A GEOCHEMICAL, TAXONOMIC, AND PHYLOGENETIC INVESTIGATION OF PALEOZOIC ARTHROPODS: CASE STUDIES ON THE CAMBRIAN SPICE EVENT AND THE SILURIAN WAUKESHA LAGERSTÄTTE

A Thesis

presented to

the Faculty of the Graduate School

at the University of Missouri-Columbia

In Partial Fulfillment

of the Requirements

for the Degree Master of Science

---

by

MIKAELA A. PULSIPHER

Dr. James D. Schiffbauer, Thesis Supervisor

December 2020

The undersigned, appointed by the dean of the Graduate School, have examined the thesis entitled

A GEOCHEMICAL, TAXONOMIC, AND PHYLOGENETIC INVESTIGATION OF PALEOZOIC ARTHROPODS: CASE STUDIES ON THE CAMBRIAN SPICE EVENT AND THE SILURIAN WAUKESHA LAGERSTÄTTE

presented by Mikaela A. Pulsipher,

a candidate for the degree of Master of Science,

and hereby certify that, in their opinion, it is worthy of acceptance.

_____

Professor James D. Schiffbauer

_____

Professor John Warren Huntley

_____

Professor Sarah M. Jacquet

_____

Professor Kevin L. Shelton

_____

Professor Kevin M. Middleton

ACKNOWLEDGMENTS

The authors of Chapters 1 and 2 would like to thank P. Scheel and the staff at the McCracken Core Library and Research Center, Missouri Department of Natural Resources for core access and assistance; S. Jacquet (University of Missouri) for sample collection assistance; S. Moore (Washington University in St. Louis) for IRMS processing; and S. Rosbach (University of Missouri) for RStudio assistance. We additionally thank M. Brown, M. Chisholm, V. Beckham, E. Bunton, and G. Halliwell for project inspiration. Funding: This work was supported by the University of Missouri Research Council to KLS; the University of Missouri Department of Geological Sciences to MAP [James H. Stitt Memorial Fellowship, Keller Opportunities for Excellence, and Marshall Opportunities for Excellence]; and the National Science Foundation to JDS [EAR CAREER #1652351] and JWH [EAR CAREER #1650745].

The authors of Chapter 3 would like to thank the Waukesha Lime & Stone Co. and Franklin Aggregate Inc. quarries in Waukesha, WI for providing tours to see the Brandon Bridge Formation; C. Eaton at the University of Wisconsin-Madison Geology Museum for accessing and loaning specimens; S. Turpin Cheavens at the University of Missouri School of Medicine for professional illustrations; and S. Jacquet and W. Leibach for GIGAmacro imaging of holotypes. We additionally thank K. Sebert for keeping our interests engaged in the project. Funding: This work was supported by the University of Missouri Department of Geological Sciences to MAP [John and Betty Marshall Opportunities for Excellence Fund];

the Paleontological Society [James M. & Thomas J.M. Schopf Student Research Award] to MAP; the Association of Women Geoscientists [Winifred Goldring award] to MAP; and the National Science Foundation to JDS [EAR CAREER #1652351] and EPA [EAR-PF #1725762].

On a more personal note, I would like to thank the following people:

Jim Schiffbauer – For putting up with my bullshit, learning me a thing or two, supplying memes, and inspiring the best group Halloween costume there ever was. Thanks, yo.

Evan Anderson – For your magical eyes that can see all the things on all the fossils, and your sage advice along my quest into the hot mess that is crustacean morphology.

John Huntley, Sarah Jacquet, Kevin Shelton, & Kevin Middleton – For putting in the time and effort to read this thing and providing feedback to improve the stuff I wrote.

My fellow grad students – For helping and listening and laughing and drinking beers on Fridays whether we were in bars or in parks 6 feet away from each other.

My friends – For Zooming and FaceTimeing, proofreading and proofwatching (even if you didn't totally understand it), and reminding me to take a brain break and go outside.

My family – For finding ways to help me adult from 1200 miles away, participating in the Sunday chats that I forced upon you, and mailing me care packages of dried apples.

Tl;dr: I couldn't have done this thing on my own. Y'all are pretty great.

TABLE OF CONTENTS

LIST OF FIGURES

LIST OF TABLES

ABSTRACT

This thesis details two stand-alone projects: Chapters 1 and 2 comprise a quantitative investigation of controls on the $\delta^{13}C$ record of the Steptoean Positive Carbon Isotope Excursion (SPICE); Chapter 3 describes a taxonomic and phylogenetic assessment of a previously unnamed arthropod from the Silurian Waukesha Lagerstätte. Despite the disparate nature of these projects, they are united by an underpinning theme of Paleozoic arthropods.

The SPICE event is a prominent, global disturbance in the $\delta^{13}C$ record of the Cambrian that is temporally linked to trilobite biomere turnover at the Marjuman–Steptoean and equivalent Guzhangian–Paibian stage boundaries. The SPICE has been used as a tool for global chemostratigraphic correlation despite the fact that individual $\delta^{13}C$ records display marked variability. To quantitatively evaluate its utility as a chemostratigraphic marker, we constructed the Steptoean Positive Carbon Isotope Excursion repository for quantitative analysis (the SPICEraq) containing $\delta^{13}C$ values and associated metadata from known records of the SPICE. Results from Wilcoxon Rank Sum and χ^2 tests indicate that regional/local conditions do have a statistically significant impact on the expression of the SPICE, with paleolatitude and approximate water depth bearing the most appreciable impact. Furthermore, this investigation confirms that the SPICE event is immediately preceded by a short-lived negative $\delta^{13}C$ excursion which potentially has bearing on the associated trilobite extinction event.

The Silurian Waukesha Lagerstätte is hosted in the Brandon Bridge Formation, and only known from exposures in the Waukesha, Wisconsin area. This lagerstätte is significant as it is dominated by soft-bodied organisms, and particularly arthropods, rather than the shelly fauna typical of other Silurian biotas. Included in this soft-bodied assemblage are several unnamed and undescribed taxa; the most abundant of the unnamed soft-bodied forms is a vermiform arthropod bearing a cephalic carapace, a suite of five raptorial head appendages, and a long, homonomously segmented trunk adorned with small swimming appendages. Taxonomic and phylogenetic analyses indicate that this taxon represents a new genus of arthropods, comprising two species: *Acheronauta stimulapis* gen. et sp. nov. and *Acheronauta leonidas* gen. et sp. nov. distinguished by the morphology of the cephalic carapace and trunk terminus. *Acheronauta* gen. nov. is a basal mandibulate, closely related to the fuxianhuiids and/or hymenocarinids. Scanning electron microscopy indicates that these fossils are preserved as calcium phosphate compressions in a carbonate-cemented siliciclastic host rock. The preservation of soft-bodied organisms in the Waukesha Lagerstätte may provide evidence of evolutionary pathways connecting Cambrian arthropods to later Paleozoic and Modern fauna and thus warrants further investigation.

CHAPTER 1:

A META-ANALYSIS OF THE STEPTOEAN POSITIVE CARBON ISOTOPE EXCURSION: THE SPICEraq DATA REPOSITORY

Mikaela A. Pulsipher[a], James D. Schiffbauer[a,b], Matthew J. Jeffrey[c,a], John Warren Huntley[a], David A. Fike[d], Kevin L. Shelton[a]

[a]Department of Geological Sciences, University of Missouri, Columbia, MO 65211 USA

[b]X-ray Microanalysis Core Facility, University of Missouri, Columbia, MO 65211 USA

[c]Department of Environmental Studies, Bellarmine University, Louisville, KY 40205 USA

[d]Department of Earth and Planetary Sciences, Washington University in St. Louis, St. Louis, MO 63130 USA

Abstract

The Steptoean Positive Isotopic Carbon Excursion (SPICE) is a prominent chemostratigraphic feature in the Lower Paleozoic. It has been used to correlate Upper Cambrian carbonate strata globally and is cited as intimately linked to the *Crepicephalus-Aphelaspis* trilobite extinction event and the Sauk II-Sauk III megasequence transition. Despite the global nature of the SPICE event, regional/local conditions serve as a control on the expression of the SPICE event in the rock record. In light of this, and to better understand

how reliable the SPICE event is as a chemostratigraphic tool for correlation, we have compiled the "SPICEraq," a data repository comprising 78 SPICE-bearing sections containing 6669 individual $\delta^{13}C$ analyses. In this study, we quantitatively evaluate the variability in SPICE records and document that, while the excursion is a global signature, its stratigraphic expression is influenced by such conditions as paleolatitude, paleocontinent, water depth, and facies. While the magnitude of the SPICE excursion is generally consistent (an ~4‰ increase), the peak $\delta^{13}C$ values are quite variable (ranging from +0.35 to +5.87‰). Specifically, sections located between 30 and 60°S paleolatitude ca. 500 Ma record $\delta^{13}C$ values ~1 to 2‰ lower than those from lower paleolatitudes. Sections deposited in shallow water depths and facies also record lower $\delta^{13}C$ values than intermediate and deep-water facies; the deep-water facies exhibit the most ^{13}C-enriched carbonates at the peak of the SPICE and post-excursion. The stratigraphic thickness of the excursion varies widely, ranging from <3 to ~884 m, and is significantly impacted by all categorical variables investigated in this study. This study documents that the rising limb of the SPICE is immediately preceded by a small negative $\delta^{13}C$ excursion in 75% of sections with data collected pre-SPICE. While 32% of sections record a $\delta^{13}C$ plateau during peak SPICE, its presence in the $\delta^{13}C$ record does not appear to be influenced by any environmental conditions investigated herein. Altogether, these analyses indicate that regional/local conditions impact the stratigraphic expression of $\delta^{13}C$ records, and thus care should be taken to use robust, quantitative measures to compare and correlate excursions.

1.1 Introduction

The carbon isotope record of the Cambrian Period (~540–485 Ma) shows considerable variation. Through the first two Cambrian Series (~540–497 Ma), fluctuating positive and negative excursions are common and characteristic (Maloof et al., 2005; Dilliard et al., 2007; Saltzman & Thomas, 2012). Following the end of Series 2, the $\delta^{13}C_{carb}$ record stabilizes around 0‰ V-PDB (Vienna Pee Dee Belemnite standard; hereafter, $\delta^{13}C$ refers to carbonate carbon), and is punctuated, mostly, by only lower magnitude excursions. The exception is the prominent Steptoean Positive Isotopic Carbon Excursion (SPICE) event near the Guzhangian–Paibian Stage boundary (which also corresponds to the North American Marjuman–Steptoean Stage boundary and the Miaolingian–Furongian Series boundary; Fig. 1-1) (Saltzman et al., 2000; Saltzman & Thomas, 2012; Zhao et al., 2019).

First named by Saltzman et al. (1998), the SPICE is a ~4 to 5‰ increase in $\delta^{13}C$ values that has been used in global chemostratigraphic correlation. The SPICE has been documented in carbonate stratigraphic sections around the world, including North America (e.g., Saltzman et al., 1998; Hurtgen et al., 2009), South America (e.g., Sial et al., 2008), Europe (e.g., Pruss et al., 2019; Álvaro et al., 2008), Asia (e.g., Kouchinsky et al., 2008; Ng et al., 2014; Lim et al., 2015; Wotte & Strauss, 2015), and Australia (e.g., Schmid et al., 2018). With such a broad geographic occurrence of this pronounced excursion, the inference commonly adopted is that the SPICE represents a global perturbation of the carbon cycle (Saltzman et al., 1998). Further, not only has the excursion been identified in both shallow and deep water carbonates (Saltzman et al., 2000; Glumac & Mutti, 2007; Zuo et al., 2018), but also in a smaller magnitude excursion (+1 to +2‰) of organic carbon isotope values ($\delta^{13}C_{org}$) from organic-rich shales (Álvaro et al., 2008; Ahlberg et al., 2009, 2018; Baker, 2010; Saltzman et al., 2011; Woods et al., 2011).

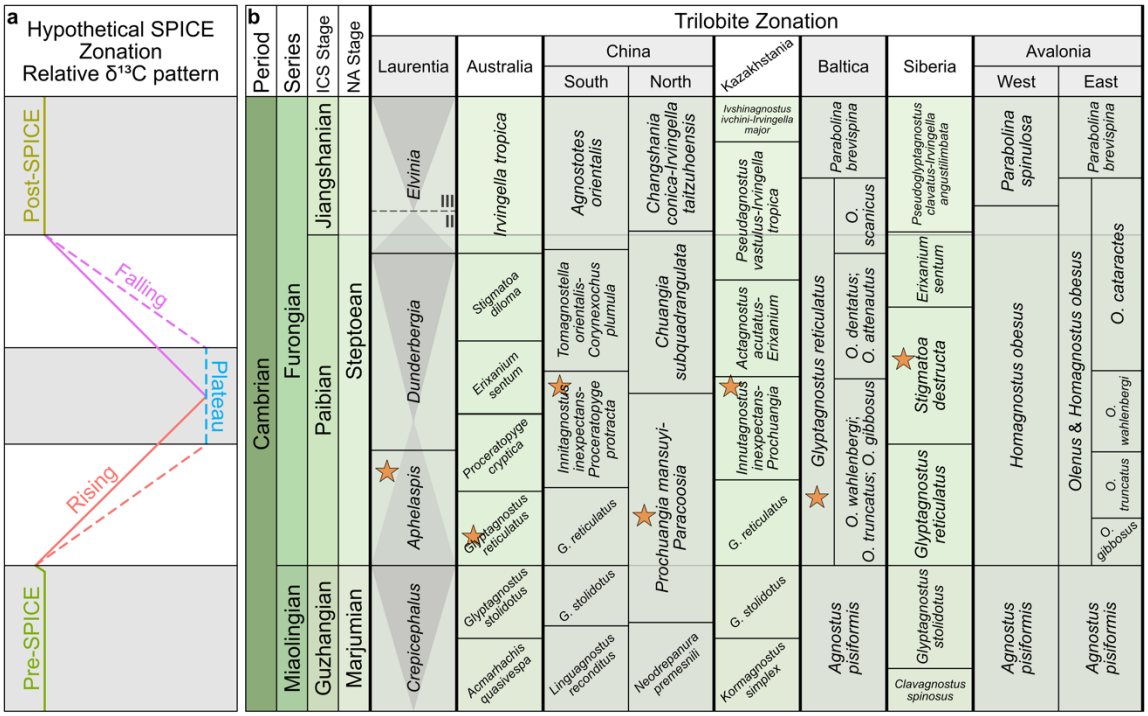

Figure 1-1. Representative SPICE curve, Cambrian Series and Stage framework, and trilobite biozonation. (a) Idealized $\delta^{13}C$ curve illustrating the 5 possible SPICE zones used to evaluate the stratigraphic expression of the SPICE (labeled, from lower to upper): Pre-SPICE, Rising limb, Plateau, Falling limb, and Post-SPICE. The zonation color-coding used here is also adopted in further figures. (b) Global correlation scheme of trilobite biozones, after Geyer (2019). Orange stars indicate the timing of the onset of the rising limb of the SPICE as identified on different paleocontinents (from Saltzman et al., 2000; Kouchinsky et al., 2008; Ahlberg et al., 2009; Ng et al., 2014; Schmid et al., 2018; and Pruss et al., 2019, as noted by Geyer, 2019). The transgressive and regressive packages within the Sauk II and Sauk III megasequences (after Palmer et al., 2012) are indicated by the triangle diagrams overprinted on the Laurentian trilobite zones; the Sauk II–Sauk III boundary is indicated by the dashed line in the Laurentia column. Note that (a) and (b) are not intended to directly correlate, their positions are only relative.

Other geochemical analyses have been utilized to investigate the SPICE event, including oxygen, sulfur, and uranium isotopes, as well as other elemental proxies (e.g., Elrick et al., 2011; Gill et al., 2011; Dahl et al., 2014; Wotte & Strauss, 2015; LeRoy & Gill, 2019). Unlike $\delta^{13}C$ values, $\delta^{18}O$ values do not show a consistent global pattern. In some sections,

$\delta^{18}O$ has an inverse relationship with $\delta^{13}C$, with the nadir of $\delta^{18}O$ values corresponding to the peak $\delta^{13}C$ values (Elrick et al., 2011). In other cases, $\delta^{18}O$ values covary with $\delta^{13}C$ and record a positive $\delta^{18}O$ excursion, such as in the Kyrshabakty section in Kazakhstan (+1‰ V-PDB) (Wotte & Strauss, 2015) and the Kulyumbe section in Siberia (+4‰ V-PDB) (Kouchinsky et al., 2008). In many instances, however, $\delta^{18}O$ does not covary with $\delta^{13}C$ and may be virtually invariant through the SPICE, such as in multiple boreholes from Australia (Schmid, 2017), the Tangwangzhai section in China (Zhu et al., 2004), and the Shingle Pass section in Nevada, United States (Baker, 2010). A positive $\delta^{34}S$ excursion of varying amplitudes has also been shown to correlate with the SPICE in multiple sections around the globe (Hurtgen et al., 2009; Gill et al., 2011; Saltzman et al., 2011; Wotte & Strauss, 2015; LeRoy and Gill, 2019). Dahl et al. (2014) measured uranium isotopes in the Mt. Whelan core from Australia to further investigate the relationship between the SPICE event and possible euxinia. Iron, mercury, and molybdenum concentrations have been analyzed to evaluate the paleoredox conditions of SPICE occurrences in North America (LeRoy & Gill, 2019), Sweden (Gill et al., 2011), and Scotland (Pruss et al., 2019). Results from these studies suggest that the timing of anoxic and/or euxinic conditions in different sections is variable with respect to trilobite extinctions and peak $\delta^{13}C$ values of the SPICE (Gill et al., 2011; Dahl et al., 2014; LeRoy & Gill, 2019; Pruss et al., 2019). Additionally, phosphatic brachiopods from Laurentia display $\delta^{13}C$ values preserving the SPICE event in a manner similar to that of corresponding bulk carbonate analyses (Cowan et al., 2005; Auerbach, 2004; Elrick et al., 2011).

The SPICE event may have also been biologically important. It occurred coincidentally with a trilobite biomere turnover, but whether it was causally or only temporally linked remains a question (Saltzman et al., 1998, 2000; Gill et al., 2011; Gerhardt, 2014; Gerhardt & Gill, 2016; Schiffbauer et al., 2017). The onset of the rising limb is coincident with the first appearance

datum (FAD) of the trilobite *Glyptagnostus reticulatus* and the base of the Pterocephaliid biomere (Fig. 1-1; Saltzman et al., 2000; Glumac, 2011). The FAD of *G. reticulatus* is also correlative with the base of the *Aphelaspis* zone following the two-phase extinction of *Crepicephalus*-zone and *Coosella perplexa*-subzone trilobites (Glumac, 2011; Schiffbauer et al., 2017). $\delta^{13}C$ values rise toward a maximum of approximately +4 to +5‰ in the late *Dunderbergia* or early *Elvinia* zones, with the peak preceding the FAD of *Irvingella major* and coinciding with the Sauk II-Sauk III megasequence boundary (Sloss, 1963; Saltzman et al., 2000, 2004; Glumac, 2011; Wotte & Strauss, 2015). The return to background $\delta^{13}C$ values occurs within the *Elvinia* zone and the latest Pterocephaliid biomere, preceding the Marjumiid-Pterocephaliid boundary and extinction event (Glumac, 2011; Wotte and Strauss, 2015; Saltzman et al., 2004). Much more broadly, the SPICE event occurred between the Cambrian radiation and the Great Ordovician Biodiversification Event (GOBE) and has been posited to reflect changes in paleoenvironmental conditions leading to either the GOBE or the Ordovician Plankton Revolution (Servais et al., 2016). Although no direct link has been established between the SPICE and these biotic events, the SPICE may record conditions that set the stage for development of the appropriate oxygenation and/or nutrient conditions for later biodiversification (Servais et al., 2008; 2016; Saltzman et al., 2011).

Several authors have documented the peak of the SPICE being coincident with the Sauk II–Sauk III megasequence boundary in Laurentian sections (Saltzman et al., 1998; 2004; Glumac & Mutti, 2007; Glumac, 2011). This necessitates deposition of strata recording the rising limb of the SPICE during the tail end of a regressive event, and subsequent deposition of strata capturing the falling limb during the beginning of a transgression. While the Sauk sequences specifically are directly applicable to Laurentian strata, some authors have suggested that sections elsewhere in the world may also record a shallowing event coincident with the

SPICE (e.g., Chen et al., 2011; Wotte & Strauss, 2015; Wang et al., 2020), although this is not ubiquitous (e.g., Schiffbauer et al., 2017; LeRoy & Gill, 2019; Labotka & Freiburg, 2020). The SPICE is not the only carbon isotope excursion in the Paleozoic that is associated with eustatic sea-level changes. For instance, the positive Upper Ordovician Hirnantian isotopic carbon excursion (HICE) has been attributed to glacioeustacy (Melchin et al., 2013; Jones et al., 2020); and comparably, the positive $\delta^{13}C$ excursion of the Silurian Ireviken event is suggested to have been linked to climate change (Rose et al., 2019). This latter excursion is sometimes recorded in regressive facies packages (Baltica and Canada), and sometimes in transgressive facies packages (USA, Great Britain, and Tunisia) (Rose et al., 2019), similar to what is observed for the SPICE.

Despite its reputed global nature, some workers have suggested that the SPICE event may be more strongly affected by regional/local depositional conditions than previously thought—and thus its utility for correlation may be imprecise. Some workers have cited regional tectonics, heterogeneity in the chemical gradients of seawater in the Furongian, and paleo-water depth as potential driving forces for this variability (Wotte & Strauss, 2015; Schiffbauer et al., 2017; Barili et al., 2018). Furthermore, the SPICE interval varies widely in stratigraphic thickness, from <3 m in the Wanliangyu section, China (Rising limb: ~1 m; Chen et al., 2011) to >800 m in the Kulyumbe section, Siberia (Rising limb: ~380 m; Kouchinsky et al., 2008). In addition to demonstrable local variability, some sections that have been previously identified as Steptoean in age do not capture an easily identifiable SPICE signal in their $\delta^{13}C$ records, despite clear documentation of the event in nearby time-equivalent units (e.g., Pruss et al., 2016). The fossil assemblages in some of these sections indicate a likely Steptoean age (e.g., Huang et al., 2019), whereas in other sections, fossil data are sparse, causing ambiguity about the age of the units (e.g., Glumac & Mutti, 2007).

These disparities, among others later discussed, in published SPICE data make its use as a tool for global correlation more complicated than previously assumed. To date, no robust statistical analyses have been employed to quantitatively compare and contrast the stratigraphic expressions of the SPICE. Identification of the excursion has been done predominantly through C-isotope pattern-matching, for lack of a better term, and biostratigraphic and/or lithologic correlation. Here, we present a compilation of data from the published literature and the results of a meta-analysis to test for emergent patterns in the $\delta^{13}C$ records of the SPICE and explore a variety of regional/local conditions during deposition and diagenesis that may have impacted its stratigraphic expression.

1.2 Materials & Methods

1.2.1 Construction of the SPICEraq

To test the variability of the stratigraphic and isotopic expression of the SPICE signal, we compiled SPICE records published from 1992–2020 (data collection was stopped on February 29, 2020). In sum, the entire compilation encompassed a total of 95 individual sections from 36 published journal articles and theses/dissertations—78 of which were subjected to statistical analyses (see Table 1-1 for summary), and 17 of which were excluded for their lack of an apparent excursion. Hereafter, we refer to this data compilation as the Steptoean Positive Isotopic Carbon Excursion repository for quantitative analysis (the SPICEraq). Three publications prior to Saltzman et al. (1998), where the SPICE received its formal definition, were included in this study because they report data that are likely to have recorded the then-unnamed SPICE event: Laudon (1992), He (1995), and Saltzman et al. (1995). Carbon isotope data, and, if noted, lithology and/or facies, were taken from

supplemental files and in-text tables provided for each published SPICE dataset. If not provided in tables, lithology and/or facies were extracted from the text and/or figures of the corresponding publication. Where necessitated by the lack of published data tables, $\delta^{13}C$ values and stratigraphic thickness measurements were extracted from figures using WebPlot Digitizer (WPD; Rohatgi, 2019—all extracted data are included in the SPICEraq). In many cases, WPD was used for extracting metadata other than isotope values and stratigraphic heights/core depths, for instance including Series/Stage boundary positions, Formation boundary positions, lithologic package thicknesses, biostratigraphic index or biozone boundary positions, and other information included in figures but not reported in data tables (this information is explicitly provided in Section 2.1

TABLE 1-1.

SPICEraq SUMMARY DATA

E #	Lc	δ13C (‰ V-PDB)						Stratigraphic thickness (m)					Metadata						
		Pre med	Rise min	Rise max	Plat med	Fall min	Post med	Pre	Rise	Plat	Fall	Post	Exc	Fac	Dep	Lith	PCont	PLat°	Ref
1	North America	1.64	1.40	5.30	4.63	0.12	0.71	32.80	115.20	44.00	55.00	53.00	214.20	ISB	Int	C	Laur	0–30N	Baker, 2010
2		0.62	0.32	5.47	4.39	-0.09	0.55	24.00	92.50	77.10	17.20	48.20	186.80	ISB	Int	C	Laur	0–30S	Baker, 2010
3		-1.20	-1.10	1.59	1.65	—	—	21.25	5.25	9.00	—	—	14.25	Shelf	Int	D	Laur	30–60S	Barili et al., 2018
4		-1.23	-1.61	1.13	—	-1.74	-1.53	48.00	22.50	—	7.25	14.50	29.75	Shelf	Int	D	Laur	30–60S	Barili et al., 2018
5		0.31	-1.20	2.90	—	—	—	26.00	20.00	—	—	—	20.00	ISB	Int	C	Laur	0–30S	Gerhardt & Gill, 2016
6		0.53	0.40	4.06	—	1.99	—	26.00	19.00	—	4.50	—	23.50	ISB	Int	C	Laur	0–30S	Gerhardt & Gill, 2016
7		0.37	-3.82	3.70	3.48	—	—	26.25	7.52	7.28	—	—	14.80	ISB	Int	C	Laur	0–30S	Gerhardt & Gill, 2016
8		0.25	-0.06	3.41	—	—	—	7.00	28.00	—	—	—	28.00	ISB	Int	C	Laur	0–30S	Gerhardt & Gill, 2016
9		0.17	-0.10	3.77	2.32	-0.32	-0.31	16.80	2.52	4.22	29.28	5.84	36.02	ISB	Int	L	Laur	0–30S	Gill et al., 2011
10		1.48	1.14	3.26	3.65	0.62	0.84	9.14	5.42	53.86	12.74	10.23	72.02	Shelf	Int	L	Laur	0–30S	Glumac, 2011
11		2.69	2.51	4.53	4.01	2.34	3.39	2.58	5.89	27.79	4.36	12.94	38.04	Shelf	Int	L	Laur	0–30S	Glumac, 2011
12		-0.87	-1.83	2.91	—	1.07	1.25	2.90	2.05	—	1.00	0.10	3.05	Basin	Dp	L	Laur	30–60S	Glumac & Mutti, 2007
13		0.33	0.33	4.09	3.18	-0.85	—	10.70	22.80	29.15	30.35	—	82.30	ShNS	Sh	L	Laur	0–30S	Glumac & Walker, 1998
14		-0.03	0.53	2.94	—	-0.80	-0.85	63.00	20.00	—	16.00	29.00	36.00	ShNS	Sh	L	Laur	0–30S	He, 1995
15		-1.28	-1.75	1.83	—	-3.00	—	52.14	16.17	—	29.98	—	46.15	Shelf	Int	C	Laur	30–60S	Hurtgen et al., 2009
16		—	0.00	4.40	4.40	-2.40	-2.30	—	6.10	7.70	13.80	1.30	27.60	Shelf	Int	D	Laur	0–30S	Labotka & Freiburg, 2020
17		0.40	-0.50	2.40	—	—	—	59.70	19.10	—	—	—	19.10	ShNS	Sh	C	Laur	0–30S	Laudon, 1992
18		-0.25	-0.50	3.90	—	—	—	57.50	34.90	—	—	—	34.90	ShNS	Sh	C	Laur	0–30S	Laudon, 1992
19		0.30	-1.46	2.89	—	—	—	38.13	11.07	—	—	—	11.07	ISB	Int	L	Laur	0–30S	LeRoy & Gill, 2019
20		0.56	0.47	1.83	—	—	—	12.60	6.80	—	—	—	6.80	ISB	Int	D	Laur	0–30S	LeRoy & Gill, 2019
21		0.70	0.19	2.10	—	—	—	19.30	13.13	—	—	—	13.13	ISB	Int	L	Laur	0–30S	LeRoy & Gill, 2019
22		-0.61	-0.30	4.03	3.77	2.94	—	54.00	30.00	20.00	7.00	—	57.00	Shelf	Int	D	Laur	0–30S	Mackey & Stewart, 2019
23		0.72	0.63	1.89	—	0.88	0.99	6.75	3.00	—	4.50	2.25	7.50	ISB	Int	L	Laur	0–30N	Saltzman et al., 1995
24		0.57	-0.30	2.76	—	1.07	1.21	25.66	4.84	—	11.50	10.50	16.34	ISB	Int	L	Laur	0–30S	Saltzman et al., 1995
25		0.03	0.05	1.08	—	—	—	8.90	12.54	—	—	—	12.54	Shelf	Int	D	Laur	0–30S	Saltzman et al., 1995
26		0.35	0.47	1.11	0.92	0.75	—	5.50	2.00	9.50	4.00	—	15.50	Shelf	Int	L	Laur	0–30S	Saltzman et al., 1995
27		0.37	0.08	4.65	4.20	0.68	0.70	85.40	165.20	43.10	53.50	28.00	261.80	ISB	Int	L	Laur	0–30N	Saltzman et al., 1998

TABLE 1-1 (CONTINUED)

28	North America	1.97	1.39	4.85	4.40	0.37	0.59	76.50	1.50	75.00	21.00	52.10	97.50	ISB	Int	L	Laur	0–30S	Saltzman et al., 1998
29		—	0.77	4.38	—	1.11	1.03	—	39.90	—	21.70	43.40	61.60	ISB	Int	L	Laur	0–30S	Saltzman et al., 1998
30		—	-1.61	2.19	1.96	-2.27	-1.16	—	29.48	7.46	15.93	38.97	52.87	Shelf	Int	L	Laur	30–60S	Saltzman et al., 2004
31		0.90	0.96	3.81	—	0.22	0.47	8.44	6.72	—	7.78	15.29	14.50	Shelf	Int	L	Laur	0–30S	Saltzman et al., 2004
32		0.22	-0.10	4.75	3.96	0.05	0.95	24.72	19.02	26.63	16.49	15.69	62.14	Shelf	Int	L	Laur	0–30S	Saltzman et al., 2004
33		0.04	0.58	5.67	—	1.66	—	50.29	15.70	—	11.89	—	27.59	ISB	Int	L	Laur	0–30S	Schiffbauer et al., 2017
34		0.11	-0.38	2.97	—	-1.46	-0.27	35.36	8.53	—	4.27	27.13	12.80	ISB	Int	D	Laur	0–30S	Schiffbauer et al., 2017
35		-1.01	-2.32	2.40	—	-0.99	-0.39	37.79	15.55	—	13.11	13.71	28.66	ISB	Int	D	Laur	0–30S	Schiffbauer et al., 2017
36		0.16	0.03	3.64	2.30	-1.09	-0.40	26.52	3.05	16.15	8.38	20.27	27.58	ISB	Int	D	Laur	0–30S	Schiffbauer et al., 2017
37		0.18	-0.19	2.59	2.37	—	—	16.31	1.37	11.74	—	—	13.11	ISB	Int	L	Laur	0–30S	Schiffbauer et al., 2017
38		-0.45	-1.37	4.10	—	-1.84	-1.13	44.81	2.89	—	7.62	114.61	10.51	ShNS	Sh	D	Laur	0–30S	Jeffrey, 2017
39		0.25	0.39	4.67	3.68	0.38	0.44	120.09	6.71	39.16	31.09	38.87	76.96	Shelf	Int	D	Laur	0–30S	Jeffrey, 2017
40	SA	-1.30	-2.10	5.70	—	—	—	210.90	210.10	—	—	—	210.10	ShNS	Sh	L	Gond	30–60S	Sial et al., 2008
41		—	-0.50	0.80	0.60	-0.90	-0.80	—	28.00	38.70	44.50	59.40	111.20	ShNS	Sh	D	Gond	30–60S	Sial et al., 2013
42	EU	-2.09	-1.67	3.02	—	-0.89	-0.29	38.70	9.00	—	1.97	20.10	10.97	ShNS	Sh	L	Gond	30–60S	Álvaro et al., 2008
43		-0.70	-0.27	2.72	—	-0.99	-0.72	37.70	12.30	—	20.00	69.60	32.30	ShNS	Sh	C	Laur	30–60S	Pruss et al., 2019
44	Asia	0.39	0.15	3.46	—	1.20	1.17	3.70	1.10	—	1.75	6.15	2.85	ShNS	Sh	L	Gond	0–30S	Chen et al., 2011
45		0.90	0.60	4.10	3.80	1.70	1.70	47.90	18.45	91.20	10.05	26.38	119.70	Slope	Dp	L	Gond	0–30N	Chung et al., 2011
46		0.03	-0.80	3.84	—	-0.83	0.21	1216.00	378.00	—	506.00	340.00	884.00	Shelf	Int	C	Sib	0–30S	Kouchinsky et al., 2008
47		-0.22	-3.43	4.60	—	0.09	0.26	289.10	283.60	—	102.30	508.80	385.90	Shelf	Int	C	Sib	0–30S	Kouchinsky et al., 2008
48		—	-0.27	3.75	—	0.82	—	—	111.00	—	28.00	—	139.00	Slope	Dp	L	Gond	0–30N	Li et al., 2018b
49		—	—	—	—	0.71	—	—	—	—	47.50	—	47.50	Slope	Dp	NA	Gond	0–30N	Li et al., 2018b
50		—	2.10	5.06	—	3.57	3.95	—	88.50	—	7.00	14.50	95.50	Slope	Dp	L	Gond	0–30N	Li et al., 2018b
51		0.23	0.15	2.81	1.73	-2.34	-1.84	17.77	7.81	7.84	26.13	1.78	41.78	Shelf	Int	L	Gond	0–30N	Lim et al., 2015
52		-2.29	-1.09	3.59	—	0.32	0.46	66.21	19.26	—	23.47	51.77	42.73	Shelf	Int	L	Gond	0–30S	Liu et al., 2017
53		1.03	0.52	4.14	—	2.20	2.10	1.30	3.60	—	2.80	3.30	6.40	ShNS	Sh	L	Gond	0–30S	Ng et al., 2014
54		0.23	-0.53	1.31	—	—	—	177.70	99.80	—	—	—	99.80	Slope	Dp	L	Gond	0–30N	Saltzman et al., 2000
55		0.51	0.19	5.03	4.28	1.26	1.66	82.35	150.20	110.25	120.00	230.00	380.45	Slope	Dp	L	Gond	0–30N	Saltzman et al., 2000
56		-0.45	-0.51	4.82	—	0.62	0.47	116.00	63.50	—	52.50	208.00	116.00	Slope	Dp	L	Kazk	0–30S	Saltzman et al., 2000
57		—	-0.33	3.87	3.87	2.34	—	—	10.50	11.00	2.70	—	24.20	ShNS	Sh	C	Gond	0–30N	Wang et al., 2020
58		0.42	-1.00	3.71	—	1.36	1.36	17.90	1.20	—	2.65	7.67	3.85	ShNS	Sh	C	Gond	0–30S	Wang et al., 2020
59		0.05	0.04	3.37	—	-0.34	1.40	42.70	10.00	—	0.20	4.00	10.20	ShNS	Sh	C	Gond	0–30S	Wang et al., 2020
60		—	0.55	2.26	—	—	—	—	0.59	—	—	—	0.59	ShNS	Sh	C	Gond	0–30S	Wang et al., 2020
61		-0.40	-0.30	5.00	—	0.70	0.80	82.10	61.00	—	53.20	19.50	114.20	Slope	Dp	L	Kazk	0–30S	Wotte & Strauss, 2015
62		0.18	0.21	2.23	—	0.08	0.44	30.10	2.70	—	8.20	35.40	10.90	ShNS	Sh	L	Gond	0–30S	Zhu et al., 2004
63		0.20	0.00	3.00	—	—	—	124.00	70.50	—	—	—	70.50	Slope	Dp	L	Gond	0–30N	Zhu et al., 2004
64		-0.20	0.80	3.70	3.30	0.90	0.90	108.00	24.00	14.00	21.00	44.00	59.00	Basin	Dp	L	Gond	0–30N	Zuo et al., 2018
65		-0.10	-0.70	4.40	—	0.50	1.50	490.00	150.00	—	125.00	450.00	275.00	Slope	Dp	L	Gond	0–30N	Zuo et al., 2018
66	Australia	—	2.41	4.16	—	0.97	—	—	127.05	—	131.30	—	258.35	ShNS	Sh	L	Gond	0–30N	Gill et al., 2011
67		-0.36	-0.05	3.91	—	-0.43	-0.23	166.04	50.93	—	152.10	57.21	203.03	ShNS	Sh	C	Gond	0–30N	Lindsay et al., 2005
68		-0.47	-0.39	5.87	—	1.04	—	110.65	135.50	—	55.64	—	191.14	Basin	Dp	L	Gond	0–30N	Saltzman et al., 2000
69		-0.97	-1.16	1.93	—	-1.30	—	344.42	179.84	—	164.59	—	344.43	ShNS	Sh	C	Gond	0–30N	Schmid, 2017
70		-1.87	-1.89	1.53	—	-0.12	—	27.44	109.72	—	39.63	—	149.35	ShNS	Sh	C	Gond	0–30N	Schmid, 2017
71		-0.86	-1.16	2.54	—	-1.29	-1.97	73.15	173.74	—	124.97	164.59	298.71	ShNS	Sh	C	Gond	0–30N	Schmid et al., 2018
72		-0.31	-0.42	4.86	—	1.12	1.77	50.35	71.95	—	15.40	20.20	87.35	ShNS	Sh	D	Gond	0–30N	Schmid et al., 2018
73		-1.13	-1.32	3.01	—	-2.88	—	64.01	103.63	—	158.50	—	262.13	ShNS	Sh	C	Gond	0–30N	Schmid et al., 2018

TABLE 1-1 (CONTINUED)

74	Australia	-0.75	-1.34	2.49	—	-1.07	—	40.00	140.00	—	100.00	—	240.00	ShNS	Sh	C	Gond	0–30N	Schmid et al., 2018
75		—	-3.76	1.85	—	-2.78	—	—	146.30	—	85.34	—	231.64	ShNS	Sh	C	Gond	0–30N	Schmid et al., 2018
76		—	-5.01	0.35	—	-3.04	—	—	204.21	—	54.87	—	259.08	ShNS	Sh	C	Gond	0–30N	Schmid et al., 2018
77		-0.71	-1.81	2.24	2.26	1.52	—	90.11	69.17	93.55	11.17	—	173.89	ShNS	Sh	C	Gond	0–30N	Schmid et al., 2018
78		—	-4.17	1.44	—	—	—	—	152.30	—	—	—	152.30	ShNS	Sh	D	Gond	0–30N	Schmid et al., 2018

Summary table of important $\delta^{13}C$ values, stratigraphic thicknesses, and metadata for each entry. For both $\delta^{13}C$ values and stratigraphic thicknesses, all samples marked "Omit" in the SPICEraq were also excluded from these calculations and dashes indicate that a particular SPICE zone was not sampled in that entry. Metadata outlined in this table include paleolatitude, paleocontinent, water depth, simplified facies, and publication reference. See full SPICEraq in SOM for more details, including the name of sections/boreholes. Abbreviations: E# = entry number; Lc = modern geographic location [SA = South America, EU = Europe]; Pre = pre-SPICE; Rise = rising limb; Plat = plateau; Fall = falling limb; Post = post-SPICE; Exc = Excursion (Rise + Plateau [if present] + Fall); med = median; min = minimum; max = maximum; Fac = facies and Dep = depth [ISB = intrashelf basin, ShNS = shallow/ nearshore, Int = intermediate, dp = deep]; Lith = lithology [C = "carbonate", L = limestone, D = dolostone]; PCont = paleocontinent [Gond = Gondwana, Kazk = Kazakhstania, Laur = Laurentia, Sib = Siberia]; and PLat° = paleolatitude.

In order to quantitatively evaluate the expression of the SPICE event, $\delta^{13}C$ curves were divided into 5 possible "SPICE zones" based on the shape of the curve and/or the greater stratigraphic context of the section as relayed in the text and figures of the corresponding papers (Fig. 1-1a). To be clear, while the excursion itself is commonly defined as a 4 to 5‰ shift in $\delta^{13}C$ values, we chose not to demarcate the SPICE zones designated herein either by specific $\delta^{13}C$ values or magnitudes of change. Instead, because marked variation is observable both across and within entries, we visually assessed all of the compiled data, scaled equally within groups organized by stratigraphic thickness. From our observations, we have defined the SPICE zones as follows, largely based on changes in the slope of the $\delta^{13}C$ profile over stratigraphic distance: (1) Pre-SPICE: background $\delta^{13}C$ values prior to the onset of the SPICE. (2) Rising limb: the onset of the SPICE, beginning with the negative-most value immediately preceding the rising $\delta^{13}C$ values and ending with the maximum $\delta^{13}C$ value prior to a plateau or fall in the values. (3) Plateau: for those sections that hovered near the peak $\delta^{13}C$ value for a minimum of 5 m, a plateau was demarcated between the maxima of the rising and falling limbs. (4) Falling limb: the zone over which $\delta^{13}C$ values return to a stabilized background, beginning with the maximum $\delta^{13}C$ value or the end of the rising limb or the plateau, and ending with the negative-most $\delta^{13}C$ value before stabilization. (5) Post-SPICE: stabilized background $\delta^{13}C$ values following termination of the falling limb (Fig. 1-1a). In order to preserve the full stratigraphic extent of each SPICE zone in subsequent analyses, the sample marking the boundary between adjacent SPICE zones was included in both the preceding and succeeding zones. Note that these duplicated points do not otherwise affect the analyses conducted herein as all calculations were restricted to individual SPICE zones and did not cross the boundaries between adjacent zones.

In several sections, the pre- and/or post-SPICE zones covered 10s to 100s of meters, capturing other excursions/fluctuations either before or after the SPICE. These zones were truncated in an attempt to remove these fluctuations and calculate median $\delta^{13}C$ values that more accurately reflect the baselines immediately under- and overlying the SPICE. The samples excluded from this study remain in the SPICEraq but have been coded as "Omit" for the SPICE zone. A corrected meters-above-the-bottom value was calculated for each section, with the 1st non-omitted sample used as the bottom-most value. However, to mitigate variation in stratigraphic thickness across datasets and to pin sections on an identifiable chemostratigraphic feature, the stratigraphic height or borehole depth of each sample was recalculated as meters relative to the onset of the rising limb of the SPICE event.

Five grouping variables were used to test for emerging patterns in the SPICEraq: paleolatitude, paleocontinent, water depth, facies, and lithology. Approximate paleolatitude and paleocontinent for each study locality were determined based on the 500 Ma paleogeographic reconstruction in GPlates (Müller et al., 2018). Six paleolatitudinal categories, as approximations of climate zones, were demarcated in 30° increments symmetrically about the equator (0–30°N and S; 30–60°N and S; and 60–90°N and S). The precise location of Kazakhstanian sections is not known at 500 Ma; following Saltzman et al. (2000), those sections are assumed to have been located between 0–30°S because the island arc that would later become Kazakhstania spans from the lower portion of 0–30°N zone to the upper portion of the 30–60°S zone (Fig. 1-2). The facies description for each section was simplified to one of five categories based on the description provided in the text for the onset of the SPICE: (1) Shallow/nearshore, (2) Shelf, (3) Intrashelf basin, (4) Slope, and (5) Basin. Water depth was approximated from these simplified facies categories, with 1 corresponding to shallow, 2 and 3 corresponding to intermediate, and 4 and 5 corresponding to deep. Table 2-1 lists the

facies/depth descriptors that served as keywords for our categorical assignment; such an approach was necessary because not all of the publications assessed for the SPICEraq provide an approximate water depth for the deposition of the analyzed carbonates. Water depth thus operates as a more relaxed approximation of depositional environment than the facies descriptor. In order to evaluate the effects of lithology on $\delta^{13}C$ values, the lithology of the specific sample recording the peak $\delta^{13}C$ value for the rising limb of the SPICE was noted and simplified to one of three categories: (1) "Carbonate", (2) Limestone, and (3) Dolostone (n = 77 total). Samples included in the "carbonates" category represent those for which a more precise lithology (i.e., limestone or dolostone) could not be ascertained from data tables, stratigraphic columns, or the text of the original publications. Within individual entries, lithologies were not assessed for all samples nor were the effects of lithology on $\delta^{13}C$ values evaluated for the entire SPICE interval because several entries comprise data obtained from both limestones and dolostones and thus cannot be assigned to a single lithologic category. Note that entry #49 was excluded from lithologic analysis because samples within this entry comprise only the falling limb of the SPICE.

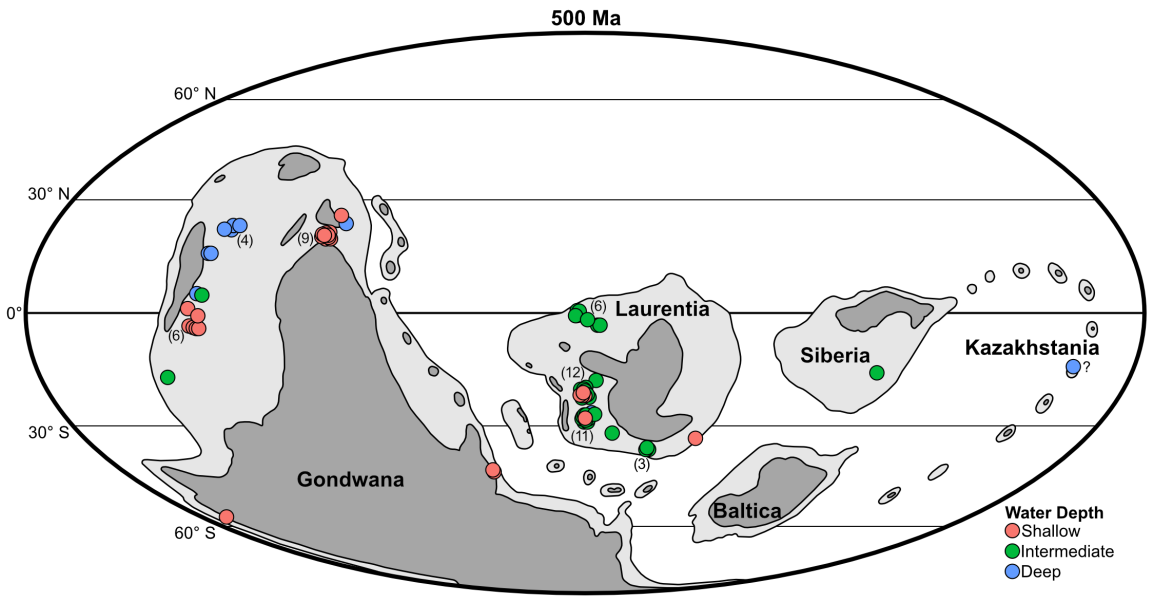

Figure 1-2. Paleogeographic map ca. 500 Ma. The location of each of the 78 entries included in the SPICEraq is marked by a circle, color-coded by categorical water depth. The numbers in parentheses denote how many total entries are included within each overlapping cluster. A question mark denotes an uncertain paleogeographic location. Dark gray regions denote exposed continental land masses, whereas light gray regions denote continental shelves. Reconstruction based on the 500 Ma raster from GPlates (Müller et al., 2018).

Some of the sections included in our compilation, although identified as Steptoean in age, do not illustrate the characteristic positive $\delta^{13}C$ excursion (n = 17; including some or all sections from Perfetta et al., 1999; Glumac & Spivak-Birndorf, 2002; Buggisch et al., 2003; Glumac & Mutti, 2007; Sial et al., 2008; Ahlberg et al., 2009; Peng et al., 2016; Pruss et al., 2016; Jeffrey, 2017; Azmy, 2019; Huang et al., 2019). As a result, these sections cannot be broken down into the five "SPICE zones" used in this study to describe the excursion and have thus been excluded from further analysis of the SPICEraq. This group of sections is hereafter referred to as the "SWEETS" group (sections without evident expression of the SPICE) because of their apparent lack of "SPICE-y-ness". Some of the sections in the SWEETS group may show portions of the SPICE, for instance a part of the rising or falling

limbs. However, not enough detail is reported to confirm that they unequivocally capture the SPICE event or to justify their inclusion in further analyses.

Two publications that do unambiguously present SPICE-bearing sections were unfortunately necessary to exclude from both the SPICEraq and the SWEETS group. The first is Brasier's (1993) seminal composite carbon isotope curve from the Great Basin, which is commonly regarded as the first documentation of the SPICE event (Saltzman et al. 2004; Barili et al., 2018). These data could not be evaluated because: (1) no data tables are provided in text; and (2) the isotope versus stratigraphy illustration (his figure 1) has no vertical scale. The second exclusion was Li et al. (2018a), which captures the SPICE event in a suite of well logs from south China. However, much like the other exclusion, these data are inaccessible because: (1) no data tables are provided; and (2) the figures do not show individual data points that could have been assessed via WPD (and arbitrarily picking any "points" along the published curves may capture "smoothed" or otherwise filtered data).

The full SPICEraq data repository is formatted as a Microsoft® Excel® file, which is too massive to include as an appendix to this thesis. The work presented in Chapters 1 and 2 is currently in press at *Earth Science Reviews*, (Pulsipher et al., *in press*) where the SPICEraq will be included as part of the Supplementary Online Materials. Associated metadata for the SPICEraq is included in Section 2.1 and a column key for the SPICEraq datasheet is included in Section 2.7. In addition, metadata descriptions for the SWEETS group are included in Section 2.2; paleogeographic locations of the SWEETS sections are included in Figure 2-1; and all SWEETS $\delta^{13}C$ data are plotted in Figure 2-2. Where discussing any SPICEraq or SWEETS entries in the main text that follows, we include the entry numbers (corresponding to the repository in #X format for SPICEraq entries and #SX format for SWEETS entries), along with their corresponding locations and references at their first in-text mention. Lastly,

Section 2.3 includes additional details on WPD data collection, as well as verification of the accuracy and precision of WPD through cross-checking of published sections with both figures and data tables available (examples shown in Fig. 2-3).

1.2.2 Quantitative Analysis of the SPICEraq

RStudio (v. 1.2.1335 © 2009–2019 RStudio, Inc.) packages base and stats (v. 3.6.1; R Core Team, 2019) were used to identify the following $\delta^{13}C$ values: pre-SPICE median, rising limb minimum, rising limb maximum, plateau median, falling limb minimum, and post-SPICE median. The ranges of both stratigraphic thicknesses and $\delta^{13}C$ values for the SPICE zones were also calculated. Data wrangling and transformation in RStudio was accomplished with the dplyr (v. 0.8.3; Wickham et al., 2019) and tidyr (v. 0.8.3; Wickham and Henry, 2019) packages. Wilcoxon rank-sum tests were conducted using the stats package (v. 3.6.1; R Core Team, 2019) to compare pre-SPICE medians, rising limb minima, rising limb maxima, and post-SPICE medians among the identified grouping variables: paleolatitude, paleocontinent, water depth, facies, and lithology. This tests the alternative hypothesis that the data come from populations with the same median values. The statistical significance of differences in peak $\delta^{13}C$ values across paleolatitudinal bins was further evaluated through randomization, the details of which are provided in the Section 2.4. In addition, χ^2 tests were conducted in PAST (v. 4.0; Hammer et al., 2001) in order to determine whether or not the presence of a plateau in SPICE data was related to paleolatitude, paleocontinent, water depth, or facies. The null hypothesis for the χ^2 tests is that the proportion of plateaus among grouping variables is indistinguishable from the proportion of all observations among those same grouping variables (i.e., the likelihood of a plateau is unaffected by grouping variable). An alpha value of 0.05 was assumed for all analyses, with marginally significant *p*-values constrained to

$0.05<p\leq0.1$. The ggplot2 (v. 3.2.1; Wickham, 2016) and ggridges (v. 0.5.1; Wilke, 2018) packages in RStudio were used to produce figures. See Section 2.6 for a copy of our R code inputs.

1.2.3 Additional data from southeast Missouri

In addition to previously published data, detailed samples for isotope analysis were collected from two cores from southeast Missouri, housed at the Missouri Geological Survey McCracken Core Library and Research Center in Rolla, MO (Jeffrey et al., 2017). These cores augment data reported by Schiffbauer et al. (2017) for the Central Missouri Intrashelf Basin. Core LO-5 represents a shallow marine section deposited on the Lebanon Arch, and core 319-11A represents a shelf section deposited on a down-dropping, fault-bounded block adjacent to the Reelfoot Rift (Fig. 1-3a; entries #38 and #39, respectively). Samples were sawn and examined via binocular microscopy to identify their lithological and mineralogical components. Carbonate portions were micro-drilled; care was taken to target homogeneous carbonate components, including micritic and oolitic calcite, and micritic, planar, and fabric-retentive dolomite (Sibley & Gregg, 1987). In addition, two southeast Missouri outcrops taken from the Jeffrey (2017) thesis are also reported for completeness, although they do not unequivocally record the SPICE and are thus placed in the SWEETS group. See Section 2.2 for a further description of these outcrops and the corresponding $\delta^{13}C$ and $\delta^{18}O$ data (entries #S9 and #S10).

Analyses of carbon and oxygen isotopes were conducted at Washington University in St. Louis, MO, using a GasBench II peripheral on a Delta V Advantage isotope ratio mass spectrometer (IRMS). Isotopic results are reported on the V-PDB scale; NBS 19 was used as

the house standard, with replicate analyses giving a standard error of $<\pm 0.05‰$ for both carbon and oxygen values.

Figure 1-3. Location map and geochemical analyses of two southeast Missouri cores collected by Jeffrey (2017). (a) Map of southeast Missouri, United States, showing the locations (yellow circles) of cores LO-5 and 319-11A, as well as sampled outcrops (data shown in Fig. 2-2), relative to the central Missouri Intrashelf Basin, Lebanon Arch, and Reelfoot Rift. (b) Lithologic core logs and geochemical analyses of LO-5 and 319-11A. Note that while the ‰ V-PDB scales on the x-axis for both sections are identical, the vertical scales are different.

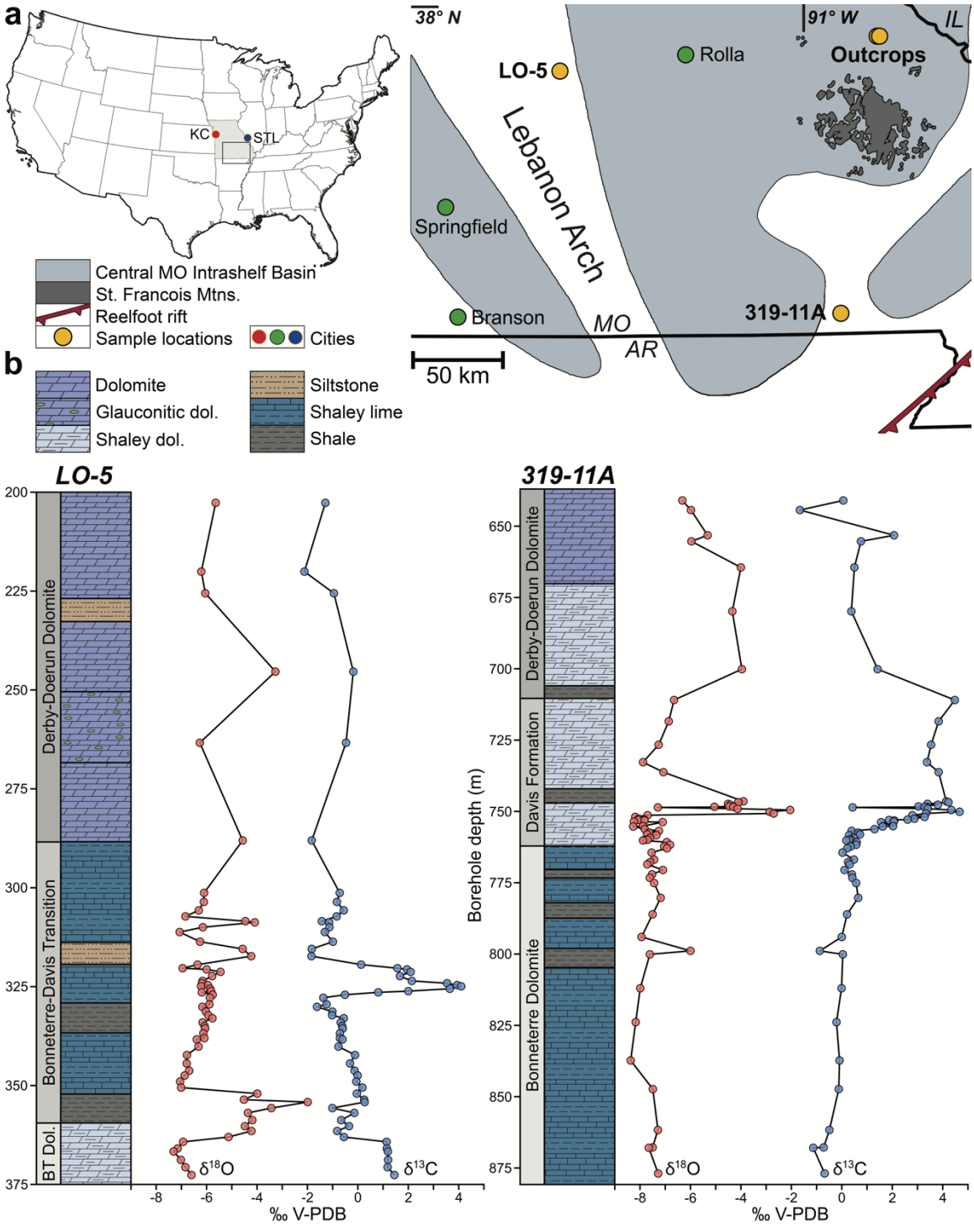
a
KC
STL
38° N
91° W
IL
LO-5
Rolla
Outcrops
Lebanon Arch
Springfield
Branson
MO
AR
319-11A
50 km
Central MO Intrashelf Basin
St. Francois Mtns.
Reelfoot rift
Sample locations
Cities
b
Dolomite
Glauconitic dol.
Shaley dol.
Siltstone
Shaley lime
Shale
LO-5
319-11A
Derby-Doerun Dolomite
Bonneterre-Davis Transition
BT Dol.
Davis Formation
Bonneterre Dolomite
Borehole depth (m)
δ18O
δ13C
‰ V-PDB

1.3 Results

1.3.1 New $\delta^{13}C$ and $\delta^{18}O$ data from southeast Missouri

Previously unpublished core data from southeast Missouri, cores LO-5 and 319-11A, are included in the SPICEraq as entries #38 and #39. Biostratigraphic control is lacking for both cores in the original drilling reports, so correlation is limited to $\delta^{13}C$ data and lithostratigraphy (Jeffrey, 2017; He et al., 1997). The LO-5 section is 169.93 meters in length and comprises 67 analyzed samples. This section spans the upper Bonneterre Dolomite, the mixed carbonate-siliciclastic Bonneterre-Davis transition, and the lower Derby-Doerun Dolomite (Fig. 1-3b). The Davis Formation is not easily distinguishable in this shallow-water section. The SPICE event is recorded in a silty limestone interval near the middle of the Bonneterre-Davis transition as an ~5.5‰ positive shift in $\delta^{13}C$ values over a thickness of ~3 m, with a peak $\delta^{13}C$ value of +4.1‰. No correlative excursion is exhibited in the $\delta^{18}O$ data over the same interval.

The 319-11A section contains 72 samples, covers an interval of 235.92 m, and spans the Bonneterre Dolomite, the Davis Formation, and the lower Derby-Doerun Dolomite (Fig. 1-3b). In this section, the rising limb of the SPICE begins in the uppermost Bonneterre Dolomite and continues through the Davis Formation into the lowermost Derby-Doerun Dolomite. The magnitude of the positive $\delta^{13}C$ shift is ~5.0‰, and spans a stratigraphic interval of ~6.5 m, with a peak $\delta^{13}C$ value of +4.67‰. An ~5.0‰ positive shift in $\delta^{18}O$ values correlates with the uppermost rising limb of the SPICE.

1.3.2 Results of the SPICEraq

Of the 95 sections assessed for compilation of the SPICEraq, a total of 78 SPICE occurrences, comprising 6669 individual $\delta^{13}C$ analyses, were included in the statistical evaluation presented here (Table 1-1; Figs. 1-4 to 1-7; Section 2.1). The remaining 17 sections comprise the SWEETS group (Figs. 2-1 & 2-2; Section 2.2), which as described previously do not unequivocally show the excursion and are thus excluded from all results presented herein. Individual occurrences of stratigraphic sections/cores are referred to hereafter by their entry number in the SPICEraq (Table 1-1; Figs. 1-4 to 1-7). To avoid unnecessary repetition of lengthy figure captions, please refer to Table 1-2 for details pertaining to Figures 1-4 to 1-7. These entries are from 40 unique stratigraphic sections and 25 unique drill cores, 12 of which have been sampled by more than one study. Importantly, sections with repeated analyses from more than one study were included in evaluation of the SPICEraq because they presented additional, rather than repeated, data. The following sections are represented by more than one entry in the SPICEraq: Felix Cove, Canada (entries #3 [Barili et al., 2018] and #30 [Saltzman et al., 2004]); House Range, United States (entries #2 [Baker, 2010], #24 [Saltzman et al., 1995], and #28 [Saltzman et al., 1998]); Shingle Pass, United States (entries #1 [Baker, 2010] and #27 [Saltzman et al., 1998]); TE-1 core, United States (entries #9 [Gill et al., 2011] and #37 [Schiffbauer et al., 2017]); Duibian A, China (entries #48 [Li et al., 2018b] and #64 [Zuo et al., 2018]); Kulyumbe, Siberia (entries #46 and #47 [Kouchinsky et al., 2008]); Kyrshabakty, Kazakhstan (entries #56 [Saltzman et al., 2000] and #61 [Wotte & Strauss, 2015]); Wa'ergang, China (entries #50 [Li et al., 2018b] and #55 [Saltzman et al., 2000]); Wangcun, China (entries #63 [Zhu et al., 2004] and #65 [Zuo et al., 2018]); Wanliangyu, China (entries #44 [Chen et al., 2011] and #60 [Wang et al., 2020]); Alice 1 core, Australia (entries

#69 [Schmid, 2017] and #71 [Schmid et al., 2018]); and East Johnny's Creek 1 core, Australia (entries #70 [Schmid, 2017] and #75 [Schmid et al., 2018]).

All studied sections were located between paleolatitudes of 30°N and 60°S, ca. 500 Ma, with the majority located from 0 to 30°S. Collection sites are located in 10 modern countries, sorted by number of included localities: United States (n = 35), China (n = 16), Australia (n = 13), Canada (n = 4), Kazakhstan (n = 2), Siberia (n = 2), South Korea (n = 2), Argentina (n = 2), France (n = 1), and Scotland (n = 1). These localities represent four paleocontinents—Gondwana, Kazakhstania, Laurentia, and Siberia—although all but four of the sections were located on either Laurentia or Gondwana. Shallow/nearshore (n = 28) and intrashelf basin (n = 21) facies are the most abundant categories, although the majority of these sections are from intermediate water depths (n = 37). Deeper-water environments are represented mostly by slope facies (n = 10), with rarer basin facies (n = 3) (Table 1-3).

Figure 1-4. Carbon isotope data for all SPICEraq entries designated herein as "short" sections/drill cores, i.e., <70 m in total thickness. For details on interpreting this figure, see Table 1-2.

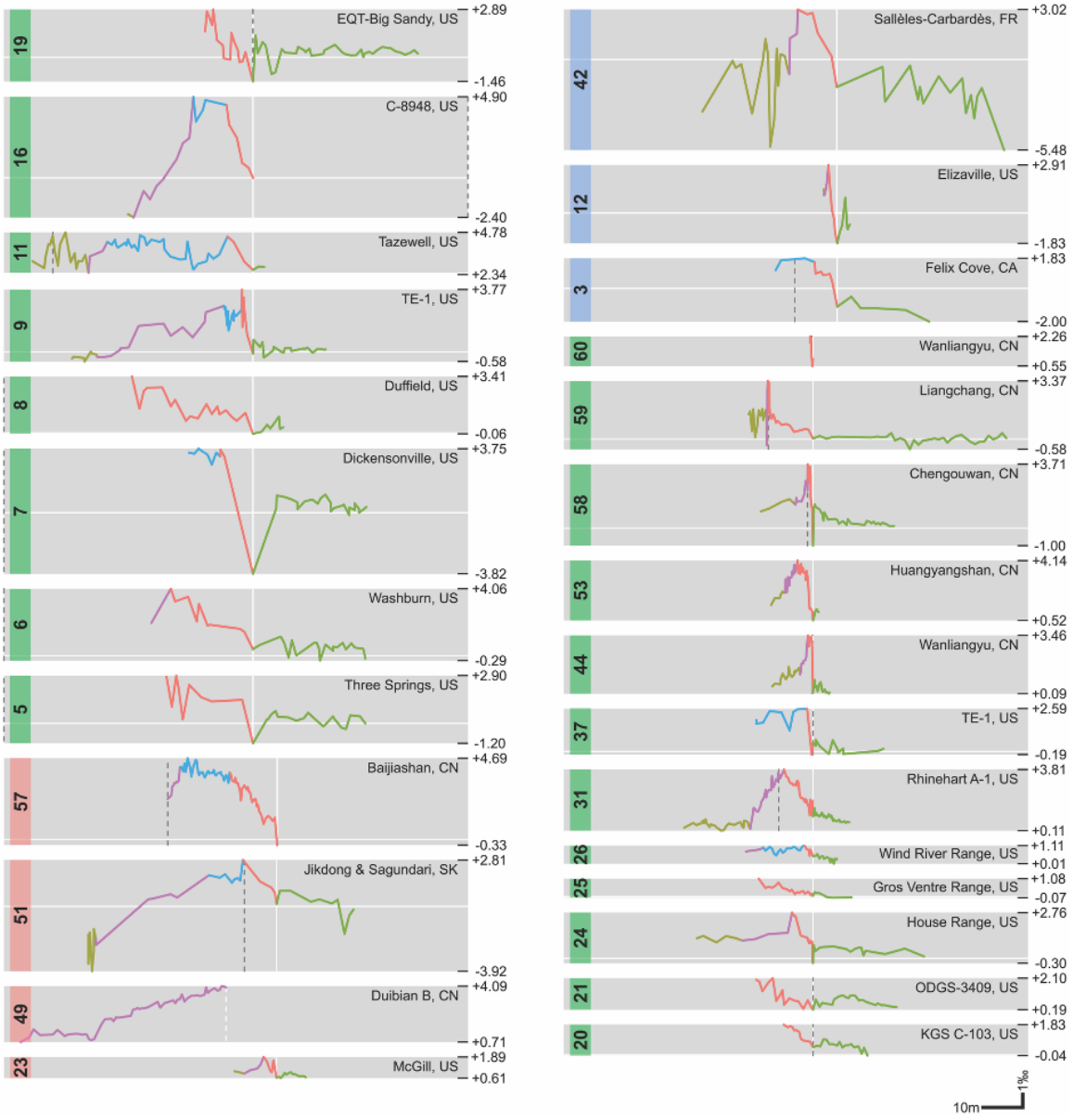
19
EQT-Big Sandy, US
+2.89
-1.46
16
C-8948, US
+4.90
-2.40
11
Tazewell, US
+4.78
+2.34
9
TE-1, US
+3.77
-0.58
8
Duffield, US
+3.41
-0.06
7
Dickensonville, US
+3.75
-3.82
6
Washburn, US
+4.06
-0.29
5
Three Springs, US
+2.90
-1.20
57
Baijiashan, CN
+4.69
-0.33
51
Jikdong & Sagundari, SK
+2.81
-3.92
49
Duibian B, CN
+4.09
+0.71
23
McGill, US
+1.89
+0.61
42
Sallèles-Carbardès, FR
+3.02
-5.48
12
Elizaville, US
+2.91
-1.83
3
Felix Cove, CA
+1.83
-2.00
60
Wanliangyu, CN
+2.26
+0.55
59
Liangchang, CN
+3.37
-0.58
58
Chengouwan, CN
+3.71
-1.00
53
Huangyangshan, CN
+4.14
+0.52
44
Wanliangyu, CN
+3.46
+0.09
37
TE-1, US
+2.59
-0.19
31
Rhinehart A-1, US
+3.81
+0.11
26
Wind River Range, US
+1.11
+0.01
25
Gros Ventre Range, US
+1.08
-0.07
24
House Range, US
+2.76
-0.30
21
ODGS-3409, US
+2.10
+0.19
20
KGS C-103, US
+1.83
-0.04
1‰
10m

Figure 1-5. Carbon isotope data for all SPICEraq entries designated herein as "intermediate" sections/drill cores, i.e., ≥70 and <200 m in total thickness. For details on interpreting this figure, see Table 1-2.

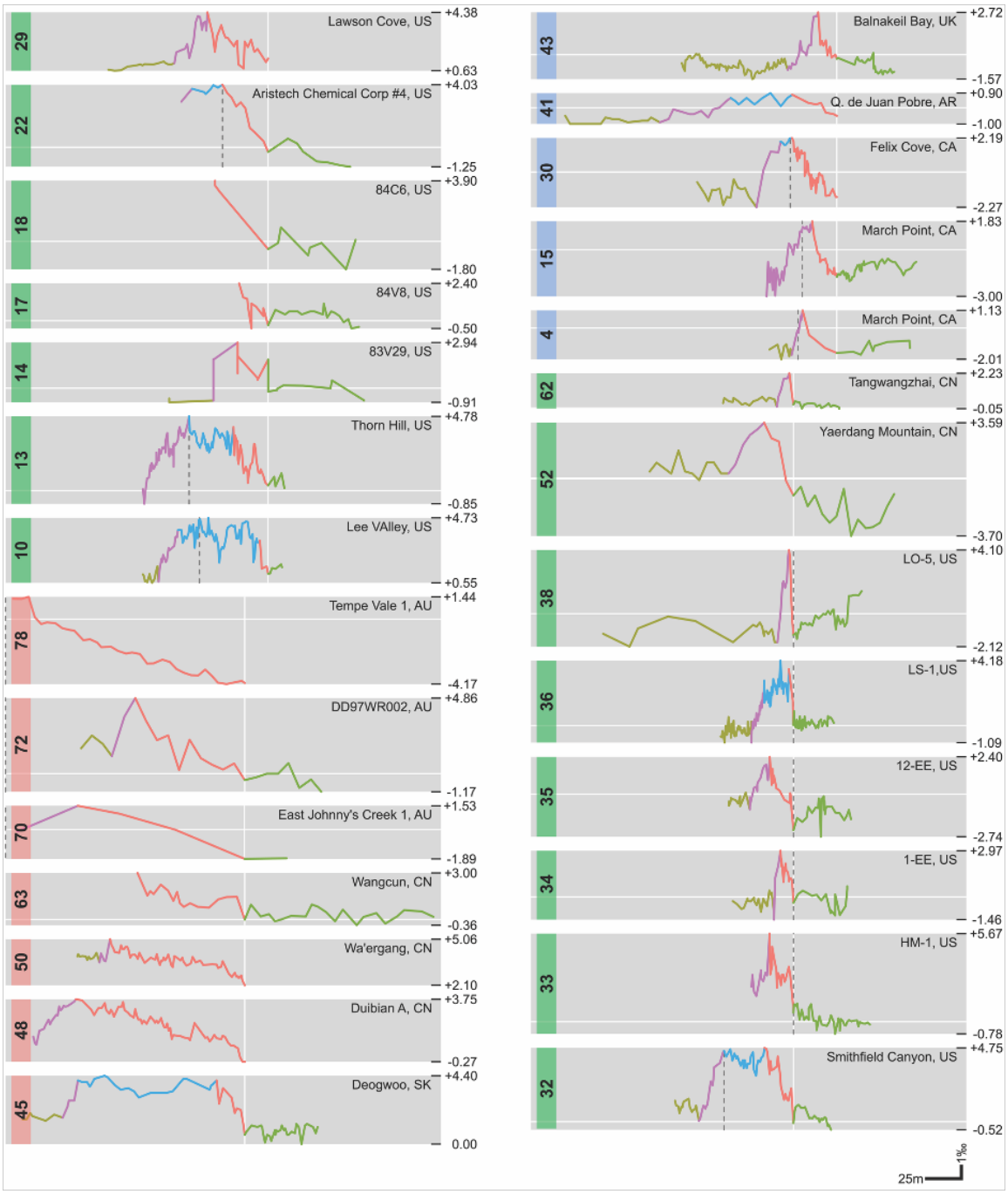
29
Lawson Cove, US
+4.38
+0.63
22
Aristech Chemical Corp #4, US
+4.03
-1.25
18
84C6, US
+3.90
-1.80
17
84V8, US
+2.40
-0.50
14
83V29, US
+2.94
-0.91
13
Thorn Hill, US
+4.78
-0.85
10
Lee VAlley, US
+4.73
+0.55
78
Tempe Vale 1, AU
+1.44
-4.17
72
DD97WR002, AU
+4.86
-1.17
70
East Johnny's Creek 1, AU
+1.53
-1.89
63
Wangcun, CN
+3.00
-0.36
50
Wa'ergang, CN
+5.06
+2.10
48
Duibian A, CN
+3.75
-0.27
45
Deogwoo, SK
+4.40
0.00
43
Balnakeil Bay, UK
+2.72
-1.57
41
Q. de Juan Pobre, AR
+0.90
-1.00
30
Felix Cove, CA
+2.19
-2.27
15
March Point, CA
+1.83
-3.00
4
March Point, CA
+1.13
-2.01
62
Tangwangzhai, CN
+2.23
-0.05
52
Yaerdang Mountain, CN
+3.59
-3.70
38
LO-5, US
+4.10
-2.12
36
LS-1,US
+4.18
-1.09
35
12-EE, US
+2.40
-2.74
34
1-EE, US
+2.97
-1.46
33
HM-1, US
+5.67
-0.78
32
Smithfield Canyon, US
+4.75
-0.52
1‰
25m

Figure 1-6. Carbon isotope data for all SPICEraq entries designated herein as "long" sections/drill cores, i.e., ≥200 and <700 m in total thickness. For details on interpreting this figure, see Table 1-2.

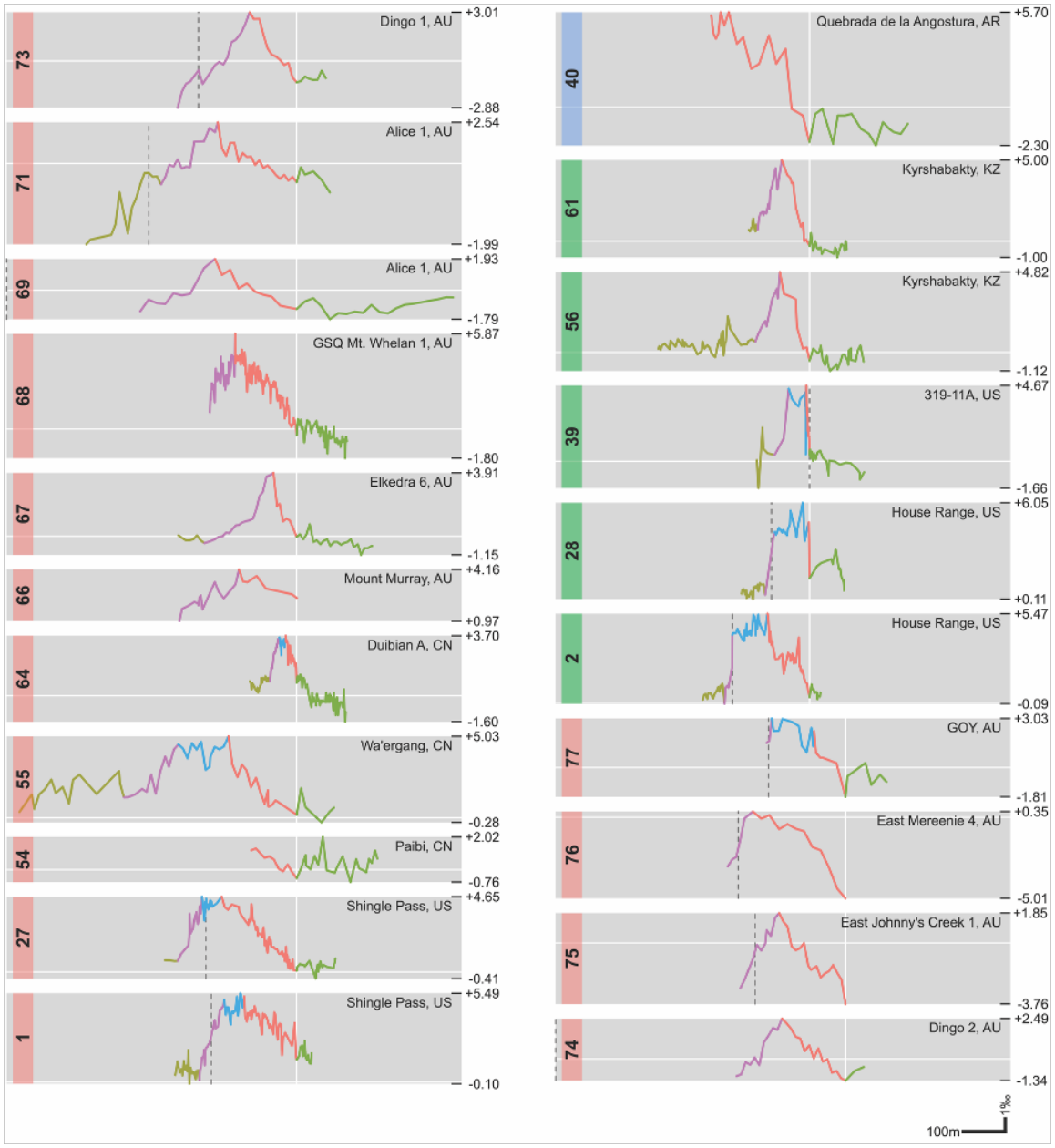
73
Dingo 1, AU
+3.01
-2.88
71
Alice 1, AU
+2.54
-1.99
69
Alice 1, AU
+1.93
-1.79
68
GSQ Mt. Whelan 1, AU
+5.87
-1.80
67
Elkedra 6, AU
+3.91
-1.15
66
Mount Murray, AU
+4.16
+0.97
64
Duibian A, CN
+3.70
-1.60
55
Wa'ergang, CN
+5.03
-0.28
54
Paibi, CN
+2.02
-0.76
27
Shingle Pass, US
+4.65
-0.41
1
Shingle Pass, US
+5.49
-0.10
40
Quebrada de la Angostura, AR
+5.70
-2.30
61
Kyrshabakty, KZ
+5.00
-1.00
56
Kyrshabakty, KZ
+4.82
-1.12
39
319-11A, US
+4.67
-1.66
28
House Range, US
+6.05
+0.11
2
House Range, US
+5.47
-0.09
77
GOY, AU
+3.03
-1.81
76
East Mereenie 4, AU
+0.35
-5.01
75
East Johnny's Creek 1, AU
+1.85
-3.76
74
Dingo 2, AU
+2.49
-1.34
1‰
100m

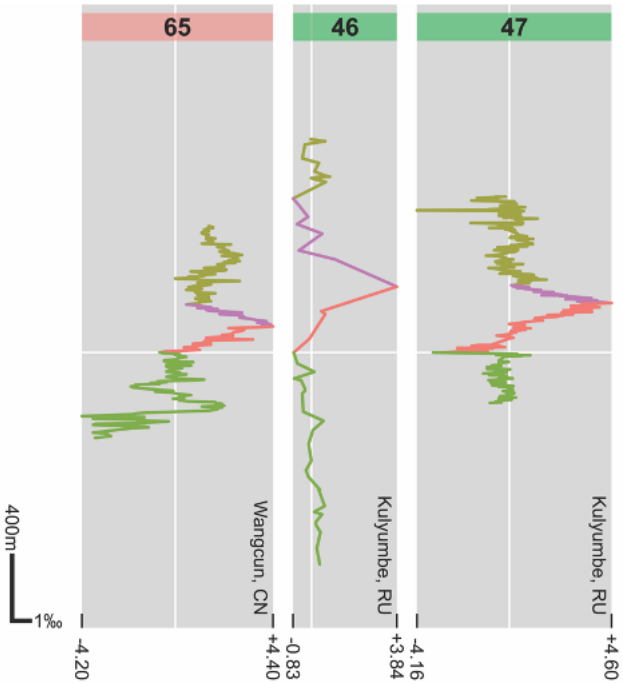

Figure 1-7. Carbon isotope data for all SPICEraq entries designated herein as "super long" sections/drill cores, i.e., ≥700 m in total thickness. For details on interpreting this figure, see Table 1-2.

TABLE 1-2.

KEY DETAILS FOR INTERPRETING FIGURES 1-4 THROUGH 1-7 & 2-2

Entries are grouped according to total length (in meters) of the section (based on natural breaks in the data), excluding samples omitted from the pre- and post-SPICE zones for analytical purposes:

- Short (x<70 m; Fig. 1-4)
- Intermediate (70≤x<200 m; Fig. 1-5)
- Long (200≤x<700 m; Fig. 1-6)
- Super long (x≥700 m; Fig. 1-7)
- Y-axis scale (stratigraphic thickness) is maintained within each figure (except in Fig. 2-2, where thickness groupings are labeled)

Within each plot:

- Section entry numbers, corresponding to the SPICEraq, are noted at the top of each plot
- Section name/location is included at lower-end of each plot
  - Locations abbreviated as follows:
    - US = United States
    - CA = Canada
    - AR = Argentina
    - FR = France
    - SK = South Korea
    - CN = China
    - KZ = Kazakhstan
    - AU = Australia
    - RU = Russia
    - SE = Sweden (only used in Fig. 2-2)
- X-axis scale ($\delta^{13}C$ ‰ V-PDB) is identical for all plots
- Grey boxes demarcate the range of $\delta^{13}C$ values in each entry, with the minimum and maximum values denoted at the bottom of each plot
- Vertical white lines within the grey boxes indicate the position of 0‰ if it falls within the plotted range
- Entries are aligned on the minimum $\delta^{13}C$ value of the rising limb (the onset of the excursion), the position of which is denoted by the horizontal white line within the grey boxes
  - Note that the position of entry #49 in Figure 1-4 relative to others in this figure is only approximate; data from this section lie entirely within the falling limb
- The Sauk II–Sauk III boundary is denoted by a black dashed horizontal line if its position relative to the plotted $\delta^{13}C$ data was provided in the original publication (regardless of paleocontinent)

Sections are categorically grouped by paleolatitude, with color-coded entry number label flags to match paleolatitude groupings in other figures within both Chapter 1 and Chapter 2:

- 0–30° N = red
- 0–30° S = green
- 30–60° S = blue

Carbon isotope data is color-coded according to SPICE zone, matching those used in Figure 1-1a

- Pre-SPICE = green
- Rising limb = red
- Plateau [if present] = blue
- Falling Limb = purple
- Post-SPICE = olive

TABLE 1-3.

DISTRIBUTION OF DATA ACROSS SPICE ZONES

Grouping variables	Grouping categories	Total entries (#)	Number of SPICE zones				
			Pre	Rising	Plateau	Falling	Post
Paleolatitude	0–30° N	27	19	26	8	24	12
	0–30° S	42	39	42	14	31	26
	30–60° S	9	7	9	3	7	6
Paleocontinent	Gondwana	34	24	33	7	29	17
	Kazakhstania	2	2	2	0	2	2
	Laurentia	40	37	40	18	29	23
	Siberia	2	2	2	0	2	2
Depth	Shallow	28	21	28	4	23	13
	Intermediate	37	34	37	18	28	23
	Deep	13	10	12	3	11	8
Facies	Shallow/nearshore	28	21	28	4	23	13
	Shelf	16	15	16	9	14	11
	Intrashelf basin	21	19	21	9	14	12
	Slope	10	7	9	2	8	6
	Basin	3	3	3	1	3	2
Total		78	65	77	25	62	44
Lithology	"Carbonate"	25	—	—	—	—	—
	Limestone	38	—	—	—	—	—
	Dolostone	14	—	—	—	—	—
	Total	77	—	—	—	—	—

Distribution of entire entries, as well as individual SPICE zones across the categorical variables of interest to this study: paleolatitude, paleocontinent, water depth, facies, and lithology. Lithologic categories were not applied to entire SPICE zones.

1.3.2.1 General $\delta^{13}C$ data summary

The $\delta^{13}C$ values, stratigraphic thicknesses, and regional/local conditions of each entry are summarized in Table 1-1. The background median $\delta^{13}C$ values prior to the onset of the SPICE range from -2.29 to +2.69‰ (entries #52 [Yaerdang Mountain, China; Liu et al., 2017] and #11 [Tazewell, Tennessee, US; Glumac, 2011], respectively). The maximum values of the rising limb, and thus the peak $\delta^{13}C$ value of the SPICE event, range from +0.35 to +5.87‰

(entries #76 [East Mereenie 4, Australia; Schmid et al., 2018] and #68 [Mt. Whelan, Australia; Saltzman et al., 2000], respectively). The magnitude of the excursion ranges from 0.64 to 8.03‰ (entries #26 [Wind River Range, Wyoming, US; Saltzman et al., 1995] and #47 [Kulyumbe, Russia; Kouchinsky et al., 2008], respectively). After the peak, $\delta^{13}C$ returns to lower values, stabilizing at a median post-SPICE background between -2.30 and +3.95‰ (entries #16 [C-8948, Illinois, US; Labotka & Freiburg, 2020] and #50 [Wa'ergang, China; Li et al., 2018b], respectively).

1.3.2.2 Stratigraphic thickness

The stratigraphic thickness of SPICE zones varies widely. Rising limb zones are between < 1 and 378 m thick (entries #60 [Wanliangyu, China; Wang et al., 2020] and #46 [Kulyumbe, Russia; Kouchinsky et al., 2008], respectively) and falling limb zones are between <1 and 506 m thick (entries #59 [Liangchang, China; Wang et al., 2020] and #46, respectively). If present, the plateau can be up to 110 m thick (entry #55 [Wa'ergang, China; Saltzman et al., 2000]). The stratigraphic thickness of the entire SPICE interval (Rising limb + Plateau + Falling limb) ranges from 2.85 m (Wanliangyu, China; Chen et al., 2011) to 884 m (Kulyumbe, Russia; Kouchinsky et al., 2008).

Scatter plots (Figs. 1-8 & 2-4) show stratigraphic thicknesses relative to the peak magnitude of the SPICE event in an attempt to visualize sediment accumulation by the various groupings. These types of data visualizations are organized by thickness of only the rising limb (Fig. 1-8) and then also as the thickness of the full excursion (Fig. 2-4), in order to differentiate any potential stratigraphic biases from the presence or absence of a plateau. While rising limb thickness does not necessarily correlate directly with overall excursion thickness at the entry

level, many of the same overall trends are present when viewed by various groupings. That is, the groups with statistically significant differences (by Wilcoxon rank sum tests) in rising limb thicknesses are also the groups that have statistically significant differences in total SPICE interval thicknesses (Table 2-2).

When stratigraphic thickness data are grouped by paleolatitude (Figs. 1-8a & 2-4a; Table 2-2a), the points, minus three apparent outliers (entries #40 [Quebrada de La Angostura, Argentina; Sial et al., 2008], #46, and #47), form two clusters of stratigraphically thinner sections located in the southern hemisphere (Laurentia), and thicker sections located in the northern hemisphere (Gondwana). That the Laurentian sections are thinner than those in Gondwana is statistically significant (Table 2-2b). The Kazakhstanian sections, limited to two in number (entries #56 and #61), plot within the cluster for 0–30°S for both total and rising limb thicknesses (Figs. 1-8a–b & 2-4a–b). The Siberian sections are outliers (entries #46 and #47), bearing the thickest rising limbs over all, and being the only sections with rising limbs thicker than 100 m to have been deposited in the southern hemisphere (Figs 1-8a–b & 2-4a–b). Entry #46 also records the thickest total SPICE interval, which is at least 500 m greater than any other section (Fig. 2-4b).

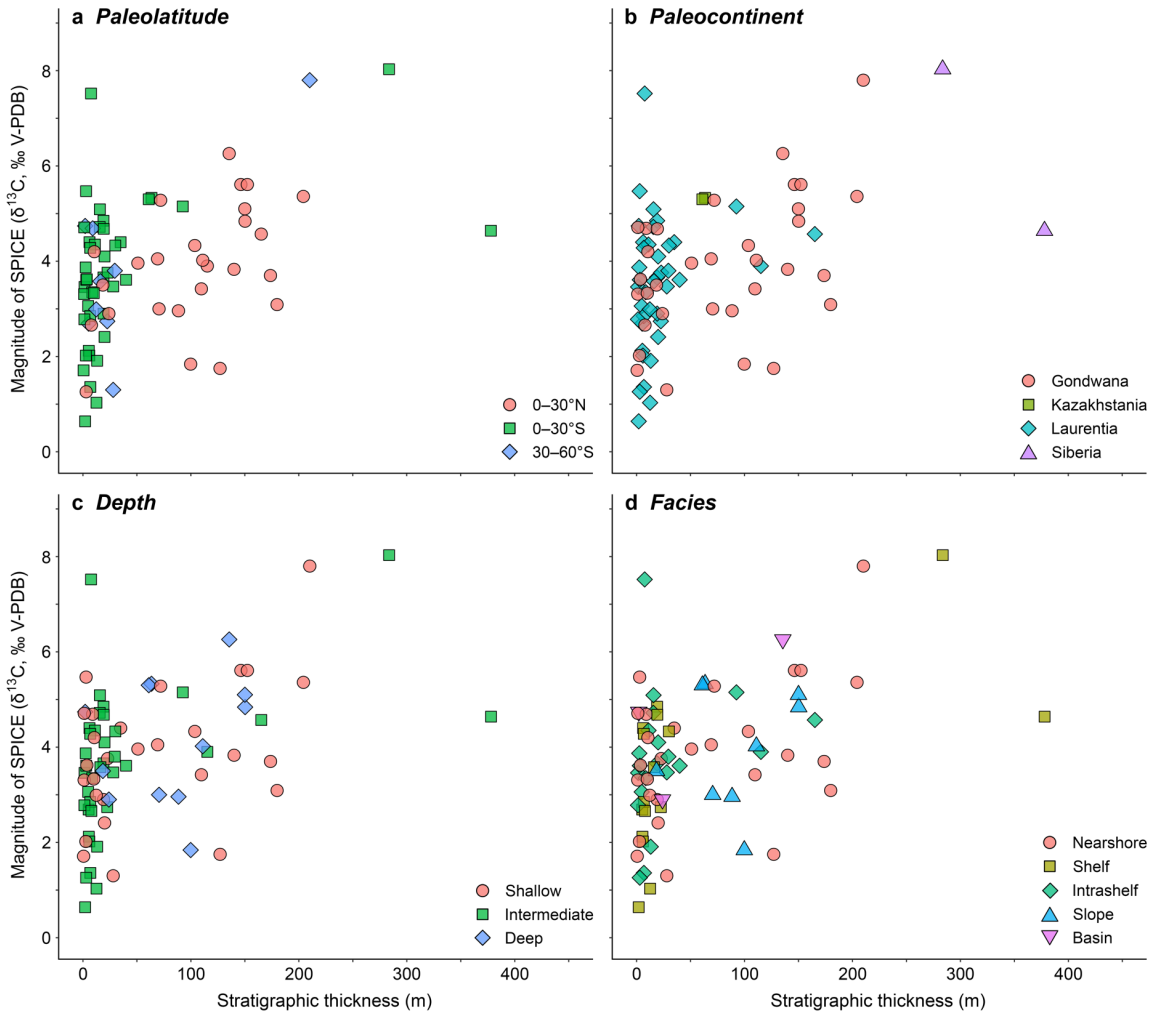

Figure 1-8. Stratigraphic thickness of the rising limb of the SPICE. Scatter plots comparing the magnitude of the SPICE event (the difference between the maximum and minimum $\delta^{13}C$ values of the rising limb) to the stratigraphic thickness (in meters) of the rising limb of the excursion. Together, these variables serve as a proxy for the rate of onset of the SPICE event. Entries are labelled according to the following grouping variables: (a) paleolatitudinal zone; (b) paleocontinent; (c) water-depth; (d) facies.

There is significant overlap between groups when the sections are classified by water depth or facies (Figs. 1-8c–d & 2-4c–d). Intermediate water depths and facies tend to have stratigraphically thin total SPICE intervals and rising limbs (Figs. 1-8c & 2-4c). With the exception of the two notable Siberian outliers (entries #46 and #47), shelf facies display the

narrowest range of stratigraphic thicknesses, with total SPICE intervals <100 m thick and rising limbs <50 m thick (Figs. 1-8d & 2-4d). Similarly, the majority of sections from intrashelf basin facies also have rising limbs <50 m thick and total SPICE intervals <100 m thick, with the exception of three outliers (entries #1 [Baker, 2010], #2 [Baker, 2010], and #27 [Saltzman et al., 1998]; all of which were deposited in the House Range Embayment within the Great Basin region of Laurentia). All but one of the slope sections (#45 [Deogwoo, South Korea; Chung et al., 2011]) plot between 50 and 150 m of stratigraphic thickness in the rising limb. While sections from intermediate water depths and the corresponding facies have significantly shorter rising limbs and total SPICE intervals than sections deposited in slope settings, no further patterns are otherwise apparent across depth and facies groupings (Table 2-2c–d).

Supplementing the patterns observable in the scatter plots, box and whisker plots shown in supplemental Figures 2-5 and 2-6 highlight the similarities in the distribution of total excursion and rising limb thicknesses, respectively, across the grouping variables. Visually, the patterns in the equivalent figure panels are nearly identical, although the precise positions of median values and interquartile ranges may have shifted. The box and whisker plots further illustrate that the broader groups with stratigraphically thin rising limbs also tend to have stratigraphically thin total SPICE intervals (Figs. 2-5 & 2-6).

1.3.2.3 Statistical evaluation of the presence of a plateau

Twenty-five of the 78 (32%) total sections exhibit a plateau in elevated $\delta^{13}C$ values between the rising and falling limbs. We used χ^2 tests to evaluate the null hypothesis that there is no association between the presence of a plateau in individual SPICE entries and the

grouping variables evaluated in this study. For all grouping variables, the resultant *p*-values for the χ^2 distributions are >0.1 (Table 1-4), and thus we failed to reject our null hypothesis.

TABLE 1-4.

χ^2 TEST RESULTS

Grouping variables	Grouping categories	Plateau observed	Plateau expected	χ^2 test results
Paleolatitude	0–30° N	8	8.15	$\chi^2 = 0.005$ df = 3 $p = 0.99$
	0–30° S	14	13.92	
	30–60° S	3	2.93	
	Total	25	25	
Paleocontinent	Gondwana	7	10.07	$\chi^2 = 2.24$ df = 3 $p = 0.13$
	Kazakhstania	0	0.73	
	Laurentia	18	13.46	
	Siberia	0	0.73	
	Total	25	25	
Depth	Shallow	4	8.15	$\chi^2 = 4.47$ df = 2 $p = 0.11$
	Intermediate	18	12.82	
	Deep	3	4.03	
	Total	25	25	
Facies	Shallow/nearshore	4	8.15	$\chi^2 = 4.64$ df = 4 $p = 0.33$
	Shelf	9	5.95	
	Intrashelf basin	9	6.87	
	Slope	2	2.93	
	Basin	1	1.10	
	Total	25	25	

Results for χ^2 tests evaluating the distribution of plateaus among grouping variables

1.3.2.4 Distribution and variation of SPICE zones and $\delta^{13}C$ values

Joy plots (or ridgeline plots; stacked density plots) illustrate changes in $\delta^{13}C$ values through the progression of the SPICE across the categorical variables. In the case of paleolatitude, the sections in the 30–60°S zone have $\delta^{13}C$ values approximately 1 to 2‰ lower

than those from more equatorial regions (Fig. 1-9a). The differences between 30–60°S and 0–30°S sections are statistically significant in all cases, whereas the differences between 30–60°S and 0–30°N sections are only marginally significant for all cases except the maximum $\delta^{13}C$ value of the SPICE (Table 2-3a). 0–30°N and 0–30°S sections have similar distributions; only the pre-SPICE median $\delta^{13}C$ value is marginally significant (Fig. 1-9a; Table 2-3a). Randomization results indicate that the true difference in median peak $\delta^{13}C$ values for higher latitude (30–60° S) sections relative to the combined median peak $\delta^{13}C$ value of tropical (0–30° N and 0–30° S) sections is statistically significant (Section 2.4; Fig. 2-7). Siberian and Kazakhstanian sections are omitted from the paleocontinent joy plot (Fig. 1-9b) because each has only two sections, rendering density plots impractical as tools for analysis or visualization. The overall shape of the distributions for Gondwanan and Laurentian sections are quite similar (Fig. 1-9b), except in the case of the pre-SPICE median $\delta^{13}C$ values, in which Laurentian sections have a more pronounced peak about the median value, and a longer right tail. Figure 1-9b confirms that the pre-SPICE median $\delta^{13}C$ is significantly higher in Laurentia than in Gondwana; whereas the post-SPICE median $\delta^{13}C$ is marginally higher in Gondwana than in Laurentia (Table 2-3b), as is described in more detail below in Section 1.3.2.5. Most other differences in $\delta^{13}C$ values between paleocontinents have no statistical significance (Table 2-3b).

Figure 1-9. $\delta^{13}C$ values before, during, and after the SPICE event. From bottom to top the individual joy plot panels show the distribution in $\delta^{13}C$ values for the median pre-SPICE background, the minimum of the rising limb (the onset of the SPICE event), the maximum of the rising limb (the peak of the SPICE event), and the median post-SPICE background. The vertical black line within each curve denotes the median value of that distribution. In (a), sections are grouped according to paleolatitude; in (b), sections are grouped according to paleocontinent.

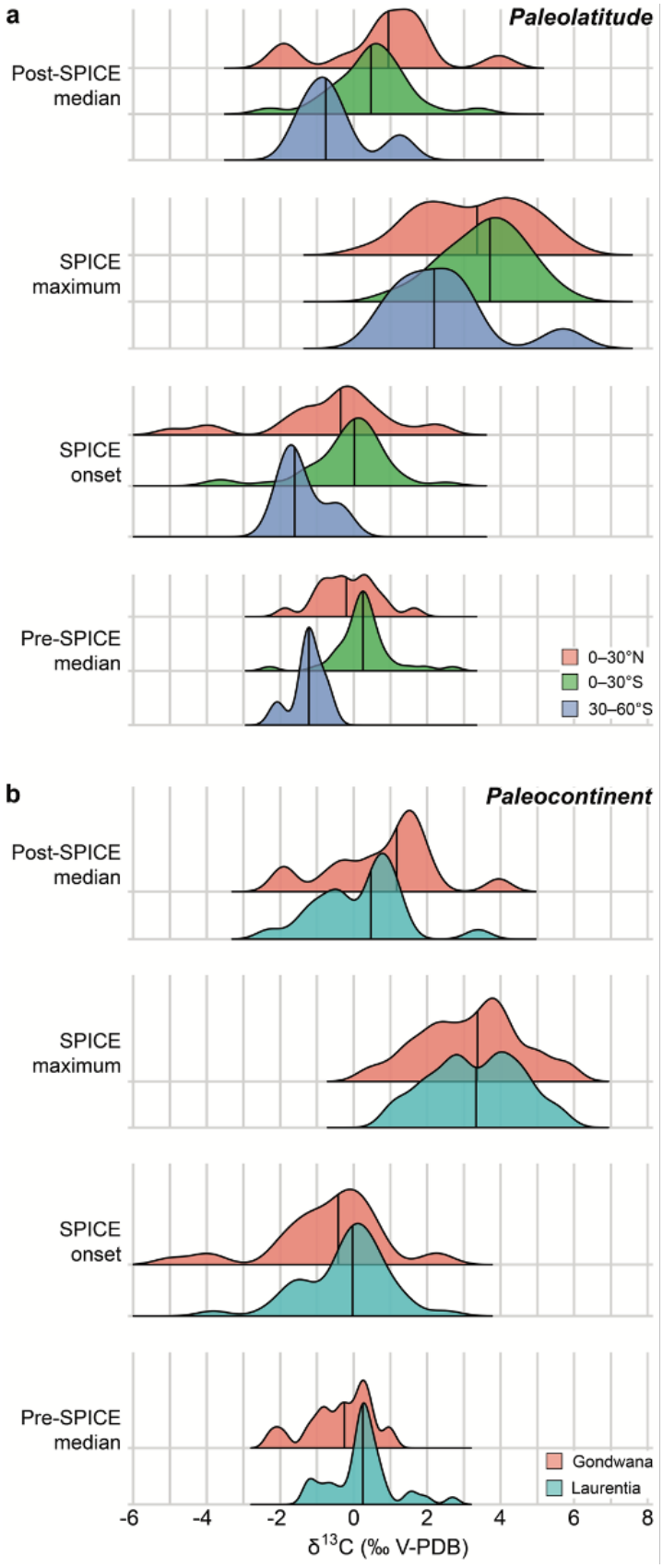
a
Paleolatitude
Post-SPICE median
SPICE maximum
SPICE onset
Pre-SPICE median
0–30°N
0–30°S
30–60°S
b
Paleocontinent
Post-SPICE median
SPICE maximum
SPICE onset
Pre-SPICE median
Gondwana
Laurentia
-6
-4
-2
0
2
4
6
8
δ13C (‰ V-PDB)

Depth and facies joy plots show that, generally, the minimum and median $\delta^{13}C$ values for the peak of the SPICE and the median of the post-SPICE background decrease with decreasing water depth (Fig. 1-10a). This trend is less obvious when sections are grouped according to facies (Fig. 1-10b) rather than water depth. For the pre-SPICE median and rising limb minimum, the higher $\delta^{13}C$ values are found in intermediate depth (specifically intrashelf basin facies) sections, whereas shallow and deep-water sections have a nearly identical median value (Fig. 1-10; Table 2-3c). In contrast, the peak value of the SPICE excursion, and the median of the post-SPICE zone are highest in the deep-water (specifically slope facies) sections. (Fig. 1-10; Table 2-3d).

Figure 1-10. $\delta^{13}C$ values before, during, and after the SPICE event. From bottom to top the individual joy plot panels show the distribution in $\delta^{13}C$ values for the median pre-SPICE background, the minimum of the rising limb (the onset of the SPICE event), the maximum of the rising limb (the peak of the SPICE event), and the median post-SPICE background. The vertical black line within each curve denotes the median value of that distribution. In (a), sections are grouped according to water depth; in (b), sections are grouped according to facies.

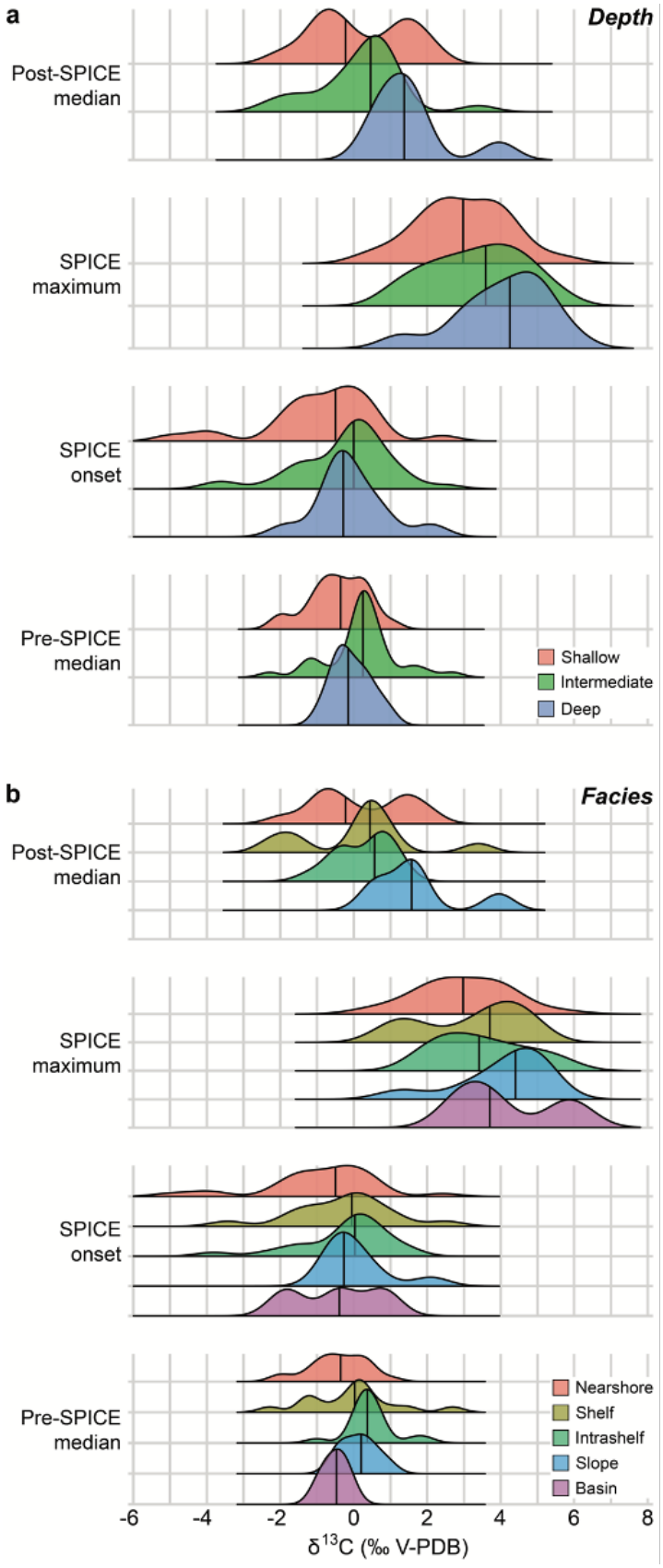
a
Depth
Post-SPICE median
SPICE maximum
SPICE onset
Pre-SPICE median
Shallow
Intermediate
Deep
b
Facies
Post-SPICE median
SPICE maximum
SPICE onset
Pre-SPICE median
Nearshore
Shelf
Intrashelf
Slope
Basin
-6
-4
-2
0
2
4
6
8
δ13C (‰ V-PDB)

Box and whisker plots illustrate the magnitude of the $\delta^{13}C$ excursion captured by the rising limb of the SPICE event (as the difference between the peak and onset $\delta^{13}C$ values). The interquartile ranges and median values for the southern hemisphere are nearly identical, with no statistically significant differences (Fig. 1-11a; Table 2-3a). High magnitude $\delta^{13}C$ excursions of ~8‰ are limited to sections from the southern hemisphere. Laurentian and Gondwanan sections have nearly identical interquartile ranges and similar overall ranges (Fig. 1-11b; Table 2-3b). Kazakhstanian and Siberian sections are included in Figure 1-11b, although little can be said about their distributions relative to other paleocontinents due to conspicuously uneven sampling, except for the fact that both paleocontinents plot toward the higher end of the observed range. These high-magnitude $\delta^{13}C$ excursions of ~8‰ are limited to shallow and intermediate depths, and thus shallow/nearshore, shelf, and intrashelf basin facies (Fig. 1-11c–d). The interquartile range and median magnitude of shelf sections are both skewed more toward lower $\delta^{13}C$ values than for any other facies (Fig. 1-11d). Slope and shelf settings have the widest interquartile ranges, whereas intrashelf basins have the narrowest range (Fig. 1-11d). For intermediate and deep-water facies, minimum and median $\delta^{13}C$ magnitudes increase with water depth, with the highest minimum and median values found in basinal facies (Fig. 1-11c–d). Shallow/nearshore sections are exceptions to this trend, and are shifted more toward higher $\delta^{13}C$ values relative to the sections deposited in shelf settings. (Fig. 1-11d). Note, however, that there are no statistically significant differences between these distributions of magnitudes (Table 2-3c–d).

Figure 1-11. Magnitude of the $\delta^{13}C$ excursion. Box and whisker plots illustrate the magnitude of the $\delta^{13}C$ excursion captured by the rising limb of the SPICE (maximum $\delta^{13}C$ value of the rising limb minus the minimum $\delta^{13}C$ value of the rising limb). Black dots show the magnitude for individual entries. The colored boxes show the interquartile range (IQR = Q3-Q1) of the distribution, with the center black line indicating the median value. Solid line whiskers extend beyond the box by a factor of 1.5 * IQR, where the upper whisker = min(max(x), Q3 + 1.5 * IQR) and the lower whisker = max(min(x), Q1 - 1.5 * IQR). Dashed line whiskers extend to the absolute minimum or maximum of the distribution, if necessary. Entries are labelled according to the following grouping variables: (a) paleolatitudinal zone; (b) paleocontinent; (c) water-depth; (d) facies.

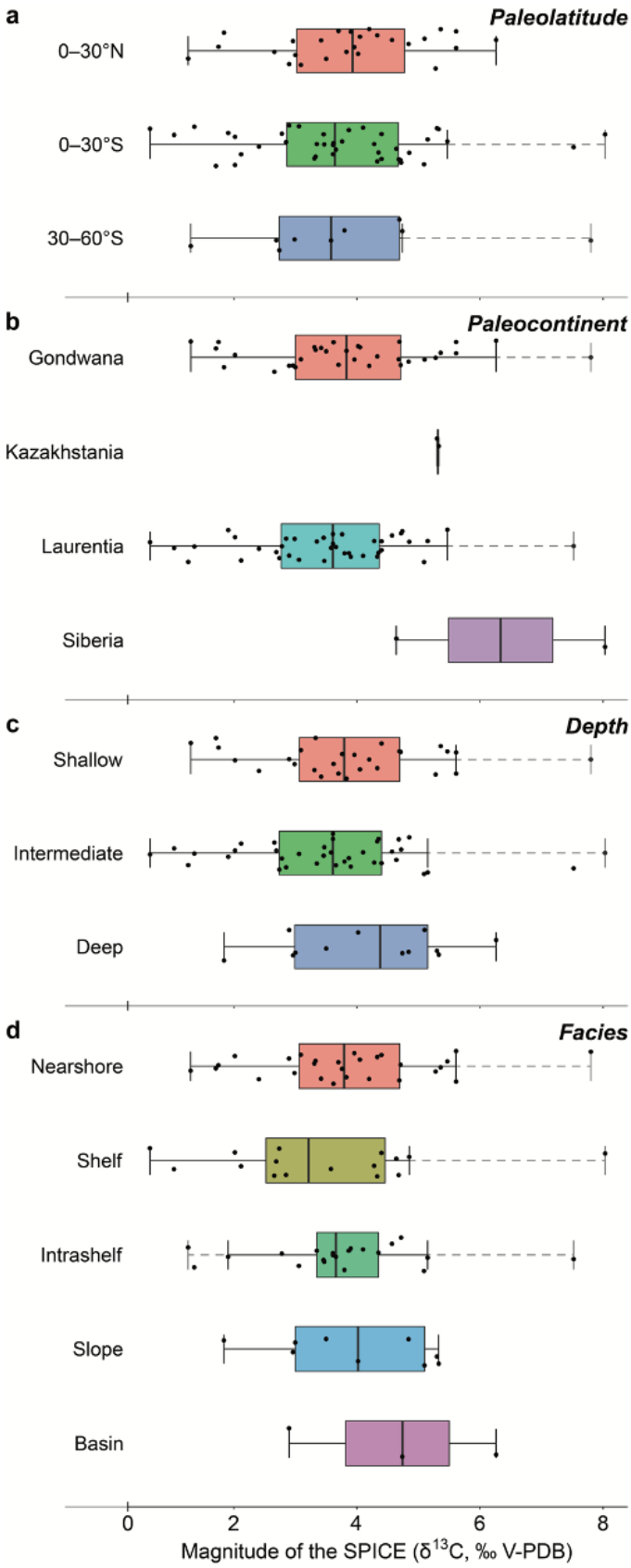
a
Paleolatitude
0–30°N
0–30°S
30–60°S
b
Paleocontinent
Gondwana
Kazakhstania
Laurentia
Siberia
c
Depth
Shallow
Intermediate
Deep
d
Facies
Nearshore
Shelf
Intrashelf
Slope
Basin
0
2
4
6
8
Magnitude of the SPICE (δ13C, ‰ V-PDB)

1.3.2.5 Trends at the SPICE onset, and pre- to post-SPICE $\delta^{13}C$ shifts

In all cases, comparison of the $\delta^{13}C$ value of the onset of the rising limb to the median $\delta^{13}C$ value of the pre-SPICE zone in Figures 1-9 and 1-10 shows a shift in the left tail of the distribution toward lower values. Forty-eight of the 78 total sections (62%) included in this repository have minimum rising limb $\delta^{13}C$ values that are lower than the median $\delta^{13}C$ value of the pre-SPICE background. Twelve of the sections in the SPICEraq do not sample any of the pre-SPICE zone, which means that a median background $\delta^{13}C$ value can only be calculated for 65 of the sections. Taking this into consideration, 74% of the sections with a recorded pre-SPICE zone display a small negative excursion immediately prior to the onset of the SPICE event (Perfetta et al., 1999). This "negative kick" has an average magnitude of 0.62‰, and a maximum magnitude of 4.19‰ (Table 1-1). Depending on which grouping variable is used, the negative-most onset $\delta^{13}C$ values of the SPICE are found in the 0–30°N zone; in Gondwana; and in shallow/nearshore settings (Figs. 1-9 & 1-10; Table 2-3). For further investigation of trends in rising limb, pre-, and post-SPICE data, see also data visualization in Figs. 2-8–2-10.

1.3.2.6 Lithology

Figure 1-12 illustrates the distribution of maximum rising limb $\delta^{13}C$ values for those samples that could be identified as either limestone or dolostone. Samples limited to "carbonate" (n = 25) for their lithologic description were excluded from this figure for visualization purposes. Results from the Wilcoxon rank sum tests are presented in Table 2-4. Limestone samples record marginally significantly higher peak-SPICE $\delta^{13}C$ values (median = +3.76‰; n = 38) relative to dolostone samples (median = +2.69‰; n = 14).

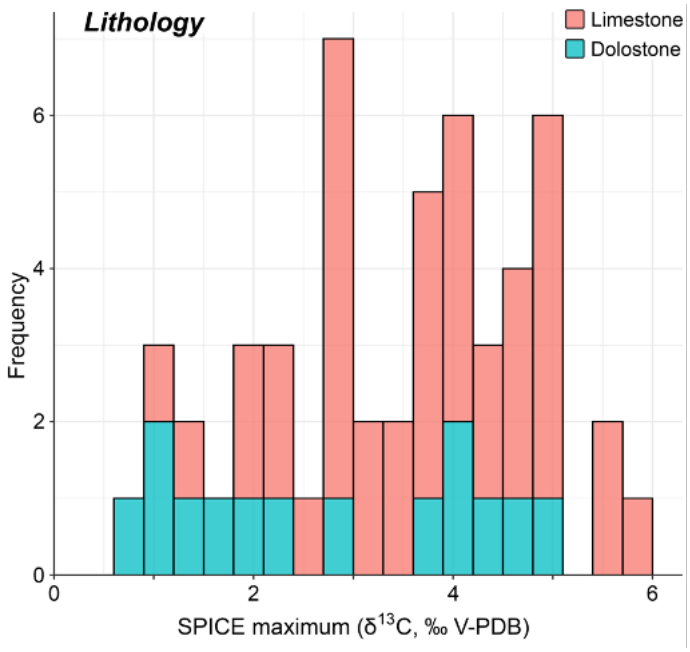

Figure 1-12. Influence of lithology on $\delta^{13}C$ values. This histogram illustrates the distribution of individual maximum $\delta^{13}C$ values for the rising limb of the SPICE, color-coded by lithology. Samples belonging to the "carbonates" group have been excluded from this figure for visualization purposes. Bin-width = 0.3‰, with hard upper boundary.

1.4 Discussion

1.4.1 Synopsis of the SPICE and potential causes

The SPICE is the most prominent positive carbon isotope excursion in the late Cambrian (Saltzman & Thomas, 2012). It has been hypothesized to be the result of such driving forces as: increased atmospheric oxygenation (Saltzman et al., 2011); higher rates of biological productivity (Saltzman et al., 1998; 2000); global cooling (Glumac & Walker, 1998; Saltzman et al., 1998); enhanced coastal upwelling (Saltzman et al., 2000); eustatic sea level change (Glumac & Walker, 1998; Saltzman et al., 2000; 2004); and an expansion of carbonate platforms (Álvaro et al., 2008). Most commonly, however, the SPICE event is attributed to:

(1) an increased rate of burial of organic carbon (Glumac & Walker, 1998; Saltzman et al., 1998; Álvaro et al., 2008; Gill et al., 2011); (2) anoxic/euxinic conditions (Saltzman et al., 1998; 2000; Gill et al., 2011; Dahl et al., 2014; Bond & Grasby, 2017; LeRoy & Gill, 2019; Pruss et al., 2019); and/or (3) an increased rate of continental weathering associated with the sea level lowstand between the Sauk II and Sauk III megasequences (Glumac & Walker, 1998; Saltzman et al., 2000; Harper et al., 2019). In addition, anoxia and/or euxinia are commonly cited as the specific driver of the trilobite biomere turnover event associated with the SPICE, and it is therefore appealing to also assign this change in seawater chemistry as the source of the SPICE event itself. Documentation of correlative positive $\delta^{34}S$ excursions in SPICE sections from the United States (Gill et al., 2007; 2011; Saltzman et al., 2011; LeRoy and Gill, 2019), Newfoundland (Hurtgen et al., 2009), Sweden (Gill et al., 2011), Kazakhstan (Wotte & Strauss, 2015), China (Saltzman et al., 2011), and Australia (Gill et al., 2011) may provide supporting evidence for anoxia and euxinia. Our methodology was specifically chosen in order to conduct a comprehensive analysis of the publication history of the SPICE event over the last 2+ decades and evaluate the potential significance of regional/local controls on the expression of the purportedly global signature of the SPICE in the rock record.

The SPICE is often depicted as an asymmetric excursion, with the rising limb noticeably thicker stratigraphically than the falling limb (see fig. 1 in Glumac, 2011; fig. 1 in Elrick et al., 2011; and fig. 1 in Gerhardt & Gill, 2016), which does reflect the shapes of some SPICE excursions (e.g., entries #1, #4 [March Point, Canada; Barili et al., 2018], and #27). However, the stratigraphic expression of the SPICE is quite variable and does not typically display that geometry (Figs. 1-4 to 1-7). For example, in some sections, the excursion is recorded as a sharp rising limb and much thicker falling limb (e.g., entries #9 [TE-1, United States; Gill et al., 2011] and #15 [March Point, Canada; Hurtgen et al., 2009]). Through the

compilation conducted herein, however, we can observe that the SPICE has a more symmetrical appearance, with the rising and falling limbs covering comparable stratigraphic thicknesses (e.g., entries #31 [Rhinehart A-1, United States; Saltzman et al., 2004] and #32 [Smithfield Canyon, United States; Saltzman et al., 2004]). Perhaps more importantly, the SPICE interval varies widely in stratigraphic thickness, from <3 m in the Wanliangyu section, China (Chen et al., 2011) to >800 m in the Kulyumbe section, Siberia (Kouchinsky et al., 2008).

Our meta-analysis additionally demonstrates that the magnitude and peak values of the SPICE event are more variable than previously described. Following the classic account by Saltzman et al. (1998), the SPICE has typically been described as a positive $\delta^{13}C$ shift, ~4 to 5‰ in magnitude. However, we illustrate through the SPICEraq data compilation that, in fact, the magnitudes of the excursion range from 0.64 to 8.03‰ (median = 3.76‰), while the peak SPICE $\delta^{13}C$ values range from +0.35 to +5.87‰ (median = +3.46‰). This should not necessarily be unexpected, as the amount of research on SPICE-hosting sections has increased dramatically since Saltzman et al.'s (1998) report—hence the motivation for this study. Despite the fact that the same general pattern can be seen in all sections that document the SPICE, the expression of the excursion in distinct sections appears fundamentally different in terms of the $\delta^{13}C$ pattern and the stratigraphic thickness of the event. For example, see SPICEraq entries #9 (Missouri, US; Gill et al., 2011; short section with thin rising limb and plateau and a drawn-out falling limb), #43 (Balnakeil Bay, Scotland; Pruss et al., 2019; intermediate section with rising and falling limbs of similar thickness and a prolonged plateau), and #59 (Liangcheng, China; Wang et al., 2020; super-long section with relatively symmetric rising and falling limbs and no plateau; Figs. 1-4 to 1-7).

1.4.2 Interpretation of results

1.4.2.1 Plateaus

Although 32% of the entries included in the SPICEraq display a plateau, defined as persistently high $\delta^{13}C$ values for 5 meters or more of section (e.g., entry #28 [House Range, Utah, US; Saltzman et al., 1998]), χ^2 tests revealed that there is no significant association between the presence of a plateau in the SPICE record and any of the categorical variables investigated. Eighteen of the 25 plateau-bearing sections were deposited in intermediate water depths, indicating that shelf and intrashelf basin settings are the most likely to record a plateau, perhaps as a result of the combination of sediment supply and accommodation space (Schlager, 1993). However, 18 of 25 recorded plateaus are in sections from Laurentia, whereas the other 7 are in Gondwana, which may indicate higher sedimentation accumulation in Laurentia ca. 500 Ma. Contrary to this, the prevalence of stratigraphically thinner total excursions and rising limbs for Laurentian entries relative to those of Gondwana appears to suggest that, of the two paleocontinents, Laurentia may have been more sediment-starved during the onset of the SPICE (Figs. 1-8 & 2-4). An alternative explanation to this phenomenon is that Laurentia may have been more tectonically quiescent than Gondwana at this time, and therefore would not have generated much new accommodation space, independent of sediment supply and delivery.

The uneven distribution of $\delta^{13}C$ plateaus across Laurentia and Gondwana could be a product of the relationship between the SPICE event and the Sauk II–Sauk III transition. The peak of the SPICE has been described as correlating with the boundary between the Sauk II and Sauk III megasequences (Saltzman et al., 1998; 2004; Glumac & Mutti, 2007; Glumac, 2011). This would suggest that the rising limb of the SPICE was deposited during the tail end

of a major regressive event, while the falling limb was deposited early during a transgression. However, Schiffbauer et al. (2017) suggested that the rising limb of the SPICE, at least in Missouri, United States, instead correlates with the early transgression of the Sauk III megasequence as evidenced by lithostratigraphic relationships in the studied cores. In those cores (entries #33–37), the rising limb of the SPICE is preserved in a package of deeper-water shales deposited atop shallow-shelf carbonates, which requires a deepening at or prior to the onset of the rising limb, rather than at the peak of the SPICE event as others have suggested (e.g., Brasier, 1993; Saltzman et al., 2004; Glumac, 2011). The SPICE in the Franconia Formation (entry #16; Labotka & Freiburg 2020) of the regionally comparable Illinois Basin is preserved entirely within the Sauk III megasequence as also evidenced by stratigraphic relationships. Following a period of sea level fall prior to the onset of the SPICE, LeRoy & Gill (2019) additionally present evidence of sea level rise at the initiation of the positive excursion in the Conasauga Intrashelf Basin (entries #19–21; Appalachians), again in the form of deeper-water shales being deposited over shallower carbonate units. If, as Schiffbauer et al. (2017), Labotka & Freiburg (2020), and LeRoy & Gill (2019) suggest, sea level began to rise (at the beginning of the Sauk III transgression) at or prior to the onset of the rising limb, accommodation space likely would be greater on Laurentia at the time of the SPICE-maximum than on the other paleocontinents. Given that the Sauk megasequence, like all Sloss sequences, is a Laurentia-centric, craton-wide sea level flux package (Sloss, 1963), this could help explain the higher proportion of plateaus (although not statistically significant) in the $\delta^{13}C$ excursions of Laurentian sections. More importantly, it is worth noting that these lithostratigraphic relationships documenting the onset of the SPICE during the Sauk III transgression (Schiffbauer et al., 2017; LeRoy & Gill, 2019; Labotka & Freiburg, 2020) run counter to those of other sections showing the excursion beginning during the Sauk II

regression (Saltzman et al., 1998; 2004; Glumac & Mutti, 2007; Glumac, 2011)—which can be visualized in Figs. 1-4 to 1-7. This could be a product of deposition in regionally restricted intrashelf basinal paleoenvironments where local tectonic activity overrides the broader Laurentian Sauk sequence signal, or alternatively may imply that the excursion is indeed more asynchronous than perhaps previously accounted for (Schiffbauer et al., 2017).

An additional hypothesis also warrants consideration, however. Myrow et al. (2012) investigated the cyclic depositional patterns of Upper Cambrian sections from the Laurentian inner detrital belt. They found that sections in Montana and Wyoming record meter-scale deepening upward packages composed, from bottom to top, of shales, grainstones, flat pebble conglomerates, and thrombolites. These cycles were deposited entirely in subaqueous conditions below fair-weather wave base, within a stable craton; thus, neither tectonic processes nor regional fluctuations in sea level are likely drivers of the observed cyclicity. Rather, Myrow et al. (2012) argue that these cycles are driven by changes in the amount of terrigenous sediment being added to the system as a result of eustatic changes, and the subsequent impact of clastic sediment flux on the carbonate factory. They interpret that the lowermost shale layers were deposited during a regressive period, whereby significant input of siliciclastic material derived from nearby fluvial and shoreline processes caused a reduction in carbonate productivity—and thus are shallow-water shales. As conditions shifted into a transgressive system, siliciclastic input diminished and allowed for the return of carbonate precipitation with increasing quantity and thickness up section, with the uppermost microbial communities developing once waters were devoid of suspended sediment. The topmost beds are sharply capped by the basal shales of the overlying cycle, indicating renewed regression and subsequent suffocation of the carbonate factory (Myrow et al., 2012). Nonetheless, regardless of whether the sections from Schiffbauer et al. (2017), LeRoy & Gill (2019), or

others document regression or transgression, these records of the SPICE event appear to be intimately linked to eustatic sea level fluctuations associated with the Sauk II–Sauk III megasequence boundary, although perhaps in a different manner than previously supposed.

1.4.2.2 Pre-SPICE negative excursion

The Marjumiid-Pterocephaliid extinction event is typically described as corresponding to the onset of the rising limb of the SPICE (e.g., Glumac & Walker, 1998; Saltzman et al., 1998; Saltzman et al., 2000; Peng et al., 2004; Gill et al., 2011). The current study documents that most SPICE occurrences are immediately preceded by a relatively small negative carbon isotope excursion (Table 1-1), contra the assertion by Gerhardt and Gill (2016). Indeed, as observed in Figures 1-9 and 1-10, the negative shift in the left tail of the minimum $\delta^{13}C$ values for the rising limb relative to the median $\delta^{13}C$ values for the pre-SPICE baseline suggests that, although not ubiquitous, there is an observable negative $\delta^{13}C$ "kick" immediately preceding the onset of the SPICE event in perhaps as many as three-quarters of localities (Table 1-1).

First documented by Saltzman et al. (1995) in the House Range section (entry #24) and later identified by Perfetta et al. (1999) in the Black Hills, South Dakota, United States (entries #S5–S7), this short-lived negative excursion has been suggested to be coincident with the *Marjumiid-Pterocephaliid* extinction boundary. In the Black Hills, the magnitude of this negative $\delta^{13}C$ excursion ranged from 0.48‰ to 0.78‰ (increasing magnitude with depth), with a minimum value between -1.10‰ and -0.40‰. Both Saltzman et al. (1995) and Perfetta et al. (1999) ascribed this negative excursion to the influx of cold, deep ^{12}C-enriched waters into the shallower ^{13}C-enriched shelf environments where these sections were deposited—where the trilobite extinction boundary is marked by the replacement of the shallow-shelf fauna of the

Crepicephalus zone by the deeper-water fauna of the *Aphelaspis* zone (Stitt, 1975; Palmer, 1984; Saltzman et al., 1995; Perfetta et al., 1999; Palmer et al., 2012; Schiffbauer et al., 2017). It is plausible that the trilobite extinction event was thus correlative with the negative excursion, rather than the transition to the positive excursion as previously proposed. Nonetheless, because it is short-lived and generally small in magnitude, this negative excursion could easily be missed by coarse sampling intervals, thus giving the appearance that the extinction corresponds to the onset of the rising limb of the SPICE. Furthermore, it is not entirely unexpected that an extinction event should correspond to a negative carbon isotope excursion. In a review of mass extinctions and their causes, Bond & Grasby (2017) document 10 Paleozoic extinction events that co-occur with negative $\delta^{13}C$ excursions with magnitudes ranging from -2 to -7‰, including the end-Permian, end-Triassic, and end-Jurassic extinctions. A biotic crash can lead to a negative $\delta^{13}C$ excursion; reduced biological activity could cause an enrichment of ^{12}C in ocean water, pulling the $\delta^{13}C$ record toward lower values (Saltzman et al., 1995).

One of the important findings by Schiffbauer et al. (2017) was that the record of the SPICE event in Missouri, United States (entries #33–37), is decoupled from trilobite extinction events. Specifically, the onset of the SPICE showed an inconsistent relationship with the *Crepicephalus-Aphelaspis* turnover and the FAD of *Aphelaspis*. This is contrary to claims made by others that pin the onset of the SPICE rising limb at the beginning of the *Pterocephaliid* biomere (e.g., Glumac & Walker, 1998; Saltzman et al., 1998; Saltzman et al., 2000; Peng et al., 2004; Gill et al., 2011; Fig. 1-1). In a recent contribution, Geyer (2019) presents a comprehensive correlation chart of Cambrian series, biozones, and carbon isotope excursions. The biozone correlation for the regions of interest to this study are redrafted in Fig. 1-1b for reference. Importantly, Geyer (2019) shows that the timing of the SPICE event is variable. In

some regions (Australia, Baltica, Laurentia, North China) the SPICE falls near the base of the Paibian. In other regions, however, the SPICE falls more toward the middle to late Paibian (Kazakhstania, Siberia, South China). Albeit a cursory look at chronostratigraphic placement of the SPICE signal, Geyer's (2019) compilation (Fig. 1-1b) further corroborates the work by Schiffbauer et al. (2017) and supports the argument that the SPICE event is time-transgressive.

Nevertheless, it is plausible, if not probable, that the Marjumiid-Pterocephaliid extinction event itself is also geologically asynchronous, leaving neither biological turnover nor the SPICE event applicable for precise global correlation. For example, recent work by Sundberg et al. (2020) and Karlstrom et al. (2020) highlight the asynchronous nature of trilobite extinction events. Refined U-Pb detrital zircon ages presented by Karlstrom et al. (2020) indicate that the extinction of olenellid- and redlichiid-group trilobites, along with the appearance of paradoxidid-group trilobites, did not occur synchronously at the Series 2-Miaolingian boundary as previously assumed (Sundberg et al., 2020). Rather, these events were asynchronous and protracted, with the FAD of paradoxidids (ca. 509 Ma) notably predating the last appearance datum (LAD) of olenellids (ca. 506.5 Ma), the LAD of redlichiids (ca. 506 Ma), and the Series 2-Miaolingian boundary (506 Ma) by approximately 3 m.y. (Karlstrom et al., 2020; Sundberg et al., 2020). While this example is at the Series boundary prior to the SPICE event at the Miaolingian-Furongian transition, it highlights the need for high-resolution investigation of other trilobite extinction events, as they may be equally as likely to have occurred over similarly protracted time scales rather than as globally synchronous events. However, even if these events are not synchronous on the global-scale, resolving whether or not the *Crepicephalus-Aphelaspis* turnover co-varies temporally with the SPICE event will be an important step towards resolving any plausible causal relationship.

1.4.2.3 Paleolatitude and paleocontinent

The most consistent trend in $\delta^{13}C$ data through the SPICE event is observed when sections are grouped by paleolatitude; there are significantly lower $\delta^{13}C$ values for the 30–60°S sections relative to the more tropical sections located between 30° N and 30° S (Figs. 1-9a & 2-7). The correlation between high latitudes and low $\delta^{13}C$ values could be due to lower primary productivity in the temperate and polar regions relative to the tropics (e.g., Westberry et al., 2008). Increased biological activity in the lower latitudes regardless of water depth, and more generally in productive shallow coastal ecosystems, could lead to an enrichment of ^{13}C in the water and thus higher $\delta^{13}C$ values of the carbonates (Knoll et al., 1986; Saltzman et al., 2000). The magnitude of the $\delta^{13}C$ excursion is fairly consistent across paleolatitudinal zones (Fig. 1-11a), although smaller magnitude changes are limited to the lower latitude sections, and the highest magnitude changes are limited to the southern hemisphere (Figs. 1-9a & 1-11a). One may infer that the consistency in excursion magnitudes across all paleolatitude zones indicates a global nature of the SPICE event, but this would be highly complicated from a chronological perspective as evidenced by the varying relationships with the Sauk II-Sauk III megasequences and trilobite biomeres. Instead, we suggest that the underlying geochemical signal may be asynchronous and has been filtered through regional/local conditions. Specifically, the paleolatitudinal gradient appears to have a significant effect on the baseline conditions and thus the minimum and maximum $\delta^{13}C$ values of the rising limb of the SPICE—or effectively, how the SPICE is expressed in the rock record (Table 2-3a).

The trends observed in the stratigraphic thickness of the SPICE across the paleolatitudinal zones (Figs. 1-10, 2-4, & 2-8) are heavily influenced by the geographic position of the paleocontinents (Fig. 1-2) at 500 Ma, as well as their respective amounts of accommodation space and sediment supply. Sections with the stratigraphically thinnest rising

limbs are generally restricted to the Laurentian sections (which is located almost entirely in the southern hemisphere), whereas the stratigraphically thicker sections are restricted generally to Gondwana (which spanned all three paleolatitude zones of interest in this study) and Siberia (which was located dominantly in the 0–30°S zone) (Figs. 1-2, 1-8, & 2-4). This further supports the suggestion that Laurentia as a whole had the least amount of accommodation space and/or the lowest sediment supply during the onset of the SPICE, while Siberia had the greatest.

1.4.2.4 Water depth and facies

Generally, deeper water SPICE sections have higher $\delta^{13}C$ values than shallower water sections, to differing degrees of significance (Figs. 1-10, 1-11, & 2-9; Table 2-3c–d). With the exception of the extreme outliers #46 and #47, shelf sections host the stratigraphically thinnest excursions overall, and capture the smallest magnitude excursions of all the facies groups (Figs. 1-8, 1-11, & 2-4). The minimum magnitudes of the SPICE event show a steady increase with water depth starting with shelf sections, whereas the higher magnitude excursions are limited to shallow and intermediate sections (Fig. 1-11). The negative excursion immediately preceding the onset of the SPICE is most pronounced in shallow/nearshore sections (Fig. 1-10). These results support assertions by Schiffbauer et al. (2017), Li et al. (2018b), and Huang et al. (2019) that the stratigraphic expression of the SPICE is dependent on regional/local depositional conditions.

Kump (1991) established a steady-state equation describing the isotopic composition of carbon in surface vs. deep waters. One of the important fluxes in this equation is the input of riverine carbon derived from continental weathering into the surface ocean carbon

reservoir. Presuming this carbon flux is depleted in ^{13}C in the Cambrian, it would have the potential to cause the shallow marine carbon isotope signature to shift toward lower values relative to the deep ocean reservoir. Some authors (e.g., Saltzman et al., 2004; Chen et al., 2011; Wotte & Strauss, 2015; Wang et al., 2020) document increased continental erosion coeval with the onset of the SPICE excursion, which is interpreted to be the result of sea level change. In some sections, this is based on stratigraphic evidence for subaerial exposure (e.g., Saltzman et al., 2004; Chen et al., 2011; Wang et al., 2020) and thus indicates both deposition in shallower water settings and a period of non-deposition. Wotte & Strauss (2015), however, documented high $^{87}Sr/^{86}Sr$ values in a slope section (entry #61), which suggests an influx of material derived from continental weathering rather than subaerial exposure. In both cases, these lines of evidence document a period of increased continental erosion, which could serve to reduce the $\delta^{13}C$ values of the shallow water sections by adding a weathered carbon component to the reservoir (Kump, 1991; Wotte & Strauss, 2015). However, in order for continental weathering to have an appreciable effect on local dissolved inorganic carbon (DIC), the depositional setting would need to be proximal to riverine input and/or brackish conditions, not in fully marine conditions.

It is not surprising that regional/local conditions could impact the stratigraphic expression of the SPICE event, and this has likely been the case through much of the history of the planet. Modern ocean waters exhibit heterogeneity in their $\delta^{13}C$ values that are influenced by many factors (Knoll et al., 1986; Saltzman & Thomas, 2012). For example, Swart and Eberli (2005) assessed carbon isotope values in a transect of modern sediment cores across the Great Bahamas Bank in water depths ranging from 10 to 650 m. The uppermost portions of the shallowest cores were markedly depleted in ^{13}C, which they attributed to a reduced influence of pelagic carbonate as well as diagenetic alteration of the sediments by meteoric

waters during times of regression and platform exposure. Comparatively, the platform sediments are instead much more enriched in ^{13}C, likely owing to increased photic zone primary productivity. Likewise, Patterson & Walter (1994) documented a 4‰ decrease in $\delta^{13}C$ values in modern carbonate platforms of Florida and the Bahamas relative to open ocean waters, again from the input of ^{13}C-depleted terrestrial waters. They concluded that depositional environment is an important consideration in carbon isotope studies because $\delta^{13}C$ values vary with depth as a result of meteoric influx and evaporation. These modern studies highlight the need for basin-scale lateral investigations in the geologic record in order to more fully appreciate local variability in isotopic signatures.

Other workers have cited early marine diagenesis as the driving force for variation in the geochemical record of carbonates along depth gradients. For example, also from transects across modern carbonate platform and slope environments in the Bahamas, Higgins et al. (2018) document concurrent $\delta^{13}C$, $\delta^{18}O$, $\delta^{44}Ca$, and $\delta^{26}Mg$ data, with the shallowest water sediments enriched in $\delta^{44}Ca$ and depleted in $\delta^{13}C$ values. Similarly, Jones et al. (2020) present $\delta^{13}C$, $\delta^{44}Ca$, and Sr/Ca data from the Hirnantian isotopic carbon excursion (HICE) in the Upper Ordovician that indicate depth-dependence of the recorded $\delta^{13}C$ (showing an increase with increasing depth) and $\delta^{44}Ca$ values (showing a decrease with increasing depth). Both Higgins et al. (2018) and Jones et al. (2020) attribute these results to the variation in the style of early diagenesis that carbonates experience as a result of water depth, depositional environment, and elemental system.

Carbonate diagenesis displays two end-member conditions: fluid-buffered (open diagenesis) or sediment-buffered (closed diagenesis) (Ahm et al., 2018; Higgins et al., 2018; Jones et al., 2020). In fluid-buffered conditions, the chemistry of the diagenetic minerals is controlled by the chemistry of the pore-fluids, which, in carbonate marine environments, is

overwhelmingly dominated by seawater. Other types of fluids may certainly affect shallow marine environments; however, the degree to which these fluids may influence the $\delta^{13}C$ record is likely ultimately dwarfed by the impact that seawater has on fluid-buffered systems on a geologic time scale. In sediment-buffered conditions, the chemistry of the diagenetic minerals is controlled by the chemistry of the primary carbonate minerals. Fluid-buffered conditions dominate in shallow marine environments largely as a result of high rates of fluid flow induced by external processes such a sea-level change (Higgins et al., 2018; Jones et al., 2020). In deeper water environments, where fluid flow-rates are lower, sediment-buffered conditions will prevail (Ahm et al., 2018; Higgins et al., 2018; Jones et al., 2020). Thus, shallow-water carbonates are more likely to record $\delta^{13}C$ similar to ambient seawater values as a result of fluid-buffered diagenetic conditions that force sediment geochemistry toward that of seawater (Higgins et al., 2018; Jones et al., 2020). Because the style of early marine diagenesis that affects carbonate deposits is largely controlled by depositional environment water-depth, eustatic sea-level changes can alter the diagenetic conditions of a particular carbonate deposit. Thus, widespread records of correlative $\delta^{13}C$ excursions may not always indicate global perturbations to the carbon cycle, but instead may record synchronous change in the diagenetic conditions of shallow-water environments driven by eustatic sea-level change (Ahm et al., 2018; Higgins et al., 2018; Jones et al., 2020).

Together, these processes (early marine diagenesis, continental weathering, sea-level change) could help explain the lower $\delta^{13}C$ values identified here in shallow water sections relative to intermediate and deep-water sections. The greatest isotopic variability in the ocean is confined to the surface ocean reservoir where depositional environments, primary productivity, carbonate precipitation, and other local environmental factors will have the most appreciable impact (Kump, 1991).

1.4.2.5 Lithology

Of the 52 peak SPICE samples whose lithology could be identified as either limestone or dolostone, limestone samples had a marginally significantly higher median $\delta^{13}C$ value (Fig. 1-12; Table 2-4). The implications of this evaluation are unfortunately limited by the quantity of samples whose lithology could not be refined further than "carbonate," and thus further work is necessary. Regardless, these results do indicate that the specific carbonate chemistry possibly has an appreciable impact on the $\delta^{13}C$ record, implicating a role for diagenesis in modulating the expression of the SPICE signal, and thus it is important to note the mineralogy of sampled material (i.e., limestone vs. dolostone).

1.4.3 Caveats and assumptions

There are several assumptions associated with the above analyses that need to be mentioned. One important caveat to note is that we are assuming that the stratigraphic sections used in this study are complete, i.e., portions of the rising or falling limbs of the SPICE are not missing due to erosion or any other cause for incompleteness. In a related point, some sections (e.g., entry #3) are missing the falling and/or post-SPICE zones, whereas other sections are missing the pre-SPICE zone (e.g., entry #16). In both instances, the stratigraphic extent and $\delta^{13}C$ magnitude of the rising limb is compromised and it is possible that they are missing the peak SPICE value and/or the minimum $\delta^{13}C$ value signaling the onset of the SPICE event. Likewise, our demarcation of a plateau at a minimum stratigraphic thickness of 5 m is notably arbitrary and potentially biases against condensed sections.

However, in such cases, we may be competing against poor sampling density for appropriate identification of a plateau. That is, if the distance between individual samples is relatively large versus the overall thickness of the excursion, a plateau may be artificially created simply by the spacing of sampling (e.g., by missing the SPICE peak in collected samples). Admittedly, these are limitations of our study. The total quantity of sections analyzed is sufficiently numerous that it is not feasible to ground-truth the stratigraphic completeness of each section nor to provide additional samples should sampling density be a concern. As such, we must assume that each original publication reports, to the best of the authors' ability, a complete and accurate stratigraphic section with accounts of any observed unconformity or other stratigraphic limitation. We cannot exclude the possibility that the low peak-$\delta^{13}C$ values and smaller magnitude shifts identified in some sections could be a result of either incomplete sampling or poor sampling density.

Similarly, the significance of our analyses is also affected by the accuracy and completeness of the biostratigraphic framework provided by the original authors. Some sections (e.g., entries #3, #4, #38 [Outcrop 1, Missouri, US; Jeffrey, 2017], #39 [Outcrop 2, Missouri, US; Jeffrey, 2017]) have little to no biostratigraphic control, either because the units contained few fossils or because original fossil fabrics have been obscured by diagenesis. For the majority of the entries, biostratigraphic control relies upon a framework established by previous authors (e.g., entries #22 [Aristech Chemical Corp. #4, Ohio, US; Mackey & Stewart, 2019], and #33–37). Indeed, few studies included in the SPICEraq described collecting their own fossil samples to build a biostratigraphic framework tied to their isotopic analyses (e.g., entry #32 [Saltzman et al., 2004]). Sections with limited fossil control have dubious age constraints and thus prevent us from using the SPICEraq to further evaluate the apparent time-transgressive nature of the SPICE (Schiffbauer et al., 2017; Geyer, 2019). It is possible

that sections with sparse fossil evidence may not actually be the correct age to capture the SPICE event and may instead be capturing a preceding or succeeding excursion; however, the entries included in the SPICEraq were all identified as the SPICE by the original authors, and we have taken these interpretations at face value. No attempts were made to re-evaluate these interpretations based on the fossil evidence described in the original papers.

Lastly, in order to compare individual sections, it was necessary to simplify some of the categorical description included per entry. The first example of this is the relegation of the paleolatitude classifications to a categorical variable, rather than as a quantitative/numerical variable. This was necessitated because not every publication provides precise location metadata for each section, and thus paleolatitudinal coordinates were sometimes approximated by the nearest identifiable city. Had truly quantitative data been uniformly available, for instance, two-dimensional density plots could have been used to evaluate more accurate paleolatitudinal trends. Because categorical variables were necessitated, we chose 30°-incremental bins in order to capture ample localities per bin as well as approximate modern climate zones in our resulting analyses. A second simplification is that the facies description of each entry was reduced to a single descriptor. Simplified facies categories were based on in-text descriptions for the majority of samples from the rising limb and plateau zones of the $\delta^{13}C$ data and applied to all other samples in that entry. Noteworthy examples of this generalization are sections that capture the Nolichucky and Maynardville formations of the Conasauga Group in the Appalachians, United States (entries #5–8 [Gerhardt & Gill, 2016], #10–13 [Glumac, 2011; Glumac & Mutti, 2007; Glumac & Walker, 1998], and #19-21 [LeRoy & Gill, 2019]). The majority of these sections displays an overall shallowing upward trend from the deep ramp, intrashelf basinal facies of the Nolichucky Formation to the shallow marine, peritidal facies of the upper Maynardville Formation (Markello & Read, 1981; Glumac &

Walker, 1998). We recognize that this oversimplifies the data by possibly obscuring more detailed variation in the depositional environment and/or sea level through the progression of the SPICE, and thus likely underestimates the true variability of the SPICE records.

1.4.4 SWEETS entries

When viewed by paleogeographic location (Fig. 2-2), all SWEETS sections except for one (entry #S13 [Andrarum 3, Sweden; Ahlberg et al., 2009]) are regionally correlative with perhaps less-altered, more savory sections where the SPICE has been positively identified. This may suggest that the absence of an identifiable SPICE signal in the SWEETS sections is not due to a lack of an original excursion in those locations, but rather, several scenarios are plausible: (1) The record of the SPICE was locally masked by diagenetic alteration. (2) The sections are the correct age, but the SPICE event is now absent as a result of a condensed section or erosional activity. Or (3), these sections are not well-constrained biostratigraphically or geochronologically, and thus the portion of the section sampled for $\delta^{13}C$ analysis was not time-equivalent to the SPICE. Previous studies such as Saltzman et al. (1998), Glumac & Spivak-Birndorf (2002), Glumac & Mutti (2007), and Pruss et al. (2016) have come to similar conclusions regarding the absence of the SPICE signal in some sections.

1.4.5 The importance of regional/local conditions on the stratigraphic expression of the carbon isotope record

Ocean circulation patterns are difficult to model for the early Phanerozoic because of the vastly different, and still fairly poorly constrained, tectonic plate configuration relative to the modern (Servais et al., 2014). Regardless of the specific details of ancient upwelling zones

and surface water currents, the amalgamation of landmasses in the southern hemisphere left a vast open ocean in the northern hemisphere. This, along with differences in Earth's prevailing wind patterns, albedo, and ice cover is likely to have had an appreciable effect on circulation (Brenchley et al., 1994; Saltzman et al., 2000; Servais et al., 2014). It is plausible, if not likely, that the geographic record of the SPICE was affected by these patterns; perhaps the latitudinal variation in the minimum and maximum values of the excursions is a result of this. More work is necessary to better model ocean circulation patterns of the late Cambrian in order to confirm this and determine what effects it may have had on the global record of the SPICE.

This study is not the first to suggest that regional/local conditions have had an effect on how the SPICE event is recorded. For example, Barili et al. (2018) seconded the idea by Saltzman et al. (2004) that local conditions served as a driving force for the low-magnitude excursion (~+2‰) documented at Felix Cove, Newfoundland (entries #3 and #30). Both studies argued that regional tectonics created a restricted, marginal marine environment that became more enriched in ^{12}C as compared to other locations globally (Saltzman et al., 2004; Barili et al., 2018). In three sections from South China spanning ~650 km, ranging from upper to lower slope depositional environments, the peak of the SPICE event ranges from +3.7 to +5.1‰ (entries #48–50; Li et al., 2018b); these discrepancies were interpreted as likely due to prolonged ocean stratification as a result of poorly mixed Cambrian seas. Wotte & Strauss (2015) compared a suite of seven SPICE sections from around the globe (entries #9, #15, #27, #29, #61, #66, #68), which included new data they collected as well as previously published data (Saltzman et al., 1998; Saltzman et al., 2000; Gill et al., 2007; Gill et al., 2011), and found that peak $\delta^{13}C$ values ranged from +1.8‰ (entry #15; Newfoundland; Hurtgen et al., 2009) to >+6.0‰ (entry #68; Australia; Saltzman et al., 2000). They similarly concluded that regional conditions led to heterogeneity in the chemical gradients of seawater in the

Furongian, and thus the variable $\delta^{13}C$ records (Wotte & Strauss, 2015). In a case study of five cores (entries #33-37) taken over a paleodepth gradient across ~85 km in southeast Missouri, United States, Schiffbauer et al. (2017) documented that the SPICE event is facies-dependent, time-transgressive, and decoupled from trilobite biotic crises. Thus, the record of the SPICE event displays variation on both local and global scales.

$\delta^{13}C$ is not the only geochemical signal to display regional variation during the time of the SPICE event. Investigations of paleoredox proxies have documented discrepancies in the timing of peak anoxia relative to extinction events and the $\delta^{13}C$ maxima in different sections. Positive $\delta^{34}S$ excursions documented from selected, globally distributed localities exhibit marked variability in both the peak values and the magnitudes of the excursions (Hurtgen et al., 2009; Gill et al., 2011). In the Andrarum-3 drill core from southern Sweden (entry #S13; $\delta^{13}C$ reported in Ahlberg et al., 2009), paleoredox proxies (reported by Gill et al., 2011), including iron speciation ratios and molybdenum concentrations, indicate persistent euxinic conditions during the SPICE, as well as before and after the excursion. The investigation by LeRoy & Gill (2019) of the Conasauga Intrashelf Basin, Appalachians, United States, however, shows more complexity. Iron speciation data document the presence of anoxic conditions in two shallower sections, although conditions change from euxinic (entry #20) to ferruginous (entry #21) with increasing distance offshore. The most distal Conasauga section does not display any evidence for anoxic conditions, either before or during the onset of the SPICE (LeRoy & Gill, 2019). Using mercury as a paleoredox proxy for the Eilean Dubh Formation (entry #43) in Scotland, Pruss et al. (2019) documented that anoxic conditions began to develop during the rising limb of the SPICE but peaked during the falling limb. Uranium isotope excursions can also be utilized to track the development of anoxic and euxinic conditions globally. Samples from the deep-water Mt. Whelan core (entry #68; $\delta^{13}C$ reported

by Saltzman et al., 2000) in Queensland, Australia indicate that peak anoxic and euxinic conditions are correlative with the trilobite extinction event, but precede the return to baseline values in $\delta^{13}C$ and $\delta^{34}S$ proxies (uranium analyses conducted by Dahl et al., 2014).

1.4.6 The utility of the SPICE for global chemostratigraphic correlation

Many workers have used carbon isotope stratigraphy as a method for correlating sections globally through many periods of earth history (e.g., Kaufman et al., 1992; Vahrenkamp, 1996; Ferreri et al., 1997; Saltzman et al., 1998; Saltzman & Thomas, 2012; Voigt et al., 2012). This method of correlation relies on two fundamental assumptions: (1) that stratigraphic variability in $\delta^{13}C$ records is the result of secular change in the global marine DIC reservoir; and (2) that excursions in question are synchronous and the result of widespread/global perturbations to the carbon cycle that are relatively unaffected by regional/local conditions during deposition and subsequent diagenesis such that the main signature can still be identified (Saltzman & Thomas, 2012).

We are not arguing the fact that the SPICE event is globally recorded; that is evident in the global distribution of outcrop and core sections bearing records of the SPICE. This study does document, however, that regional/local conditions have a significant impact on the stratigraphic expression of the SPICE event, and presumably on other carbon isotope excursions as well. The variability in $\delta^{13}C$ records documented in this study suggests that there is the possibility that other records of the SPICE event may have gone unrecognized because they do not fit the typical description of the excursion. Smaller magnitude or shorter stratigraphic records of the SPICE could be misidentified as a different excursion or missed entirely by coarse sampling densities. Similarly, inadequate fossil control and the time-

transgressive nature of the excursion presents the possibility that some identified SPICE sections are not actually representative of the SPICE event. Attempts should be made to give more attention to the context of chemostratigraphic excursions beyond the magnitude of their rising limb. How are the segments of the excursion expressed over stratigraphic thickness? How do lithologic or diagenetic changes in the strata relate to the expression of the excursion? How do excursions from new sampling locations relate to the results of regional/global meta-analyses? Addressing these questions moving forward may allow for a greater understanding of processes leading to the patterns observed and may additionally generate new testable hypotheses as opposed to relying on pattern-matching or biostratigraphy alone.

1.5 Conclusions

In summary, emergent trends are identified from a meta-analysis of 78 globally distributed stratigraphic sections that record the SPICE event.

- Sections deposited between 30 and 60°S paleolatitude have consistently lower $\delta^{13}C$ values throughout the SPICE than those sections deposited in the tropics. This may result from reduced primary productivity and/or colder water temperatures at higher latitudes.
- Shallow water sections tend to have lower $\delta^{13}C$ values than sections from deeper water environments. This trend is likely driven by the differing diagenetic conditions experienced by shallow- and deep-water carbonates and is related to the Sauk II-Sauk III transition.
- Host-rock lithology, i.e., limestone versus dolostone, appears to have an appreciable effect on the recording of $\delta^{13}C$ during the SPICE, implicating a role for diagenesis in

modulating the expression of the SPICE signal. As such, it is important to note the mineralogy of sampled material when measuring and reporting carbon isotopic data.

- Regional/local conditions have a significant impact on the stratigraphic expression of the SPICE event and presumably other carbon isotope excursions.
- There is an identifiable negative $\delta^{13}C$ excursion immediately preceding the onset of the SPICE in the majority of the entries included in the SPICEraq. Thus, this negative excursion may be global in nature; its absence from some sections could be an artifact of sampling density or erosional activity.
- The apparent time-transgressive nature of the SPICE challenges assumptions that it is mediated by a change in the isotopic composition of marine DIC, which would impact all sections synchronously.

[See section 2.8 for corresponding reference list to Chapter 1.]

CHAPTER 2:

SUPPLEMENTARY MATERIALS FOR THE SPICEraq DATA REPOSITORY

2.1 Description of entries in the SPICEraq

Each of the 78 SPICEraq entries has been described below according to the following format (next page) and organized by entry number. Datasets obtained using WebPlot Digitizer (Rohatgi, 2019) have been designated by the qualifier WPD. Entries that had no associated data tables and thus limited our isotopic value vs. stratigraphic height/core depth data collection to WPD extraction from published figures exclusively have been noted (n = 8).

- **Entry #: Location – Type of section (Measured stratigraphic section or core)**
    - Complete reference for the original publication
    - Number of individual analyses and length (m) of complete section as published by the original authors
        - Number of analyses omitted for statistical evaluation in this study (if any)
    - List of SPICE zones present in the section
        - Whether or not the section exhibits a plateau
        - Whether or not the section records the Pre-SPICE negative kick
    - Simplified facies and water depth assigned to the section in this study
        - Reasoning for this designation
        - Lithology designation ("carbonate", limestone, dolostone) for rising limb peak $\delta^{13}C$ sample
    - Paleocontinent and paleolatitude of the section based on the 500 Ma paleogeographic reconstruction in GPlates (Müller et al., 2018).
    - Data collected:
        - Description of where specific data was collected, including figure(s) and table(s) numbers in the original publication
    - Other notes (if applicable)

- **Entry 1: Shingle Pass, Nevada, United States — Measured section**
    - Baker, J.L., 2010. Carbon isotopic fractionation across a late Cambrian carbonate platform: A regional response to the SPICE event as recorded in the Great Basin (MS thesis). University of Nevada, Las Vegas.
    - 121 analyses over 300.0 m
        - No analyses omitted
    - SPICE zones present: Pre, Rising, Falling, Post
        - Exhibits plateau
        - Records pre-SPICE negative kick
    - Deposited in intrashelf basin setting in intermediate water
        - Based on text in sections 2 and 6 and deposition of section within the House Range Embayment
        - "Carbonate"
    - Located on paleocontinent Laurentia from 0–30° N
    - Data collected:
        - Sample numbers, meters, lithologies, and $\delta^{13}C$, $\delta^{18}O$, TOC, and $\delta^{13}C_{org}$ values from Appendix
        - Formations and members from fig. 15
        - Stages from fig. 5
    - A second separate dataset from the Shingle Pass section is presented in Saltzman et al., 1998 (entry #61)

- **Entry 2: House Range, Utah, United States — Measured section**
    - Baker, J.L., 2010. Carbon isotopic fractionation across a late Cambrian carbonate platform: A regional response to the SPICE event as recorded in the Great Basin (MS thesis). University of Nevada, Las Vegas.
    - 132 analyses over 339.0 m
        - Post-SPICE: 24 analyses over 80.0 m omitted
    - SPICE zones present: Pre, Rising, Plateau, Falling, Post
        - Exhibits plateau
        - Does record pre-SPICE negative kick
    - Deposited in intrashelf basin setting in intermediate water
        - Based on text in sections 2 and 6 and deposition of section within the House Range Embayment
        - "Carbonate"
    - Located on paleocontinent Laurentia from 0–30° S
    - Data collected:
        - Sample numbers, meters, lithologies, and $\delta^{13}C$, $\delta^{18}O$, TOC, and $\delta^{13}C_{org}$ values from Appendix
        - Formations and members from fig. 15
        - Stages from fig. 5
    - Two other separate datasets from the House Range section are presented in Saltzman et al., 1995 (entry #24) and Saltzman et al., 1998 (entry #28)

- **Entry 3: Felix Cove, Newfoundland, Canada — Measured section**
    - Barili, R., Neilson, J.E., Brasier, A.T., Goldberg, K., Pastro Bardola, T., De Ros, L.F., Leng, M., 2018. Carbon isotopes, stratigraphy, and environmental change: the Middle–Upper Cambrian Positive Excursion (SPICE) in Port au Port Group, western Newfoundland, Canada. Can. J. Earth Sci. 55, 1209–1222. https://doi.org/10.1139/cjes-2018-0025
    - 16 analyses over 35.5 m
        - No analyses omitted
    - SPICE zones present: Pre, Rising
        - Exhibits plateau
        - Does not record pre-SPICE negative kick
    - Deposited in shelf setting in intermediate water
        - Based on text in "Geologic Setting" section
        - Dolostone
    - Located on paleocontinent Laurentia from 30–60° S
    - Data collected:
        - Meters, lithologies, and $\delta^{13}C$, $\delta^{13}C_{org}$, %C, and $\delta^{18}O$ values, from table 3
        - Formations from fig. 8 via WPD
    - A second separate dataset from the Felix Cove section is presented in Saltzman et al., 2004 (entry #30)

- **Entry 4: March Point, Newfoundland, Canada — Measured section**
    - Barili, R., Neilson, J.E., Brasier, A.T., Goldberg, K., Pastro Bardola, T., De Ros, L.F., Leng, M., 2018. Carbon isotopes, stratigraphy, and environmental change: the Middle–Upper Cambrian Positive Excursion (SPICE) in Port au Port Group, western Newfoundland, Canada. Can. J. Earth Sci. 55, 1209–1222. https://doi.org/10.1139/cjes-2018-0025
    - 41 analyses over 235.3 m
        - Pre-SPICE: 13 analyses over 131.0 m omitted
    - SPICE zones present: Pre, Rising, Falling, Post.
        - Does not exhibit plateau
        - Records pre-SPICE negative kick.
    - Deposited in shelf setting in intermediate water
        - Based on text in "Geologic Setting" section
        - Dolostone
    - Located on paleocontinent Laurentia from 30–60° S
    - Data collected:
        - Meters, lithologies, and $\delta^{13}C$, $\delta^{13}C_{org}$, %C, and $\delta^{18}O$ values, from table 3
        - Formations from fig. 7 via WPD

- **Entry 5: Three Springs, Tennessee, United States — Measured section**
    - Gerhardt, A.M., Gill, B.C., 2016. Elucidating the relationship between the later Cambrian end-Marjuman extinctions and SPICE Event. Palaeogeogr. Palaeoclimatol. Palaeoecol. 461, 362–373. https://doi.org/10.1016/j.palaeo.2016.08.031
    - 32 analyses over 46.0 m
        - No analyses omitted
    - SPICE zones present: Pre, Rising
        - Does not exhibit plateau
        - Records pre-SPICE negative kick
    - Deposited in intrashelf basin setting in intermediate water
        - Based on deposition of section within the Conasauga Intrashelf Basin and description of same section in Gerhardt (2014)
        - "Carbonate"
    - Located on paleocontinent Laurentia from 0–30° S
    - Data collected:
        - Sample numbers, meters, lithologies, and $\delta^{13}C$ and $\delta^{18}O$ values from supplementary online materials
        - Formations and biozones from fig. 7 via WPD

- **Entry 6: Washburn, Tennessee, United States – Measured section**
    - Gerhardt, A.M., Gill, B.C., 2016. Elucidating the relationship between the later Cambrian end-Marjuman extinctions and SPICE Event. Palaeogeogr. Palaeoclimatol. Palaeoecol. 461, 362–373. https://doi.org/10.1016/j.palaeo.2016.08.031
    - 33 analyses over 49.5 m
        - No analyses omitted
    - SPICE zones present: Pre, Rising, Falling
        - Does not exhibit plateau
        - Records Pre-SPICE negative kick
    - Deposited in intrashelf basin setting in intermediate water
        - Based on deposition of section within the Conasauga Intrashelf Basin and description of same section in Gerhardt (2014)
        - "Carbonate"
    - Located on paleocontinent Laurentia from 0–30° S
    - Data collected:
        - Sample numbers, meters, lithologies, and $\delta^{13}C$ and $\delta^{18}O$ values from supplementary online materials
        - Formations and biozones from fig. 7 via WPD

- **Entry 7: Dickensonville, Virginia, United States – Measured section**
    - Gerhardt, A.M., Gill, B.C., 2016. Elucidating the relationship between the later Cambrian end-Marjuman extinctions and SPICE Event. Palaeogeogr. Palaeoclimatol. Palaeoecol. 461, 362–373. https://doi.org/10.1016/j.palaeo.2016.08.031
    - 59 analyses over 67.7 m
        - Pre-SPICE: 24 analyses over 22.4 m omitted
    - SPICE zones present: Pre, Rising
        - Exhibits plateau
        - Records Pre-SPICE negative kick
    - Deposited in intrashelf basin setting in intermediate water
        - Based on deposition of section within the Conasauga Intrashelf Basin and description of same section in Gerhardt (2014)
        - "Carbonate"
    - Located on paleocontinent Laurentia from 0–30° S
    - Data collected:
        - Sample numbers, meters, lithologies, and $\delta^{13}C$ and $\delta^{18}O$ values from supplementary online materials
        - Formations and biozones from fig. 7 via WPD

- **Entry 8: Duffield, Virginia, United States – Measured section**
    - Gerhardt, A.M., Gill, B.C., 2016. Elucidating the relationship between the later Cambrian end-Marjuman extinctions and SPICE Event. Palaeogeogr. Palaeoclimatol. Palaeoecol. 461, 362–373. https://doi.org/10.1016/j.palaeo.2016.08.031
    - 26 analyses over 35.0 m
        - No analyses omitted
    - SPICE zones present: Pre, Rising
        - Does not exhibit plateau
        - Records Pre-SPICE negative kick
    - Deposited in intrashelf basin setting in intermediate water
        - Based on deposition of section within the Conasauga Intrashelf Basin and description of same section in Gerhardt (2014)
        - "Carbonate"
    - Located on paleocontinent Laurentia from 0–30° S
    - Data collected:
        - Sample numbers, meters, lithologies, and $\delta^{13}C$ and $\delta^{18}O$ values from supplementary online materials
        - Formations and biozones from fig. 7 via WPD

- **Entry 9: TE-1, Missouri, United States – Core**
    - Gill, B.C., Lyons, T.W., Young, S.A., Kump, L.R., Knoll, A.H., Saltzman, M.R., 2011. Geochemical evidence for widespread euxinia in the Later Cambrian ocean. Nature 469, 80–83. https://doi.org/10.1038/nature09700
    - 66 analyses over 61.1 m
        - Post-SPICE: 2 analyses over 1.1 m omitted
    - SPICE zones present: Pre, Rising, Falling, Post
        - Exhibits plateau
        - Records Pre-SPICE negative kick
    - Deposited in intrashelf basin setting in intermediate water
        - Based on deposition of section within the Central Missouri Intrashelf Basin
        - Limestone
    - Located on paleocontinent Laurentia from 0–30° S
    - Data collected:
        - Meters, lithologies, formations, biozones, and $\delta^{13}C$ and $\delta^{18}O$ values from supplementary online materials
        - Epochs and Stages from fig. 2 via WPD
    - A second separate dataset from the TE-1 section is presented in Schiffbauer et al., 2017 (entry #37)

- **Entry 10: Lee Valley, Tennessee, United States – Measured section**
    - Glumac, B., 2011. High-resolution stratigraphy and correlation of Cambrian strata using carbon isotopes: an example from the southern Appalachians, USA. Carbonates and Evaporites 26, 287–297. https://doi.org/10.1007/s13146-011-0065-2
    - 96 analyses over 91.4 m
        - No analyses omitted
    - SPICE zones present: Pre, Rising, Falling, Post
        - Exhibits plateau
        - Records Pre-SPICE negative kick
    - Deposited in shelf setting in intermediate water
        - Based on fig. 3 and text in "Depositional Environments" section
        - Limestone
    - Located on paleocontinent Laurentia from 0–30° S
    - Data collected:
        - Meters, $\delta^{13}C$ values, lithologies, formations, and members from figs. 6 & 7 via WPD
        - Biozones and Stages from fig. 5
        - No data tables were provided for this entry in the original publication, neither in the text nor in the supplement. Data collection was limited to that obtained through WPD.

- **Entry 11: Tazewell, Tennessee, United States – Measured section**
    - Glumac, B., 2011. High-resolution stratigraphy and correlation of Cambrian strata using carbon isotopes: an example from the southern Appalachians, USA. Carbonates and Evaporites 26, 287–297. https://doi.org/10.1007/s13146-011-0065-2
    - 58 analyses over 53.6 m
        - No analyses omitted
    - SPICE zones present: Pre, Rising, Falling, Post
        - Exhibits plateau
        - Records Pre-SPICE negative kick
    - Deposited in shelf setting in intermediate water
        - Based on fig. 3 and text in "Depositional Environments" section
        - Limestone
    - Located on paleocontinent Laurentia from 0–30° S
    - Data collected:
        - Meters, $\delta^{13}C$ values, lithologies, formations, and members from figs. 6 & 7 via WPD
        - Biozones and Stages from fig. 5
        - No data tables were provided for this entry in the original publication, neither in the text nor in the supplement. Data collection was limited to that obtained through WPD.

- **Entry 12: Elizaville, New York, United States – Measured section**
    - Glumac, B., Mutti, L.E., 2007. Late Cambrian (Steptoean) sedimentation and responses to sea-level change along the northeastern Laurentian margin: Insights from carbon isotope stratigraphy. Geol. Soc. Am. Bull. 119, 623–636. https://doi.org/10.1130/B25897.1
    - 22 analyses over 17.3 m
        - Post-SPICE: 6 analyses over 1.2 m omitted
    - SPICE zones present: Pre, Rising, Falling, Post
        - Does not exhibit plateau
        - Records Pre-SPICE negative kick
    - Deposited in basin setting in deep water
        - Based on fig. 3 and text in "Conclusions" section
        - Limestone
    - Located on paleocontinent Laurentia from 30–60° S
    - Data collected:
        - Meters, lithologies, and $\delta^{13}C$ and $\delta^{18}O$ values from supplementary online materials
        - Stages from fig. 1

- **Entry 13: Thorn Hill, Tennessee, United States – Measured section**
    - Glumac, B., Walker, K.R., 1998. A Late Cambrian positive carbon-isotope excursion in the Southern Appalachians; relation to biostratigraphy, sequence stratigraphy, environments of deposition, and diagenesis. J. Sediment. Res. 68, 1212–1222. https://doi.org/10.2110/jsr.68.1212
    - 119 analyses over 93.0 m
        - No analyses omitted
    - SPICE zones present: Pre, Rising, Falling
        - Exhibits plateau
        - Does not record Pre-SPICE negative kick
    - Deposited in shallow/nearshore setting in shallow water
        - Based on fig. 1 and text in "Geologic Setting and Depositional Environments" section
        - Limestone
    - Located on paleocontinent Laurentia from 0–30° S
    - Data collected:
        - Meters, lithologies, formations, and $\delta^{13}C$ and $\delta^{18}O$ values from supplementary online materials

- **Entry 14: 83V29, Missouri, United States – Core**
    - He, Z., 1995. Sedimentary facies and variation of stable isotope composition of Upper Cambrian to Lower Ordovician strata in Southern Missouri: Implications for the origin of MVT deposits, and the geochemical and hydrological features of regional ore-forming fluids (PhD dissertation). University of Missouri-Rolla. 124 p.
    - 21 analyses over 128.0 m
        - No analyses omitted
    - SPICE zones present: Pre, Rising, Falling, Post
        - Does not exhibit plateau
        - Does not record Pre-SPICE negative kick
    - Deposited in shallow/nearshore setting in shallow water
        - Based on fig. 3 and deposition of section on the shallow Lebanon Arch
        - Limestone
    - Located on paleocontinent Laurentia from 0–30° S
    - Data collected:
        - Sample numbers, meters, lithologies, formations, and $\delta^{13}C$ and $\delta^{18}O$ values from Appendix
        - No biozone control

- **Entry 15: March Point, Newfoundland, Canada – Measured section**
    - Hurtgen, M.T., Pruss, S.B., Knoll, A.H., 2009. Evaluating the relationship between the carbon and sulfur cycles in the later Cambrian ocean: An example from the Port au Port Group, western Newfoundland, Canada. Earth Planet. Sci. Lett. 281, 288–297. https://doi.org/10.1016/j.epsl.2009.02.033
    - 305 analyses over 279.4 m
        - Pre-SPICE: 199 analyses over 179.4 m omitted
    - SPICE zones present: Pre, Rising, Falling
        - Does not exhibit plateau
        - Records Pre-SPICE negative kick
    - Deposited in shelf setting in intermediate water
        - Based on text in section 3
        - "Carbonate"
    - Located on paleocontinent Laurentia from 30–60° S
    - Data collected:
        - Sample numbers, $\delta^{13}C$ and $\delta^{18}O$ values, formations, and members from supplementary online materials
        - Meters from fig. 2 via WPD

- **Entry 16: C-8948, Illinois, United States – Core**
    - Labotka, D.M., Freiburg, J.T., 2020. Geochemical Preservation of the Steptoean Positive Carbon Isotope Excursion (SPICE) Event in Dolomites of the Furongian Franconia Formation in the Illinois Basin. Illinois State Geol. Surv. Circular 6, 11.
    - 20 analyses over 28.9 m
        - No analyses omitted
    - SPICE zones present: Rising, Falling, Post
        - Exhibits plateau
        - No Pre-SPICE zone sampled to evaluate Pre-SPICE negative kick
    - Deposited in shelf setting in intermediate water
        - Based on text in "Introduction" and "Methods" sections
        - Dolostone
    - Located on paleocontinent Laurentia from 0–30° S
    - Data collected:
        - Sample numbers, meters, $\delta^{13}C$ and $\delta^{18}O$ values from table 1
        - Formations and Stages from fig. 2 via WPD
        - Lithologies from text in "Bulk Isotope Analysis" section

- **Entry 17: 84V8, Missouri, United State – Core**
    - Laudon, P.R., 1992. Dolomite neomorphism and water-rock relationships in the mineralized Bonneterre Dolomite (Cambrian), Southeast Missouri (M.S. thesis). University of Missouri-Rolla. 165 p.
    - 27 analyses over 78.8 m
        - No analyses omitted
    - SPICE zones present: Pre, Rising
        - Does not exhibit plateau
        - Records Pre-SPICE negative kick
    - Deposited in shallow/nearshore setting in shallow water
        - Based on text in section I and fig. 5
        - "Carbonate"
    - Located on paleocontinent Laurentia from 30–60° S
    - Data collected:
        - Meters and $\delta^{13}C$ and $\delta^{18}O$ values from table 2
        - Sample numbers, lithologies, and formations from table 1

- **Entry 18: 84C6, Missouri, United States – Core**
    - Laudon, P.R., 1992. Dolomite neomorphism and water-rock relationships in the mineralized Bonneterre Dolomite (Cambrian), Southeast Missouri (M.S. thesis). University of Missouri-Rolla. 165 p.
    - 11 analyses over 92.4 m
        - No analyses omitted
    - SPICE zones present: Pre, Rising
        - Does not exhibit plateau
        - Records Pre-SPICE negative kick
    - Deposited in shallow/nearshore setting in shallow water
        - Based on text in section I and fig. 5
        - "Carbonate"
    - Located on paleocontinent Laurentia from 30–60° S
    - Data collected:
        - Meters and $\delta^{13}C$ and $\delta^{18}O$ values from table 2
        - Sample numbers, lithologies, and formations from table 1

- **Entry 19: EQT-Big Sandy, Kentucky, United States – Core**
    - LeRoy, M.A., Gill, B.C., 2019. Evidence for the development of local anoxia during the Cambrian SPICE event in eastern North America. Geobiology 17, 381–400. https://doi.org/10.1111/gbi.12334
    - 98 analyses over 112.3 m
        - Pre-SPICE: 43 analyses over 62.3 m omitted
    - SPICE zones present: Pre, Rising
        - Does not exhibit plateau
        - Records Pre-SPICE negative kick
    - Deposited in intrashelf basin setting in intermediate water
        - Based on text in section 2 and deposition of section within the Conasauga Intrashelf Basin
        - Limestone
    - Located on paleocontinent Laurentia from 0–30° S
    - Data collected:
        - Sample numbers, meters, and $\delta^{13}C$ and $\delta^{18}O$ values from supplementary online materials
        - Formations, facies, Series, and Stages from fig. 6 via WPD

- **Entry 20: KGS C-103, Kentucky, United States – Core**
    - LeRoy, M.A., Gill, B.C., 2019. Evidence for the development of local anoxia during the Cambrian SPICE event in eastern North America. Geobiology 17, 381–400. https://doi.org/10.1111/gbi.12334
    - 55 analyses over 39.8 m
        - Pre-SPICE: 27 analyses over 19.8 m omitted
    - SPICE zones present: Pre, Rising
        - Does not exhibit plateau
        - Records Pre-SPICE negative kick
    - Deposited in intrashelf basin setting in intermediate water
        - Based on text in section 2 and deposition of section within the Conasauga Intrashelf Basin
        - Dolostone
    - Located on paleocontinent Laurentia from 0–30° S
    - Data collected:
        - Sample numbers, meters, and $\delta^{13}C$ and $\delta^{18}O$ values from supplementary online materials
        - Formations, facies, Series, and Stages from fig. 4 via WPD

- **Entry 21: ODGS-3409, Ohio, United States – Core**
    - LeRoy, M.A., Gill, B.C., 2019. Evidence for the development of local anoxia during the Cambrian SPICE event in eastern North America. Geobiology 17, 381–400. https://doi.org/10.1111/gbi.12334
    - 39 analyses over 32.4 m
        - No analyses omitted
    - SPICE zones present: Pre, Rising
        - Does not exhibit plateau
        - Records Pre-SPICE negative kick
    - Deposited in intrashelf basin setting in intermediate water
        - Based on text in section 2 and deposition of section within the Conasauga Intrashelf Basin
        - Limestone
    - Located on paleocontinent Laurentia from 0–30° S
    - Data collected:
        - Sample numbers, meters, and $\delta^{13}C$ and $\delta^{18}O$ values from supplementary online materials
        - Formations, facies, Series, and Stages from fig. 5 via WPD

- **Entry 22: Aristech Chemical Corp. #4, Ohio, United States – Core**
    - Mackey, J.E., Stewart, B.W., 2019. Evidence of SPICE-related anoxia on the Laurentian passive margin: Paired $\delta^{13}C$ and trace element chemostratigraphy of the upper Conasauga Group, Central Appalachian Basin. Palaeogeogr. Palaeoclimatol. Palaeoecol. 528, 160–174. https://doi.org/10.1016/j.palaeo.2019.04.018
    - 24 analyses over 111.0 m
        - No analyses omitted
    - SPICE zones present: Pre, Rising, Falling
        - Exhibits plateau
        - Does not record Pre-SPICE negative kick
    - Deposited in shelf setting in intermediate water
        - Based on fig. 2 and text in section 2
        - Dolostone
    - Located on paleocontinent Laurentia from 0–30° S
    - Data collected:
        - Meters and $\delta^{13}C$ and $\delta^{18}O$ values from table 7
        - Lithologies, Stages, biozones, and formations from fig. 8 via WPD

- **Entry 23: McGill, Nevada, United States – Measured section**
    - Saltzman, M.R., Davidson, J.P., Holden, P., Runnegar, B., Lohmann, K.C., 1995. Sea-level-driven changes in ocean chemistry at an Upper Cambrian extinction horizon. Geology 23, 893. https://doi.org/10.1130/0091-7613(1995)023<0893:SLDCIO>2.3.CO;2
    - 27 analyses over 16.5 m
        - No analyses omitted
    - SPICE zones present: Pre, Rising, Falling, Post
        - Does not exhibit plateau
        - Records Pre-SPICE negative kick
    - Deposited in intrashelf basin setting in intermediate water
        - Based on deposition of section within the House Range Embayment
        - Limestone
    - Located on paleocontinent Laurentia from 0–30° N
    - Data collected:
        - Meters, $\delta^{13}C$ and $\delta^{18}O$ values, and lithologies from supplementary online materials
        - Formations and biozones from fig. 3 via WPD

- **Entry 24: House Range, Utah, United States – Measured section**
    - Saltzman, M.R., Davidson, J.P., Holden, P., Runnegar, B., Lohmann, K.C., 1995. Sea-level-driven changes in ocean chemistry at an Upper Cambrian extinction horizon. Geology 23, 893. https://doi.org/10.1130/0091-7613(1995)023<0893:SLDCIO>2.3.CO;2
    - 48 analyses over 52.5 m
        - No analyses omitted
    - SPICE zones present: Pre, Rising, Falling, Post
        - Does not exhibit plateau
        - Records Pre-SPICE negative kick
    - Deposited in intrashelf basin setting in intermediate water
        - Based on deposition of section within the House Range Embayment
        - Limestone
    - Located on paleocontinent Laurentia from 0–30° S
    - Data collected:
        - Meters, $\delta^{13}C$ and $\delta^{18}O$ values, and lithologies from supplementary online materials
        - Biozones from fig. 3 via WPD
    - Two other separate datasets from the House Range section are presented in Baker, 2010 (entry #2) and Saltzman et al., 1998 (entry #28)

- **Entry 25: Gros Ventre Range, Wyoming, United States – Measured section**
    - Saltzman, M.R., Davidson, J.P., Holden, P., Runnegar, B., Lohmann, K.C., 1995. Sea-level-driven changes in ocean chemistry at an Upper Cambrian extinction horizon. Geology 23, 893. https://doi.org/10.1130/0091-7613(1995)023<0893:SLDCIO>2.3.CO;2
    - 30 analyses over 21.4 m
        - No analyses omitted
    - SPICE zones present: Pre, Rising
        - Does not exhibit plateau
        - Does not record Pre-SPICE negative kick
    - Deposited in shelf setting in intermediate water
        - Based on fig. 1
        - Dolostone
    - Located on paleocontinent Laurentia from 0–30° S
    - Data collected:
        - Meters, $\delta^{13}C$ and $\delta^{18}O$ values, and lithologies from supplementary online materials
        - Biozones from fig. 3 via WPD

- **Entry 26: Wind River Range, Wyoming, United States – Measured section**
    - Saltzman, M.R., Davidson, J.P., Holden, P., Runnegar, B., Lohmann, K.C., 1995. Sea-level-driven changes in ocean chemistry at an Upper Cambrian extinction horizon. Geology 23, 893. https://doi.org/10.1130/0091-7613(1995)023<0893:SLDCIO>2.3.CO;2
    - 54 analyses over 21.0 m
        - No analyses omitted
    - SPICE zones present: Pre, Rising, Falling
        - Exhibits plateau
        - Does not record Pre-SPICE negative kick
    - Deposited in shelf setting in intermediate water
        - Based on fig. 1
        - Limestone
    - Located on paleocontinent Laurentia from 0–30° S
    - Data collected:
        - Meters, $\delta^{13}C$ and $\delta^{18}O$ values, and lithologies from supplementary online materials
        - Biozones from fig. 3 via WPD

- **Entry 27: Shingle Pass, Nevada, United States – Measured section**
    - Saltzman, M.R., Runnegar, B., Lohmann, K.C., 1998. Carbon isotope stratigraphy of Upper Cambrian (Steptoean Stage) sequences of the eastern Great Basin: Record of a global oceanographic event. Geol. Soc. Am. Bull. 110, 285–297. https://doi.org/10.1130/0016-7606(1998)110<0285:CISOUC>2.3.CO;2
    - 128 analyses over 375.2 m
        - No analyses omitted
    - SPICE zones present: Pre, Rising, Falling, Post
        - Exhibits plateau
        - Records Pre-SPICE negative kick
    - Deposited in intrashelf basin setting in intermediate water
        - Based on text in "Geologic Background" section and deposition of section within the House Range Embayment
        - Limestone
    - Located on paleocontinent Laurentia from 0–30° N
    - Data collected:
        - Meters and $\delta^{13}C$ and $\delta^{18}O$ values from supplementary online materials
        - Formations and biozones from fig. 2 via WPD
        - Facies from fig. 3 via WPD
    - A second separate dataset from the Shingle Pass section is presented in Baker, 2010 (entry #1)

- **Entry 28: House Range, Utah, United States – Measured section**
    - Saltzman, M.R., Runnegar, B., Lohmann, K.C., 1998. Carbon isotope stratigraphy of Upper Cambrian (Steptoean Stage) sequences of the eastern Great Basin: Record of a global oceanographic event. Geol. Soc. Am. Bull. 110, 285–297. https://doi.org/10.1130/0016-7606(1998)110<0285:CISOUC>2.3.CO;2
    - 92 analyses over 253.5 m
        - Post-SPICE: 33 analyses over 27.3 meters omitted
    - SPICE zones present: Pre, Rising, Falling, Post
        - Exhibits plateau
        - Records Pre-SPICE negative kick
    - Deposited in intrashelf basin setting in intermediate water
        - Based on text in "Geologic Background" section and deposition of section within the House Range Embayment
        - Limestone
    - Located on paleocontinent Laurentia from 0–30° S
    - Data collected:
        - Meters and $\delta^{13}C$ and $\delta^{18}O$ values from table 1
        - Formations and biozones from fig. 2 via WPD
        - Facies from fig. 3 via WPD
    - Two other separate datasets from the House Range section are presented in Baker, 2010 (entry #22) and Saltzman et al., 1995 (entry #24)

- **Entry 29: Lawson Cove, Utah, United States – Measured section**
    - Saltzman, M.R., Runnegar, B., Lohmann, K.C., 1998. Carbon isotope stratigraphy of Upper Cambrian (Steptoean Stage) sequences of the eastern Great Basin: Record of a global oceanographic event. Geol. Soc. Am. Bull. 110, 285–297. https://doi.org/10.1130/0016-7606(1998)110<0285:CISOUC>2.3.CO;2
    - 60 analyses over 126.0 m
        - Post-SPICE: 10 analyses over 19.6 m omitted
    - SPICE zones present: Rising, Falling, Post
        - Does not exhibit plateau
        - No Pre-SPICE zone sampled to evaluate Pre-SPICE negative kick
    - Deposited in intrashelf basin setting in intermediate water
        - Based on text in "Geologic Background" section and deposition of section within the House Range Embayment
        - Limestone
    - Located on paleocontinent Laurentia from 0–30° S
    - Data collected:
        - Meters and $\delta^{13}C$ and $\delta^{18}O$ values from table 1
        - Formations and biozones from fig. 2 via WPD
        - Facies from fig. 3 via WPD

- **Entry 30: Felix Cove, Newfoundland, Canada – Measured section**
    - Saltzman, M.R., Cowan, C.A., Runkel, A.C., Runnegar, B., Stewart, M.C., Palmer, A.R., 2004. The Late Cambrian Spice ($\delta^{13}C$) Event and the Sauk II-Sauk III Regression: New Evidence from Laurentian Basins in Utah, Iowa, and Newfoundland. J. Sediment. Res. 74, 366–377. https://doi.org/10.1306/120203740366
    - 64 analyses over 91.8 m
        - No analyses omitted
    - SPICE zones present: Rising, Falling, Post
        - Exhibits plateau
        - No Pre-SPICE zone sampled to evaluate Pre-SPICE negative kick
    - Deposited in shelf setting in intermediate water
        - Based on fig. 2 and text in "Sequence Stratigraphy, Biostratigraphy, and $\delta^{13}C$ Trends" section
        - Limestone
    - Located on paleocontinent Laurentia from 30–60° S
    - Data collected:
        - Meters, $\delta^{13}C$ values, formations, members, Stages, and biozones from fig. 6 via WPD
        - No data tables were provided for this entry in the original publication, neither in text nor supplement. Data collection was limited to WPD.
    - A second separate dataset from the Felix Cove section is presented in Barili et al., 2018 (entry #3)

- **Entry 31: Rhinehart A-1, Iowa, United States – Core**
    - Saltzman, M.R., Cowan, C.A., Runkel, A.C., Runnegar, B., Stewart, M.C., Palmer, A.R., 2004. The Late Cambrian Spice ($\delta^{13}C$) Event and the Sauk II-Sauk III Regression: New Evidence from Laurentian Basins in Utah, Iowa, and Newfoundland. J. Sediment. Res. 74, 366–377. https://doi.org/10.1306/120203740366
    - 129 analyses over 38.2 m
        - No analyses omitted
    - SPICE zones present: Pre, Rising, Falling, Post
        - Does not exhibit plateau
        - Does not record Pre-SPICE negative kick
    - Deposited in shelf setting in intermediate water
        - Based on fig. 2 and text in "Sequence Stratigraphy, Biostratigraphy, and $\delta^{13}C$ Trends" section
        - Limestone
    - Located on paleocontinent Laurentia from 0–30° S
    - Data collected:
        - Meters, $\delta^{13}C$ values, formations, members, Stages, and biozones from fig. 5 via WPD
        - No data tables were provided for this entry in the original publication, neither in the text nor in the supplement. Data collection was limited to that obtained through WPD.

- **Entry 32: Smithfield Canyon, Utah, United States – Measured section**
    - Saltzman, M.R., Cowan, C.A., Runkel, A.C., Runnegar, B., Stewart, M.C., Palmer, A.R., 2004. The Late Cambrian Spice ($\delta^{13}C$) Event and the Sauk II-Sauk III Regression: New Evidence from Laurentian Basins in Utah, Iowa, and Newfoundland. J. Sediment. Res. 74, 366–377. https://doi.org/10.1306/120203740366
    - 100 analyses over 118.7 m
        - Pre-SPICE: 5 analyses over 15.5 m omitted
    - SPICE zones present: Pre, Rising, Falling, Post
        - Exhibits plateau
        - Records Pre-SPICE negative kick
    - Deposited in shelf setting in intermediate water
        - Based on fig. 2 and text in "Sequence Stratigraphy, Biostratigraphy, and $\delta^{13}C$ Trends" section
        - Limestone
    - Located on paleocontinent Laurentia from 0–30° S
    - Data collected:
        - Meters, $\delta^{13}C$ values, formations, Stages, and biozones from fig. 4 via WPD
        - No data tables were provided for this entry in the original publication, neither in the text nor in the supplement. Data collection was limited to that obtained through WPD.

- **Entry 33: HM-1, Missouri, United States – Core**
    - Schiffbauer, J.D., Huntley, J.W., Fike, D.A., Jeffrey, M.J., Gregg, J.M., Shelton, K.L., 2017. Decoupling biogeochemical records, extinction, and environmental change during the Cambrian SPICE event. Sci. Adv. 3, e1602158. https://doi.org/10.1126/sciadv.1602158
    - 85 analyses over 106.8 m
        - Pre-SPICE: 7 analyses over 22.3 m omitted
    - SPICE zones present: Pre, Rising, Falling
        - Does not exhibit plateau
        - Does not record Pre-SPICE negative kick
    - Deposited in intrashelf basin setting in intermediate water
        - Based on text in "Geological and Paleontological Setting" section and deposition of section within the Central Missouri Intrashelf Basin
        - Limestone
    - Located on paleocontinent Laurentia from 0–30° S
    - Data collected:
        - Meters, lithologies, and $\delta^{13}C$ and $\delta^{18}O$ values from supplementary online materials.
        - Biozones from fig. S3 via WPD

- **Entry 34: 1-EE, Missouri, United States – Core**
    - Schiffbauer, J.D., Huntley, J.W., Fike, D.A., Jeffrey, M.J., Gregg, J.M., Shelton, K.L., 2017. Decoupling biogeochemical records, extinction, and environmental change during the Cambrian SPICE event. Sci. Adv. 3, e1602158. https://doi.org/10.1126/sciadv.1602158
    - 70 analyses over 119.2 m
        - Pre-SPICE: 15 analyses over 42.7 m omitted
    - SPICE zones present: Pre, Rising, Falling, Post
        - Does not exhibit plateau
        - Records Pre-SPICE negative kick
    - Deposited in intrashelf basin setting in intermediate water
        - Based on text in "Geological and Paleontological Setting" section and deposition of section within the Central Missouri Intrashelf Basin
        - Dolostone
    - Located on paleocontinent Laurentia from 0–30° S
    - Data collected:
        - Meters, lithologies, and $\delta^{13}C$ and $\delta^{18}O$ values from supplementary online materials
        - Biozones from fig. S4 via WPD

- **Entry 35: 12-EE, Missouri, United States – Core**
    - Schiffbauer, J.D., Huntley, J.W., Fike, D.A., Jeffrey, M.J., Gregg, J.M., Shelton, K.L., 2017. Decoupling biogeochemical records, extinction, and environmental change during the Cambrian SPICE event. Sci. Adv. 3, e1602158. https://doi.org/10.1126/sciadv.1602158
    - 67 analyses over 80.2 m
        - No analyses omitted
    - SPICE zones present: Pre, Rising, Falling, Post
        - Does not exhibit plateau
        - Records Pre-SPICE negative kick
    - Deposited in intrashelf basin setting in intermediate water
        - Based on text in "Geological and Paleontological Setting" section and deposition of section within the Central Missouri Intrashelf Basin
        - Dolostone
    - Located on paleocontinent Laurentia from 0–30° S
    - Data collected:
        - Meters, lithologies, and $\delta^{13}C$ and $\delta^{18}O$ values from supplementary online materials
        - Biozones from fig. S5 via WPD

- **Entry 36: LS-1, Missouri, United States – Core**
    - Schiffbauer, J.D., Huntley, J.W., Fike, D.A., Jeffrey, M.J., Gregg, J.M., Shelton, K.L., 2017. Decoupling biogeochemical records, extinction, and environmental change during the Cambrian SPICE event. Sci. Adv. 3, e1602158. https://doi.org/10.1126/sciadv.1602158
    - 210 analyses over 115.8 m
        - Pre-SPICE: 27 analyses over 36.0 m omitted
        - Post-SPICE: 7 analyses over 3.8 m omitted
    - SPICE zones present: Pre, Rising, Falling, Post
        - Exhibits plateau
        - Records Pre-SPICE negative kick
    - Deposited in intrashelf basin setting in intermediate water
        - Based on text in "Geological and Paleontological Setting" section and deposition of section within the Central Missouri Intrashelf Basin
        - Dolostone
    - Located on paleocontinent Laurentia from 0–30° S
    - Data collected:
        - Meters, lithologies, and $\delta^{13}C$ and $\delta^{18}O$ values from supplementary online materials
        - Biozones from fig. S2 via WPD

- **Entry 37: TE-1, Missouri, United States – Core**
    - Schiffbauer, J.D., Huntley, J.W., Fike, D.A., Jeffrey, M.J., Gregg, J.M., Shelton, K.L., 2017. Decoupling biogeochemical records, extinction, and environmental change during the Cambrian SPICE event. Sci. Adv. 3, e1602158. https://doi.org/10.1126/sciadv.1602158
    - 23 analyses over 29.4 m
        - No analyses omitted
    - SPICE zones present: Pre, Rising
        - Exhibits plateau
        - Records Pre-SPICE negative kick
    - Deposited in intrashelf basin setting in intermediate water
        - Based on text in "Geological and Paleontological Setting" section and deposition of section within the Central Missouri Intrashelf Basin
        - Limestone
    - Located on paleocontinent Laurentia from 0–30° S
    - Data collected:
        - Meters, lithologies, and $\delta^{13}C$ and $\delta^{18}O$ values from supplementary online materials
        - Biozones from fig. S1 via WPD
    - A second separate dataset from the TE-1 section is presented in Gill et al., 2011 (entry #9)

- **Entry 38: LO-5, Missouri, United States – Core**
    - Jeffrey, M.J., 2017. Stratigraphic variation of the Late Cambrian SPICE event in Upper Cambrian carbonates of Southern Missouri (M.S. thesis). University of Missouri-Columbia.
    - 64 analyses over 169.9 m
        - No analyses omitted
    - SPICE zones present: Pre, Rising, Falling, Post
        - Does not exhibit plateau
        - Records Pre-SPICE negative kick
    - Deposited in shallow/nearshore setting in shallow water
        - Based on fig 1, text in section 3, and deposition of section on shallow Lebanon Arch
        - Dolostone
    - Located on paleocontinent Laurentia from 0–30° S
    - Data collected:
        - Facies based on Palmer et al. (2012)
        - No biozone data available, no fossils

- **Entry 39: 319-11A, Missouri, United States – Core**
    - Jeffrey, M.J., 2017. Stratigraphic variation of the Late Cambrian SPICE event in Upper Cambrian carbonates of Southern Missouri (M.S. thesis). University of Missouri-Columbia.
    - 64 analyses over 169.9 m
        - No analyses omitted
    - SPICE zones present: Pre, Rising, Falling, Post
        - Exhibits plateau
        - Does not record Pre-SPICE negative kick
    - Deposited in shelf setting in intermediate water
        - Based on fig. 1 and deposition of section within Reelfoot Rift
        - Dolostone
    - Located on paleocontinent Laurentia from 0–30° S
    - Data collected:
        - Facies based on Palmer et al. (2012)
        - No biozone data available, no fossils

- **Entry 40: Quebrada de la Angostura, La Rioja, Argentina – Measured section**
    - Sial, A.N., Peralta, S., Ferreira, V.P., Toselli, A.J., Aceñolaza, F.G., Parada, M.A., Gaucher, C., Alonso, R.N., Pimentel, M.M., 2008. Upper Cambrian carbonate sequences of the Argentine Precordillera and the Steptoean C-Isotope positive excursion (SPICE). Gondwana Res. 13, 437–452. https://doi.org/10.1016/J.GR.2007.05.001
    - 31 analyses over 421.0 m
        - No analyses omitted
    - SPICE zones present: Pre, Rising
        - Does not exhibit plateau
        - Records Pre-SPICE negative kick
    - Deposited in shallow/nearshore setting in shallow water
        - Based on text in "Geologic Setting" section
        - Limestone
    - Located on paleocontinent Gondwana from 30–60° S
    - Data collected:
        - Sample numbers, meters, $\delta^{13}C$ and $\delta^{18}O$ values from supplementary online materials
        - Biozones, Stages, and lithologies from fig. 9 via WPD

- **Entry 41: Quebrada de Juan Pobre, San Juan, Argentina – Measured section**
    - Sial, A.N., Peralta, S., Gaucher, C., Toselli, A.J., Ferreira, V.P., Frei, R., Parada, M.A., Pimentel, M.M., Silva Pereira, N., 2013. High-resolution stable isotope stratigraphy of the upper Cambrian and Ordovician in the Argentine Precordillera: Carbon isotope excursions and correlations. Gondwana Res. 24, 330–348. https://doi.org/10.1016/j.gr.2012.10.014
    - 61 analyses over 262.1 m
        - Post-SPICE: 23 analyses over 87.5 m omitted
    - SPICE zones present: Rising, Falling, Post
        - Exhibits plateau
        - No Pre-SPICE zone sampled to evaluate Pre-SPICE negative kick
    - Deposited in shallow/nearshore setting in shallow water
        - Based on text in section 2
        - Dolostone
    - Located on paleocontinent Gondwana from 30–60° S
    - Data collected:
        - Sample numbers, meters, $\delta^{13}C$ and $\delta^{18}O$ values, and formations from table 1
        - Lithologies and biozones from fig. 3

- **Entry 42: Sallèles-Carbardès, Montagne Noire, France – Measured section**
    - Álvaro, J.J., Bauluz, B., Subias, I., Pierre, C., Vizcaino, D., 2008. Carbon chemostratigraphy of the Cambrian-Ordovician transition in a midlatitude mixed platform, Montagne Noire, France. Geol. Soc. Am. Bull. 120, 962–975. https://doi.org/10.1130/B26243.1
    - 40 analyses over 69.8 m
        - No analyses omitted
    - SPICE zones present: Pre, Rising, Falling, Post
        - Does not exhibit plateau
        - Does not record Pre-SPICE negative kick
    - Deposited in shallow/nearshore setting in shallow water
        - Based on text in "Samples and Methods" section
        - Limestone
    - Located on paleocontinent Gondwana from 30–60° S
    - Data collected:
        - Meters, $\delta^{13}C$ and $\delta^{18}O$ values, lithologies, and Series from supplementary online materials
        - Formations from fig. 4 via WPD

- **Entry 43: Balnakeil Bay, Scotland, United Kingdom – Measured section**
    - Pruss, S.B., Jones, D.S., Fike, D.A., Tosca, N.J., Wignall, P.B., 2019. Marine anoxia and sedimentary mercury enrichments during the Late Cambrian SPICE event in northern Scotland. Geology 47, 475–478. https://doi.org/10.1130/G45871.1
    - 132 analyses over 139.6 m
        - No analyses omitted
    - SPICE zones present: Pre, Rising, Falling, Post
        - Does not exhibit plateau
        - Does not record Pre-SPICE negative kick
    - Deposited in shallow/nearshore setting in shallow water
        - Based on in-text citation of Raine (2009)
        - "Carbonate"
    - Located on paleocontinent Laurentia from 30–60° S
    - Data collected:
        - Meters and $\delta^{13}C$, $\delta^{18}O$, and TOC values form supplementary online materials
        - No biozone data

- **Entry 44: Wanliangyu, Shandong Province, North China – Measured section**
    - Chen, J., Chough, S.K., Han, Z., Lee, J.-H., 2011. An extensive erosion surface of a strongly deformed limestone bed in the Gushan and Chaomidian formations (late Middle Cambrian to Furongian), Shandong Province, China: Sequence–stratigraphic implications. Sediment. Geol. 233, 129–149. https://doi.org/10.1016/j.sedgeo.2010.11.002
    - 53 analyses over 12.7 m
        - No analyses omitted
    - SPICE zones present: Pre, Rising, Falling, Post
        - Does not exhibit plateau
        - Records Pre-SPICE negative kick
    - Deposited in shallow/nearshore setting in shallow water
        - Based on text in section 4
        - Limestone
    - Located on paleocontinent Gondwana from 0–30° S
    - Data collected:
        - Sample numbers, meters, $\delta^{13}C$ and $\delta^{18}O$ values, and lithologies from table 4
        - Formations, Epochs, and biozones from fig. 16 via WPD
    - A second separate dataset from the Wanliangyu section is presented in Wang et al., 2020 (entry #60)

- **Entry 45: Deogwoo, Gangweon Province, South Korea – Measured section**
    - Chung, G.-S., Lee, J.-G., Lee, K.-S., 2011. Stable Carbon Isotope Stratigraphy of the Cambrian Machari Formation in the Yeongweol Area, Gangweon Province, Korea. J. Korean earth Sci. Soc. 32, 437–452. https://doi.org/10.5467/JKESS.2011.32.5.437
    - 71 analyses over 194.0 m
        - No analyses omitted
    - SPICE zones present: Pre, Rising, Falling, Post
        - Exhibits plateau
        - Records Pre-SPICE negative kick
    - Deposited in shallow/nearshore setting in shallow water
        - Based on fig. 4 and text in "Lithofacies and Facies Associations" section
        - Limestone
    - Located on paleocontinent Gondwana from 0–30° N
    - Data collected:
        - Sample numbers and $\delta^{13}C$ values from table 2
        - Meters and biozones from fig. 3 via WPD

- **Entry 46: Kulyumbe (Ottawa-Bochum dataset), Siberia, Russia – Measured section**
    - Kouchinsky, A., Bengton, S., Gallet, Y., Korovnikov, I., Pavlov, V., Runnegar, B., Shields, G., Veizer, J., Young, E., Ziegler, K., 2008. The SPICE carbon isotope excursion in Siberia: a combined study of the upper Middle Cambrian–lowermost Ordovician Kulyumbe River section, northwestern Siberian Platform. Geol. Mag. 145, 609–622. https://doi.org/10.1017/S0016756808004913
    - 69 analyses over 2986 m
        - Pre-SPICE: 17 samples over 234 m omitted
    - SPICE zones present: Pre, Rising, Falling, Post
        - Does not exhibit plateau
        - Records Pre-SPICE negative kick
    - Deposited in shelf setting in intermediate water
        - Based on fig. 1 and text in section 5
        - "Carbonate"
    - Located on paleocontinent Siberia from 0–30° S
    - Data collected:
        - Sample numbers, meters, $\delta^{13}C$ and $\delta^{18}O$ values, formations, and biozones from supplementary online materials [supplement #3]
    - A second separate dataset from the Kulyumbe section is presented in Kouchinsky et al., 2008 (entry #47)

- **Entry 47: Kulyumbe, Siberia, Russia – Measured section**
    - Kouchinsky, A., Bengton, S., Gallet, Y., Korovnikov, I., Pavlov, V., Runnegar, B., Shields, G., Veizer, J., Young, E., Ziegler, K., 2008. The SPICE carbon isotope excursion in Siberia: a combined study of the upper Middle Cambrian–lowermost Ordovician Kulyumbe River section, northwestern Siberian Platform. Geol. Mag. 145, 609–622. https://doi.org/10.1017/S0016756808004913
    - 1118 analyses over 2311.7 m
        - Pre-SPICE: 541 samples over 1125.3 m omitted
    - SPICE zones present: Pre, Rising, Falling, Post
        - Does not exhibit plateau
        - Records Pre-SPICE negative kick
    - Deposited in shelf setting in intermediate water
        - Based on fig. 1 and text in section 5
        - "Carbonate"
    - Located on paleocontinent Siberia from 0–30° S
    - Data collected:
        - Sample numbers, meters, $\delta^{13}C$ and $\delta^{18}O$ values, outcrops, and formations from supplementary online materials [supplement #1]
        - A second separate dataset from the Kulyumbe section is presented in Kouchinsky et al., 2008 (entry #46)

- **Entry 48: Duibian A, Zhejiang Province, South China – Measured section**
    - Li, D., Zhang, Xiaolin, Hu, D., Chen, X., Huang, W., Zhang, Xu, Li, M., Qin, L., Peng, S., Shen, Y., 2018. Evidence of a large $\delta^{13}C_{carb}$ and $\delta^{13}C_{org}$ depth gradient for deep-water anoxia during the late Cambrian SPICE event. Geology 46, 631–634. https://doi.org/10.1130/G40231.1
    - 87 analyses over 139.0 m
        - No analyses omitted
    - SPICE zones present: Rising, Falling
        - Does not exhibit plateau
        - No Pre-SPICE zone sampled to evaluate Pre-SPICE negative kick
    - Deposited in slope setting in deep water
        - Based on fig. 1 and text in "Stratigraphy and Sampling" section
        - Limestone
    - Located on paleocontinent Gondwana from 0–30° N
    - Data collected:
        - Sample numbers, meters, and $\delta^{13}C$ and $\delta^{18}O$ values from supplementary online materials
        - Lithologies, formations, and Stages from fig. 2 via WPD
    - A second separate dataset from the Duibian A section is presented in Zuo et al., 2018 (entry #64)

- **Entry 49: Duibian B, Zhejiang Province, South China – Measured section**
    - Li, D., Zhang, Xiaolin, Hu, D., Chen, X., Huang, W., Zhang, Xu, Li, M., Qin, L., Peng, S., Shen, Y., 2018. Evidence of a large $\delta^{13}C_{carb}$ and $\delta^{13}C_{org}$ depth gradient for deep-water anoxia during the late Cambrian SPICE event. Geology 46, 631–634. https://doi.org/10.1130/G40231.1
    - 62 analyses over 47.5 m
        - No analyses omitted
    - SPICE zones present: Falling
        - Does not exhibit plateau
        - No Pre-SPICE zone sampled to evaluate Pre-SPICE negative kick
    - Deposited in slope setting in deep water
        - Based on fig. 1 and text in "Stratigraphy and Sampling" section
        - Lithology NA
    - Located on paleocontinent Gondwana from 0–30° N
    - Data collected:
        - Sample numbers, meters, and $\delta^{13}C$ and $\delta^{18}O$ values from supplementary online materials
        - Lithologies, formations, and Stages from fig. 2 via WPD
    - Because all samples in this entry belong to the falling limb of the SPICE, the meters above onset value (Column G in the SPICEraq) has been calculated relative to the onset of the rising limb in Entry #48, which is a correlative section. The lowermost sample meterage in this entry corresponds to the meterage for the maximum δ13C value in the rising limb of entry #48.

- **Entry 50: Wa'ergang, Hunan Province, South China – Measured section**
    - Li, D., Zhang, Xiaolin, Hu, D., Chen, X., Huang, W., Zhang, Xu, Li, M., Qin, L., Peng, S., Shen, Y., 2018. Evidence of a large $\delta^{13}C_{carb}$ and $\delta^{13}C_{org}$ depth gradient for deep-water anoxia during the late Cambrian SPICE event. Geology 46, 631–634. https://doi.org/10.1130/G40231.1
    - 88 analyses over 141.5 m
        - Post-SPICE: 4 analyses over 6.5 m omitted
    - SPICE zones present: Rising, Falling, Post
        - Does not exhibit plateau
        - No Pre-SPICE zone sampled to evaluate Pre-SPICE negative kick
    - Deposited in slope setting in deep water
        - Based on fig. 1 and text in "Stratigraphy and Sampling" section
        - Limestone
    - Located on paleocontinent Gondwana from 0–30° N
    - Data collected:
        - Sample numbers, meters, and $\delta^{13}C$ and $\delta^{18}O$ values from supplementary online materials
        - Lithologies, formations, and Stages from fig. 2 via WPD
    - A second separate dataset from the Wa'ergang section is presented in Saltzman et al., 2000 (entry #55)

- **Entry 51: Jikdong and Sagundari, Gangwon Province, South Korea – Measured section**
    - Lim, J.N., Chung, G.S., Park, T.-Y.S., Lee, K.S., 2015. Lithofacies and stable carbon isotope stratigraphy of the Cambrian Sesong Formation in the Taebaeksan Basin, Korea. J. Korean Earth Sci. Soc. 36, 617–631. https://doi.org/10.5467/JKESS.2015.36.7.617
    - 40 analyses over 65.1 m
        - Post-SPICE: 5 analyses over 3.3 m omitted
    - SPICE zones present: Pre, Rising, Falling, Post
        - Exhibits plateau
        - Records Pre-SPICE negative kick
    - Deposited in shelf setting in shallow/nearshore water
        - Based on text in "Discussion" section
        - Limestone
    - Located on paleocontinent Gondwana from 0–30° N
    - Data collected:
        - Sample numbers, $\delta^{13}C$ and $\delta^{18}O$ values, and lithologies from table 2
        - Meters from fig. 4 via WPD
        - Series, Stages, and biozones from fig. 5 via WPD

- **Entry 52: Yaerdang Mountain, Xinjiang Province, North China – Measured section**
    - Liu, H., Liao, Z., Zhang, H., Tian, Y., Cheng, B., Yang, S., 2017. Stable isotope ($\delta^{13}C_{ker}$, $\delta^{13}C_{carb}$, $\delta^{18}O_{carb}$) distribution along a Cambrian outcrop section in the eastern Tarim Basin, NW China and its geochemical significance. Geosci. Front. 8, 163–170. https://doi.org/10.1016/j.gsf.2016.02.004
    - 46 analyses over 236.9 m
        - Pre-SPICE: 11 analyses over 71.3 m omitted
    - SPICE zones present: Pre, Rising, Falling, Post
        - Does not exhibit plateau
        - Does not record Pre-SPICE negative kick
    - Deposited in shelf setting in intermediate water
        - Based on tables 1 and 2
        - Limestone
    - Located on paleocontinent Gondwana from 0–30° S
    - Data collected:
        - Meters, $\delta^{13}C$, $\delta^{18}O$, and TOC values, and formations from fig. 2 via WPD
        - No data tables were provided for this entry in the original publication, neither in the text nor in the supplement. Data collection was limited to that obtained through WPD.

- **Entry 53: Huangyangshan, Shandong Province, North China – Measured section**
    - Ng, T.-W., Yuan, J.-L., Lin, J.-P., 2014. The North China Steptoean Positive Carbon Isotope Event: New insights towards understanding a global phenomenon. Geobios 47, 371–387. https://doi.org/10.1016/j.geobios.2014.09.003
    - 47 analyses over 11.0 m
        - No analyses omitted
    - SPICE zones present: Pre, Rising, Falling, Post
        - Does not exhibit plateau
        - Records Pre-SPICE negative kick
    - Deposited in shelf setting in intermediate water
        - Based on text in section 3
        - Limestone
    - Located on paleocontinent Gondwana from 0–30° N
    - Data collected:
        - Meters, $\delta^{13}C$ and $\delta^{18}O$ values, biozones, Series, and Stages from table 1
        - Lithologies from fig. 2 via WPD

- **Entry 54: Paibi, Hunan Province, South China – Measured section**
    - Saltzman, M.R., Ripperdan, R.L., Brasier, M.D., Lohmann, K.C., Robison, R.A., Chang, W.T., Peng, S., Ergaliev, E.K., Runnegar, B., 2000. A global carbon isotope excursion (SPICE) during the Late Cambrian: relation to trilobite extinctions, organic-matter burial and sea level. Palaeogeogr. Palaeoclimatol. Palaeoecol. 162, 211–223. https://doi.org/10.1016/S0031-0182(00)00128-0
    - 37 analyses over 369.0 m
        - Pre-SPICE: 7 analyses over 43.0 m omitted
    - SPICE zones present: Pre, Rising
        - Does not exhibit plateau
        - Records Pre-SPICE negative kick
    - Deposited in slope setting in deep water
        - Based on text in section 2
        - Limestone
    - Located on paleocontinent Gondwana from 0–30° N
    - Data collected:
        - Meters, $\delta^{13}C$ and $\delta^{18}O$ values, formations, and biozones from table 2

- **Entry 55: Wa'ergang, Hunan Province, South China – Measured section**
    - Saltzman, M.R., Ripperdan, R.L., Brasier, M.D., Lohmann, K.C., Robison, R.A., Chang, W.T., Peng, S., Ergaliev, E.K., Runnegar, B., 2000. A global carbon isotope excursion (SPICE) during the Late Cambrian: relation to trilobite extinctions, organic-matter burial and sea level. Palaeogeogr. Palaeoclimatol. Palaeoecol. 162, 211–223. https://doi.org/10.1016/S0031-0182(00)00128-0
    - 71 analyses over 862.8 m
        - Post-SPICE: 13 analyses over 175.3 m
    - SPICE zones present: Pre, Rising, Falling, Post
        - Exhibits plateau
        - Records Pre-SPICE negative kick
    - Deposited in slope setting in deep water
        - Based on text in section 2
        - Limestone
    - Located on paleocontinent Gondwana from 0–30° N
    - Data collected:
        - Meters, $\delta^{13}C$ and $\delta^{18}O$ values, formations, and biozones from table 3
    - A second separate dataset from the Wa'ergang section is presented in Li et al., 2018 (entry #50)

- **Entry 56: Kyrshabakty, Malyi Karatau region, Kazakhstan – Measured section**
    - Saltzman, M.R., Ripperdan, R.L., Brasier, M.D., Lohmann, K.C., Robison, R.A., Chang, W.T., Peng, S., Ergaliev, E.K., Runnegar, B., 2000. A global carbon isotope excursion (SPICE) during the Late Cambrian: relation to trilobite extinctions, organic-matter burial and sea level. Palaeogeogr. Palaeoclimatol. Palaeoecol. 162, 211–223. https://doi.org/10.1016/S0031-0182(00)00128-0
    - 12 analyses over 587.0 m
        - Pre-SPICE: 16 analyses over 61.0 m omitted
        - Post-SPICE: 21 analyses over 76.5 m omitted
    - SPICE zones present: Pre, Rising, Falling, Post
        - Does not exhibit plateau
        - Records Pre-SPICE negative kick
    - Deposited in slope setting in deep water
        - Based on text in section 2
        - Limestone
    - Located on paleocontinent Kazakhstania from 0–30° S
    - Data collected:
        - Meters, $\delta^{13}C$ and $\delta^{18}O$ values, formations, and biozones from table 1
    - A second separate dataset from the Kyrshabakty section is presented in Wotte & Strauss, 2015 (entry #61)

- **Entry 57: Baijiashan, Liaoning Province, North China – Core**
    - Wang, Z., Chen, J., Liang, T., Yuan, J., Han, C., Liu, J., Zhu, C., Zhu, D., Han, Z., 2020. Spatial variation in carbonate carbon isotopes during the Cambrian SPICE event across the eastern North China Platform. Palaeogeogr. Palaeoclimatol. Palaeoecol. 546, 109669. https://doi.org/10.1016/j.palaeo.2020.109669
    - 89 analyses over 24.2 m
        - No analyses omitted
    - SPICE zones present: Rising, Falling
        - Exhibits plateau
        - No Pre-SPICE zone sampled to evaluate Pre-SPICE negative kick
    - Deposited in shallow/nearshore setting in shallow water
        - Based on text in section 6
        - "Carbonate"
    - Located on paleocontinent Gondwana from 0–30° N
    - Data collected:
        - Sample numbers, meters, and $\delta^{13}C$ and $\delta^{18}O$ values from supplementary online materials
        - Facies, formations, and biozones from fig. 3

- **Entry 58: Chengouwan, Shandong Province, North China – Core**
    - Wang, Z., Chen, J., Liang, T., Yuan, J., Han, C., Liu, J., Zhu, C., Zhu, D., Han, Z., 2020. Spatial variation in carbonate carbon isotopes during the Cambrian SPICE event across the eastern North China Platform. Palaeogeogr. Palaeoclimatol. Palaeoecol. 546, 109669. https://doi.org/10.1016/j.palaeo.2020.109669
    - 88 analyses over 60.2 m
        - Post-SPICE: 26 analyses over 22.4 m omitted
    - SPICE zones present: Pre, Rising, Falling, Post
        - Does not exhibit plateau
        - Records Pre-SPICE negative kick
    - Deposited in shallow/nearshore setting in shallow water
        - Based on text in section 6
        - "Carbonate"
    - Located on paleocontinent Gondwana from 0–30° S
    - Data collected:
        - Sample numbers, meters, and $\delta^{13}C$ and $\delta^{18}O$ values from supplementary online materials
        - Facies, formations, biozones, and Epochs from fig. 7

- **Entry 59: Liangchang, Shandong Province, North China – Core**
    - Wang, Z., Chen, J., Liang, T., Yuan, J., Han, C., Liu, J., Zhu, C., Zhu, D., Han, Z., 2020. Spatial variation in carbonate carbon isotopes during the Cambrian SPICE event across the eastern North China Platform. Palaeogeogr. Palaeoclimatol. Palaeoecol. 546, 109669. https://doi.org/10.1016/j.palaeo.2020.109669
    - 7 analyses over 0.59 m
        - No analyses omitted
    - SPICE zones present: Rising
        - Does not exhibit plateau
        - Records Pre-SPICE negative kick
    - Deposited in shallow/nearshore setting in shallow water
        - Based on text in section 6
        - "Carbonate"
    - Located on paleocontinent Gondwana from 0–30° S
    - Data collected:
        - Sample numbers, meters, and $\delta^{13}C$ and $\delta^{18}O$ values from supplementary online materials
        - Facies, formations, biozones, and Epochs from fig. 7

- **Entry 60: Wanliangyu, Shandong Province, North China – Core**
    - Wang, Z., Chen, J., Liang, T., Yuan, J., Han, C., Liu, J., Zhu, C., Zhu, D., Han, Z., 2020. Spatial variation in carbonate carbon isotopes during the Cambrian SPICE event across the eastern North China Platform. Palaeogeogr. Palaeoclimatol. Palaeoecol. 546, 109669. https://doi.org/10.1016/j.palaeo.2020.109669
    - 77 analyses over 56.9 m
        - No analyses omitted
    - SPICE zones present: Pre, Rising, Falling, Post
        - Does not exhibit plateau
        - No Pre-SPICE zone sampled to evaluate Pre-SPICE negative kick
    - Deposited in shallow/nearshore setting in shallow water
        - Based on text in section 6
        - "Carbonate"
    - Located on paleocontinent Gondwana from 0–30° S
    - Data collected:
        - Sample numbers, meters, and $\delta^{13}C$ and $\delta^{18}O$ values from supplementary online materials
        - Facies, formations, biozones, and Epochs from fig. 7
    - A second separate dataset from the Wanliangyu section is presented in Chen et al., 2011 (entry #44)

- **Entry 61: Kyrshabakty, Malyi Karatau region, Kazakhstan – Measured section**
    - Wotte, T., Strauss, H., 2015. Questioning a widespread euxinia for the Furongian (Late Cambrian) SPICE event: indications from $\delta^{13}C$, $\delta^{18}O$, $\delta^{34}S$ and biostratigraphic constraints. Geol. Mag. 152, 1085–1103. https://doi.org/10.1017/S0016756815000187
    - 58 analyses over 215.8 m
        - No analyses omitted
    - SPICE zones present: Pre, Rising, Falling, Post
        - Does not exhibit plateau
        - Does not record Pre-SPICE negative kick
    - Deposited in slope setting in deep water
        - Based on fig. 2 and text in section 2
        - Limestone
    - Located on paleocontinent Kazakhstania from 0–30° S
    - Data collected:
        - Sample numbers, meters, and $\delta^{13}C$ and $\delta^{18}O$ values from table 1
        - Formations, facies, Series, and Stages from fig. 2 via WPD
    - A second separate dataset from the Kyrshabakty section is presented in Saltzman et al., 2000 (entry #56)

- **Entry 62: Tangwangzhai, Shandong Province, North China – Measured section**
    - Zhu, M.-Y., Zhang, J.-M., Li, G.-X., Yang, A.-H., 2004. Evolution of C isotopes in the Cambrian of China: implications for Cambrian subdivision and trilobite mass extinctions. Geobios 37, 287–301. https://doi.org/10.1016/j.geobios.2003.06.001
    - 54 analyses over 98.5 m
        - Pre-SPICE: 2 analyses over 1 m omitted
        - Post-SPICE: 12 analyses over 17.9 m omitted
    - SPICE zones present: Pre, Rising, Falling, Post
        - Does not exhibit plateau
        - Does not record Pre-SPICE negative kick
    - Deposited in shallow/nearshore setting in shallow water
        - Based on text in sections 2 and 5
        - Limestone
    - Located on paleocontinent Gondwana from 0–30° S
    - Data collected:
        - Meters and $\delta^{13}C$ and $\delta^{18}O$ values from table 3
        - Formations and Stages from fig. 4 via WPD

- **Entry 63: Wangcun, Hunan Province, South China – Measured section**
    - Zhu, M.-Y., Zhang, J.-M., Li, G.-X., Yang, A.-H., 2004. Evolution of C isotopes in the Cambrian of China: implications for Cambrian subdivision and trilobite mass extinctions. Geobios 37, 287–301. https://doi.org/10.1016/j.geobios.2003.06.001
    - 146 analyses over 534.6 m
        - Pre-SPICE: 109 analyses over 330.99 m omitted
    - SPICE zones present: Pre, Rising
        - Does not exhibit plateau
        - Records Pre-SPICE negative kick
    - Deposited in slope setting in deep water
        - Based on text in section 2
        - Limestone
    - Located on paleocontinent Gondwana from 0–30° N
    - Data collected:
        - Meters and $\delta^{13}C$ and $\delta^{18}O$ values from table 1
        - Formations and Stages from fig. 2 via WPD
    - A second separate dataset from the Wangcun section is presented in Zuo et al., 2018 (entry #65)

- **Entry 64: Duibian A, Zhejiang Province, South China – Measured section**
    - Zuo, J., Peng, S., Qi, Y., Zhu, X., Bagnoli, G., Fang, H., 2018. Carbon-isotope excursions recorded in the Cambrian system, South China: Implications for mass extinctions and sea-level fluctuations. J. Earth Sci. 29, 479–491. https://doi.org/10.1007/s12583-017-0963-x
    - 256 analyses over 333.0 m
        - Pre-SPICE: 29 analyses over 64.0 m omitted
        - Post-SPICE: 43 analyses over 55 m omitted
    - SPICE zones present: Pre, Rising, Falling, Post
        - Exhibits plateau
        - Does not record Pre-SPICE negative kick
    - Deposited in basin setting in deep water
        - Based on text in sections 2, 4, and 5
        - Limestone
    - Located on paleocontinent Gondwana from 0–30° N
    - Data collected:
        - Meters, lithologies, and $\delta^{13}C$ and $\delta^{18}O$ values from table 2
        - Formations, Stages, and biozones from fig. 4 via WPD
    - A second separate dataset from the Duibian A section is presented in Li et al., 2018 (entry #48)

- **Entry 65: Wangcun, Hunan Province, South China – Measured section**
    - Zuo, J., Peng, S., Qi, Y., Zhu, X., Bagnoli, G., Fang, H., 2018. Carbon-isotope excursions recorded in the Cambrian system, South China: Implications for mass extinctions and sea-level fluctuations. J. Earth Sci. 29, 479–491. https://doi.org/10.1007/s12583-017-0963-x
    - 278 analyses over 1745 m
        - Pre-SPICE: 12 analyses over 180 m omitted
        - Post-SPICE: 38 analyses over 245 m omitted
    - SPICE zones present: Pre, Rising, Falling, Post
        - Does not exhibit plateau
        - Records Pre-SPICE negative kick
    - Deposited in slope setting in deep water
        - Based on text in sections 2 and 4
        - Limestone
    - Located on paleocontinent Gondwana from 0–30° N
    - Data collected:
        - Meters, lithologies, and $\delta^{13}C$ and $\delta^{18}O$ values from table 1
        - Formations, Stages, and biozones from fig. 4 via WPD
    - A second separate dataset from the Wangcun section is presented in Zhu et al., 2004 (entry #63)

- **Entry 66: Mount Murray, Queensland, Australia – Measured section**
    - Gill, B.C., Lyons, T.W., Young, S.A., Kump, L.R., Knoll, A.H., Saltzman, M.R., 2011. Geochemical evidence for widespread euxinia in the Later Cambrian ocean. Nature 469, 80–83. https://doi.org/10.1038/nature09700
    - 20 analyses over 258.4 m
        - No analyses omitted
    - SPICE zones present: Rising, Falling
        - Does not exhibit plateau
        - No Pre-SPICE zone sampled to evaluate Pre-SPICE negative kick
    - Deposited in shallow/nearshore setting in shallow water
        - Based on text in supplementary online materials
        - Limestone
    - Located on paleocontinent Gondwana from 0–30° N
    - Data collected:
        - Meters, facies, Stages, and $\delta^{13}C$ and $\delta^{18}O$ values from supplementary online materials

- **Entry 67: Elkedra 6, Georgina Basin, Australia – Core**
    - Lindsay, J.F., Kruse, P.D., Green, O.R., Hawkins, E., Brasier, M.D., Cartlidge, J., Corfield, R.M., 2005. The Neoproterozoic–Cambrian record in Australia: A stable isotope study. Precambrian Res. 143, 113–133. https://doi.org/10.1016/j.precamres.2005.10.002
    - 91 analyses over 685.8 m
        - Pre-SPICE: 33 analyses over 245.6 m omitted
    - SPICE zones present: Pre, Rising, Falling, Post
        - Does not exhibit plateau
        - Does not record Pre-SPICE negative kick
    - Deposited in shallow/nearshore setting in shallow water
        - Based on in-text citation of Ambrose et al. (2001)
        - "Carbonate"
    - Located on paleocontinent Gondwana from 0–30° N
    - Data collected:
        - Meters, formations, members, $\delta^{13}C$ and $\delta^{18}O$ values, and lithologies from fig. 9 via WPD
        - No data tables were provided for this entry in the original publication, neither in the text nor in the supplement. Data collection was limited to that obtained through WPD.

- **Entry 68: GSQ Mt. Whelan 1, Queensland, Australia – Core**
    - Saltzman, M.R., Ripperdan, R.L., Brasier, M.D., Lohmann, K.C., Robison, R.A., Chang, W.T., Peng, S., Ergaliev, E.K., Runnegar, B., 2000. A global carbon isotope excursion (SPICE) during the Late Cambrian: relation to trilobite extinctions, organic-matter burial and sea level. Palaeogeogr. Palaeoclimatol. Palaeoecol. 162, 211–223. https://doi.org/10.1016/S0031-0182(00)00128-0
    - 265 analyses over 346.3 m
        - Pre-SPICE: 5 analyses over 5.5 m omitted
    - SPICE zones present: Pre, Rising, Falling
        - Does not exhibit plateau
        - Does not record Pre-SPICE negative kick
    - Deposited in basin setting in deep water
        - Based on text in section 2
        - Limestone
    - Located on paleocontinent Gondwana from 0–30° N
    - Data collected:
        - Meters, $\delta^{13}C$ values, biozones, and lithologies from fig. 3 via WPD
        - No data tables were provided for this entry in the original publication, neither in the text nor in the supplement. Data collection was limited to that obtained through WPD.

- **Entry 69: Alice 1, Northern Territory, Australia – Core**
    - Schmid, S., 2017. Chemostratigraphy and palaeo-environmental characterisation of the Cambrian stratigraphy in the Amadeus Basin, Australia. Chem. Geol. 451, 169–182. https://doi.org/10.1016/j.chemgeo.2017.01.019
    - 72 analyses over 1408.2 m
        - Pre-SPICE: 34 analyses over 707.1 m omitted
    - SPICE zones present: Pre, Rising, Falling
        - Does not exhibit plateau
        - Records Pre-SPICE negative kick
    - Deposited in shallow/nearshore setting in shallow water
        - Based on in section 2
        - "Carbonate"
    - Located on paleocontinent Gondwana from 0–30° N
    - Data collected:
        - Meters, formations, and $\delta^{13}C$ and $\delta^{18}O$ values from supplementary online materials
        - Stages from fig. 1
    - Data from the Alice 1 core is also presented in Schmid et al. (2018) (entry #71). Schmid (2017) and Schmid et al. (2018) present different data sets for this core so both are included in the SPICEraq

- **Entry 70: East Johnny's Creek 1, Northern Territory, Australia – Core**
    - Schmid, S., 2017. Chemostratigraphy and palaeo-environmental characterisation of the Cambrian stratigraphy in the Amadeus Basin, Australia. Chem. Geol. 451, 169–182. https://doi.org/10.1016/j.chemgeo.2017.01.019
    - 20 analyses over 1051.6 m
        - Pre-SPICE: 14 analyses over 249.9 m omitted
    - SPICE zones present: Pre, Rising, Falling
        - Does not exhibit plateau
        - Records Pre-SPICE negative kick
    - Deposited in shallow/nearshore setting in shallow water
        - Based on in section 2
        - "Carbonate"
    - Located on paleocontinent Gondwana from 0–30° N
    - Data collected:
        - Meters, formations, and $\delta^{13}C$ and $\delta^{18}O$ values from supplementary online materials
        - Stages from fig. 1
    - Data from the East Johnny's Creek 1 core is also presented in Schmid et al. (2018) (entry #75). Schmid (2017) and Schmid et al. (2018) present different data sets for this core so both are included in the SPICEraq.

- **Entry 71: Alice 1, Northern Territory, Australia – Core**
    - Schmid, S., Smith, P.M., Woltering, M., 2018. A basin-wide record of the Late Cambrian Steptoean Positive Carbon Isotope Excursion (SPICE) in the Amadeus Basin, Australia. Palaeogeogr. Palaeoclimatol. Palaeoecol. 508, 116–128. https://doi.org/10.1016/j.palaeo.2018.07.027
    - 50 analyses over 536.45 m
        - No analyses omitted
    - SPICE zones present: Pre, Rising, Falling, Post
        - Does not exhibit plateau
        - Records Pre-SPICE negative kick
    - Deposited in shallow/nearshore setting in shallow water
        - Based on text in section 2
        - "Carbonate"
    - Located on paleocontinent Gondwana from 0–30° N
    - Data collected:
        - Meters and $\delta^{13}C$ and $\delta^{18}O$ values from supplementary online materials
        - Formations from fig. 6 via WPD
        - Stages from fig. 1
    - Data from the Alice 1 core is also presented in Schmid et al. (2018) (entry #69). These data sets for this core are unique so both are included in the SPICEraq.
    - Note, that while all references to this publication are formatted as "Schmid et al. (2018)" in this study, this publication is sometimes mis-referenced as "Suzanne et al. (2018)" owing to a production error that reversed the names of all authors..

- **Entry 72: DD97WR002, Northern Territory, Australia – Core**
    - Schmid, S., Smith, P.M., Woltering, M., 2018. A basin-wide record of the Late Cambrian Steptoean Positive Carbon Isotope Excursion (SPICE) in the Amadeus Basin, Australia. Palaeogeogr. Palaeoclimatol. Palaeoecol. 508, 116–128. https://doi.org/10.1016/j.palaeo.2018.07.027
    - 23 analyses over 157.9 m
        - No analyses omitted
    - SPICE zones present: Pre, Rising, Falling, Post
        - Does not exhibit plateau
        - Records Pre-SPICE negative kick
    - Deposited in shallow/nearshore setting in shallow water
        - Based on text in section 2
        - Dolostone
    - Located on paleocontinent Gondwana from 0–30° N
    - Data collected:
        - Meters and $\delta^{13}C$ and $\delta^{18}O$ values from supplementary online materials
        - Formations from fig. 6 via WPD
        - Stages from fig. 1

- **Entry 73: Dingo 1, Northern Territory, Australia – Core**
    - Schmid, S., Smith, P.M., Woltering, M., 2018. A basin-wide record of the Late Cambrian Steptoean Positive Carbon Isotope Excursion (SPICE) in the Amadeus Basin, Australia. Palaeogeogr. Palaeoclimatol. Palaeoecol. 508, 116–128. https://doi.org/10.1016/j.palaeo.2018.07.027
    - 35 analyses over 326.1 m
        - No analyses omitted
    - SPICE zones present: Pre, Rising, Falling
        - Does not exhibit plateau
        - Records Pre-SPICE negative kick
    - Deposited in shallow/nearshore setting in shallow water
        - Based on text in section 2
        - "Carbonate"
    - Located on paleocontinent Gondwana from 0–30° N
    - Data collected:
        - Meters and $\delta^{13}C$ and $\delta^{18}O$ values from supplementary online materials
        - Formations from fig. 6 via WPD
        - Stages from fig. 1

- **Entry 74: Dingo 2, Northern Territory, Australia – Core**
    - Schmid, S., Smith, P.M., Woltering, M., 2018. A basin-wide record of the Late Cambrian Steptoean Positive Carbon Isotope Excursion (SPICE) in the Amadeus Basin, Australia. Palaeogeogr. Palaeoclimatol. Palaeoecol. 508, 116–128. https://doi.org/10.1016/j.palaeo.2018.07.027
    - 27 analyses over 280 m
        - No analyses omitted
    - SPICE zones present: Pre, Rising, Falling
        - Does not exhibit plateau
        - Records Pre-SPICE negative kick
    - Deposited in shallow/nearshore setting in shallow water
        - Based on text in section 2
        - "Carbonate"
    - Located on paleocontinent Gondwana from 0–30° N
    - Data collected:
        - Meters and $\delta^{13}C$ and $\delta^{18}O$ values from supplementary online materials
        - Formations from fig. 6 via WPD
        - Stages from fig. 1
    - Data from the Dingo 2 core is also presented in Schmid (2017). The data presented in Schmid et al. (2018) republishes the Schmid (2017) data and also adds 49 new analyses. For this reason, only the data from the Schmid et al. (2018) paper was used in the SPICEraq.

- **Entry 75: East Johnny's Creek, Northern Territory, Australia – Core**
    - Schmid, S., Smith, P.M., Woltering, M., 2018. A basin-wide record of the Late Cambrian Steptoean Positive Carbon Isotope Excursion (SPICE) in the Amadeus Basin, Australia. Palaeogeogr. Palaeoclimatol. Palaeoecol. 508, 116–128. https://doi.org/10.1016/j.palaeo.2018.07.027
    - 26 analyses over 231.6 m
        - No analyses omitted
    - SPICE zones present: Rising, Falling
        - Does not exhibit plateau
        - No Pre-SPICE zone sampled to evaluate Pre-SPICE negative kick
    - Deposited in shallow/nearshore setting in shallow water
        - Based on text in section 2
        - "Carbonate"
    - Located on paleocontinent Gondwana from 0–30° N
    - Data collected:
        - Meters and $\delta^{13}C$ and $\delta^{18}O$ values from supplementary online materials
        - Formations from fig. 6 via WPD
        - Stages from fig. 1
    - Data from the East Johnny's Creek 1 core is also presented in Schmid et al. (2018) (entry #70). Schmid (2017) and Schmid et al. (2018) present different data sets for this core so both are included in the SPICEraq

- **Entry 76: East Mereenie 4, Northern Territory, Australia – Core**
    - Schmid, S., Smith, P.M., Woltering, M., 2018. A basin-wide record of the Late Cambrian Steptoean Positive Carbon Isotope Excursion (SPICE) in the Amadeus Basin, Australia. Palaeogeogr. Palaeoclimatol. Palaeoecol. 508, 116–128. https://doi.org/10.1016/j.palaeo.2018.07.027
    - 17 analyses over 259.1 m
        - No analyses omitted
    - SPICE zones present: Rising, Falling
        - Does not exhibit plateau
        - No Pre-SPICE zone sampled to evaluate Pre-SPICE negative kick
    - Deposited in shallow/nearshore setting in shallow water
        - Based on text in section 2
        - "Carbonate"
    - Located on paleocontinent Gondwana from 0–30° N
    - Data collected:
        - Meters and $\delta^{13}C$ and $\delta^{18}O$ values from supplementary online materials
        - Formations from fig. 6 via WPD
        - Stages from fig. 1
    - Data from the East Mereenie 4 core is also presented in Schmid (2017). The data presented in Schmid et al. (2018) republishes the Schmid (2017) data and also adds 2 new analyses. For this reason, only the data from the Schmid et al. (2018) paper was used in the SPICEraq.

- **Entry 77: GOY, Northern Territory, Australia – Measured section**
    - Schmid, S., Smith, P.M., Woltering, M., 2018. A basin-wide record of the Late Cambrian Steptoean Positive Carbon Isotope Excursion (SPICE) in the Amadeus Basin, Australia. Palaeogeogr. Palaeoclimatol. Palaeoecol. 508, 116–128. https://doi.org/10.1016/j.palaeo.2018.07.027
    - 24 analyses over 264 m
        - No analyses omitted
    - SPICE zones present: Pre, Rising, Falling
        - Exhibits plateau
        - Records Pre-SPICE negative kick
    - Deposited in shallow/nearshore setting in shallow water
        - Based on text in section 2
        - "Carbonate"
    - Located on paleocontinent Gondwana from 0–30° N
    - Data collected:
        - Meters and $\delta^{13}C$ and $\delta^{18}O$ values from supplementary online materials
        - Formations from fig. 6 via WPD
        - Stages from fig. 1

- **Entry 78: Tempe Vale 1, Northern Territory, Australia – Core**
    - Schmid, S., Smith, P.M., Woltering, M., 2018. A basin-wide record of the Late Cambrian Steptoean Positive Carbon Isotope Excursion (SPICE) in the Amadeus Basin, Australia. Palaeogeogr. Palaeoclimatol. Palaeoecol. 508, 116–128. https://doi.org/10.1016/j.palaeo.2018.07.027
    - 33 analyses over 152.3 m
        - No analyses omitted
    - SPICE zones present: Rising
        - Does not exhibit plateau
        - No Pre-SPICE zone sampled to evaluate Pre-SPICE negative kick
    - Deposited in shallow/nearshore setting in shallow water
        - Based on text in section 2
        - Dolostone
    - Located on paleocontinent Gondwana from 0–30° N
    - Data collected:
        - Meters and $\delta^{13}C$ and $\delta^{18}O$ values from supplementary online materials
        - Formations from fig. 6 via WPD
        - Stages from fig. 1

2.2 Description of entries included in the SWEETS group

Descriptions of the 17 entries in the SWEETS group follows the outline below:

- **Entry S#: Location – Type of section (Measured stratigraphic section or core)**
    - Complete reference for the original publication
    - Number of individual analyses and length (m) of complete section as published by the original authors
    - Simplified facies and water depth assigned to the section in this study
        - Reasoning for this designation
    - Paleocontinent and paleolatitude of the section based on the 500 Ma paleogeographic reconstruction in GPlates (Müller et al., 2018).
    - Reason for including this entry in the SWEETS group

- **Entry S1: Martin Point, Newfoundland, Canada – Measured section**
    - Azmy, K., 2019. Carbon-isotope stratigraphy of the SPICE event (Upper Cambrian) in eastern Laurentia: implications for global correlation and a potential reference section. Geol. Mag. 156, 1311–1322. https://doi.org/10.1017/S0016756818000638
    - 50 analyses over 107.4 m
    - Deposited in slope setting in intermediate water
        - Based on text in sections 3 and 6
    - Located on paleocontinent Laurentia from 30–60° S
    - Azmy (2019) correlates this section with four others where the SPICE event has been documented (see their fig. 6): Felix Cove, Newfoundland (Saltzman et al., 2004), Shingle Pass, Nevada (Saltzman et al., 2004), Kyrshabakty River, Kazakhstan (Saltzman et al., 2000), and the Great Basin, United States (Brasier et al., 1993). Azmy (2019) places this section chemostratigraphically above the SPICE event, with the bottom most sample correlating with the uppermost end of the falling limb. Thus, this section is entirely post-SPICE, and is not applicable to the SPICEraq but is included in the SWEETS group for completeness.

- **Entry S2: Pine Plains, New York, United States – Measured section**
    - Glumac, B., Mutti, L.E., 2007. Late Cambrian (Steptoean) sedimentation and responses to sea-level change along the northeastern Laurentian margin: Insights from carbon isotope stratigraphy. Geol. Soc. Am. Bull. 119, 623–636. https://doi.org/10.1130/B25897.1
    - 36 analyses over 398.6 m
    - Deposited in shelf setting in intermediate water
        - Based on figs. 3 & 4
    - Located on paleocontinent Laurentia from 30–60° S
    - Glumac and Mutti (2007) sampled the Stockbridge, Pine Plains, and Schodack Formations of the northern Appalachians, all three of which had previously been identified as Steptoean based on "sparse" fossil evidence. The $\delta^{13}C$ record of the Stockbridge and Pine Plains Formations shows no strong positive excursion, and Glumac & Mutti (2007) cite this as evidence that neither unit is truly Steptoean. Furthermore, a cross-plot of $\delta^{13}C$ and $\delta^{18}O$ values for the Pine Plains Formation section suggests that the values have been diagenetically altered. The lack of an easily identifiable excursion precludes inclusion of this section in the SPICEraq.

- **Entry S3: Stockbridge, Massachusetts, United States – Measured section**
    - Glumac, B., Mutti, L.E., 2007. Late Cambrian (Steptoean) sedimentation and responses to sea-level change along the northeastern Laurentian margin: Insights from carbon isotope stratigraphy. Geol. Soc. Am. Bull. 119, 623–636. https://doi.org/10.1130/B25897.1
    - 70 analyses over 395.1 m
    - Deposited in shelf setting in intermediate water
        - Based on figs. 3 & 4
    - Located on paleocontinent Laurentia from 30–60° S
    - Glumac and Mutti (2007) sampled the Stockbridge, Pine Plains, and Schodack Formations of the northern Appalachians, all three of which had previously been identified as Steptoean based on "sparse" fossil evidence. The $\delta^{13}C$ record of the Stockbridge and Pine Plains Formations shows no strong positive excursion, and Glumac & Mutti (2007) cite this as evidence that neither unit is truly Steptoean. $\delta^{13}C$ values for this section consistently hover around -2‰, which the authors suggest indicates that the section is actually Sunwaptan or Trempealeauan. The lack of an easily identifiable excursion precludes inclusion of this section in the SPICEraq.

- **Entry S4: Highgate Gorge, Vermont, United States – Measured section**
    - Glumac, B., Spivak-Birndorf, M.L., 2002. Stable isotopes of carbon as an invaluable stratigraphic tool: An example from the Cambrian of the northern Appalachians, USA. Geology 30, 563. https://doi.org/10.1130/0091-7613(2002)030<0563:SIOCAA>2.0.CO;2
    - 62 analyses over 21.2 m
    - Deposited in slope setting in deep water
        - Based on text in "Geologic Setting" section
    - Located on paleocontinent Laurentia from 30–60° S
    - The lower Gorge Formation has been proposed to be Steptoean in age (Glumac & Spivak-Birndof (2002). Landing (1983) provided biostratigraphic evidence that the section has been condensed, with strata from the late *Dunderbergia* zone missing. No positive $\delta^{13}C$ excursion is documented in the data published by Glumac & Spivak-Birndorf (2002) (values hover between 0 and -1‰), hence it's inclusion in the SWEETS group. The authors take this carbon isotope data as evidence that this section is not Steptoean in age, and that the stratigraphic gap encompasses the *Aphelaspis* zone.

- **Entry S5: Dark Canyon, South Dakota, United States – Measured section**
    - Perfetta, P.J., Shelton, K.L., Stitt, J.H., 1999. Carbon isotope evidence for deep-water invasion at the Marjumiid-Pterocephaliid biomere boundary, Black Hills, USA: A common origin for biotic crises on Late Cambrian shelves. Geology 27, 403–406. https://doi.org/10.1130/0091-7613(1999)027<0403:CIEFDW>2.3.CO;2
    - 5 analyses over 1.1 m
    - Deposited in shelf setting in intermediate water
        - Based on text in the "Introduction" and "Discussion" sections
    - Located on paleocontinent Laurentia from 0–30° S
    - Perfetta et al. (1999) document the negative excursion that immediately precedes the onset of the rising limb of the SPICE in three sections from the Black Hills, South Dakota, United States. This negative excursion correlates with the Marjumiid-Pterocephaliid extinction event. The authors interpret the negative excursion as the result of an influx of deep, cold, ^{12}C-enriched water onto the warmer and shallower shelf environment. Because these sections end within the negative excursion, they lie entirely within the pre-SPICE zone and have thus been excluded from the SPICEraq. They are included in the SWEETS group because the Perfetta et al. (1999) publication was among the first to document the negative excursion that is shown by this study to be found in the majority of SPICE-bearing sections.

- **Entry S6: Little Elk Creek, South Dakota, United States – Measured section**
    - Perfetta, P.J., Shelton, K.L., Stitt, J.H., 1999. Carbon isotope evidence for deep-water invasion at the Marjumiid-Pterocephaliid biomere boundary, Black Hills, USA: A common origin for biotic crises on Late Cambrian shelves. Geology 27, 403–406. https://doi.org/10.1130/0091-7613(1999)027<0403:CIEFDW>2.3.CO;2
    - 17 analyses over 4.3 m
    - Deposited in shelf setting in intermediate water
        - Based on text in the "Introduction" and "Discussion" sections
    - Located on paleocontinent Laurentia from 0–30° S
    - Perfetta et al. (1999) document the negative excursion that immediately precedes the onset of the rising limb of the SPICE in three sections from the Black Hills, South Dakota, United States. This negative excursion correlates with the Marjumiid-Pterocephaliid extinction event. The authors interpret the negative excursion as the result of an influx of deep, cold, ^{12}C-enriched water onto the warmer and shallower shelf environment. Because these sections end within the negative excursion, they lie entirely within the pre-SPICE zone and have thus been excluded from the SPICEraq. They are included in the SWEETS group because the Perfetta et al. (1999) publication was among the first to document the negative excursion that is shown by this study to be found in the majority of SPICE-bearing sections.

- **Entry S7: Moll, South Dakota, United States – Measured section**
    - Perfetta, P.J., Shelton, K.L., Stitt, J.H., 1999. Carbon isotope evidence for deep-water invasion at the Marjumiid-Pterocephaliid biomere boundary, Black Hills, USA: A common origin for biotic crises on Late Cambrian shelves. Geology 27, 403–406. https://doi.org/10.1130/0091-7613(1999)027<0403:CIEFDW>2.3.CO;2
    - 10 analyses over 5.0 m
    - Deposited in shelf setting in intermediate water
        - Based on text in the "Introduction" and "Discussion" sections
    - Located on paleocontinent Laurentia from 0–30° S
    - Perfetta et al. (1999) document the negative excursion that immediately precedes the onset of the rising limb of the SPICE in three sections from the Black Hills, South Dakota, United States. This negative excursion correlates with the Marjumiid-Pterocephaliid extinction event. The authors interpret the negative excursion as the result of an influx of deep, cold, ^{12}C-enriched water onto the warmer and shallower shelf environment. Because these sections end within the negative excursion, they lie entirely within the pre-SPICE zone and have thus been excluded from the SPICEraq. They are included in the SWEETS group because the Perfetta et al. (1999) publication was among the first to document the negative excursion that is shown by this study to be found in the majority of SPICE-bearing sections.

- **Entry S8: Cow Head Peninsula, Newfoundland, Canada – Measured section**
    - Pruss, S.B., Castagno, K.A., Fike, D.A., Hurtgen, M.T., 2016. Carbon isotope ($\delta^{13}C_{carb}$) heterogeneity in deep-water Cambro-Ordovician carbonates, western Newfoundland. Palaeogeogr. Palaeoclimatol. Palaeoecol. 458, 52–62. https://doi.org/10.1016/j.palaeo.2015.10.004
    - 243 analyses over 255.7 m
    - Deposited in slope setting in deep water
        - Based on text in sections 2 and 6
    - Located on paleocontinent Laurentia from 30–60° S
    - Pruss et al. (2016) studied the Cow Head Group in Newfoundland, the deep-water equivalent of the shallow water members of the Port au Port Group investigated by Hurtgen et al. (2009) and Saltzman et al. (2004). Despite documentation of the SPICE in the shallower settings, Pruss et al. (2016) found no evidence for the SPICE event in the Cow Head Group. They suggested that the excursion is missing from the $\delta^{13}C$ record because the deeper water section is significantly condensed, as evidenced by biostratigraphy (Pruss et al., 2016).

- **Entry S9: Outcrop 1, Missouri, United States – Measured section**
    - Jeffrey, M.J., 2017. Stratigraphic variation of the Late Cambrian SPICE event in Upper Cambrian carbonates of Southern Missouri (M.S. thesis). University of Missouri-Columbia.
    - 20 analyses over 6.7 m
    - Deposited in intrashelf basin setting in intermediate water
        - Based on deposition of section within the Central Missouri Intrashelf Basin
    - Located on paleocontinent Laurentia from 0–30° S
    - Outcrop 1 spans the uppermost Bonneterre Dolomite to the lowermost Davis Formation. The majority of $\delta^{13}C$ analyses hover around 0.5‰, while the upper 7 analyses record an ~2.0‰ positive excursion. The entire section is less than 7 meters in length and comprises only 20 analyses. The Bonneterre Dolomite and Davis Formation are known to capture the SPICE event in a suite of other sections from Missouri. While it is plausible that this excursion captures at least part of the rising limb of the SPICE, this remains inconclusive without gathering further information. Because it may tentatively capture part of the SPICE, we have included it in the SWEETS group for completeness.

- **Entry S10: Outcrop 2, Missouri, United States – Measured section**
    - Jeffrey, M.J., 2017. Stratigraphic variation of the Late Cambrian SPICE event in Upper Cambrian carbonates of Southern Missouri (M.S. thesis). University of Missouri-Columbia.
    - 8 analyses over 4.3 m
    - Deposited in intrashelf basin setting in intermediate water
        - Based on deposition of section within the Central Missouri Intrashelf Basin
    - Located on paleocontinent Laurentia from 0–30° S
    - Outcrop 2 lies entirely within the Davis Formation. The bottom half of the section records $\delta^{13}C$ analyses around 0‰, while the upper half records an ~2.75‰ positive excursion. The entire section is less than 4.5 meters in length and comprises only 8 analyses. The Bonneterre Dolomite and Davis Formation are known to capture the SPICE event in a suite of other sections from Missouri. While it is plausible that this excursion captures at least part of the rising limb of the SPICE, this remains inconclusive without gathering further information. Because it may tentatively capture part of the SPICE, we have included it in the SWEETS group for completeness.

- **Entry S11: Cerro La Silla, San Juan, Argentina – Measured section**
    - Sial, A.N., Peralta, S., Ferreira, V.P., Toselli, A.J., Aceñolaza, F.G., Parada, M.A., Gaucher, C., Alonso, R.N., Pimentel, M.M., 2008. Upper Cambrian carbonate sequences of the Argentine Precordillera and the Steptoean C-Isotope positive excursion (SPICE). Gondwana Res. 13, 437–452. https://doi.org/10.1016/J.GR.2007.05.001
    - 55 analyses over 1120.7 m
    - Deposited in shallow/nearshore setting in shallow water
        - Based on text in "Geologic Setting" section
    - Located on paleocontinent Gondwana from 30–60° S
    - Sial et al. (2008) presents data from three Upper Cambrian sections in the Argentine Precordillera. In one of these sections, the rising limb of the SPICE event is captured within the Flecha Formation and is included in the SPICEraq as entry #40. The other two sections have instead been included in the SWEETS group, including the Cerro La Silla section which captures the upper Cambrian Flecha Formation, the Cambrian-Ordovician Silla Formation, and the lowermost Ordovician San Juan Formation. Sial et al. (2008) identify an ~1‰ positive excursion in the uppermost Flecha Formation as the SPICE event. However, the $\delta^{13}C$ record is quite variable and vacillates between -1.5‰ and 0.0‰ for its majority; the noisiest interval immediately overlies this proposed SPICE event. We were not confident enough in the designation of this excursion as the SPICE event to include it in the SPICEraq and all subsequent analyses. It is possible that this section does capture some or all of the SPICE event, which is why we chose to place this section in the SWEETS group instead of discarding it completely.

- **Entry S12: Quebrada de La Flechas, San Juan, Argentina – Measured section**
    - Sial, A.N., Peralta, S., Ferreira, V.P., Toselli, A.J., Aceñolaza, F.G., Parada, M.A., Gaucher, C., Alonso, R.N., Pimentel, M.M., 2008. Upper Cambrian carbonate sequences of the Argentine Precordillera and the Steptoean C-Isotope positive excursion (SPICE). Gondwana Res. 13, 437–452. https://doi.org/10.1016/J.GR.2007.05.001
    - 104 analyses over 1136.0 m
    - Deposited in shallow/nearshore setting in shallow water
        - Based on text in "Geologic Setting" section
    - Located on paleocontinent Gondwana from 30–60° S
    - Sial et al. (2008) presents data from three Upper Cambrian sections in the Argentine Precordillera. In one of these sections, the rising limb of the SPICE event is captured within the Flecha Formation and is included in the SPICEraq as entry #40. The other two sections have instead been included in the SWEETS group for the purposes of this study; Quebrada de La Flechas is the second of these sections. Quebrada de La Flechas spans the Cambrian Zonda and Flecha Formations. The bottom-most four samples in the section capture an ~2.5‰ excursion, which the authors tentatively suggest may correspond to the falling limb of the SPICE. Because of the lack of certainty in this designation, as well as the lack of greater carbon isotope context below this anomaly, we have opted to include this section in the SWEETS group rather than in the SPICEraq.

- **Entry S13: Andrarum 3, Scania, Sweden – Core**
    - Ahlberg, P., Axheimer, N., Babcock, L.E., Eriksson, M.E., Schmitz, B., Terfelt, F., 2009. Cambrian high-resolution biostratigraphy and carbon isotope chemostratigraphy in Scania, Sweden: first record of the SPICE and DICE excursions in Scandinavia. Lethaia 42, 2–16. https://doi.org/10.1111/j.1502-3931.2008.00127.x
    - 19 analyses over 28.7 m
    - Deposited in shallow/nearshore setting in shallow water
        - Based on text in "Geologic Setting" section
    - Located on paleocontinent Baltica from 30–60° S
    - Entry #S13 is from the Andrarum-3 drill core in southern Sweden (Ahlberg et al., 2009). The Andrarum-3 drill core is a well-known example of the SPICE in $\delta^{13}C_{org}$ isotopes, where it is recorded as an approximately 2‰ positive excursion. In addition to their $\delta^{13}C_{org}$ analyses, Ahlberg et al. (2009) also collected 19 samples for whole-rock carbon analyses. They documented an approximately 9‰ positive excursion but found that the individual $\delta^{13}C_{carb}$ values were indicative of diagenetic alteration (values range from -16.87‰ to -0.17‰). These data were thus excluded from the SPICEraq and all subsequent analyses but were included in the SWEETS group for completeness.

- **Entry S14: Tangwangzhai, Shandong Province, North China – Measured section**
    - Huang, J., Chen, Y., Chu, X., Sun, T., 2019. The geochemistry of the late Cambrian carbonate in North China: the Steptoean Positive Carbon Isotope Excursion (SPICE) record suppressed in a coastal condition? Geol. Mag. 156, 1805–1819. https://doi.org/10.1017/S0016756819000025
    - 71 analyses over 120.4 m
    - Deposited in shallow/nearshore setting in shallow water
        - Based on text in the Abstract and section 6
    - Located on paleocontinent Gondwana from 0–30° S
    - Huang et al. (2019) sampled a biostratigraphically constrained, shallow marine section near Tangwangzhai, North China. $\delta^{13}C$ values hover between 0 and +1‰ for the majority of the sampled interval, with a slight positive increase shown in the lowermost Chaomidian Formation interpreted as the SPICE. The excursion is weak, with a peak value of +1.68‰, and located within one of the noisiest intervals of data; identification of SPICE zones is not possible, hence it's inclusion in the SWEETS group. The Tangwangzhai section was also sampled by Zhu et al., 2004 (Entry #62), which shows a pronounced 2.2‰ positive carbon isotope excursion in the lowermost Changshan Formation which is equivalent to the lower portion Chaomidian Formation (BGMRSP, 1996; Chough et al., 2010). Huang et al. (2019) noted the presence of an unconformity between the Gushan Formation and the overlying Chaomidian Formation in their measured section. It is possible that some or all of the record of the SPICE is missing as a result of this erosion. It is additionally unclear whether Huang et al. (2019) and Zhu et al. (2004) sampled the exact same section, or if they sampled neighboring sections.

- **Entry S15: Sanjiang, Guangxi Province, South China – Measured section**
    - Peng, Yang, Peng, Yongbo, Lang, X., Ma, H., Huang, K., Li, F., Shen, B., 2016. Marine Carbon-Sulfur Biogeochemical Cycles during the Steptoean Positive Carbon Isotope Excursion (SPICE) in the Jiangnan Basin, South China. J. Earth Sci. 27, 242–254. https://doi.org/10.1007/s12583-016-0694-4
    - 55 analyses over 87.7 m
    - Deposited in basin setting in deep water
        - Based on fig. 1 and text in section 1
    - Located on paleocontinent Gondwana from 0–30° N
    - Peng et al. (2016) describe the Sanjiang section as capturing the SPICE event. Because the age of the sampled Qingxi Formation is poorly constrained, this assertion is predominantly based on the correlation of positive shifts in $\delta^{13}C$ and $\delta^{34}C$. This relationship is observed in other SPICE-bearing sections. In the ~90 m section, $\delta^{13}C$ rises slowly from ~-3.5‰ to ~3.2‰, while $\delta^{34}S$ rises slowly from ~+1‰ to ~40‰. Despite this concurrent rise in both values, the Sanjiang section has been included in the SWEETS group rather than the SPICEraq, particularly because the slow, relatively monotonic rise in $\delta^{13}C$ values makes it quite difficult to identify the SPICE zones used in this study to quantify and describe the excursion.

- **Entry S16: Jiagou, Anhui Province, North China – Measured section**
    - Wang, Z., Chen, J., Liang, T., Yuan, J., Han, C., Liu, J., Zhu, C., Zhu, D., Han, Z., 2020. Spatial variation in carbonate carbon isotopes during the Cambrian SPICE event across the eastern North China Platform. Palaeogeogr. Palaeoclimatol. Palaeoecol. 546, 109669. https://doi.org/10.1016/j.palaeo.2020.109669
    - 43 analyses over 36.7 m
    - Deposited in shallow/nearshore setting in shallow water
        - Based on text in section 6
    - Located on paleocontinent Gondwana from 0–30° S
    - Wang et al. (2020) presents a suite of six sections from the epeiric sea of the North China platform. Four of the six sections capture at least part of the rising limb of the SPICE event and are included in the SPICEraq (entries #57-60). Wang et al. (2020) correlate all six sections in fig. 6; they place the Jiagou section entirely within the Furongian and correlate samples at the 10 m mark with samples in the post-SPICE zone of other sections. While the bottom most samples in the Jiagou section display elevated $\delta^{13}C$ values relative the rest of the section, they peak around +1‰. Because this section does not cross the Furongian/Miaolingian boundary and does not capture what is unequivocally a portion of the SPICE event, we have elected to place this section within the SWEETS group and not the SPICEraq.

- **Entry S17: Shashan, Liaoning Province, North China – Measured section**
    - Wang, Z., Chen, J., Liang, T., Yuan, J., Han, C., Liu, J., Zhu, C., Zhu, D., Han, Z., 2020. Spatial variation in carbonate carbon isotopes during the Cambrian SPICE event across the eastern North China Platform. Palaeogeogr. Palaeoclimatol. Palaeoecol. 546, 109669. https://doi.org/10.1016/j.palaeo.2020.109669
    - 63 analyses over 20.5 m
    - Deposited in shallow/nearshore setting in shallow water
        - Based on text in section 6
    - Located on paleocontinent Gondwana from 0–30° N
    - Wang et al. (2020) presents a suite of six sections from the epeiric sea of the North China platform. Four of the six sections capture at least part of the rising limb of the SPICE event and are included in the SPICEraq (entries #57-60). Wang et al. (2020) correlate all six sections in their fig. 6; they place the Shashan section entirely within the Furongian and indicate that the bottom of this section is "roughly connected" to the Baijiashan section. The Baijiashan section captures the entire rising limb, a plateau, and part of the falling limb of the SPICE event. While the bottom most samples in the Shashan section potentially capture the uppermost region of the falling limb, we have elected to place this section within the SWEETS group and not the SPICEraq because of the dubious connection between it and the Baijiashan section.

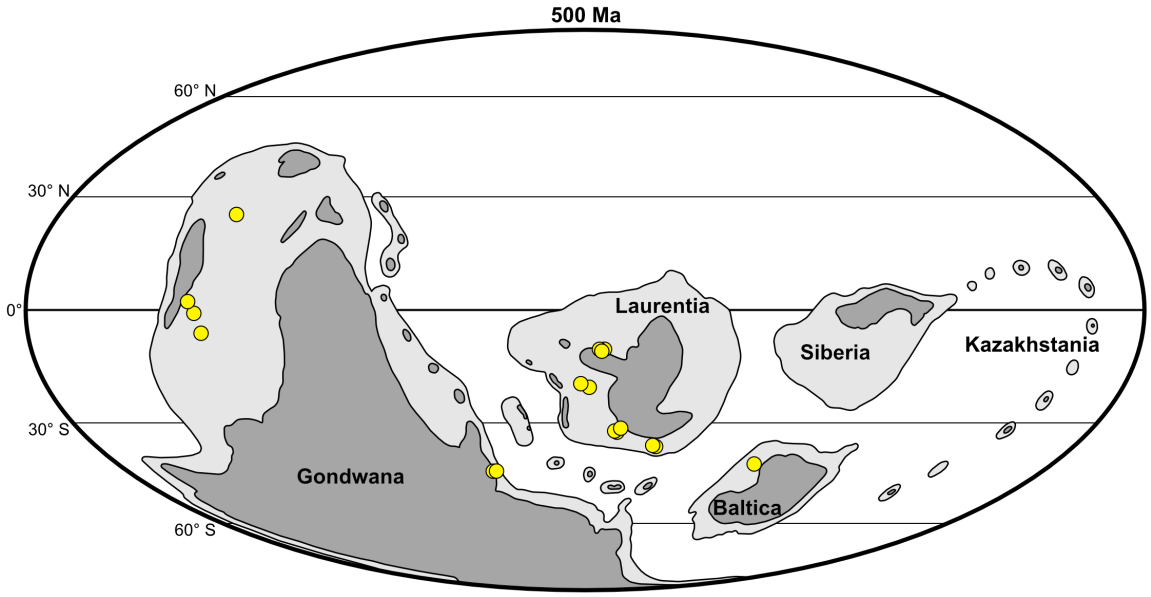

Figure 2-1. Paleogeographic map ca. 500 Ma showing the approximate locations of all 17 SWEETS entries marked by yellow circles. The dark gray denotes exposed continental land masses, whereas the light gray denotes continental shelves. Reconstruction based on the 500 Ma raster in GPlates (Müller et al., 2018).

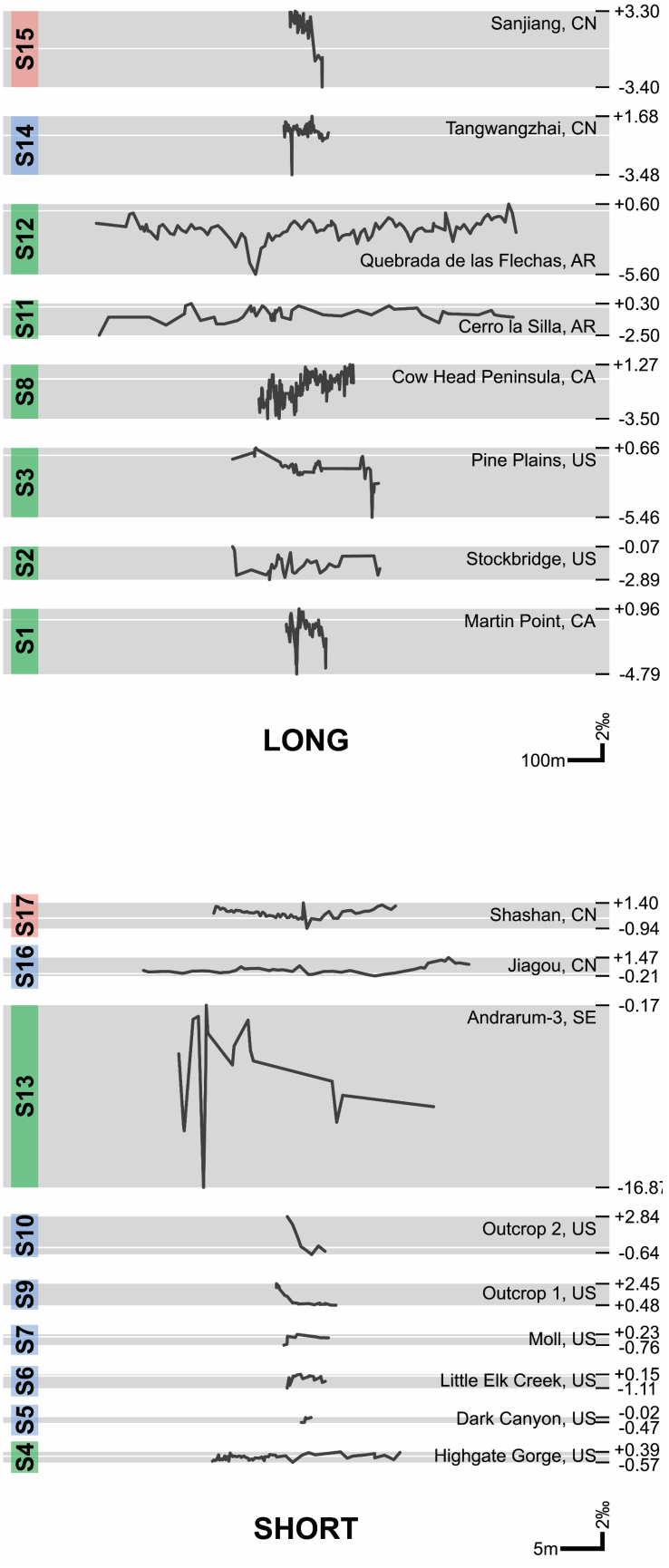

Figure 2-2. Carbon isotope data for all SWEETS entries. For details on interpreting this figure, see Table 1-2 in Chapter 1.

2.3 Evaluations of published figures vs. published data tables using WebPlot Digitizer

Four entries have been selected to document the utility of WebPlot Digitizer (WPD; Rohatgi, 2019) for extracting numerical data from published figures (Fig. 2-3). All identifying information, including precise meterage and $\delta^{13}C$ values, has been intentionally removed from Fig. 2-3 to preserve the anonymity of the original authors. While we did find some discrepancies, as detailed below, the goal here was not to lambast previous authors for poorly constructed figures, and hence the removal of any identifying features from these plots. Rather, we tested all published figures associated with SPICEraq and SWEETS entries to ensure accuracy and precision in data reporting and visualization. We provide from this exercise two important observations: (1) it illustrates the usefulness and reliability of WPD as a method for extracting accurate information from figures if data tables are unavailable; (2) it also illustrates that figures may not always be the most reliable source from which to retrieve numerical data, owing to errors in figure construction. If data tables are also available, they should be used as the primary record. In all possible cases, data tables have been used as the primary source in the SPICEraq; WPD-extracted data were only utilized if necessitated by the absence of published data tables.

Fig. 2-3 illustrates a few key differences in the level of agreement between published figures and in-text or supplemental data tables. For the large majority of entries, these data sets were quite agreeable and returned nearly identical data points in terms of both stratigraphic height and $\delta^{13}C$ value (examples shown in Fig. 2-3a–b). Because the majority of entries were agreeable, we considered WPD to be a reliable method for extracting data from figures and thus used it to obtain data from those publications that did not provide data tables—primarily as a means to increase the comprehensiveness of our dataset.

In some cases, however, WPD data extractions from figures did not agree with the data provided in tables (examples shown in Fig. 2-3c–d). The original published figures illustrating the entries shown in Fig. 2-3c–d were each evaluated twice in WPD, with the axes and data points demarcated anew both times to ensure that the WPD evaluation was correct. In both cases, the two WPD curves plotted directly atop each other, indicating that discrepancies between WPD and the published figures were not a result of user error. In the cases of poor agreement, two important types of differences were noted. (1) Data points were offset by some margin, either stratigraphically (y-axis errors), isotopically (x-axis errors), or sometimes both. In the examples illustrated in Fig. 2-3 c–d, the WPD-extracted points from the published figures are shifted vertically relative to the points from their corresponding published data tables, indicating discrepancies in the stratigraphic height values ranging from ~1.5 m to ~4 m. If offset was instead on the x-axis, such errors instead produced discrepancies in $\delta^{13}C$ values. (2) Some errors appeared to be the result of inappropriate plot boundary choices. That is, the plot boundaries chosen for published figures cut off, or excluded, some of the data points that were included in the published tables. In other cases, data reported in data tables are sometimes inexplicably missing from figure plots even with appropriate plot boundaries. Fig. 2-3c illustrates the former type of omission error: four negative $\delta^{13}C$ data points were excluded from the published figure because of the placement of the lower boundary of the plot, but those data points were still included in the associated supplementary online materials. We must note that in no way are we suggesting intentional falsification or otherwise malicious manipulation of data; it is certainly likely that discrepancies between tables and figures are accidental. In the process of creating publication-ready figures, there are many opportunities to accidentally shift the data points without realizing that it has happened. However, the choice of where to place plot boundaries is entirely up to the author's discretion,

and caution should be exercised to avoid data exclusion. If there is a justifiable reason for excluding data (for instance, high errors in measurements or similar), authors should be explicit and transparent about this reasoning. Figures should be created to visually present the collected suite of data; when constructing and assembling data plot figures, care should be taken to ensure that the figure accurately and precisely represents the complete and unaltered data.

Figure 2-3. Comparison of WPD evaluations of published figures vs. published data tables of four select entries from the SPICEraq. All identifying information, including meter and $\delta^{13}C$ values, have been removed to preserve the anonymity of the original authors. Data as presented in published tables (either in text or supplemental) are shown in red, while data illustrated in figures and assessed with WPD are shown in blue. (a & b) show examples of good agreement between tables and figures. (c & d) show examples of poor agreement between tables and figures, either as a result of data offset or data exclusion because of plot boundary placement

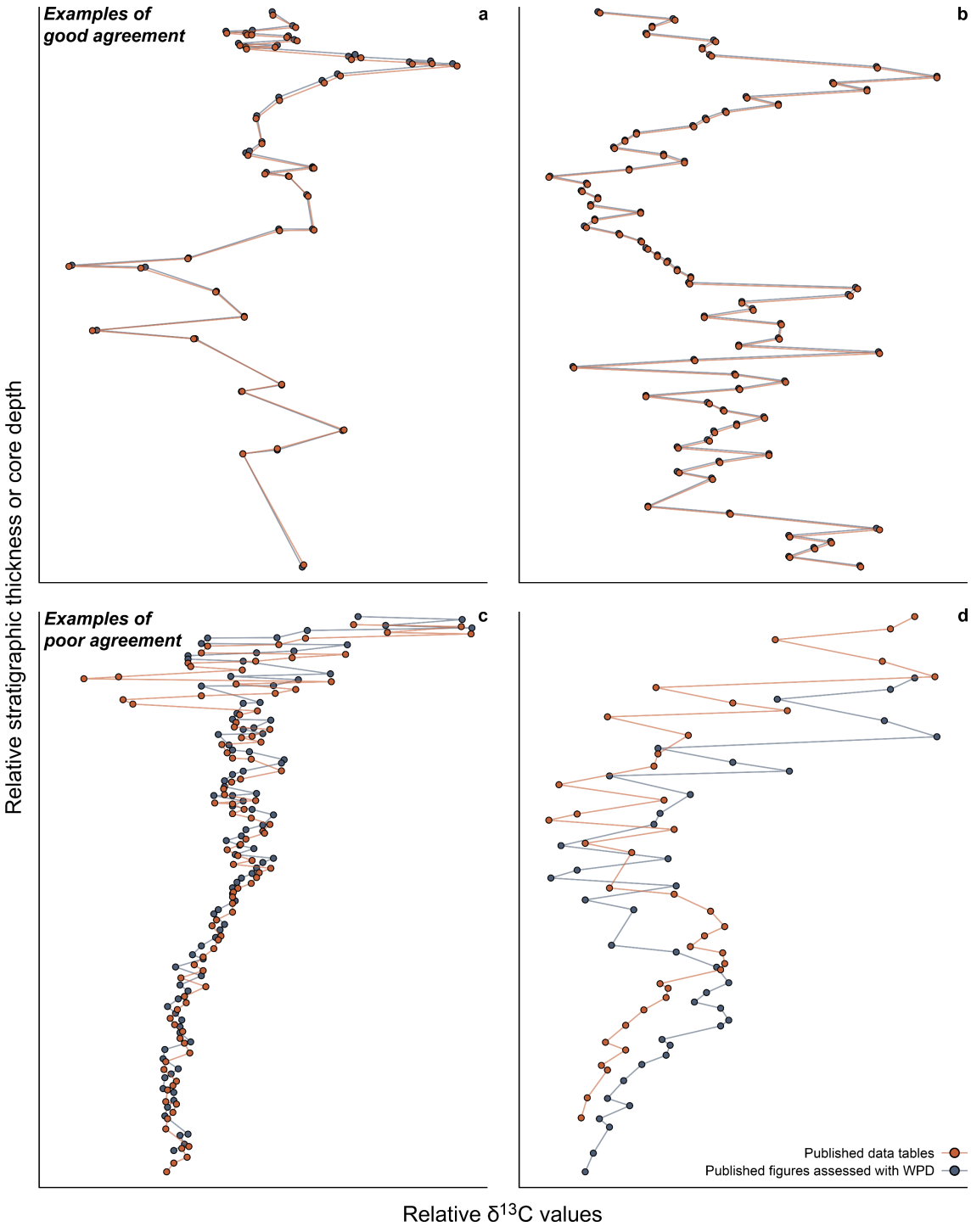
Examples of good agreement
a
b
Examples of poor agreement
c
d
Relative stratigraphic thickness or core depth
Relative δ13C values
Published data tables
Published figures assessed with WPD

2.4 Additional supplemental figures with associated captions and brief descriptions

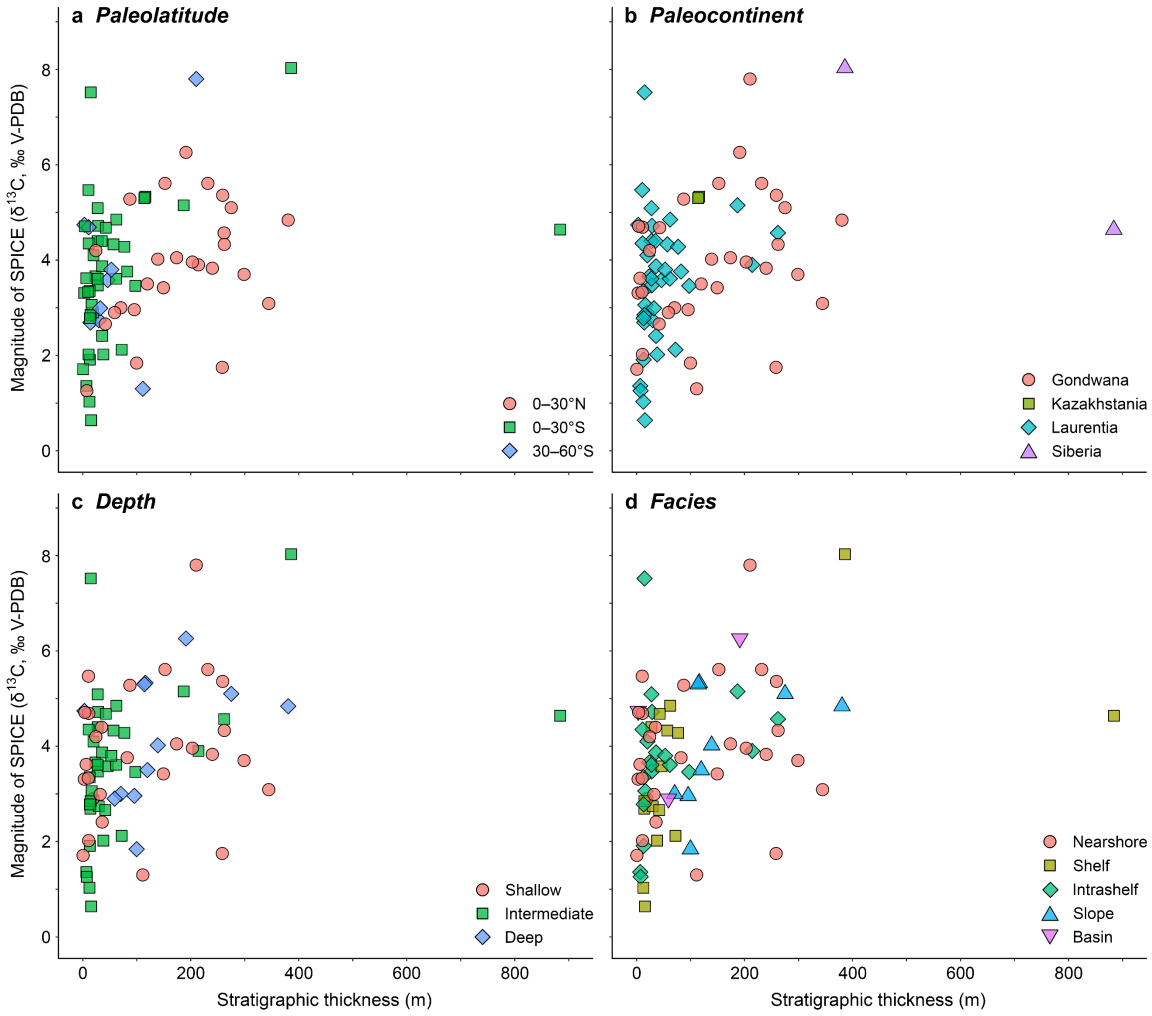

Figure 2-4. Total stratigraphic thickness of the SPICE event. XY-scatter plots comparing the magnitude of the SPICE event (the difference between the maximum and minimum $\delta^{13}C$ values of the rising limb) to the stratigraphic thickness (in meters) of the total SPICE excursion (Rising limb + Plateau [if present] + Falling limb). Entries are labelled according to the following grouping variables: (a) paleolatitudinal zone; (b) paleocontinent; (c) water-depth; (d) facies.

Figure 2-5. Stratigraphic thickness of the total excursion (rising limb + plateau [if present] + falling limb) by the four primary grouping variables. From top to bottom, these box-and-whisker plots are organized as follows: (a) paleolatitude, (b) paleocontinent, (c) water depth, and (d) facies. Black dots overprinted on the box and whisker plots show the stratigraphic thickness of the rising limb of individual entries. The colored boxes show the interquartile range (IQR = Q3-Q1) of the distribution, with the center black line indicating the median value. Solid line whiskers extend beyond the box by a factor of 1.5 * IQR, where the upper whisker = min(max(x), Q3 + 1.5 * IQR) and the lower whisker = max(min(x), Q1 - 1.5 * IQR). Dashed line whiskers extend to the absolute minimum or maximum of the distribution, if necessary.

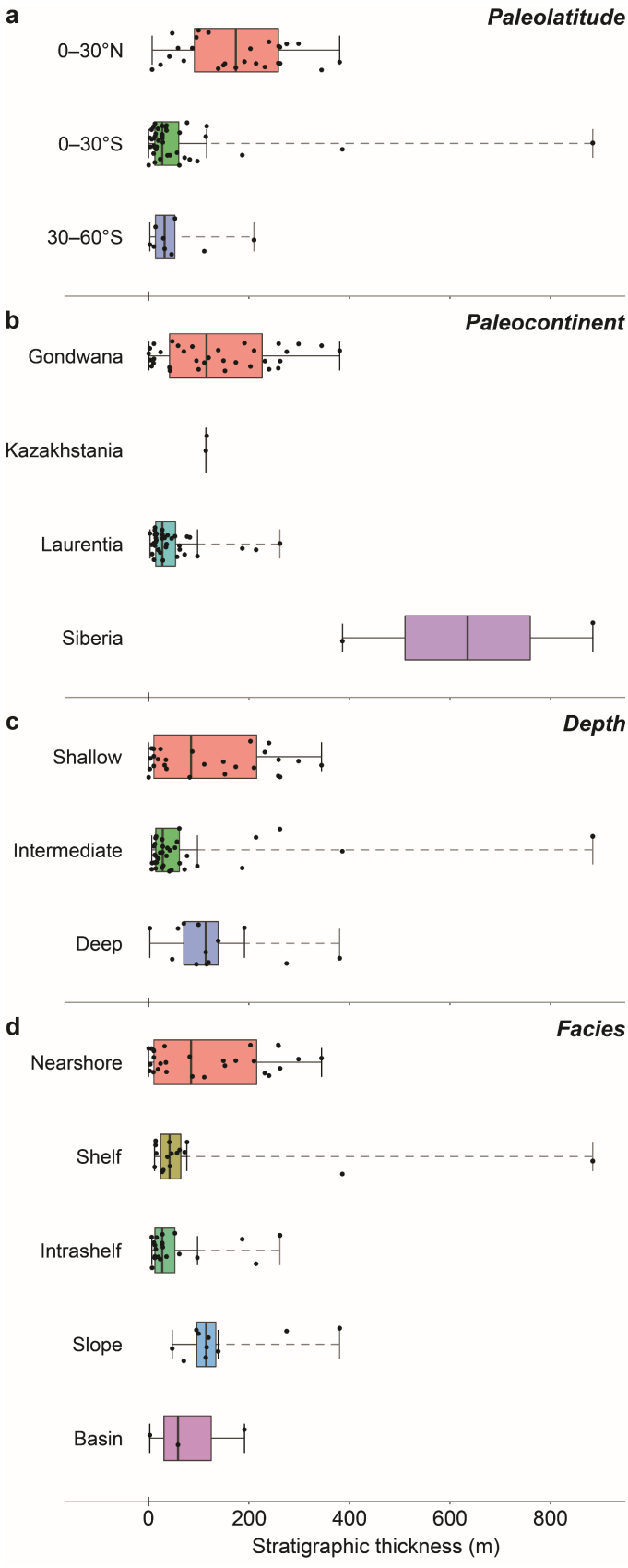
a
Paleolatitude
0–30°N
0–30°S
30–60°S
b
Paleocontinent
Gondwana
Kazakhstania
Laurentia
Siberia
c
Depth
Shallow
Intermediate
Deep
d
Facies
Nearshore
Shelf
Intrashelf
Slope
Basin
0
200
400
600
800
Stratigraphic thickness (m)

Figure 2-6. Stratigraphic thickness of the rising limb by the four primary grouping variables. From top to bottom, these box-and-whisker plots are organized as follows: (a) paleolatitude, (b) paleocontinent, (c) water depth, and (d) facies. Black dots overprinted on the box and whisker plots show the stratigraphic thickness of the rising limb of individual entries. The colored boxes show the interquartile range (IQR = Q3-Q1) of the distribution, with the center black line indicating the median value. Solid line whiskers extend beyond the box by a factor of 1.5 * IQR, where the upper whisker = min(max(x), Q3 + 1.5 * IQR) and the lower whisker = max(min(x), Q1 - 1.5 * IQR). Dashed line whiskers extend to the absolute minimum or maximum of the distribution, if necessary.

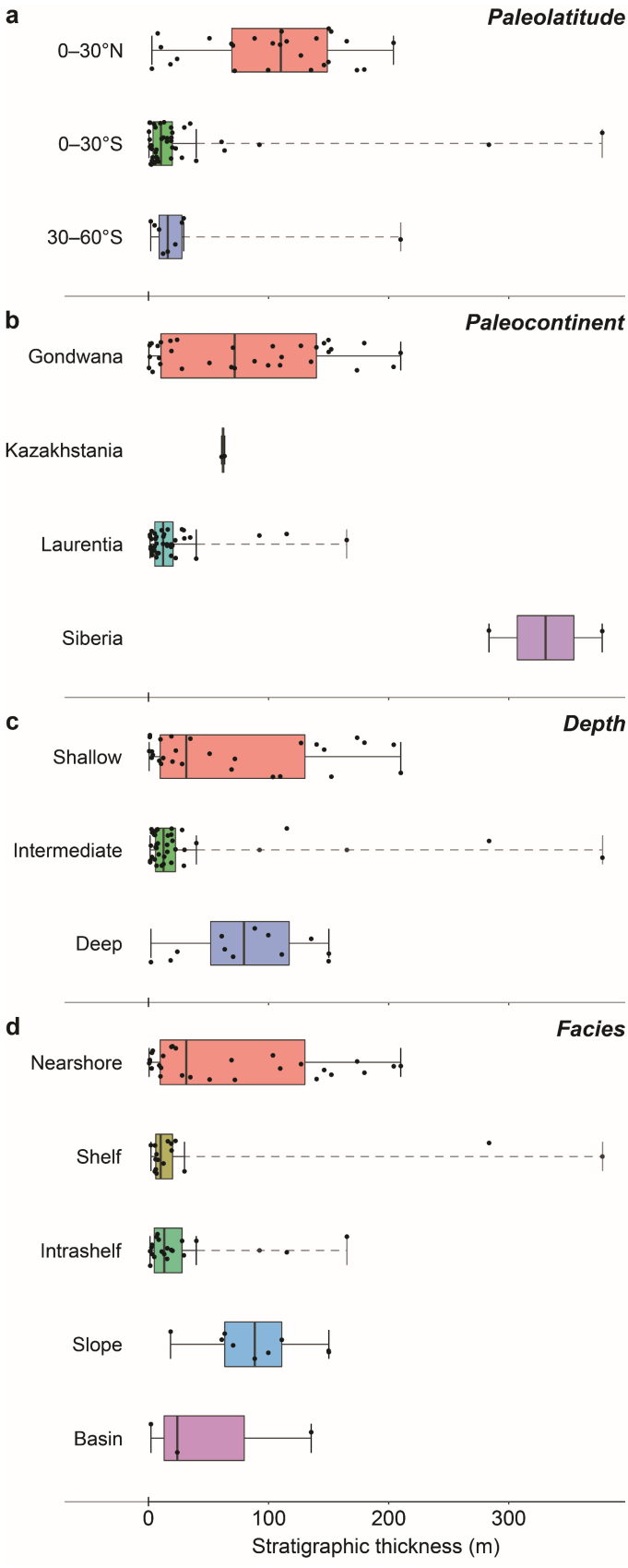
a
Paleolatitude
0–30°N
0–30°S
30–60°S
b
Paleocontinent
Gondwana
Kazakhstania
Laurentia
Siberia
c
Depth
Shallow
Intermediate
Deep
d
Facies
Nearshore
Shelf
Intrashelf
Slope
Basin
0
100
200
300
Stratigraphic thickness (m)

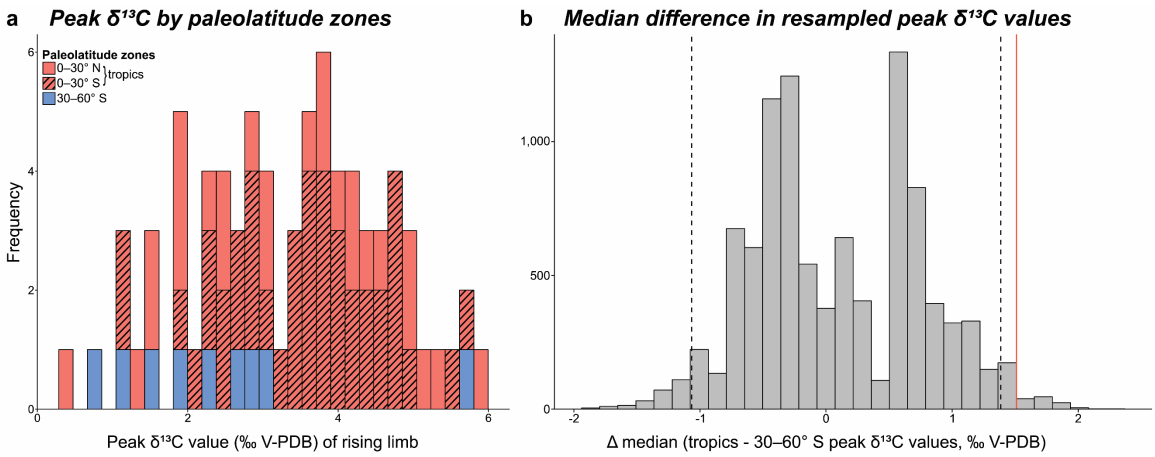

Figure 2-7. Randomization analysis of peak $\delta^{13}C$ values across paleolatitude. (a) Stacked histogram showing peak rising limb $\delta^{13}C$ values (‰), grouped according the paleolatitudinal zone. In order to evaluate the statistical significance of the apparently lower peak $\delta^{13}C$ values for sections from 30–60° S (n = 9) relative to lower latitudes, sections from 0–30° N and 0–30° S were grouped into one "tropical" bin (n = 68). (Note: we diverge from the color scheme used in other paleolatitude figures to better visually illustrate that the tropical paleolatitude bins have been grouped for this analysis, although the frequency of each is visibly separated by the addition of the diagonal hatching on the 0–30°S bin.) (b) Results from the randomization analysis. All peak rising limb $\delta^{13}C$ values (n = 77) were resampled without replacement and assigned to one of the two bins while preserving original sample sizes. The difference between median $\delta^{13}C$ value for each of the two randomized samples was calculated (tropical bin minus 30–60° S bin). Thus, a positive value indicates that a higher median peak $\delta^{13}C$ value was calculated for the 30°N–30° S sections, while a negative value indicates that a higher median peak $\delta^{13}C$ value was calculated for the 30–60°S sections. This randomization was repeated 10,000 times; and the sampling distribution of differences in median $\delta^{13}C$ values are plotted as a histogram. The 95% confidence limits were calculated as the 2.5 and 97.5 percentile values of the sampling distribution (black dashed lines), and the empirical difference in $\delta^{13}C$ values for tropical sections relative to 30–60° S sections was overlain on the plot (red line). As illustrated above, the actual difference in peak $\delta^{13}C$ values falls outside the 95% confidence limits for randomly selected samples and thus indicates that the peak $\delta^{13}C$ value for 30–60° S sections is statistically significantly lower than the peak $\delta^{13}C$ value for tropical sections.

To examine trends in the onset and peak values of the SPICE, forest plots were constructed to organize the entries in order of ascending minimum or maximum $\delta^{13}C$ value of the rising limb (Figs. 2-8 & 2-9, next two pages). All sections deposited between 30–60°S have minimum onset $\delta^{13}C$ values <0‰, whereas the other paleolatitude zones show no clear trends (Fig. 2-8a). All 30–60°S sections, except for entry #40, have maximum rising limb $\delta^{13}C$ values of ~+0.8 to +3.0‰ (Fig. 2-8b). Although there is a minor amount of overlap between shallow and deep-water sections, most shallow water sections have minimum onset values <0‰ (Fig. 2-9a), whereas most deep-water sections have minimum onset values ≥-0.70‰ (Fig. 2-9a). Plotting the sections by the maximum $\delta^{13}C$ value of the rising limb shows that the majority of deep-water sections have peaks ≥+3‰ (Fig. 2-9b).

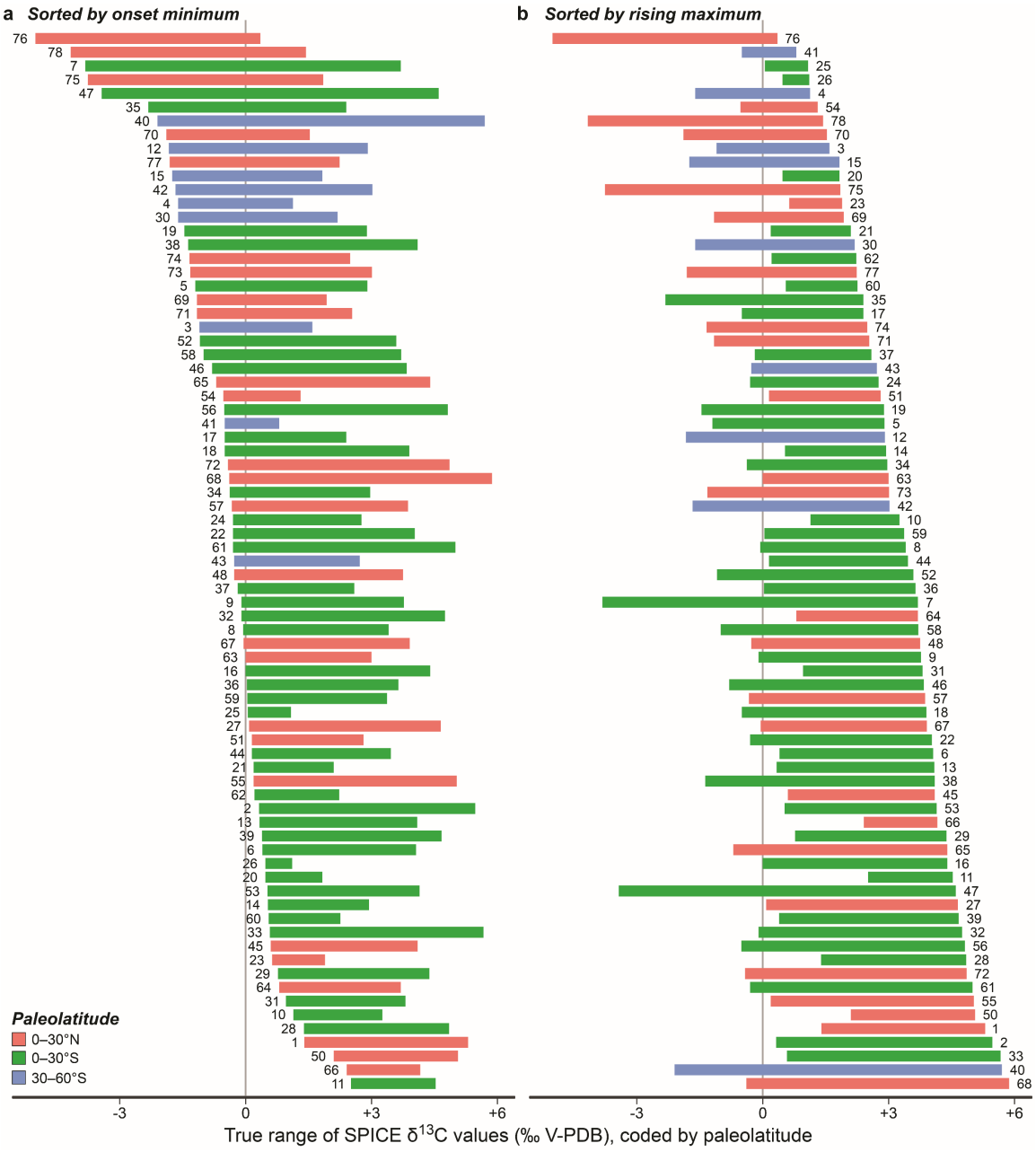

Figure 2-8. Distribution of onset and peak $\delta^{13}C$ values of the rising limb of the SPICE. Forest plots illustrate the magnitude of the $\delta^{13}C$ excursion of the SPICE event recorded in each entry, organized according to ascending minimum or maximum $\delta^{13}C$ value and colored by paleolatitude. Colored bars illustrate the magnitude of the rising limb for individual sections; the adjacent numbers denote the corresponding entry number in the SPICEraq. In (a), sections are sorted by ascending minimum $\delta^{13}C$ value of the rising limb; in (b) sections are sorted by ascending maximum $\delta^{13}C$ value of the rising limb.

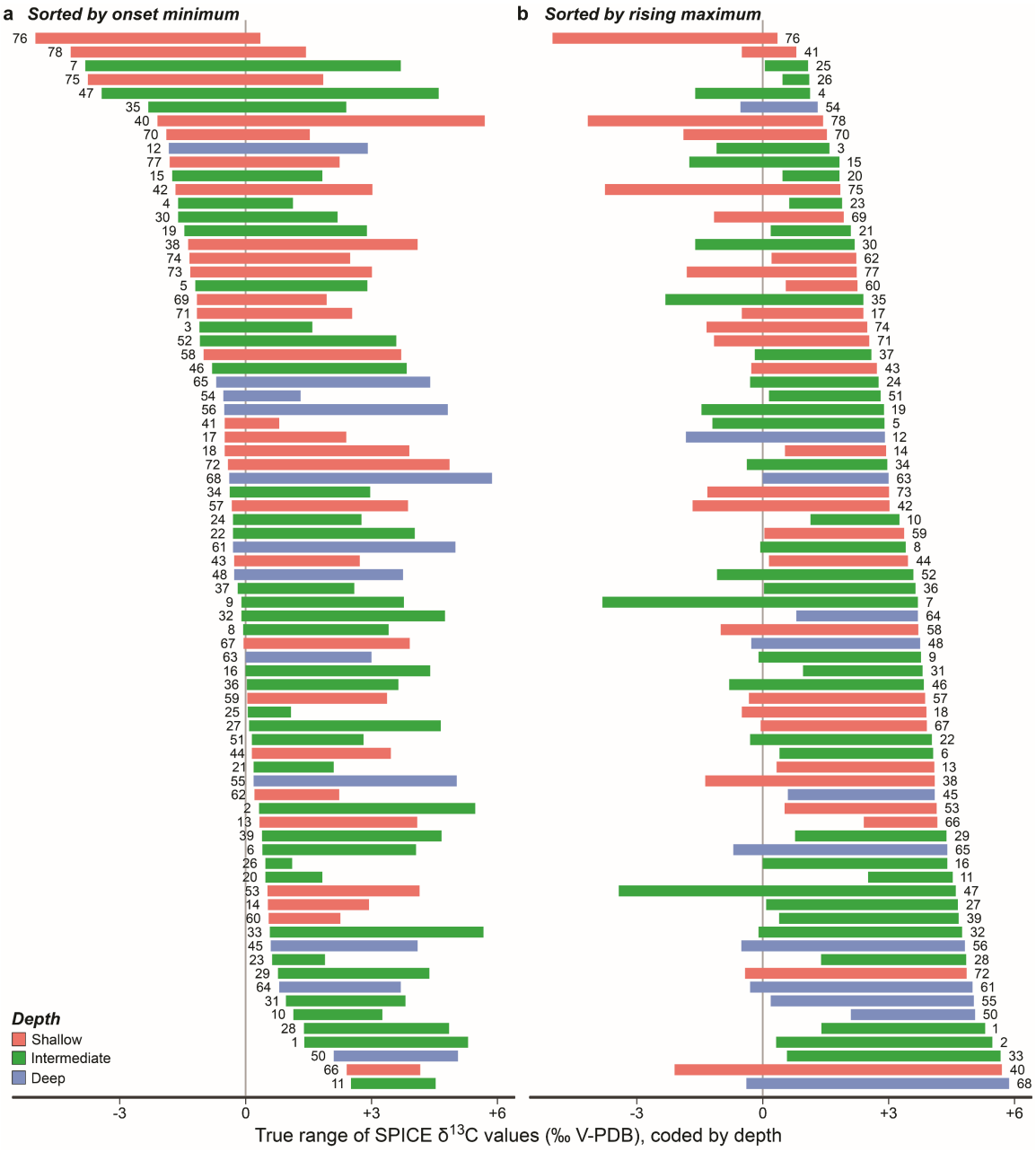

Figure 2-9. Distribution of onset and peak $\delta^{13}C$ values of the rising limb of the SPICE. Forest plots illustrate the magnitude of the $\delta^{13}C$ excursion of the SPICE event recorded in each entry, organized according to ascending minimum or maximum $\delta^{13}C$ value and colored by water depth. Colored bars illustrate the magnitude of the rising limb for individual sections; the adjacent numbers denote the corresponding entry number in the SPICEraq. In (a), sections are sorted by ascending minimum $\delta^{13}C$ value of the rising limb; in (b) sections are sorted by ascending maximum $\delta^{13}C$ value of the rising limb.

Figure 2-10 illustrates the degree to which pre- and post-SPICE median $\delta^{13}C$ values differ within a single entry (calculated as pre-SPICE median minus post-SPICE median). Thus, negative values indicate that the pre-SPICE median is lower than the post-SPICE median for a single entry, while positive values indicate that the pre-SPICE median is higher than the post-SPICE median for a single entry. Median values and Wilcoxon rank sum test results for each distribution are reported in Table 2-3. The difference in pre- and post-SPICE median values ranges from -2.75‰ (entry #52; Yaerdang Mountain, China; Liu et al., 2017) to +2.07‰ (entry #51; Jikdong; South Korea; Lim et al., 2015). Paleolatitude is the only categorical variable investigated that did not return any statistically significant *p*-values (Fig. 2-10a; Table 2-3a). Entries from the paleocontinent Laurentia recorded a median pre- to post-SPICE difference of 0.19‰, which is statistically different from the median values calculated for both Gondwana (-1.01‰) and Kazakhstania (-1.06‰; Fig. 2-10b; Table 2-3b). Deep water sections, specifically those from slope facies, record a significant difference in pre- and post-SPICE medians relative to shallow and intermediate water depths (Fig. 2-10c–d; Table 2-3c–d).

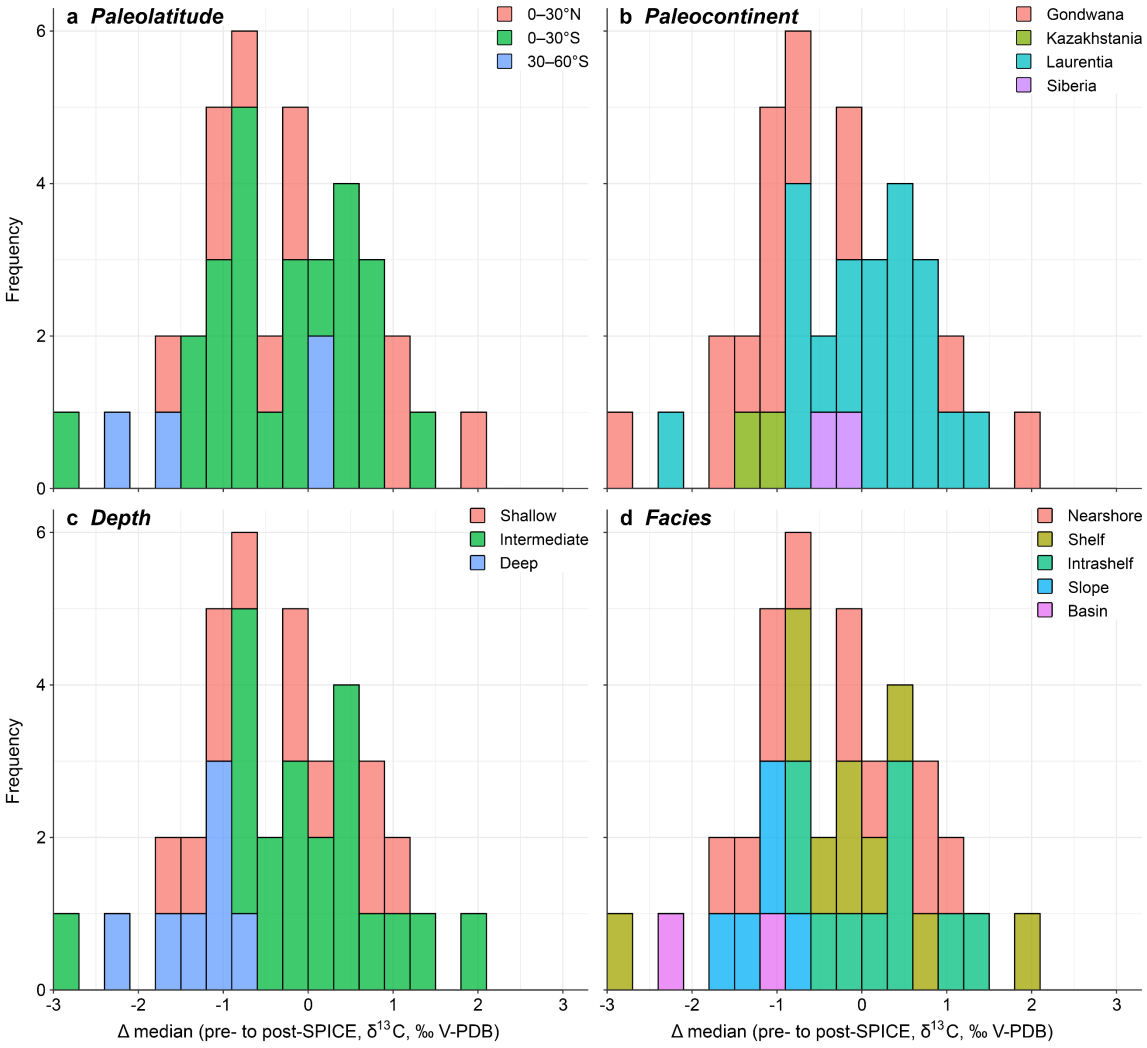

Figure 2-10. Difference in pre- and post-SPICE median $\delta^{13}C$ values. This histogram illustrates the ‰ change in pre- and post- SPICE median values for single entries, calculated as pre-SPICE median minus post-SPICE median. Positive values indicate that the pre-SPICE median is higher than the post-SPICE median; negative values indicate that the pre-SPICE median is lower than the post-SPICE median. Entries are labelled according to the following grouping variables: (a) paleolatitudinal zone; (b) paleocontinent; (c) water-depth; (d) facies. Bin-width = 0.3‰, with hard upper boundary.

2.5 Supplemental tables with associated captions

TABLE 2-1.

DEPTH AND FACIES KEYWORDS

Depth	Facies	Keywords
Shallow	Shallow/Nearshore	• Peritidal • Supratidal • Shallow water • Evaporite • Karst • Fluvial • Shallow marine • Epicontinental sea • Epeiric sea • Very shallow
Intermediate	Shelf	• Subtidal • Intertidal • Shallow to deep ramp • Inner detrital belt • Carbonate shelf • Prograding carbonate ramp • Platform carbonates • Continental shelf • Inner to outer shelf • Subtidal shoal
	Intrashelf basin	• House Range Embayment • Conasauga Intrashelf Basin • Rome Trough • Central Missouri Intrashelf Basin
Deep	Slope	• Mid to outer ramp • Turbidites • Debris flows • Suspension settling • Upper to lower slope • Slope belt • Deep water carbonates • Submarine fan • Slope
	Basin	• Basinal shales/facies • Deepwater basin

The terms listed here are taken from the respective original publications of all of the included SPICE datasets and were categorized to provide depth/facies groupings for each entry.

TABLE 2-2.

WILCOXON RANK SUM TESTS, STRATIGRAPHIC THICKNESS

(a)	Paleolatitude	0–30°N	0–30°S	30–60°S
Median	Full excursion thickness	173.89	27.59	32.30
	Rising limb thickness	110.36	10.54	16.17
Wilcoxon p-values for full excursion stratigraphic thickness				
	0–30°N	—	**1.1360×10^{-7}**	**0.0015**
	0–30°S	—	—	0.6182
	30–60°S	—	—	—
Wilcoxon p-values for rising limb stratigraphic thickness				
	0–30°N	—	**6.4050×10^{-7}**	**0.0090**
	0–30°S	—	—	0.3737
	30–60°S	—	—	—

(b)	Paleocontinent	Gondwana	Kazakhstania	Laurentia	Siberia
Median	Full excursion thickness	115.45	115.10	27.80	634.95
	Rising limb thickness	71.95	62.25	12.42	330.80
Wilcoxon p-values for full excursion stratigraphic thickness					
	Gondwana	—	1.0000	**0.0010**	**0.0032**
	Kazakhstania	—	—	**0.0372**	0.3333
	Laurentia	—	—	—	**0.0023**
	Siberia	—	—	—	—
Wilcoxon p-values for rising limb stratigraphic thickness					
	Gondwana	—	0.7563	**0.0006**	**0.0034**
	Kazakhstania	—	—	**0.0479**	0.3333
	Laurentia	—	—	—	**0.0196**
	Siberia	—	—	—	—

190

TABLE 2-2 (CONTINUED)

(c)	Depth	Shallow	Intermediate	Deep
Median	Full excursion thickness	84.83	28.66	114.20
	Rising limb thickness	31.45	12.54	79.50
Wilcoxon p-values for full excursion stratigraphic thickness				
	Shallow	—	0.3392	0.4799
	Intermediate	—	—	**0.0023**
	Deep	—	—	—
Wilcoxon p-values for rising limb stratigraphic thickness				
	Shallow	—	0.0609	0.3891
	Intermediate	—	—	**0.0022**
	Deep	—	—	—

(d)	Facies	Shallow/ nearshore	Shelf	Intrashelf basin	Slope	Basin
Median	Full excursion thickness	84.83	42.26	27.58	115.10	59.00
	Rising limb thickness	31.45	10.18	13.13	88.50	24.00
Wilcoxon p-values for full excursion stratigraphic thickness						
	Shallow/nearshore	—	0.7814	0.2239	0.2716	0.6349
	Shelf	—	—	0.1384	**0.0034**	0.9577
	Intrashelf basin	—	—	—	**0.0008**	0.8053
	Slope	—	—	—	—	0.3706
	Basin	—	—	—	—	—
Wilcoxon p-values for rising limb stratigraphic thickness						
	Shallow/nearshore	—	0.1777	0.0841	0.2264	0.7769
	Shelf	—	—	0.9397	**0.0035**	0.7121
	Intrashelf basin	—	—	—	**0.0012**	0.6798
	Slope	—	—	—	—	0.3727
	Basin	—	—	—	—	—

Results for the Wilcoxon rank sum tests evaluating the statistical significance of differences in the stratigraphic thickness (in meters) of the SPICE across the investigated categorical variables. Stratigraphic thicknesses assessed include the entire excursion interval (rising limb + plateau [if present] + falling limb), as well as that of the rising limb alone. Median values for each distribution are reported, as well as *p*-values for each test. *p*-values ≤0.05 are bolded; *p*-values >0.05 and ≤0.1 are underlined. Sections are grouped according to the following variables: (a) paleolatitude, (b) paleocontinent, (c) water depth, and (d) facies. (c) and (d) are on the following page.

TABLE 2-3.

WILCOXON RANK SUM TESTS, $\Delta^{13}C$ VALUES

(a)	Paleolatitude	0–30°N	0–30°S	30–60°S
Median value	Post-SPICE median $\delta^{13}C$	0.95	0.47	-0.76
	Rising limb maximum $\delta^{13}C$	3.36	3.71	2.19
	Rising limb minimum $\delta^{13}C$	-0.36	0.02	-1.61
	Pre-SPICE median $\delta^{13}C$	-0.20	0.25	-1.23
	Rising limb magnitude $\delta^{13}C$	3.93	3.64	3.58
	Median pre- to post-SPICE $\delta^{13}C$ difference	-0.30	-0.37	-0.89
Wilcoxon p-values for post-SPICE median $\delta^{13}C$				
	0–30°N	—	0.1719	0.0831
	0–30°S	—	—	**0.0451**
	30–60°S	—	—	—
Wilcoxon p-values for rising limb maximum $\delta^{13}C$				
	0–30°N	—	0.5363	0.1280
	0–30°S	—	—	**0.0126**
	30–60°S	—	—	—
Wilcoxon p-values for rising limb minimum $\delta^{13}C$				
	0–30°N	—	0.2257	**0.0379**
	0–30°S	—	—	**0.0007**
	30–60°S	—	—	—
Wilcoxon p-values for pre-SPICE median $\delta^{13}C$				
	0–30°N	—	0.0671	**0.0010**
	0–30°S	—	—	**0.0001**
	30–60°S	—	—	—
Wilcoxon p-values for rising limb $\delta^{13}C$ magnitude				
	0–30°N	—	0.5830	0.5334
	0–30°S	—	—	0.8336
	30–60°S	—	—	—
Wilcoxon p-values for pre- to post-SPICE $\delta^{13}C$ median difference				
	0–30°N	—	0.9556	0.4535
	0–30°S	—	—	0.3554
	30–60°S	—	—	—

192

TABLE 2-3 (CONTINUED)

(b)	Paleocontinent	Gondwana	Kazakhstania	Laurentia	Siberia
Median value	Post-SPICE median $\delta^{13}C$	1.17	0.64	0.47	0.23
	Rising limb maximum $\delta^{13}C$	3.37	4.91	3.34	4.22
	Rising limb minimum $\delta^{13}C$	-0.42	-0.41	-0.03	-2.12
	Pre-SPICE median $\delta^{13}C$	-0.26	-0.42	0.25	-0.10
	Rising limb magnitude $\delta^{13}C$	3.83	5.32	3.61	6.33
	Median pre- to post-SPICE $\delta^{13}C$ difference	-1.01	-1.06	0.19	-0.33
Wilcoxon p-values for post-SPICE median $\delta^{13}C$					
	Gondwana	—	0.7485	0.0752	0.4211
	Kazakhstania	—	—	0.6886	0.3333
	Laurentia	—	—	—	0.6087
	Siberia	—	—	—	—
Wilcoxon p-values for rising limb maximum $\delta^{13}C$					
	Gondwana	—	0.1008	0.7902	0.2723
	Kazakhstania	—	—	0.0549	0.3333
	Laurentia	—	—	—	0.3013
	Siberia	—	—	—	—
Wilcoxon p-values for rising limb minimum $\delta^{13}C$					
	Gondwana	—	0.9717	0.1181	0.2409
	Kazakhstania	—	—	0.3598	0.3333
	Laurentia	—	—	—	0.0923
	Siberia	—	—	—	—
Wilcoxon p-values for pre-SPICE median $\delta^{13}C$					
	Gondwana	—	0.7446	**0.0197**	0.8862
	Kazakhstania	—	—	0.1918	0.3333
	Laurentia	—	—	—	0.2790
	Siberia	—	—	—	—
Wilcoxon p-values for rising limb $\delta^{13}C$ magnitude					
	Gondwana	—	0.1098	0.3131	0.1265
	Kazakhstania	—	—	**0.0360**	1.0000
	Laurentia	—	—	—	0.0549
	Siberia	—	—	—	—
Wilcoxon p-values for pre- to post-SPICE $\delta^{13}C$ median difference					
	Gondwana	—	0.8167	**0.0062**	0.3333
	Kazakhstania	—	—	**0.0346**	0.3333
	Laurentia	—	—	—	0.4848
	Siberia	—	—	—	—

TABLE 2-3 (CONTINUED)

(c)	Depth	Shallow	Intermediate	Deep
Median value	Post-SPICE median $\delta^{13}C$	-0.23	0.46	1.38
	Rising limb maximum $\delta^{13}C$	2.98	3.59	4.25
	Rising limb minimum $\delta^{13}C$	-0.50	0.00	-0.29
	Pre-SPICE median $\delta^{13}C$	-0.36	0.25	-0.15
	Rising limb magnitude $\delta^{13}C$	3.80	3.61	4.38
	Median pre- to post-SPICE $\delta^{13}C$ difference	-0.26	-0.06	-1.15
Wilcoxon p-values for post-SPICE median $\delta^{13}C$				
	Shallow	—	0.9741	0.0535
	Intermediate	—	—	**0.0029**
	Deep	—	—	—
Wilcoxon p-values for rising limb maximum $\delta^{13}C$				
	Shallow	—	0.2832	**0.0155**
	Intermediate	—	—	0.0680
	Deep	—	—	—
Wilcoxon p-values for rising limb minimum $\delta^{13}C$				
	Shallow	—	**0.0413**	0.1247
	Intermediate	—	—	0.8615
	Deep	—	—	—
Wilcoxon p-values for pre-SPICE median $\delta^{13}C$				
	Shallow	—	**0.0089**	0.2678
	Intermediate	—	—	0.1834
	Deep	—	—	—
Wilcoxon p-values for rising limb $\delta^{13}C$ magnitude				
	Shallow	—	0.4422	0.5749
	Intermediate	—	—	0.1665
	Deep	—	—	—
Wilcoxon p-values for pre- to post-SPICE $\delta^{13}C$ median difference				
	Shallow	—	0.3172	**0.0346**
	Intermediate	—	—	**0.0001**
	Deep	—	—	—

TABLE 2-3 (CONTINUED)

(d)	Facies	Shallow/ nearshore	Shelf	Intrashelf basin	Slope	Basin
Median value	Post-SPICE median $\delta^{13}C$	-0.23	0.44	0.57	1.58	1.08
	Rising limb maximum $\delta^{13}C$	2.98	3.70	3.41	4.40	3.70
	Rising limb minimum $\delta^{13}C$	-0.50	-0.05	0.03	-0.27	-0.39
	Pre-SPICE median $\delta^{13}C$	-0.36	0.03	0.37	0.20	-0.47
	Rising limb magnitude $\delta^{13}C$	3.80	3.22	3.66	4.02	4.74
	Median pre- to post-SPICE $\delta^{13}C$ difference	-0.26	-0.19	0.22	-1.15	-1.61
Wilcoxon p-values for post-SPICE median $\delta^{13}C$						
	Shallow/nearshore	—	0.9095	0.9787	**0.0462**	0.5714
	Shelf	—	—	0.5254	**0.0207**	0.1538
	Intrashelf basin	—	—	—	**0.0135**	0.1319
	Slope	—	—	—	—	0.6429
	Basin	—	—	—	—	—
Wilcoxon p-values for rising limb maximum $\delta^{13}C$						
	Shallow/nearshore	—	0.5221	0.2753	**0.0214**	0.2848
	Shelf	—	—	0.6456	0.0792	0.5593
	Intrashelf basin	—	—	—	0.1779	0.3593
	Slope	—	—	—	—	0.8636
	Basin	—	—	—	—	—
Wilcoxon p-values for rising limb minimum $\delta^{13}C$						
	Shallow/nearshore	—	0.1570	0.0537	0.1110	0.6639
	Shelf	—	—	0.7475	0.7128	0.7121
	Intrashelf basin	—	—	—	0.8209	0.6798
	Slope	—	—	—	—	0.7273
	Basin	—	—	—	—	—
Wilcoxon p-values for pre-SPICE median $\delta^{13}C$						
	Shallow/nearshore	—	0.3689	**0.0009**	0.1009	0.7421
	Shelf	—	—	0.0461	0.6216	0.4067
	Intrashelf basin	—	—	—	0.2034	**0.0167**
	Slope	—	—	—	—	0.0667
	Basin	—	—	—	—	—
Wilcoxon p-values for rising limb $\delta^{13}C$ magnitude						
	Shallow/nearshore	—	0.3413	0.7086	0.8180	0.4226
	Shelf	—	—	0.5098	0.2285	0.1713
	Intrashelf basin	—	—	—	0.5263	0.3826
	Slope	—	—	—	—	0.8386
	Basin	—	—	—	—	—
Wilcoxon p-values for pre- to post-SPICE $\delta^{13}C$ median difference						
	Shallow/nearshore	—	0.6539	0.2230	0.1149	0.1026
	Shelf	—	—	0.4359	**0.0127**	0.1212
	Intrashelf basin	—	—	—	**0.0007**	**0.0303**
	Slope	—	—	—	—	0.5714
	Basin	—	—	—	—	—

Results for the Wilcoxon rank sum tests evaluating the statistical significance of differences in the distribution of $\delta^{13}C$ values across the investigated categorical variables. Distributions evaluated include the median pre- and post-SPICE $\delta^{13}C$ values, maximum and minimum rising limb $\delta^{13}C$ values, magnitude of the $\delta^{13}C$ excursion recorded in the rising limb, and difference between pre- and post-SPICE median $\delta^{13}C$ values per entry. See Table 1 in the main text for the specific $\delta^{13}C$ values used in these tests. Rising limb magnitude is defined as the maximum $\delta^{13}C$ value for the rising limb minus the minimum $\delta^{13}C$ value for the rising limb. The difference in pre- and post-SPICE medians is defined as the median pre-SPICE $\delta^{13}C$ value minus the median post-SPICE $\delta^{13}C$ value. Median values for each distribution are reported, as well as *p*-values for each test. *p*-values <0.05 are bolded; *p*-values <0.1 are underlined. Sections are grouped according to the following variables: (a) paleolatitude, (b) paleocontinent, (c) water depth, and (d) facies. Table panels after (a) are on subsequent pages.

TABLE 2-4.

WILCOXON RANK SUM TESTS, LITHOLOGY

Lithology	**"Carbonate"**	**Limestone**	**Dolostone**
Median SPICE maximum $\delta^{13}C$	3.01	3.76	2.69
Wilcoxon p-values for SPICE maximum $\delta^{13}C$			
"Carbonate"	—	0.0543	0.5483
Limestone	—	—	0.0564
Dolostone	—	—	—

Results for the Wilcoxon rank sum tests evaluating the statistical significance of differences in the peak $\delta^{13}C$ value of the SPICE across lithology. Lithologic categories are determined based on the lithology of the specific sample that records the maximum $\delta^{13}C$ value of the rising limb in each entry. Sections are grouped according to the following lithologies: "Carbonate," Limestone, and Dolostone. Samples labelled "Carbonate" represent those for which a more detailed mineralogy of the sampled carbonate material could not be determined based on the information provided in the original publication. *p*-values <0.05 are bolded; *p*-values <0.1 are underlined.

2.6 R code inputs

A copy of the code used in RStudio to construct figures and conduct statistical analyses is provided below for transparency and reproducibility. Much of the same code was executed several times, with the only difference being the specific variables or observations used to group the data (ie. Joy plots arranged by paleolatitude vs. joy plots arranged by facies). For the sake of brevity, each section of code was only included once, with specific variable callouts replaced by the following generic placeholders:

`VARIABLE.1`, `VARIABLE.2`, `VARIABLE.3`, etc.

Indicates where a specific grouping variable (as listed in Table 1-3) should be input

i.e., Paleolatitude, Paleocontinent, Depth, Facies, Lithology

`CATEGORY.1`, `CATEGORY.2`, `CATEGORY.3`, etc.

Indicates were a specific grouping category (as listed in Table 1-3) should be input

i.e., 0–30° N, Gondwana, Intermediate, Intrashelf basin, Limestone, etc.

`VALUE.1`, `VALUE.2`, `VALUE.3`, etc.

Indicates where the entry number for a desired section should be input

i.e., 1, 2, 3, etc.

2.6.1 Data wrangling

```
#packages
library(dplyr)
library(tidyr)
library(ggplot2)
library(ggthemes)
library(ggridges)
library(gridExtra)
```

```
#every_nth function for labelling plot axes
every_nth <- function(x, nth, empty = TRUE, inverse = FALSE)
{
  if (!inverse) {
    if(empty) {
      x[1:nth == 1] <- ""
      x
    } else {
      x[1:nth != 1]
    }
  } else {
    if(empty) {
      x[1:nth != 1] <- ""
      x
    } else {
      x[1:nth == 1]
    }
  }
}

#Attach SPICEraq and set levels of variables so legends will be in the right order
SPICEraq <- read.csv("SPICEraq_2.29.csv", header = TRUE, sep=",")
SPICEraq$Simplified.facies <- factor(SPICEraq$Simplified.facies, levels =
c("Shallow/nearshore", "Shelf", "Intrashelf basin", "Slope", "Basin"))
SPICEraq$Paleolatitude <- factor(SPICEraq$Paleolatitude, levels = c("60-90 N",
"30-60 N", "0-30 N", "0-30 S", "30-60 S", "60-90 S"))
SPICEraq$SPICE.zone <- factor(SPICEraq$SPICE.zone, levels = c("Post", "Falling",
"Plateau", "Rising", "Pre", "Omit"))
SPICEraq$Paleolatitude <- factor(SPICEraq$Paleolatitude, levels = c("60-90 N",
"30-60 N", "0-30 N", "0-30 S", "30-60 S", "60-90 S"))
SPICEraq$Paleocontinent <- factor(SPICEraq$Paleocontinent, levels = c("Gondwana",
"Kazakhstania", "Laurentia", "Siberia"))
attach(SPICEraq)

#Create a summary table that reports min, max, and median d13C + min and max
meters.above.onset by Entry.number and Spice.zone
mind13C <- SPICEraq %>% group_by(Entry.number, SPICE.zone) %>%
summarise(min(d13C))
maxd13C <- SPICEraq %>% group_by(Entry.number, SPICE.zone) %>%
summarise(max(d13C))
mediand13C <- SPICEraq %>% group_by(Entry.number, SPICE.zone) %>%
summarise(median(d13C))
minMeters <- SPICEraq %>% group_by(Entry.number, SPICE.zone) %>%
summarise(min(Meters.above.onset))
maxMeters <- SPICEraq %>% group_by(Entry.number, SPICE.zone) %>%
summarise(max(Meters.above.onset))
```

```
#Start to construct SPICEsummary table, export to Excel for editing, and import for further analyses
minmaxd13C <- full_join(mind13C, maxd13C)
minmaxmediand13C <- full_join(minmaxd13C,mediand13C)
minmaxmediand13CminMeters <- full_join(minmaxmediand13C, minMeters)
minmaxmediand13CminMetersmaxMeters <- full_join(minmaxmediand13CminMeters, maxMeters)
write.csv(minmaxmediand13CminMetersmaxMeters, "minmaxmediand13Cminmetersmaxmeters.csv")

#Attach SPICEraq.sum and set levels of variables so legends will be in the right order
SPICEraq.sum <- read.csv("SPICEraq_2.29_summary.csv", header = TRUE, sep = ",")
SPICEraq.sum$SPICE.zone <- factor(SPICEraq.sum$SPICE.zone, levels = c("Post", "Falling", "Plateau", "Rising", "Pre", "Omit"))
SPICEraq.sum$Facies <- factor(SPICEraq.sum$Facies, levels = c("Shallow/nearshore", "Shelf", "Intrashelf basin", "Slope", "Basin"))
SPICEraq.sum$Depth <- factor(SPICEraq.sum$Depth, levels = c("Shallow", "Intermediate", "Deep"))
SPICEraq.sum$Paleolatitude <- factor(SPICEraq.sum$Paleolatitude, levels = c("60-90 N", "30-60 N", "0-30 N", "0-30 S", "30-60 S", "60-90 S"))
SPICEraq.sum$Paleocontinent <- factor(SPICEraq.sum$Paleocontinent, levels = c("Gondwana", "Kazakhstania", "Laurentia", "Siberia"))
attach(SPICEraq.sum)

#create metadata table with one row for each entry
SPICEraq.meta <- read.csv("SPICEraq_2.29_metadata.csv", header = TRUE, sep = ",")
SPICEraq.meta$Facies <- factor(SPICEraq.meta$Facies, levels = c("Shallow/nearshore", "Shelf", "Intrashelf basin", "Slope", "Basin"))
SPICEraq.meta$Depth <- factor(SPICEraq.meta$Depth, levels = c("Shallow", "Intermediate", "Deep"))
SPICEraq.meta$Paleolatitude <- factor(SPICEraq.meta$Paleolatitude, levels = c("60-90 N", "30-60 N", "0-30 N", "0-30 S", "30-60 S", "60-90 S"))
SPICEraq.meta$Paleocontinent <- factor(SPICEraq.meta$Paleocontinent, levels = c("Gondwana", "Kazakhstania", "Laurentia", "Siberia"))
attach(SPICEraq.meta)

#create tables that only have one SPICE zone
SumPre <- subset(SPICEraq.sum, SPICE.zone == "Pre")
write.csv(SumPre, "SumPre_2.29.csv")
SumRising <- subset(SPICEraq.sum, SPICE.zone == "Rising")
write.csv(SumRising, "SumRising_2.29.csv")
SumPlateau <- subset(SPICEraq.sum, SPICE.zone == "Plateau")
write.csv(SumPlateau, "SumPlateau_2.29.csv")
SumFalling <- subset(SPICEraq.sum, SPICE.zone == "Falling")
write.csv(SumFalling, "SumFalling_2.29.csv")
```

```
SumPost <- subset(SPICEraq.sum, SPICE.zone == "Post")
write.csv(SumPost, "SumPost_2.29.csv")
```

2.6.2 Scatter plots

```
#strat thickness of rising limb (x) and d13C rising limb magnitude (y)
ggplot(data = subset(SPICEraq.sum, SPICE.zone == "Rising"), aes(x =
(max.Meters.above.onset. - min.Meters.above.onset.), y = (max.d13C. -
min.d13C.))) +
  geom_point(aes(shape = VARIABLE.1, fill = VARIABLE.1), size = 5, alpha = 1) +
  geom_text(aes(label = Entry.number), size = 3) +
  scale_shape_manual(values = c(21, 22, 23, 24, 25)) +
  labs(x = "Stratigraphic Range (m)", y = "Magnitude of SPICE d13C (Rising)",
title = "Rising limb d13C/m", color = "VARIABLE.1") +
  scale_x_continuous(limits = c(0,450), breaks = seq(0,450,50), labels =
every_nth(seq(0,450,50), 2, inverse = TRUE)) +
  scale_y_continuous(limits = c(0,9), breaks = seq(0,9,1), labels =
every_nth(seq(0,9,1), 2, inverse = TRUE)) +
  theme_classic() +
  theme(axis.text = element_text(size = 16, color = "black"), axis.title =
element_text(size = 16), axis.line = element_line(color = "black")) +
  #theme(axis.text.x = element_blank(), axis.text.y = element_blank(),
legend.position = "none") +
  theme(plot.title = element_text(hjust = 0.5, size = 16)) +
  theme(legend.text = element_text(size = 16))
#total strat thickness (x) and d13C rising limb magnitude (y)
ggplot(data = subset(SPICEraq.meta), aes(x = (Total.strat), y = (Rising.mag))) +
  geom_point(aes(shape = VARIABLE.1, fill = VARIABLE.1), size = 5, alpha = 1) +
  geom_text(aes(label = Entry.number), size = 3) +
  scale_shape_manual(values = c(21, 22, 23, 24, 25)) +
  labs(x = "Total Stratigraphic Range (m)", y = "Magnitude of SPICE d13C
(Rising)", title = "Total thickness vs rising magnitude", color = " VARIABLE.1")
+
  scale_x_continuous(limits = c(0,900), breaks = seq(0,900,100), labels =
every_nth(seq(0,900,100), 2, inverse = TRUE)) +
  scale_y_continuous(limits = c(0,9), breaks = seq(0,9,1), labels =
every_nth(seq(0,9,1), 2, inverse = TRUE)) +
  theme_classic() +
  theme(axis.text = element_text(size = 16, color = "black"), axis.title =
element_text(size = 16), axis.line = element_line(color = "black")) +
  #theme(axis.text.x = element_blank(), axis.text.y = element_blank(),
legend.position = "none") +
  theme(plot.title = element_text(hjust = 0.5, size = 16)) +
  theme(legend.text = element_text(size = 16))
```

2.6.3 Joy plots

```
#Stacked density plots - d13C values through SPICE by organized grouping variable
j1 <- ggplot(data = subset(SPICEraq.sum, SPICE.zone == "Pre"), aes(x =
median.d13C., y = factor(VARIABLE.1, levels = rev(levels(VARIABLE.1))))) +
  geom_density_ridges2(aes(fill = factor(VARIABLE.1)), quantile_lines = TRUE,
quantiles = 2, size = 0.5) +
  labs(x = "Median d13C of pre SPICE", y = " VARIABLE.1") +
  theme_minimal(base_size = 14) +
  theme(axis.text.x = element_text(hjust = 0.3), axis.text.y = element_text(vjust
= 0)) +
  #theme(axis.text.x = element_blank(), axis.text.y = element_blank(),
legend.position = "none") +
  scale_x_continuous(expand = c(0.01, 0), limits = c(-6, 8), breaks = seq(-6, 8,
1), labels = every_nth(seq(-6, 8, 1), 2, inverse = TRUE)) +
  scale_y_discrete(expand = c(0.01, 0)) +
  coord_cartesian(clip = "off")
j2 <- ggplot(data = subset(SPICEraq.sum, SPICE.zone == "Rising"), aes(x =
min.d13C., y = factor(VARIABLE.1, levels = rev(levels(VARIABLE.1))))) +
  geom_density_ridges2(aes(fill = factor(VARIABLE.1)), quantile_lines = TRUE,
quantiles = 2, size = 0.5) +
  labs(x = "Minimum d13C of rising limb", y = " VARIABLE.1") +
  theme_minimal(base_size = 14) +
  theme(axis.text.x = element_text(hjust = 0.3), axis.text.y = element_text(vjust
= 0)) +
  #theme(axis.text.x = element_blank(), axis.text.y = element_blank(),
legend.position = "none") +
  scale_x_continuous(expand = c(0.01, 0), limits = c(-6, 8), breaks = seq(-6, 8,
1), labels = every_nth(seq(-6, 8, 1), 2, inverse = TRUE)) +
  scale_y_discrete(expand = c(0.01, 0)) +
  coord_cartesian(clip = "off")
j3 <- ggplot(data = subset(SPICEraq.sum, SPICE.zone == "Rising"), aes(x =
max.d13C., y = factor(VARIABLE.1, levels = rev(levels(VARIABLE.1))))) +
  geom_density_ridges2(aes(fill = factor(VARIABLE.1)), quantile_lines = TRUE,
quantiles = 2, size = 0.5) +
  labs(x = "Maximum d13C of rising limb", y = " VARIABLE.1") +
  theme_minimal(base_size = 14) +
  theme(axis.text.x = element_text(hjust = 0.3), axis.text.y = element_text(vjust
= 0)) +
  #theme(axis.text.x = element_blank(), axis.text.y = element_blank(),
legend.position = "none") +
  scale_x_continuous(expand = c(0.01, 0), limits = c(-6, 8), breaks = seq(-6, 8,
1), labels = every_nth(seq(-6, 8, 1), 2, inverse = TRUE)) +
  scale_y_discrete(expand = c(0.01, 0)) +
  coord_cartesian(clip = "off")
```

```
j4 <- ggplot(data = subset(SPICEraq.sum, SPICE.zone == "Post"), aes(x =
median.d13C., y = factor(VARIABLE.1, levels = rev(levels(VARIABLE.1))))) +
  geom_density_ridges2(aes(fill = factor(VARIABLE.1)), quantile_lines = TRUE,
quantiles = 2, size = 0.5) +
  labs(x = "Median d13C of post SPICE", y = " VARIABLE.1") +
  theme_minimal(base_size = 14) +
  theme(axis.text.x = element_text(hjust = 0.3), axis.text.y = element_text(vjust
= 0)) +
  #theme(axis.text.x = element_blank(), axis.text.y = element_blank(),
legend.position = "none") +
  scale_x_continuous(expand = c(0.01, 0), limits = c(-6, 8), breaks = seq(-6, 8,
1), labels = every_nth(seq(-6, 8, 1), 2, inverse = TRUE)) +
  scale_y_discrete(expand = c(0.01, 0)) +
  coord_cartesian(clip = "off")
grid.arrange(j4, j3, j2, j1, ncol = 1)
```

2.6.4 Box plots

```
#box plots for d13C magnitude of rising limb
ggplot(data = subset(SPICEraq.sum, SPICE.zone == "Rising"), aes(x =
factor(VARIABLE.1, levels = rev(levels(VARIABLE.1))), y = (max.d13C.- min.d13C.),
fill = VARIABLE.1)) +
  stat_boxplot(geom = "errorbar", width = 0.2) +
  geom_boxplot(width = 0.3, outlier.shape = NA) +
  coord_flip() +
  theme_classic() +
  theme(legend.position = "bottom") +
  geom_jitter(width = 0.15)
  #theme(axis.text.x = element_blank(), axis.text.y = element_blank(),
legend.position = "none")

#box plot for rising limb strat thickness
ggplot(data = subset(SPICEraq.sum, SPICE.zone == "Rising"), aes(x =
factor(VARIABLE.1, levels = rev(levels(VARIABLE.1))), y =
(max.Meters.above.onset.- min.Meters.above.onset.), fill = VARIABLE.1)) +
  stat_boxplot(geom = "errorbar", width = 0.2) +
  geom_boxplot(width = 0.3, outlier.shape = NA) +
  coord_flip() +
  theme_classic() +
  theme(legend.position = "bottom") +
  #theme(axis.text.x = element_blank(), axis.text.y = element_blank(),
legend.position = "none") +
  geom_jitter(width = 0.15)
```

```
#box plot for total strat thickness
ggplot(data = subset(SPICEraq.meta), aes(x = factor(VARIABLE.1, levels =
rev(levels(VARIABLE.1))), y = (Total.strat), fill = VARIABLE.1)) +
  stat_boxplot(geom = "errorbar", width = 0.2) +
  geom_boxplot(width = 0.3, outlier.shape = NA) +
  scale_y_continuous(limits = c(0,900), breaks = seq(0,900,100), labels =
every_nth(seq(0,900,100), 2, inverse = TRUE)) +
  coord_flip() +
  theme_classic() +
  theme(legend.position = "bottom") +
  #theme(axis.text.x = element_blank(), axis.text.y = element_blank(),
legend.position = "none") +
  geom_jitter(width = 0.15)
```

2.6.5 Facet figures

```
#create palette rearranging default ggplot2 colors to make zones more
distinguishable
SPICEpal <- c(Post = "#A3A500", Falling = "#E76BF3", Plateau = "#00B0F6", Rising
= "#F8766D", Pre = "#7CAE00", Omit = "black")

#create plot for each SHORT entry. export at 400x655 as .eps (x<75 Corrected MAB)
ggplot(data = subset(SPICEraq, Entry.number == "VALUE.1" & SPICE.zone != "Omit"),
aes(x = d13C, y = Meters.above.onset, color = SPICE.zone)) +
  geom_path(size = 1) +
  #facet_wrap(Entry.number ~ .) +
  labs(x = "d13C", y = "meters above the bottom", title = "Short - VALUE.1", color
= "SPICE zone") +
  theme(plot.title = element_text(hjust = 0.5)) +
  scale_y_continuous(limits = c(-100,75), breaks = seq(-100,75,20), labels =
every_nth(seq(-100,75,20), 1, inverse = TRUE)) +
  scale_x_continuous(limits = c(-6,6), breaks = seq(-6,6,2), labels =
every_nth(seq(-6,6,2), 1, inverse = TRUE)) +
  scale_color_manual (values = SPICEpal) +
  theme_bw() +
  theme(axis.text.x = element_blank(), axis.text.y = element_blank(),
legend.position = "none")

#create plot for each INTERMEDIATE entry. export at 400x655 as .eps (75<x<200
Corrected MAB)
ggplot(data = subset(SPICEraq, Entry.number == " VALUE.1" & SPICE.zone != "Omit"),
aes(x = d13C, y = Meters.above.onset, color = SPICE.zone)) +
  geom_path(size = 1) +
  labs(x = "d13C", y = "meters above the bottom", title = "Intermediate - VALUE.1",
color = "SPICE zone") +
```

```
  theme(plot.title = element_text(hjust = 0.5)) +
  scale_y_continuous(limits = c(-100,200), breaks = seq(-100,200,50), labels =
every_nth(seq(-100,200,50), 1, inverse = TRUE)) +
  scale_x_continuous(limits = c(-6,6), breaks = seq(-6,6,2), labels =
every_nth(seq(-6,6,2), 1, inverse = TRUE)) +
  scale_color_manual (values = SPICEpal) +
  theme_bw() +
  theme(axis.text.x = element_blank(), axis.text.y = element_blank(),
legend.position = "none")

#create plot for each LONG entry. export at 400x655 as .eps (200<x<700 Corrected
MAB)
ggplot(data = subset(SPICEraq, Entry.number == " VALUE.1" & SPICE.zone != "Omit"),
aes(x = d13C, y = Meters.above.onset, color = SPICE.zone)) +
  geom_path(size = 1) +
  labs(x = "d13C", y = "meters above the bottom", title = "Long - VALUE.1", color
= "SPICE zone") +
  theme(plot.title = element_text(hjust = 0.5)) +
  scale_y_continuous(limits = c(-100,700), breaks = seq(-100,700,100), labels =
every_nth(seq(-100,700,100), 1, inverse = TRUE)) +
  scale_x_continuous(limits = c(-6,6), breaks = seq(-6,6,2), labels =
every_nth(seq(-6,6,2), 1, inverse = TRUE)) +
  scale_color_manual (values = SPICEpal) +
  theme_bw() +
  theme(axis.text.x = element_blank(), axis.text.y = element_blank(),
legend.position = "none")

#create plot for each SUPERLONG entry. export at 400x655 as .eps (x>700 Corrected
MAB)
ggplot(data = subset(SPICEraq, Entry.number == " VALUE.1" & SPICE.zone != "Omit"),
aes(x = d13C, y = Meters.above.onset, color = SPICE.zone)) +
  geom_path(size = 1) +
  labs(x = "d13C", y = "meters above the bottom", title = "Superlong - VALUE.1",
color = "SPICE zone") +
  theme(plot.title = element_text(hjust = 0.5)) +
  scale_y_continuous(limits = c(-1500,1500), breaks = seq(-1500,1500,400), labels
= every_nth(seq(-1500,1500,400), 1, inverse = TRUE)) +
  scale_x_continuous(limits = c(-6,6), breaks = seq(-6,6,2), labels =
every_nth(seq(-6,6,2), 1, inverse = TRUE)) +
  scale_color_manual (values = SPICEpal) +
  theme_bw() +
  theme(legend.position = "none")
```

2.6.6 Forest figures

```
#new matrix with min and max and Entry number for the rising limb
#includes all of the columns needed to color the lines by different variables
SPICE_forest_allzones <- data.frame("Entry.number" = SPICEraq.sum$Entry.number,
"SPICEzone" = SPICEraq.sum$SPICE.zone,
                          "min.d13C." = SPICEraq.sum$min.d13C., "max.d13C." =
SPICEraq.sum$max.d13C.,
                          "median.d13C." = SPICEraq.sum$median.d13C.,
"Paleolatitude" = SPICEraq.sum$Paleolatitude,
                          "Paleocontinent" = SPICEraq.sum$Paleocontinent,
"Facies" = SPICEraq.sum$Facies,
                          "Depth" = SPICEraq.sum$Depth)

#Selecting only the rising limbs
SPICE_forest <- subset(SPICE_forest_allzones, SPICEraq.sum$SPICE.zone ==
"Rising")
#sorting by min to add a new column that will plot them from smallest to largest
min values
SPICE_forest <- SPICE_forest[order(SPICE_forest$min.d13C.,
SPICE_forest$max.d13C.),]
SPICE_forest$min_plot_order <- seq(from = nrow(SPICE_forest), to = 1, by = -1)

#Sorting by max d13C values to add a new column that will plot them from smallest
to largest max values
SPICE_forest <- SPICE_forest[order(SPICE_forest$max.d13C.,
SPICE_forest$min.d13C.),]
SPICE_forest$max_plot_order <- seq(from = nrow(SPICE_forest), to = 1, by = -1)

#Plot by minimum d13C rising limb
ggplot(data = SPICE_forest, aes(x = SPICE_forest$min_plot_order, y =
SPICE_forest$median.d13C.,
                                ymin = SPICE_forest$min.d13C., ymax =
SPICE_forest$max.d13C.,
                                color = SPICE_foresxt$VARIABLE.1)) +
  geom_pointrange(size = 2, fatten = 0.1) +
  geom_text(aes(label = Entry.number), size = 3, color = "black") +
  coord_flip() +  # flip coordinates (puts labels on y axis)
  xlab("Label") + ylab("d13C range") +
  theme_bw() +
  theme(axis.text.x = element_blank(), axis.text.y = element_blank(),
legend.position = "none") +
  labs(title = " VARIABLE.1 by min d13C")
```

```
#Plot by minimum d13C rising limb
ggplot(data = SPICE_forest, aes(x = SPICE_forest$max_plot_order, y =
SPICE_forest$median.d13C.,
                                ymin = SPICE_forest$min.d13C., ymax =
SPICE_forest$max.d13C.,
                                color = SPICE_forest$VARIABLE.1)) +
  geom_pointrange(size = 2, fatten = 0.1) +
  geom_text(aes(label = Entry.number), size = 3, color = "black") +
  coord_flip() +  # flip coordinates (puts labels on y axis)
  xlab("Label") + ylab("d13C range") +
  theme_bw() +
  theme(axis.text.x = element_blank(), axis.text.y = element_blank(),
legend.position = "none") +
  labs(title = " VARIABLE.1 by max d13C")
```

2.6.7 $\delta^{13}C$ and $\delta^{18}O$ plots for LO-5 (#38) and 319-11A (#39)

```
#LO-5 d13C + d18O
ggplot(data = subset(SPICEraq, Entry.number == "38"), aes(y = (Borehole.depth)))
+
  geom_path(aes(x = (d13C))) +
  geom_point(aes(x = (d13C)), size = 2, shape = 21, fill = "blue") +
  geom_path(aes(x = (d18O))) +
  geom_point(aes(x = (d18O)), size = 2, shape = 21, fill = "red") +
  scale_y_reverse() +
  scale_x_continuous(limits = c(-9,5), breaks = seq(-9,5,1), labels =
every_nth(seq(-9,5,1), 2, inverse = FALSE)) +
  theme_classic()

#319-11A d13C + d18O
ggplot(data = subset(SPICEraq, Entry.number == "39"), aes(y = (Borehole.depth)))
+
  geom_path(aes(x = (d13C))) +
  geom_point(aes(x = (d13C)), size = 2, shape = 21, fill = "blue") +
  geom_path(aes(x = (d18O))) +
  geom_point(aes(x = (d18O)), size = 2, shape = 21, fill = "red") +
  scale_y_reverse() +
  scale_x_continuous(limits = c(-9,5), breaks = seq(-9,5,1), labels =
every_nth(seq(-9,5,1), 2, inverse = FALSE)) +
  theme_classic()
```

2.6.8 Stacked histogram for peak SPICE value vs. lithology

```
#attach correct csv file
SPICEraq.rise <- read.csv("SumRising_2.29.csv", header = TRUE, sep = ",")
SPICEraq.rise$Lithology <- factor(SPICEraq.rise$Lithology, levels =
c("Carbonate", "Limestone", "Dolostone"))
attach(SPICEraq.rise)

#stacked histogram, exclude "Carbonate"
ggplot(data = subset(SPICEraq.rise, Lithology != "Carbonate"), aes(x =
(max.d13C.), fill = Lithology)) +
  geom_histogram(binwidth = 0.3, boundary = 0, closed = "right", color = "black",
na.rm = TRUE) +
  theme_bw() +
  labs(title = "Rising limb max d13C - Lithology") +
  #theme(axis.text.x = element_blank(), axis.text.y = element_blank(),
legend.position = "none") +
  scale_x_continuous(limits = c(0,6), breaks = seq(0,6,1))

#Shapiro-Wilk test for normality
shapiro.test(SPICEraq.rise$max.d13C.)

#Wilcox tests to compare Pre.Post.med for lithology
wilcox.test(x=subset(SPICEraq.rise$max.d13C., Lithology=="Carbonate"),
y=subset(SPICEraq.rise$max.d13C., Lithology=="Limestone"))
wilcox.test(x=subset(SPICEraq.rise$max.d13C., Lithology=="Carbonate"),
y=subset(SPICEraq.rise$max.d13C., Lithology=="Dolostone"))
wilcox.test(x=subset(SPICEraq.rise$max.d13C., Lithology=="Limestone"),
y=subset(SPICEraq.rise$max.d13C., Lithology=="Dolostone"))
median(subset(SPICEraq.rise$max.d13C., Lithology=="Carbonate"), na.rm = TRUE)
median(subset(SPICEraq.rise$max.d13C., Lithology=="Limestone"), na.rm = TRUE)
median(subset(SPICEraq.rise$max.d13C., Lithology=="Dolostone"), na.rm = TRUE)
```

2.6.9 Stacked histogram for pre median minus post median

```
ggplot(data = SPICEraq.meta, aes(x = (Pre.Post.med), fill = VARIABLE.1)) +
  geom_histogram(binwidth = 0.3, boundary = 0, closed = "right", color = "black",
na.rm = TRUE) +
  theme_bw() +
  labs(title = "Pre median minus post median - VARIABLE.1") +
  #theme(axis.text.x = element_blank(), axis.text.y = element_blank(),
legend.position = "none") +
  scale_x_continuous(limits = c(-3,3), breaks = seq(-3,3,1))
```

```
#Shapiro-Wilk test for normality
shapiro.test(SPICEraq.meta$Pre.Post.med)

#One-sample T test to compare mean change in Pre and Post meds to hypothetical
mean of zero
t.test(SPICEraq.meta$Pre.Post.med, mu = 0, alternative = "two.sided")

#Wilcox tests to compare Pre.Post.med
wilcox.test(x=subset(SPICEraq.meta$Pre.Post.med,      VARIABLE.1=="CATEGORY.1"),
y=subset(SPICEraq.meta$Pre.Post.med, VARIABLE.1=="CATEGORY.2"))
wilcox.test(x=subset(SPICEraq.meta$Pre.Post.med,      VARIABLE.1=="CATEGORY.1"),
y=subset(SPICEraq.meta$Pre.Post.med, VARIABLE.1=="CATEGORY.3"))
wilcox.test(x=subset(SPICEraq.meta$Pre.Post.med,      VARIABLE.1=="CATEGORY.1"),
y=subset(SPICEraq.meta$Pre.Post.med, VARIABLE.1=="CATEGORY.4"))
wilcox.test(x=subset(SPICEraq.meta$Pre.Post.med,      VARIABLE.1=="CATEGORY.1"),
y=subset(SPICEraq.meta$Pre.Post.med, VARIABLE.1=="CATEGORY.5"))
wilcox.test(x=subset(SPICEraq.meta$Pre.Post.med,      VARIABLE.1=="CATEGORY.2"),
y=subset(SPICEraq.meta$Pre.Post.med, VARIABLE.1=="CATEGORY.3"))
wilcox.test(x=subset(SPICEraq.meta$Pre.Post.med,      VARIABLE.1=="CATEGORY.2"),
y=subset(SPICEraq.meta$Pre.Post.med, VARIABLE.1=="CATEGORY.4"))
wilcox.test(x=subset(SPICEraq.meta$Pre.Post.med,      VARIABLE.1=="CATEGORY.2"),
y=subset(SPICEraq.meta$Pre.Post.med, VARIABLE.1=="CATEGORY.5"))
wilcox.test(x=subset(SPICEraq.meta$Pre.Post.med,      VARIABLE.1=="CATEGORY.3"),
y=subset(SPICEraq.meta$Pre.Post.med, VARIABLE.1=="CATEGORY.4"))
wilcox.test(x=subset(SPICEraq.meta$Pre.Post.med,      VARIABLE.1=="CATEGORY.3"),
y=subset(SPICEraq.meta$Pre.Post.med, VARIABLE.1=="CATEGORY.5"))
wilcox.test(x=subset(SPICEraq.meta$Pre.Post.med,      VARIABLE.1=="CATEGORY.4"),
y=subset(SPICEraq.meta$Pre.Post.med, VARIABLE.1=="CATEGORY.5"))
median(subset(SPICEraq.meta$Pre.Post.med,  VARIABLE.1=="CATEGORY.1"),  na.rm  =
TRUE)
median(subset(SPICEraq.meta$Pre.Post.med,  VARIABLE.1=="CATEGORY.2"),  na.rm  =
TRUE)
median(subset(SPICEraq.meta$Pre.Post.med,  VARIABLE.1=="CATEGORY.3"),  na.rm  =
TRUE)
median(subset(SPICEraq.meta$Pre.Post.med,  VARIABLE.1=="CATEGORY.4"),  na.rm  =
TRUE)
median(subset(SPICEraq.meta$Pre.Post.med,  VARIABLE.1=="CATEGORY.5"),  na.rm  =
TRUE)
```

2.6.10 Statistical tests

```
#Mann-Whitney U median tests comparing median.d13C. for post-SPICE compared by
VARIABLE.1
wilcox.test(x=subset(SPICEraq.sum$median.d13C.,       SPICE.zone=="Post"       &
VARIABLE.1=="CATEGORY.1"),                    y=subset(SPICEraq.sum$median.d13C.,
SPICE.zone=="Post" & VARIABLE.1=="CATEGORY.2"))
wilcox.test(x=subset(SPICEraq.sum$median.d13C.,       SPICE.zone=="Post"       &
VARIABLE.1=="CATEGORY.1"),                    y=subset(SPICEraq.sum$median.d13C.,
SPICE.zone=="Post" & VARIABLE.1=="CATEGORY.3"))
wilcox.test(x=subset(SPICEraq.sum$median.d13C.,       SPICE.zone=="Post"       &
VARIABLE.1=="CATEGORY.1"),                    y=subset(SPICEraq.sum$median.d13C.,
SPICE.zone=="Post" & VARIABLE.1=="CATEGORY.4"))
wilcox.test(x=subset(SPICEraq.sum$median.d13C.,       SPICE.zone=="Post"       &
VARIABLE.1=="CATEGORY.1"),                    y=subset(SPICEraq.sum$median.d13C.,
SPICE.zone=="Post" & VARIABLE.1=="CATEGORY.5"))
wilcox.test(x=subset(SPICEraq.sum$median.d13C.,       SPICE.zone=="Post"       &
VARIABLE.1=="CATEGORY.2"),                    y=subset(SPICEraq.sum$median.d13C.,
SPICE.zone=="Post" & VARIABLE.1=="CATEGORY.3"))
wilcox.test(x=subset(SPICEraq.sum$median.d13C.,       SPICE.zone=="Post"       &
VARIABLE.1=="CATEGORY.2"),                    y=subset(SPICEraq.sum$median.d13C.,
SPICE.zone=="Post" & VARIABLE.1=="CATEGORY.4"))
wilcox.test(x=subset(SPICEraq.sum$median.d13C.,       SPICE.zone=="Post"       &
VARIABLE.1=="CATEGORY.2"),                    y=subset(SPICEraq.sum$median.d13C.,
SPICE.zone=="Post" & VARIABLE.1=="CATEGORY.5"))
wilcox.test(x=subset(SPICEraq.sum$median.d13C.,       SPICE.zone=="Post"       &
VARIABLE.1=="CATEGORY.3"),                    y=subset(SPICEraq.sum$median.d13C.,
SPICE.zone=="Post" & VARIABLE.1=="CATEGORY.4"))
wilcox.test(x=subset(SPICEraq.sum$median.d13C.,       SPICE.zone=="Post"       &
VARIABLE.1=="CATEGORY.3"),                    y=subset(SPICEraq.sum$median.d13C.,
SPICE.zone=="Post" & VARIABLE.1=="CATEGORY.5"))
wilcox.test(x=subset(SPICEraq.sum$median.d13C.,       SPICE.zone=="Post"       &
VARIABLE.1=="CATEGORY.4"),                    y=subset(SPICEraq.sum$median.d13C.,
SPICE.zone=="Post" & VARIABLE.1=="CATEGORY.5"))
median(subset(SPICEraq.sum$median.d13C.,          SPICE.zone=="Post"          &
VARIABLE.1=="CATEGORY.1"))
median(subset(SPICEraq.sum$median.d13C.,          SPICE.zone=="Post"          &
VARIABLE.1=="CATEGORY.2"))
median(subset(SPICEraq.sum$median.d13C.,          SPICE.zone=="Post"          &
VARIABLE.1=="CATEGORY.3"))
median(subset(SPICEraq.sum$median.d13C.,          SPICE.zone=="Post"          &
VARIABLE.1=="CATEGORY.4"))
median(subset(SPICEraq.sum$median.d13C.,          SPICE.zone=="Post"          &
VARIABLE.1=="CATEGORY.5"))
```

```
#Mann-Whitney U median tests comparing max.d13C for Rising limb compared by
VARIABLE.1
wilcox.test(x=subset(SPICEraq.sum$max.d13C.,        SPICE.zone=="Rising"        &
VARIABLE.1=="CATEGORY.1"), y=subset(SPICEraq.sum$max.d13C., SPICE.zone=="Rising"
& VARIABLE.1=="CATEGORY.2"))
wilcox.test(x=subset(SPICEraq.sum$max.d13C.,        SPICE.zone=="Rising"        &
VARIABLE.1=="CATEGORY.1"), y=subset(SPICEraq.sum$max.d13C., SPICE.zone=="Rising"
& VARIABLE.1=="CATEGORY.3"))
wilcox.test(x=subset(SPICEraq.sum$max.d13C.,        SPICE.zone=="Rising"        &
VARIABLE.1=="CATEGORY.1"), y=subset(SPICEraq.sum$max.d13C., SPICE.zone=="Rising"
& VARIABLE.1=="CATEGORY.4"))
wilcox.test(x=subset(SPICEraq.sum$max.d13C.,        SPICE.zone=="Rising"        &
VARIABLE.1=="CATEGORY.1"), y=subset(SPICEraq.sum$max.d13C., SPICE.zone=="Rising"
& VARIABLE.1=="CATEGORY.5"))
wilcox.test(x=subset(SPICEraq.sum$max.d13C.,        SPICE.zone=="Rising"        &
VARIABLE.1=="CATEGORY.2"), y=subset(SPICEraq.sum$max.d13C., SPICE.zone=="Rising"
& VARIABLE.1=="CATEGORY.3"))
wilcox.test(x=subset(SPICEraq.sum$max.d13C.,        SPICE.zone=="Rising"        &
VARIABLE.1=="CATEGORY.2"), y=subset(SPICEraq.sum$max.d13C., SPICE.zone=="Rising"
& VARIABLE.1=="CATEGORY.4"))
wilcox.test(x=subset(SPICEraq.sum$max.d13C.,        SPICE.zone=="Rising"        &
VARIABLE.1=="CATEGORY.2"), y=subset(SPICEraq.sum$max.d13C., SPICE.zone=="Rising"
& VARIABLE.1=="CATEGORY.5"))
wilcox.test(x=subset(SPICEraq.sum$max.d13C.,        SPICE.zone=="Rising"        &
VARIABLE.1=="CATEGORY.3"), y=subset(SPICEraq.sum$max.d13C., SPICE.zone=="Rising"
& VARIABLE.1=="CATEGORY.4"))
wilcox.test(x=subset(SPICEraq.sum$max.d13C.,        SPICE.zone=="Rising"        &
VARIABLE.1=="CATEGORY.3"), y=subset(SPICEraq.sum$max.d13C., SPICE.zone=="Rising"
& VARIABLE.1=="CATEGORY.5"))
wilcox.test(x=subset(SPICEraq.sum$max.d13C.,        SPICE.zone=="Rising"        &
VARIABLE.1=="CATEGORY.4"), y=subset(SPICEraq.sum$max.d13C., SPICE.zone=="Rising"
& VARIABLE.1=="CATEGORY.5"))
median(subset(SPICEraq.sum$max.d13C.,           SPICE.zone=="Rising"           &
VARIABLE.1=="CATEGORY.1"))
median(subset(SPICEraq.sum$max.d13C.,           SPICE.zone=="Rising"           &
VARIABLE.1=="CATEGORY.2"))
median(subset(SPICEraq.sum$max.d13C.,           SPICE.zone=="Rising"           &
VARIABLE.1=="CATEGORY.3"))
median(subset(SPICEraq.sum$max.d13C.,           SPICE.zone=="Rising"           &
VARIABLE.1=="CATEGORY.4"))
median(subset(SPICEraq.sum$max.d13C.,           SPICE.zone=="Rising"           &
VARIABLE.1=="CATEGORY.4"))
```

```
#Mann-Whitney U median tests comparing min.d13C for Rising limb compared by
VARIABLE.1
wilcox.test(x=subset(SPICEraq.sum$min.d13C,        SPICE.zone=="Rising"        &
VARIABLE.1=="CATEGORY.1"),  y=subset(SPICEraq.sum$min.d13C,  SPICE.zone=="Rising"
& VARIABLE.1=="CATEGORY.2"))
wilcox.test(x=subset(SPICEraq.sum$min.d13C,        SPICE.zone=="Rising"        &
VARIABLE.1=="CATEGORY.1"),  y=subset(SPICEraq.sum$min.d13C,  SPICE.zone=="Rising"
& VARIABLE.1=="CATEGORY.3"))
wilcox.test(x=subset(SPICEraq.sum$min.d13C,        SPICE.zone=="Rising"        &
VARIABLE.1=="CATEGORY.1"),  y=subset(SPICEraq.sum$min.d13C,  SPICE.zone=="Rising"
& VARIABLE.1=="CATEGORY.4"))
wilcox.test(x=subset(SPICEraq.sum$min.d13C,        SPICE.zone=="Rising"        &
VARIABLE.1=="CATEGORY.1"),  y=subset(SPICEraq.sum$min.d13C,  SPICE.zone=="Rising"
& VARIABLE.1=="CATEGORY.5"))
wilcox.test(x=subset(SPICEraq.sum$min.d13C,        SPICE.zone=="Rising"        &
VARIABLE.1=="CATEGORY.2"),  y=subset(SPICEraq.sum$min.d13C,  SPICE.zone=="Rising"
& VARIABLE.1=="CATEGORY.3"))
wilcox.test(x=subset(SPICEraq.sum$min.d13C,        SPICE.zone=="Rising"        &
VARIABLE.1=="CATEGORY.2"),  y=subset(SPICEraq.sum$min.d13C,  SPICE.zone=="Rising"
& VARIABLE.1=="CATEGORY.4"))
wilcox.test(x=subset(SPICEraq.sum$min.d13C,        SPICE.zone=="Rising"        &
VARIABLE.1=="CATEGORY.2"),  y=subset(SPICEraq.sum$min.d13C,  SPICE.zone=="Rising"
& VARIABLE.1=="CATEGORY.5"))
wilcox.test(x=subset(SPICEraq.sum$min.d13C,        SPICE.zone=="Rising"        &
VARIABLE.1=="CATEGORY.3"),  y=subset(SPICEraq.sum$min.d13C,  SPICE.zone=="Rising"
& VARIABLE.1=="CATEGORY.4"))
wilcox.test(x=subset(SPICEraq.sum$min.d13C,        SPICE.zone=="Rising"        &
VARIABLE.1=="CATEGORY.3"),  y=subset(SPICEraq.sum$min.d13C,  SPICE.zone=="Rising"
& VARIABLE.1=="CATEGORY.5"))
wilcox.test(x=subset(SPICEraq.sum$min.d13C,        SPICE.zone=="Rising"        &
VARIABLE.1=="CATEGORY.4"),  y=subset(SPICEraq.sum$min.d13C,  SPICE.zone=="Rising"
& VARIABLE.1=="CATEGORY.5"))
median(subset(SPICEraq.sum$min.d13C,           SPICE.zone=="Rising"           &
VARIABLE.1=="CATEGORY.1"))
median(subset(SPICEraq.sum$min.d13C,           SPICE.zone=="Rising"           &
VARIABLE.1=="CATEGORY.2"))
median(subset(SPICEraq.sum$min.d13C,           SPICE.zone=="Rising"           &
VARIABLE.1=="CATEGORY.3"))
median(subset(SPICEraq.sum$min.d13C,           SPICE.zone=="Rising"           &
VARIABLE.1=="CATEGORY.4"))
median(subset(SPICEraq.sum$min.d13C,           SPICE.zone=="Rising"           &
VARIABLE.1=="CATEGORY.5"))
```

```
#Mann-Whitney U median tests comparing median.d13C for Pre SPICE compared by
VARIABLE.1
wilcox.test(x=subset(SPICEraq.sum$median.d13C.,        SPICE.zone=="Pre"        &
VARIABLE.1=="CATEGORY.1"), y=subset(SPICEraq.sum$median.d13C., SPICE.zone=="Pre"
& VARIABLE.1=="CATEGORY.2"))
wilcox.test(x=subset(SPICEraq.sum$median.d13C.,        SPICE.zone=="Pre"        &
VARIABLE.1=="CATEGORY.1"), y=subset(SPICEraq.sum$median.d13C., SPICE.zone=="Pre"
& VARIABLE.1=="CATEGORY.3"))
wilcox.test(x=subset(SPICEraq.sum$median.d13C.,        SPICE.zone=="Pre"        &
VARIABLE.1=="CATEGORY.1"), y=subset(SPICEraq.sum$median.d13C., SPICE.zone=="Pre"
& VARIABLE.1=="CATEGORY.4"))
wilcox.test(x=subset(SPICEraq.sum$median.d13C.,        SPICE.zone=="Pre"        &
VARIABLE.1=="CATEGORY.1"), y=subset(SPICEraq.sum$median.d13C., SPICE.zone=="Pre"
& VARIABLE.1=="CATEGORY.5"))
wilcox.test(x=subset(SPICEraq.sum$median.d13C.,        SPICE.zone=="Pre"        &
VARIABLE.1=="CATEGORY.2"), y=subset(SPICEraq.sum$median.d13C., SPICE.zone=="Pre"
& VARIABLE.1=="CATEGORY.3"))
wilcox.test(x=subset(SPICEraq.sum$median.d13C.,        SPICE.zone=="Pre"        &
VARIABLE.1=="CATEGORY.2"), y=subset(SPICEraq.sum$median.d13C., SPICE.zone=="Pre"
& VARIABLE.1=="CATEGORY.4"))
wilcox.test(x=subset(SPICEraq.sum$median.d13C.,        SPICE.zone=="Pre"        &
VARIABLE.1=="CATEGORY.2"), y=subset(SPICEraq.sum$median.d13C., SPICE.zone=="Pre"
& VARIABLE.1=="CATEGORY.5"))
wilcox.test(x=subset(SPICEraq.sum$median.d13C.,        SPICE.zone=="Pre"        &
VARIABLE.1=="CATEGORY.3"), y=subset(SPICEraq.sum$median.d13C., SPICE.zone=="Pre"
& VARIABLE.1=="CATEGORY.4"))
wilcox.test(x=subset(SPICEraq.sum$median.d13C.,        SPICE.zone=="Pre"        &
VARIABLE.1=="CATEGORY.3"), y=subset(SPICEraq.sum$median.d13C., SPICE.zone=="Pre"
& VARIABLE.1=="CATEGORY.5"))
wilcox.test(x=subset(SPICEraq.sum$median.d13C.,        SPICE.zone=="Pre"        &
VARIABLE.1=="CATEGORY.4"), y=subset(SPICEraq.sum$median.d13C., SPICE.zone=="Pre"
& VARIABLE.1=="CATEGORY.5"))
median(subset(SPICEraq.sum$median.d13C.,           SPICE.zone=="Pre"           &
VARIABLE.1=="CATEGORY.1"))
median(subset(SPICEraq.sum$median.d13C.,           SPICE.zone=="Pre"           &
VARIABLE.1=="CATEGORY.2"))
median(subset(SPICEraq.sum$median.d13C.,           SPICE.zone=="Pre"           &
VARIABLE.1=="CATEGORY.3"))
median(subset(SPICEraq.sum$median.d13C.,           SPICE.zone=="Pre"           &
VARIABLE.1=="CATEGORY.4"))
median(subset(SPICEraq.sum$median.d13C.,           SPICE.zone=="Pre"           &
VARIABLE.1=="CATEGORY.5"))
```

2.6.11 Randomization comparing median peak SPICE values across paleolatitude bins

```
library(coin)
library(ggplot2)
library(ggthemes)

SpiceSummary <- read.csv("SPICESummary.csv", header = TRUE, sep = ",")
attach(SpiceSummary)

#Conduct a randomization to compare median SPICE peak values between two groups
(middle southern latitudes and tropical latitudes)
#Methodology                                                                from:
https://www.uvm.edu/~statdhtx/StatPages/ResamplingWithR/Random2Medians/MedianDi
fference.r

#SpiceSummary data from Table 1
n1                                                                          <-
length(SpiceSummary$Rise.max.d13C[SpiceSummary$Paleo.Latitude.Binned=="Tropics"
])
n2                                                                          <-
length(SpiceSummary$Rise.max.d13C[SpiceSummary$Paleo.Latitude.Binned=="Middle.S
outh"])
N <- n1 + n2

Group1                                                                      <-
SpiceSummary$Rise.max.d13C[SpiceSummary$Paleo.Latitude.Binned=="Tropics"]
Group2                                                                      <-
SpiceSummary$Rise.max.d13C[SpiceSummary$Paleo.Latitude.Binned=="Middle.South"]

md1 <- median(Group1, na.rm = TRUE)
md2 <- median(Group2, na.rm = TRUE)

par(mfrow = c(2,1))
hist(Group1, col = "red", xlim = c(min(SpiceSummary$Rise.max.d13C, na.rm = TRUE),
max(SpiceSummary$Rise.max.d13C, na.rm = TRUE)) )
hist(Group2, col = "green", xlim = c(min(SpiceSummary$Rise.max.d13C, na.rm =
TRUE), max(SpiceSummary$Rise.max.d13C, na.rm = TRUE)) )

obt.med.diff <- md1 - md2
cat("The obtained median difference is ", '\n', obt.med.diff, '\n')

nreps = 10000
set.seed(1086)
samp.med.dff <- numeric(nreps)
for(i in 1:nreps) {
```

```
  resamp.data <- sample(SpiceSummary$Rise.max.d13C,
length(SpiceSummary$Rise.max.d13C), replace = FALSE)
  Grp1 <- resamp.data[1:n1]
  Grp2 <- resamp.data[(n1+1):N]
  md1 <- median(Grp1, na.rm = TRUE)
  md2 <- median(Grp2, na.rm = TRUE)
  samp.med.dff[i] <- md1 - md2
}
obt.med.diff <- abs(obt.med.diff)
pUpper <- length(samp.med.dff[samp.med.dff >= obt.med.diff])/nreps
pLower <- length(samp.med.dff[samp.med.dff <= (-1)*obt.med.diff])/nreps
pExtreme <- pLower + pUpper
cat("The two-tailed probability under the null hypothesis is =", '\n', pExtreme,
'\n')

#Calculate Confidence limits
CIupper <- quantile(samp.med.dff, 0.975)
CIlower <- quantile(samp.med.dff, 0.025)
cat("The 95% confidence limits are = ", '\n', CIlower, "and", CIupper, '\n')

#Create more visually appealing histograms of peak SPICE values and sampling
distribution from randomization
SamplingDistribution <- data.frame(samp.med.dff)
ggplot() + geom_histogram(data = SamplingDistribution,
aes(SamplingDistribution$samp.med.dff))

attach(SpiceSummary)
ggplot(data = SpiceSummary) + geom_histogram(aes(Rise.max.d13C,
fill=Paleo.Latitude.Binned)) + scale_fill_colorblind() + theme_classic() +
xlab("Maximum Value of SPICE Rising Limb (d13C)") + ylab("Frequency") + theme(text
= element_text(size=20))

attach(SamplingDistribution)
ggplot() + geom_histogram(data = SamplingDistribution, aes(samp.med.dff),
fill="black") + theme_classic() + xlab("Median Tropics - Median 30-60* S Peak
SPICE Value (d13C)") + ylab("Frequency") + geom_vline(aes(xintercept=CIlower),
linetype=2, size=1) + geom_vline(aes(xintercept=CIupper), linetype=2, size=1) +
geom_vline(aes(xintercept=(md1-md2)), color="red", size=1) + ggtitle("10,000
Iteration Randomization") + theme(text = element_text(size=20))
```

2.7 Description of variables in the SPICEraq and SWEETS group

Below is a description of all columns in the SPICEraq and SWEETS group data tables, included as a single Excel file in the SOM. Any information not provided by the original publication, or not applicable to a specific sample, is marked "NA".

- Column A — Reference
    - Reference for the original publication the data was taken from.
- Column B — Entry number
    - Each section was assigned a unique entry number. Entries are organized according to modern geographic region, then alphabetically by first author, and then chronologically by publication year.
- Column C — Sample
    - Sample number/name, if provided in the original data tables or figures.
- Column D — Strat Height
    - Stratigraphic height (in meters) of samples as published in the original papers, if the entry is from a measured stratigraphic section on outcrop.
- Column E — Borehole depth
    - Borehole depth (in meters) of samples as published in the original papers, if entry is from a measured section on core.
- Column F — Meters above the bottom
    - To mitigate stratigraphic variation across entries, the stratigraphic height or borehole depth of each sample was recalculated as meters above the bottommost sample in that entry.
- Column G — Meters above onset
    - For purposes of aligning the SPICE, Column F was modified such that the onset of the rising limb was set to a value of 0.0 m. Pre-SPICE strat heights/borehole depths are then recorded as negative values. All samples marked "Omit" for the SPICE zone (Column H) are marked "NA" for this column. For the SWEETS group, this entire column is marked "NA" as no SPICE zones are identified.
- Column H — SPICE zone
    - Each entry was broken down into 5 possible SPICE zones: 1) Pre, 2) Rising, 3) Plateau [if present], 4) Falling, 5) Post. For some entries, the bottommost samples in the Pre-SPICE zone or the uppermost Post-SPICE zone were omitted because they captured other $\delta^{13}C$ excursions besides the SPICE. These samples are labelled as "Omit" for the SPICE zone. See the main text for a detailed description of these zones. For the SWEETS group, this entire column is marked "NA" as no SPICE zones are identified.

- Column I — d13C
    - $\delta^{13}C_{carb}$ (‰ V-PDB) values as provided in the original publication
- Column J —d18O
    - $\delta^{18}O_{carb}$ (‰ V-PDB) values as provided in the original publication
- Column K — d13C org
    - For those publications that provided $\delta^{13}C_{org}$ data on the same samples used for $\delta^{13}C_{carb}$, those values are included here (‰).
- Column L — TOC
    - For those publications that provided TOC (%) data for the samples, the values are reproduced here.
- Column M — Lithology
    - Sample lithology, as denoted by data tables, stratigraphic column figures, or in-text description. This is a more specific lithological description than the "carbonate", limestone, or dolostone designations for the SPICE peak, as is noted in the above entry descriptions and in-text Table 1.
- Column N — Simplified facies
    - The simplified facies description for each entry as used for all analyses in this study: Shallow/nearshore, Shelf, Intrashelf basin, Slope, Basin. Shallow/nearshore facies correspond to shallow water; Shelf and Intrashelf basin facies correspond to intermediate water depth; Slope and Basin facies correspond to deep water. All samples in one entry have the same simplified facies descriptor. For details on how the simplified facies descriptor was chosen, see the entry descriptions at the beginning of this SOM file.
- Column O — Facies
    - More detailed facies descriptions for samples/entries, as provided in the original publication.
- Column P — Group/Formation
    - Geologic group or formation the sample is from. If only one unit subdivision was noted in the original publication, it is included in this column regardless of its position within the hierarchy of unit names.
- Column Q — Unit/Member
    - If a group or formation was further subdivided into a unit or a member (or any additional information was provided), it is noted here.
- Column R — Borehole
    - If applicable, the name of the borehole a core section is from.
- Column S — Section
    - If applicable, the name of the measured stratigraphic section an entry is from.
- Column T — Biozone
    - Biostratigraphic trilobite zones, as indicated by the original publication.

- Column U — Epoch/Series
    - Chronostratigraphic Epoch or Series of each sample, as indicated by the original publication.
- Column V — Stage/Age
    - Chronostratigraphic Stage or age of each sample, as indicated by the original publication.
- Column W — Location
    - Present day geographic location of the section including country, state/province, and/or county/city.
- Column X — Present latitude
    - Present day latitude of the section in decimal degrees. If the precise latitude of the section was noted in the original publication, it is copied here. If no precise latitude was provided in the original publication, the latitude of the nearest city as shown on in-text location maps is recorded here.
- Column Y — Present longitude
    - Present day longitude of the section in decimal degrees. If the precise longitude of the section was noted in the original publication, it is copied here. If no precise latitude was provided in the original publication, the longitude of the nearest city as shown on in-text location maps is recorded here.
- Column Z — Paleocontinent
    - Paleocontinent where the section was located ca. 500 Ma: Gondwana, Kazakhstania, Laurentia, Siberia. Based on the 500 Ma paleogeographic reconstruction in GPlates (Müller et al., 2018).
- Column AA — Paleolatitude
    - Paleolatitudinal zone of the section ca. 500 Ma, with the globe divided into 6 zones: 1) 90–60° N, 2) 60–30° N, 3) 30–0° N, 4) 0–30° S, 5) 30–60° S, 6) 60–90° S. Based on the 500 Ma paleogeographic reconstruction in GPlates (Müller et al., 2018).
- Column AB — Placeholder
    - This is a simple sequential number series to aid in resorting.

2.8 Complete reference list for Chapters 1 and 2

The reference lists for Chapters 1 and 2 (both of which are about the SPICEraq) have been combined into a single list categorized herein as Section 2.8. This was done to prevent unnecessary repetition as the vast majority of the following references were cited in both chapters.

Ahlberg, P., Axheimer, N., Babcock, L.E., Eriksson, M.E., Schmitz, B., Terfelt, F., 2009. Cambrian high-resolution biostratigraphy and carbon isotope chemostratigraphy in Scania, Sweden: first record of the SPICE and DICE excursions in Scandinavia. Lethaia 42, 2–16. https://doi.org/10.1111/j.1502-3931.2008.00127.x

Ahlberg, P., Lundberg, F., Erlström, M., Calner, M., Lindskog, A., Dalhqvist, P., Joachimski, M.M., 2019. Integrated Cambrian biostratigraphy and carbon isotope chemostratigraphy of the Grönhögen-2015 drill core, Öland, Sweden. Geol. Mag. 156, 935–949. https://doi.org/10.1017/S0016756818000298

Ahm, A.S.C., Bjerrum, C.J., Blättler, C.L., Swart, P.K., Higgins, J.A., 2018. Quantifying early marine diagenesis in shallow-water carbonate sediments. Geochim. Cosmochim. Acta 236, 140–159. https://doi.org/10.1016/j.gca.2018.02.042

Álvaro, J.J., Bauluz, B., Subias, I., Pierre, C., Vizcaino, D., 2008. Carbon chemostratigraphy of the Cambrian-Ordovician transition in a midlatitude mixed platform, Montagne Noire, France. Geol. Soc. Am. Bull. 120, 962–975. https://doi.org/10.1130/B26243.1

Auerbach, D.J., 2004. The Steptoean Positive Isotopic Carbon Excursion (SPICE) in siliciclastic facies of the Upper Mississippi Valley: Implications for mass extinction and sea level change in the Upper Cambrian. Carleton College.

Azmy, K., 2019. Carbon-isotope stratigraphy of the SPICE event (Upper Cambrian) in eastern Laurentia: implications for global correlation and a potential reference section. Geol. Mag. 156, 1311–1322. https://doi.org/10.1017/S0016756818000638

Baker, J.L., 2010. Carbon isotopic fractionation across a late Cambrian carbonate platform: A regional response to the SPICE event as recorded in the Great Basin (M.S. thesis). University of Nevada, Las Vegas.

Barili, R., Neilson, J.E., Brasier, A.T., Goldberg, K., Pastro Bardola, T., De Ros, L.F., Leng, M., 2018. Carbon isotopes, stratigraphy, and environmental change: the Middle–Upper Cambrian Positive Excursion (SPICE) in Port au Port Group, western Newfoundland, Canada. Can. J. Earth Sci. 55, 1209–1222. https://doi.org/10.1139/cjes-2018-0025

Bond, D.P.G., Grasby, S.E., 2017. On the causes of mass extinctions. Palaeogeogr. Palaeoclimatol. Palaeoecol. 478, 3–29. https://doi.org/10.1016/j.palaeo.2016.11.005

Brasier, M.D., 1993. Towards a carbon isotope stratigraphy of the Cambrian System: potential of the Great Basin succession. Geol. Soc. London, Spec. Publ. 70, 341–350. https://doi.org/10.1144/GSL.SP.1993.070.01.22

Brenchley, P.J., Marshall, J.D., Carden, G.A.F., Robertson, D.B.R., Long, D.G.F., Meidla, T., Hints, L., Anderson, T.F., 1994. Bathymetric and isotopic evidence for a short-lived Late Ordovician glaciation in a greenhouse period. Geology 22, 295–298. https://doi.org/10.1130/0091-7613(1994)022<0295:BAIEFA>2.3.CO;2

Buggisch, W., Keller, M., Lehnert, O., 2003. Carbon isotope record of Late Cambrian to Early Ordovician carbonates of the Argentine Precordillera. Palaeogeogr. Palaeoclimatol. Palaeoecol. 195, 357–373. https://doi.org/10.1016/S0031-0182(03)00365-1

Bureau of Geology and Mineral Resources of Shandong Province (BGMRSP), 1996. Stratigraphy (Lithostratigraphic) of Shandong Province. China University of Geoscience Press, Beijing, China. (in Chinese)

Chen, J., Chough, S.K., Han, Z., Lee, J.-H., 2011. An extensive erosion surface of a strongly deformed limestone bed in the Gushan and Chaomidian formations (late Middle Cambrian to Furongian), Shandong Province, China: Sequence–stratigraphic implications. Sediment. Geol. 233, 129–149. https://doi.org/10.1016/j.sedgeo.2010.11.002

Chough, S.K., Lee, H.S., Woo, J., Chen, J., Choi, D.K., Lee, S., Kang, I., Park, T., Han, Z., 2010. Cambrian stratigraphy of the North China Platform: revisiting principal sections in Shandong Province, China. Geosci. J. 14, 235–268. https://doi.org/10.1007/s12303-010-0029-x

Chung, G.-S., Lee, J.-G., Lee, K.-S., 2011. Stable Carbon Isotope Stratigraphy of the Cambrian Machari Formation in the Yeongweol Area, Gangweon Province, Korea. J. Korean earth Sci. Soc. 32, 437–452. https://doi.org/10.5467/JKESS.2011.32.5.437

Cowan, C.A., Fox, D.L., Runkel, A.C., Saltzman, M.R., 2005. Terrestrial-marine carbon cycle coupling in ~500-m.y.-old phosphatic brachiopods. Geology 33, 661. https://doi.org/10.1130/G21434.1

Dahl, T.W., Boyle, R.A., Canfield, D.E., Connelly, J.N., Gill, B.C., Lenton, T.M., Bizzarro, M., 2014. Uranium isotopes distinguish two geochemically distinct stages during the later Cambrian SPICE event. Earth Planet. Sci. Lett. 401, 313–326. https://doi.org/10.1016/j.epsl.2014.05.043

Dilliard, K.A., Pope, M.C., Coniglio, M., Hasiotis, S.T., Lieberman, B.S., 2007. Stable isotope geochemistry of the lower Cambrian Sekwi Formation, Northwest Territories, Canada: Implications for ocean chemistry and secular curve generation. Palaeogeogr. Palaeoclimatol. Palaeoecol. 256, 174–194. https://doi.org/10.1016/j.palaeo.2007.02.031

Elrick, M., Rieboldt, S., Saltzman, M., McKay, R.M., 2011. Oxygen-isotope trends and seawater temperature changes across the Late Cambrian Steptoean positive carbon-isotope excursion (SPICE event). Geology 39, 987–990. https://doi.org/10.1130/G32109.1

Ferreri, V., Weissert, H., D'Argenio, B., Buonocunto, F.P., 1997. Carbon isotope stratigraphy: A tool for basin to carbonate platform correlation. Terra Nov. 9, 57–61. https://doi.org/10.1111/j.1365-3121.1997.tb00002.x

Gerhardt, A.M., 2014. Carbon cycle changes during the end-Marjuman (Cambrian) extinction int he Southern Appalachians. Virginia Polytechnic Institute and State University.

Gerhardt, A.M., Gill, B.C., 2016. Elucidating the relationship between the later Cambrian end-Marjuman extinctions and SPICE Event. Palaeogeogr. Palaeoclimatol. Palaeoecol. 461, 362–373. https://doi.org/10.1016/j.palaeo.2016.08.031

Geyer, G., 2019. A comprehensive Cambrian correlation chart. Episodes 42, 321–332. https://doi.org/10.18814/epiiugs/2019/019026

Gill, B.C., Lyons, T.W., Saltzman, M.R., 2007. Parallel, high-resolution carbon and sulfur isotope records of the evolving Paleozoic marine sulfur reservoir. Palaeogeogr. Palaeoclimatol. Palaeoecol. 256, 156–173. https://doi.org/10.1016/j.palaeo.2007.02.030

Gill, B.C., Lyons, T.W., Young, S.A., Kump, L.R., Knoll, A.H., Saltzman, M.R., 2011. Geochemical evidence for widespread euxinia in the Later Cambrian ocean. Nature 469, 80–83. https://doi.org/10.1038/nature09700

Glumac, B., 2011. High-resolution stratigraphy and correlation of Cambrian strata using carbon isotopes: an example from the southern Appalachians, USA. Carbonates and Evaporites 26, 287–297. https://doi.org/10.1007/s13146-011-0065-2

Glumac, B., Mutti, L.E., 2007. Late Cambrian (Steptoean) sedimentation and responses to sea-level change along the northeastern Laurentian margin: Insights from carbon isotope stratigraphy. Geol. Soc. Am. Bull. 119, 623–636. https://doi.org/10.1130/B25897.1

Glumac, B., Spivak-Birndorf, M.L., 2002. Stable isotopes of carbon as an invaluable stratigraphic tool: An example from the Cambrian of the northern Appalachians, USA. Geology 30, 563. https://doi.org/10.1130/0091-7613(2002)030<0563:SIOCAA>2.0.CO;2

Glumac, B., Walker, K.R., 1998. A Late Cambrian positive carbon-isotope excursion in the Southern Appalachians; relation to biostratigraphy, sequence stratigraphy, environments of deposition, and diagenesis. J. Sediment. Res. 68, 1212–1222. https://doi.org/10.2110/jsr.68.1212

Hammer, Ø., Harper, D.A.T., Ryan, P.D., 2001. PAST: Paleontological statistics software package for education and data analysis. Palaeontol. Electron. 4, 9pp.

Harper, D.A.T., Topper, T.P., Cascales-Miñana, B., Servais, T., Zhang, Y.-D., Ahlberg, P., 2019. The Furongian (late Cambrian) Biodiversity Gap: Real or apparent? Palaeoworld 28, 4–12. https://doi.org/10.1016/j.palwor.2019.01.007

He, Z., 1995. Sedimentary facies and variation of stable isotope composition of Upper Cambrian to Lower Ordovician strata in Southern Missouri: Implications for the origin of MVT deposits, and the geochemical and hydrological features of regional ore-forming fluids (Ph.D. dissertation). University of Missouri-Rolla. 124 p.

He, Z., Gregg, J.M., Shelton, K.L., Palmer, J.R., 1997. Sedimentary facies control of fluid flow and mineralization in Cambro-Ordovician strata, Southern Missouri, in: Basin-Wide Diagenetic Patterns: Integrated Petrologic, Geochemical, and Hydrological Considerations. SEPM Special Publication No. 57.

Higgins, J.A., Blättler, C.L., Lundstrom, E.A., Santiago-Ramos, D.P., Akhtar, A.A., Crüger Ahm, A.S., Bialik, O., Holmden, C., Bradbury, H., Murray, S.T., Swart, P.K., 2018. Mineralogy, early marine diagenesis, and the chemistry of shallow-water carbonate sediments. Geochim. Cosmochim. Acta 220, 512–534. https://doi.org/10.1016/j.gca.2017.09.046

Huang, J., Chen, Y., Chu, X., Sun, T., 2019. The geochemistry of the late Cambrian carbonate in North China: the Steptoean Positive Carbon Isotope Excursion (SPICE) record suppressed in a coastal condition? Geol. Mag. 156, 1805–1819. https://doi.org/10.1017/S0016756819000025

Hurtgen, M.T., Pruss, S.B., Knoll, A.H., 2009. Evaluating the relationship between the carbon and sulfur cycles in the later Cambrian ocean: An example from the Port au Port Group, western Newfoundland, Canada. Earth Planet. Sci. Lett. 281, 288–297. https://doi.org/10.1016/j.epsl.2009.02.033

Jeffrey, M.J., 2017. Stratigraphic variation of the Late Cambrian SPICE event in Upper Cambrian carbonates of southern Missouri (M.S. thesis). University of Missouri-Columbia.

Jeffrey, M.J., Huntley, J.W., Schiffbauer, J.D., Fike, D.A., Shelton, K.L., 2017. Influences of environmental variation and sedimentation rate on the recording of the Steptoean Positive Carbon Isotope Excursion (SPICE) in Missouri, in: GSA Program with Abstracts. p. 300613. https://doi.org/10.1130/abs/2017AM-300613

Jones, D.S., Brothers, R.W., Ahm, A.S.C., Slater, N., Higgins, J.A., Fike, D.A., 2020. Sea level, carbonate mineralogy, and early diagenesis controlled $\delta^{13}C$ records in Upper Ordovician carbonates. Geology 48, 194–199. https://doi.org/10.1130/G46861.1

Karlstrom, K.E., Mohr, M.T., Schmitz, M.D., Sundberg, F.A., Rowland, S.M., Blakey, R., Foster, J.R., Crossey, L.J., Dehler, C.M., Hagadorn, J.W., 2020. Redefining the Tonto Group of Grand Canyon and recalibrating the Cambrian time scale. Geology 48, 425–430. https://doi.org/10.1130/G46755.1

Kaufman, A.J., Knoll, A.H., Awramik, S.M., 1992. Biostratigraphic and chemostratigraphic correlation of Neoproterozoic sedimentary successions: Upper Tindir Group, northwestern Canada, as a test case. Geology 20, 181. https://doi.org/10.1130/0091-7613(1992)020<0181:BACCON>2.3.CO;2

Knoll, A.H., Hayes, J.M., Kaufman, A.J., Swett, K., Lambert, I.B., 1986. Secular variation in carbon isotope ratios from Upper Proterozoic successions of Svalbard and East Greenland. Nature 321, 832–838. https://doi.org/10.1038/321832a0

Kouchinsky, A., Bengton, S., Gallet, Y., Korovnikov, I., Pavlov, V., Runnegar, B., Shields, G., Veizer, J., Young, E., Ziegler, K., 2008. The SPICE carbon isotope excursion in Siberia: a combined study of the upper Middle Cambrian–lowermost Ordovician Kulyumbe River section, northwestern Siberian Platform. Geol. Mag. 145, 609–622. https://doi.org/10.1017/S0016756808004913

Kump, L.R., 1991. Interpreting carbon-isotope excursions: Strangelove oceans. Geology 19, 299. https://doi.org/10.1130/0091-7613(1991)019<0299:ICIESO>2.3.CO;2

Labotka, D.M., Freiburg, J.T., 2020. Geochemical Preservation of the Steptoean Positive Carbon Isotope Excursion (SPICE) Event in Dolomites of the Furongian Franconia Formation in the Illinois Basin. Illinois State Geol. Surv. Circular 6, 11.

Laudon, P.R., 1992. Dolomite neomorphism and water-rock relationships in the mineralized Bonneterre Dolomite (Cambrian), Southeast Missouri (M.S. thesis). University of Missouri-Rolla. 165 p.

LeRoy, M.A., Gill, B.C., 2019. Evidence for the development of local anoxia during the Cambrian SPICE event in eastern North America. Geobiology 17, 381–400. https://doi.org/10.1111/gbi.12334

Li, D., Zhang, X., Hu, D., Chen, X., Huang, W., Zhang, Xu, Li, M., Qin, L., Peng, S., Shen, Y., 2018b. Evidence of a large $\delta^{13}C_{carb}$ and $\delta^{13}C_{org}$ depth gradient for deep-water anoxia during the late Cambrian SPICE event. Geology 46, 631–634. https://doi.org/10.1130/G40231.1

Li, W., Jia, P., Fan, R., Lu, Y., Li, X., Deng, S., 2018a. Carbon isotope characteristics of the Middle–Upper Cambrian Xixiangchi Group and bottom boundary marks of Furongian Series in the Sichuan Basin and its adjacent areas. Nat. Gas Ind. B 5, 177–184. https://doi.org/10.1016/j.ngib.2018.04.004

Lim, J.N., Chung, G.S., Park, T.-Y.S., Lee, K.S., 2015. Lithofacies and Stable Carbon Isotope Stratigraphy of the Cambrian Sesong Formation in the Taebaeksan Basin, Korea. J. Korean earth Sci. Soc. 36, 617–631. https://doi.org/10.5467/JKESS.2015.36.7.617

Lindsay, J.F., Kruse, P.D., Green, O.R., Hawkins, E., Brasier, M.D., Cartlidge, J., Corfield, R.M., 2005. The Neoproterozoic–Cambrian record in Australia: A stable isotope study. Precambrian Res. 143, 113–133. https://doi.org/10.1016/j.precamres.2005.10.002

Liu, H., Liao, Z., Zhang, H., Tian, Y., Cheng, B., Yang, S., 2017. Stable isotope ($\delta^{13}C_{ker}$, $\delta^{13}C_{carb}$, $\delta^{18}O_{carb}$) distribution along a Cambrian outcrop section in the eastern Tarim Basin, NW China and its geochemical significance. Geosci. Front. 8, 163–170. https://doi.org/10.1016/j.gsf.2016.02.004

Mackey, J.E., Stewart, B.W., 2019. Evidence of SPICE-related anoxia on the Laurentian passive margin: Paired $\delta^{13}C$ and trace element chemostratigraphy of the upper Conasauga Group, Central Appalachian Basin. Palaeogeogr. Palaeoclimatol. Palaeoecol. 528, 160–174. https://doi.org/10.1016/j.palaeo.2019.04.018

Maloof, A.C., Schrag, D.P., Crowley, J.L., Bowring, S.A., 2005. An expanded record of Early Cambrian carbon cycling from the Anti-Atlas Margin, Morocco. Can. J. Earth Sci. 42, 2195–2216. https://doi.org/10.1139/e05-062

Markello, J.R., Read, J.F., 1981. Carbonate ramp-to-deeper shale shelf transitions of an Upper Cambrian intrashelf basin, Nolichucky Formation, Southwest Virginia Appalachians. Sedimentology 28, 573–597. https://doi.org/10.1111/j.1365-3091.1981.tb01702.x

Melchin, M.J., Mitchell, C.E., Holmden, C., Štorch, P., 2013. Environmental changes in the late ordovician-early silurian: Review and new insights from black shales and nitrogen isotopes. Bull. Geol. Soc. Am. 125, 1635–1670. https://doi.org/10.1130/B30812.1

Müller, R.D., Cannon, J., Qin, X., Watson, R.J., Gurnis, M., Williams, S., Pfaffelmoser, T., Seton, M., Russell, S.H.J., Zahirovic, S., 2018. GPlates: Building a Virtual Earth Through Deep Time. Geochemistry, Geophys. Geosystems 19, 2243–2261. https://doi.org/10.1029/2018GC007584

Myrow, P.M., Taylor, J.F., Runkel, A.C., Ripperdan, R.L., 2012. Mixed Siliciclastic-Carbonate Upward-Deepening Cycles of the Upper Cambrian Inner Detrital Belt of Laurentia. J. Sediment. Res. 82, 216–231. https://doi.org/10.2110/jsr.2012.20

Ng, T.-W., Yuan, J.-L., Lin, J.-P., 2014. The North China Steptoean Positive Carbon Isotope Event: New insights towards understanding a global phenomenon. Geobios 47, 371–387. https://doi.org/10.1016/j.geobios.2014.09.003

Palmer, A.R., 1984. The biomere problem: Evolution of an idea. J. Paleontol. 58, 599–611.

Palmer, J., Thompson, T.L., Seeger, C., Miller, J.F., Gregg, J.M., 2012. The Sauk Megasequence from the Reelfoot Rift to Southwestern Missouri. Gt. Am. carbonate bank Geol. Econ. Resour. Cambrian-Ordovician Sauk megasequence Laurentia AAPG Memoi, 1013–1030. https://doi.org/10.1306/13331527M983518

Patterson, W.P., Walter, L.M., 1994. Depletion of ^{13}C in seawater ΣCO_2 on modern carbonate platforms: Significance for the carbon isotopic record of carbonates. Geology 22, 885. https://doi.org/10.1130/0091-7613(1994)022<0885:DOCISC>2.3.CO;2

Peng, S., Babcock, L., Robison, R., Lin, H., Rees, M., Saltzman, M., 2004. Global Standard Stratotype-section and Point (GSSP) of the Furongian Series and Paibian Stage (Cambrian). Lethaia 37, 365–379. https://doi.org/10.1080/00241160410002081

Peng, Y., Peng, Y., Lang, X., Ma, H., Huang, K., Li, F., Shen, B., 2016. Marine Carbon-Sulfur Biogeochemical Cycles during the Steptoean Positive Carbon Isotope Excursion (SPICE) in the Jiangnan Basin, South China. J. Earth Sci. 27, 242–254. https://doi.org/10.1007/s12583-016-0694-4

Perfetta, P.J., Shelton, K.L., Stitt, J.H., 1999. Carbon isotope evidence for deep-water invasion at the Marjumiid-Pterocephaliid biomere boundary, Black Hills, USA: A common origin for biotic crises on Late Cambrian shelves. Geology 27, 403–406. https://doi.org/10.1130/0091-7613(1999)027<0403:CIEFDW>2.3.CO;2

Pruss, S.B., Castagno, K.A., Fike, D.A., Hurtgen, M.T., 2016. Carbon isotope ($\delta^{13}C_{carb}$) heterogeneity in deep-water Cambro-Ordovician carbonates, western Newfoundland. Palaeogeogr. Palaeoclimatol. Palaeoecol. 458, 52–62. https://doi.org/10.1016/j.palaeo.2015.10.004

Pruss, S.B., Jones, D.S., Fike, D.A., Tosca, N.J., Wignall, P.B., 2019. Marine anoxia and sedimentary mercury enrichments during the Late Cambrian SPICE event in northern Scotland. Geology 47, 475–478. https://doi.org/10.1130/G45871.1

Pulsipher, M.A., Schiffbauer, J.D., Jeffrey, M.M., Huntley, J.W., Fike, D.A., & Shelton, K.L., in press. A meta-analysis of the Steptoean positive carbon isotope excursion: The SPICEraq database. *Earth-Science Reviews.* https://doi.org/10.1016/j.earscirev.2020.103442

R Core Team, 2019. R: A language and environment for statistical computing. R foundation for Statistical Computing, Vienna, Austria. https://www.R-project.org/

Rohatgi, A., 2019. WebPlot Digitizer (Version 4.2) [Computer software]. https://automeris.io/WebPlotDigitizer (accessed 16 March 2020).

Rose, C. V., Fischer, W.W., Finnegan, S., Fike, D.A., 2019. Records of carbon and sulfur cycling during the Silurian Ireviken Event in Gotland, Sweden. Geochim. Cosmochim. Acta 246, 299–316. https://doi.org/10.1016/j.gca.2018.11.030

Saltzman, M.R., 2005. Phosphorus, nitrogen, and the redox evolution of the Paleozoic oceans. Geology 33, 573. https://doi.org/10.1130/G21535.1

Saltzman, M.R., Cowan, C.A., Runkel, A.C., Runnegar, B., Stewart, M.C., Palmer, A.R., 2004. The Late Cambrian Spice ($\delta^{13}C$) Event and the Sauk II-Sauk III Regression: New Evidence from Laurentian Basins in Utah, Iowa, and Newfoundland. J. Sediment. Res. 74, 366–377. https://doi.org/10.1306/120203740366

Saltzman, M.R., Davidson, J.P., Holden, P., Runnegar, B., Lohmann, K.C., 1995. Sea-level-driven changes in ocean chemistry at an Upper Cambrian extinction horizon. Geology 23, 893. https://doi.org/10.1130/0091-7613(1995)023<0893:SLDCIO>2.3.CO;2

Saltzman, M.R., Ripperdan, R.L., Brasier, M.D., Lohmann, K.C., Robison, R.A., Chang, W.T., Peng, S., Ergaliev, E.K., Runnegar, B., 2000. A global carbon isotope excursion (SPICE) during the Late Cambrian: relation to trilobite extinctions, organic-matter burial and sea level. Palaeogeogr. Palaeoclimatol. Palaeoecol. 162, 211–223. https://doi.org/10.1016/S0031-0182(00)00128-0

Saltzman, M.R., Runnegar, B., Lohmann, K.C., 1998. Carbon isotope stratigraphy of Upper Cambrian (Steptoean Stage) sequences of the eastern Great Basin: Record of a global oceanographic event. Geol. Soc. Am. Bull. 110, 285–297. https://doi.org/10.1130/0016-7606(1998)110<0285:CISOUC>2.3.CO;2

Saltzman, M.R., Thomas, E., 2012. Carbon Isotope Stratigraphy, in: Gradstein, F.M., Ogg, J.G., Schmitz, M.D., Ogg, G.M. (Eds.), The Geologic Time Scale. Elsevier, pp. 207–232. https://doi.org/10.1016/B978-0-444-59425-9.00011-1

Saltzman, M.R., Young, S.A., Kump, L.R., Gill, B.C., Lyons, T.W., Runnegar, B., 2011. Pulse of atmospheric oxygen during the late Cambrian. Proc. Natl. Acad. Sci. 108, 3876–3881. https://doi.org/10.1073/pnas.1011836108

Schiffbauer, J.D., Huntley, J.W., Fike, D.A., Jeffrey, M.J., Gregg, J.M., Shelton, K.L., 2017. Decoupling biogeochemical records, extinction, and environmental change during the Cambrian SPICE event. Sci. Adv. 3, e1602158. https://doi.org/10.1126/sciadv.1602158

Schlager, W., 1993. Accommodation and supply—a dual control on stratigraphic sequences. Sediment. Geol. 86, 111–136. https://doi.org/10.1016/0037-0738(93)90136-S

Schmid, S., 2017. Chemostratigraphy and palaeo-environmental characterisation of the Cambrian stratigraphy in the Amadeus Basin, Australia. Chem. Geol. 451, 169–182. https://doi.org/10.1016/j.chemgeo.2017.01.019

Schmid, S., Smith, P.M., Woltering, M., 2018. A basin-wide record of the Late Cambrian Steptoean positive carbon isotope excursion (SPICE) in the Amadeus Basin, Australia. Palaeogeogr. Palaeoclimatol. Palaeoecol. 508, 116–128. https://doi.org/10.1016/j.palaeo.2018.07.027

Servais, T., Danelian, T., Harper, D.A.T., Munnecke, A., 2014. Possible oceanic circulation patterns, surface water currents and upwelling zones in the Early Palaeozoic. GFF 136, 229–233. https://doi.org/10.1080/11035897.2013.876659

Servais, T., Lehnert, O., Li, J., Mullins, G.L., Munnecke, A., Nützel, A., Vecoli, M., 2008. The Ordovician Biodiversification: revolution in the oceanic trophic chain. Lethaia 41, 99–109. https://doi.org/10.1111/j.1502-3931.2008.00115.x

Servais, T., Perrier, V., Danelian, T., Klug, C., Martin, R., Munnecke, A., Nowak, H., Nützel, A., Vandenbroucke, T.R.A., Williams, M., Rasmussen, C.M.Ø., 2016. The onset of the 'Ordovician Plankton Revolution' in the late Cambrian. Palaeogeogr. Palaeoclimatol. Palaeoecol. 458, 12–28. https://doi.org/10.1016/j.palaeo.2015.11.003

Sial, A.N., Peralta, S., Ferreira, V.P., Toselli, A.J., Aceñolaza, F.G., Parada, M.A., Gaucher, C., Alonso, R.N., Pimentel, M.M., 2008. Upper Cambrian carbonate sequences of the Argentine Precordillera and the Steptoean C-Isotope positive excursion (SPICE). Gondwana Res. 13, 437–452. https://doi.org/10.1016/J.GR.2007.05.001

Sial, A.N., Peralta, S., Gaucher, C., Toselli, A.J., Ferreira, V.P., Frei, R., Parada, M.A., Pimentel, M.M., Silva Pereira, N., 2013. High-resolution stable isotope stratigraphy of the upper Cambrian and Ordovician in the Argentine Precordillera: Carbon isotope excursions and correlations. Gondwana Res. 24, 330–348. https://doi.org/10.1016/j.gr.2012.10.014

Sibley, D.F., Gregg, J.M., 1987. Classification of Dolomite Rock Textures. SEPM J. Sediment. Res. Vol. 57, 967–975. https://doi.org/10.1306/212F8CBA-2B24-11D7-8648000102C1865D

Sloss, L.L., 1963. Sequences in the Cratonic Interior of North America. Geol. Soc. Am. Bull. 74, 93–114. https://doi.org/10.1130/0016-7606(1963)74

Stitt, J.H., 1975. Adaptive radiation, trilobite paleoecology, and extinction, Ptychaspid biomere, Late Cambrian of Oklahoma. Fossils and Strata. 4 381-390.

Sundberg, F.A., Karlstrom, K.E., Geyer, G., Foster, J.R., Hagadorn, J.W., Mohr, M.T., Schmitz, M.D., Dehler, C.M., Crossey, L.J., 2020. Asynchronous trilobite extinctions at the early to middle Cambrian transition. Geology 48, 441–445. https://doi.org/10.1130/G46913.1

Swart, P.K., Eberli, G., 2005. The nature of the $\delta^{13}C$ of periplatform sediments: Implications for stratigraphy and the global carbon cycle. Sediment. Geol. 175, 115–129. https://doi.org/10.1016/j.sedgeo.2004.12.029

Vahrenkamp, V.C., 1996. Carbon Isotope Stratigraphy of the Upper Kharaib and Shuaiba Formations: Implications for the Early Cretaceous Evolution of the Arabian Gulf Region. Am. Assoc. Pet. Geol. Bull. 80, 647–661. https://doi.org/10.1306/64ED8868-1724-11D7-8645000102C1865D

Voigt, S., Gale, A.S., Jung, C., Jenkyns, H.C., 2012. Global correlation of upper Campanian-Maastrichtian successions using carbon-isotope stratigraphy: Development of a new Maastrichtian timescale. Newsletters Stratigr. 45, 25–53. https://doi.org/10.1127/0078-0421/2012/0016

Wang, Z., Chen, J., Liang, T., Yuan, J., Han, C., Liu, J., Zhu, C., Zhu, D., Han, Z., 2020. Spatial variation in carbonate carbon isotopes during the Cambrian SPICE event across the eastern North China Platform. Palaeogeogr. Palaeoclimatol. Palaeoecol. 546, 109669. https://doi.org/10.1016/j.palaeo.2020.109669

Westberry, T., Behrenfeld, M.J., Siegel, D.A., Boss, E., 2008. Carbon-based primary productivity modeling with vertically resolved photoacclimation. Global Biogeochem. Cycles 22, GB2024. https://doi.org/10.1029/2007GB003078

Wickham, H., 2016. ggplot2: Elegant graphics for data analysis. Springer-Verlag, New York. https://ggplot2.tidyverse.org

Wickham, H., François, R., Henry, L., Müller, K., 2019. dplyr: A grammar of data manipulation. R package version 0.8.3. https://CRAN.R-project.org/package=dplyr

Wickham, H., Henry, L., 2019. tidyr: Easily tidy data with "spread()" and "gather()" functions. R package version 0.8.3. https://CRAN.R-project.org/package=tidyr

Wilke, C.O., 2018. ggridges: Ridgeline plots in "ggplot2". R package version 0.5.1. https://CRAN.R-project.org/package=ggridges

Woods, M.A., Wilby, P.R., Leng, M.J., Rushton, A.W.A., Williams, M., 2011. The Furongian (late Cambrian) Steptoean Positive Carbon Isotope Excursion (SPICE) in Avalonia. J. Geol. Soc. London. 168, 851–862. https://doi.org/10.1144/0016-76492010-111

Wotte, T., Strauss, H., 2015. Questioning a widespread euxinia for the Furongian (Late Cambrian) SPICE event: indications from $\delta^{13}C$, $\delta^{18}O$, $\delta^{34}S$ and biostratigraphic constraints. Geol. Mag. 152, 1085–1103. https://doi.org/10.1017/S0016756815000187

Zhao, Y., Yuan, J., Babcock, L.E., Guo, Q., Peng, J., Yin, L., Yang, X., Peng, S., Wang, C., Gaines, R.R., Esteve, J., Tai, T., Yang, R., Wang, Y., Sun, H., Yang, Y., 2019. Global Standard Stratotype-Section and Point (GSSP) for the conterminous base of the Miaolingian Series and Wuliuan Stage (Cambrian) at Balang, Jianhe, Guizhou, China. Episodes 42, 165–184. https://doi.org/10.18814/epiiugs/2019/019013

Zhu, M.-Y., Zhang, J.-M., Li, G.-X., Yang, A.-H., 2004. Evolution of C isotopes in the Cambrian of China: implications for Cambrian subdivision and trilobite mass extinctions. Geobios 37, 287–301. https://doi.org/10.1016/j.geobios.2003.06.001

Zuo, J., Peng, S., Qi, Y., Zhu, X., Bagnoli, G., Fang, H., 2018. Carbon-isotope excursions recorded in the Cambrian system, South China: Implications for mass extinctions and sea-level fluctuations. J. Earth Sci. 29, 479–491. https://doi.org/10.1007/s12583-017-0963-x

CHAPTER 3:

DESCRIPTION OF *ACHERONAUTA* GEN. NOV., A VERMIFORM BASAL MANDIBULATE FROM THE SILURIAN BRANDON BRIDGE FORMATION, WAUKESHA, WISCONSIN, USA

Mikaela A. Pulsipher[1], Evan P. Anderson[1], Lauren S. Wright[2], Donald G. Mikulic[3], Joanne Kluessendorf[4†], James D. Schiffbauer[1,5]

[1]Department of Geological Sciences, University of Missouri, Columbia, Missouri, USA 65211

[2]Battle High School, 7575 East St. Charles Road, Columbia, Missouri, USA 65202

[3]Illinois State Geological Survey, 615 E Peabody Drive, Champaign, Illinois, USA 61820

[4]Weis Earth Science Museum, University of Wisconsin – Oshkosh, 1478 Midway Road, Menasha Wisconsin, USA 54952

[5]X-Ray Microanalysis Core, University of Missouri, Columbia, Missouri, USA 65211

[†]Deceased

Abstract

The Brandon Bridge Formation of Waukesha, Wisconsin, USA, hosts a konservat-lagerstätte of distinctive Silurian soft-bodied organisms (including a range of worms, trilobites, and uncommon arthropods) and otherwise lacks most of the shelly fauna typical of contemporaneous biotas. While several distinct species have already been described, much of

the Waukesha biota remains understudied. Further investigation of the biota of this lagerstätte is warranted, however, as these organisms may provide evidence of a unique evolutionary bridge between arthropods of the Cambrian and later Paleozoic to Modern faunas. Included in this assemblage are numerous specimens of a previously unnamed and undescribed vermiform arthropod which bears a cephalic carapace, a suite of specialized head appendages, a long, segmented trunk, and a battery of small swimming appendages. The taxonomic and phylogenetic evaluations presented herein establish this taxon as a novel genus, positioned within the basal mandibulates, and comprising two species: *Acheronauta stimulapis* gen. et sp. nov. and *Acheronauta leonidas* sp. nov.

3.1 Introduction

Since its initial discovery and report in 1985 by Mikulic and colleagues, the Waukesha Lagerstätte has been recognized as a noteworthy fossil locality, unusual for a Silurian deposit in its biotic make-up and the diversity of its soft-bodied fauna (Mikulic et al., 1985a; 1985b). However, until recently, the deposit and the fossil organisms hosted there remained relatively understudied, with taxa being only intermittently described (e.g., Moore et al., 2005; Haug et al., 2014; Jones et al., 2015; Wendruff et al., 2020a). With the desire to understand Paleozoic soft-bodied fossilization expanding beyond the Burgess Shale-type, as well as to better realize the diversity of arthropods through the first half of the Paleozoic, the Waukesha has received renewed interest as of late along with the discovery of other Ordovician/Silurian lagerstätten (von Bitter et al., 2007; Liu et al., 2006*;* Lamsdell et al., 2017). At the Waukesha, these most recent pursuits have manifested in work on the sedimentology and taphonomy of the lagerstätte (Wendruff et al. 2020b), a description of an alleged scorpion (Wendruff et al.,

2020a), and its subsequent redescription as an enigmatic arthropod, possibly with fuxianhuiid affinity by Anderson et al. (*in press*).

The biota of the Waukesha Lagerstätte represents a diverse flora and fauna, primarily soft-bodied. Arthropods are abundant and represented by trilobites (Mikulic & Kluessendorf, 1999) as well as a suite of non-trilobite arthropods including thylacocephalans (Haug et al., 2014), phyllocarids (Jones et al., 2015), chelicerates (Moore et al., 2005; Wendruff et al., 2020a), potential myriapods (Wilson et al., 2004; Westberg, 2019), and others, many of which are currently undescribed and unnamed. Several "worm" specimens are present, including both paleoscolecids and polychaetes (Mikulic et al., 1985a, 1985b; Wendruff, 2016; Westberg, 2019; Wendruff et al., 2020b). Multiple specimens of conulariids, graptolites, and conodonts are also found in the lagerstätte (Mikulic et al., 1985a; 1985b; Miller et al., 2020; Wendruff et al, 2020b). Rare and/or poorly preserved taxa include brachiopods, lobopods, algae, cnidaria, cephalopods, and echinoderms (Mikulic et al., 1985a; 1985b; LoDuca et al., 2003; Wendruff et al., 2016; Wendruff et al, 2020b). While many of these specimens are outwardly similar to Burgess Shale-type fossils, appearing as two-dimensional compressions in a fine-grained host rock, they are predominantly preserved via phosphatization (Mikulic et al., 1985b; Jones et a., 2015; Wendruff et al., 2020b; Anderson et al., *in press*).

Aside from an undescribed dalmanitid trilobite (Kluessendorf, 1990), the most abundant arthropod at the Waukesha is probably a multisegmented vermiform organism with a small head carapace. Although sometimes mentioned (Mikulic et al., 1985a; 1985b Wendruff et al. 2020a) or investigated (Westberg, 2019), it has yet to be formally described. This unnamed vermiform arthropod bears a cephalic carapace, raptorial appendages, and a battery of small swimming appendages along a homonomously segmented trunk. Our investigations of these organisms indicate that they belong to a new arthropod genus, *Acheronauta* gen. nov.,

and have revealed two distinct morphologies which should be designated as separate species. The more abundant of the two forms is here designated as *Acheronauta stimulapis* sp. nov. The rarer form is designated as *Acheronauta leonidas* sp. nov. and is distinguished by a projecting anterior keel on the carapace and trunk segments that begin constricting well before the terminus. Both species suggest phylogenetic positioning as an intriguing stem-group mandibulate, with compound eyes, antennulate antennules, and gnathiform mandibles, but self-similar second, fourth, and fifth head appendages. The first three trunk somites are reduced and functionally incorporated into the head tagma, bearing three long walking legs; the remaining trunk limbs are homonomous, shortened, and setose, and were likely useful for swimming. The purpose of this paper is to: (i) taxonomically describe the new genus and its included species; (ii) elucidate its placement in the arthropod family tree; and (iii) describe its taphonomy in comparison to works on other Waukesha deposit taxa (Jones et al. 2015; Wendruff et al. 2020b; Anderson et al., *in press*).

3.2 Geologic setting

The Waukesha Lagerstätte is housed in the lower portion of the Silurian Brandon Bridge Formation (Fig. 3-1). While not well-constrained chronostratigraphically, conodont biostratigraphy places the Waukesha Lagerstätte and Brandon Bridge Formation within the upper Llandovery epoch (Kleffner et al., 2018). This unit is found in both southern Wisconsin and northern Illinois where it is conformably overlain by the Waukesha Dolomite and the stratigraphically equivalent Markgraf Member of the Joliet Formation, respectively (Kluessendorf, 1990; Kluessendorf & Mikulic, 1996). For most of its extent, the Brandon Bridge Formation unconformably overlies the Silurian Kankakee Dolomite. However, in the

Milwaukee area a unique stratigraphic relationship is observed: here, the Brandon Bridge Formation pinches out against a southward-facing paleoslope of the Silurian Manistique Formation and is thus not exposed north of Waukesha proper (Mikulic, 1977; Mikulic et al., 1985a; 1985b; Kluessendorf, 1990; Kluessendorf & Mikulic, 1996). In this area, the Brandon Bridge Formation is only exposed within two active quarries: the Waukesha Lime & Stone Co. quarry (43.03° N, 88.21° W) in Waukesha and the Franklin Aggregate Inc. Quarry (42.91° N, 87.99° W) in Greenfield, WI (Fig. 3-1). In both quarries, the Brandon Bridge Formation is now inaccessible: at the Waukesha Lime & Stone Co. quarry the horizon is located several meters above the quarry floor, and at the Franklin Aggregate Inc. quarry the horizon is buried under overgrown piles of debris.

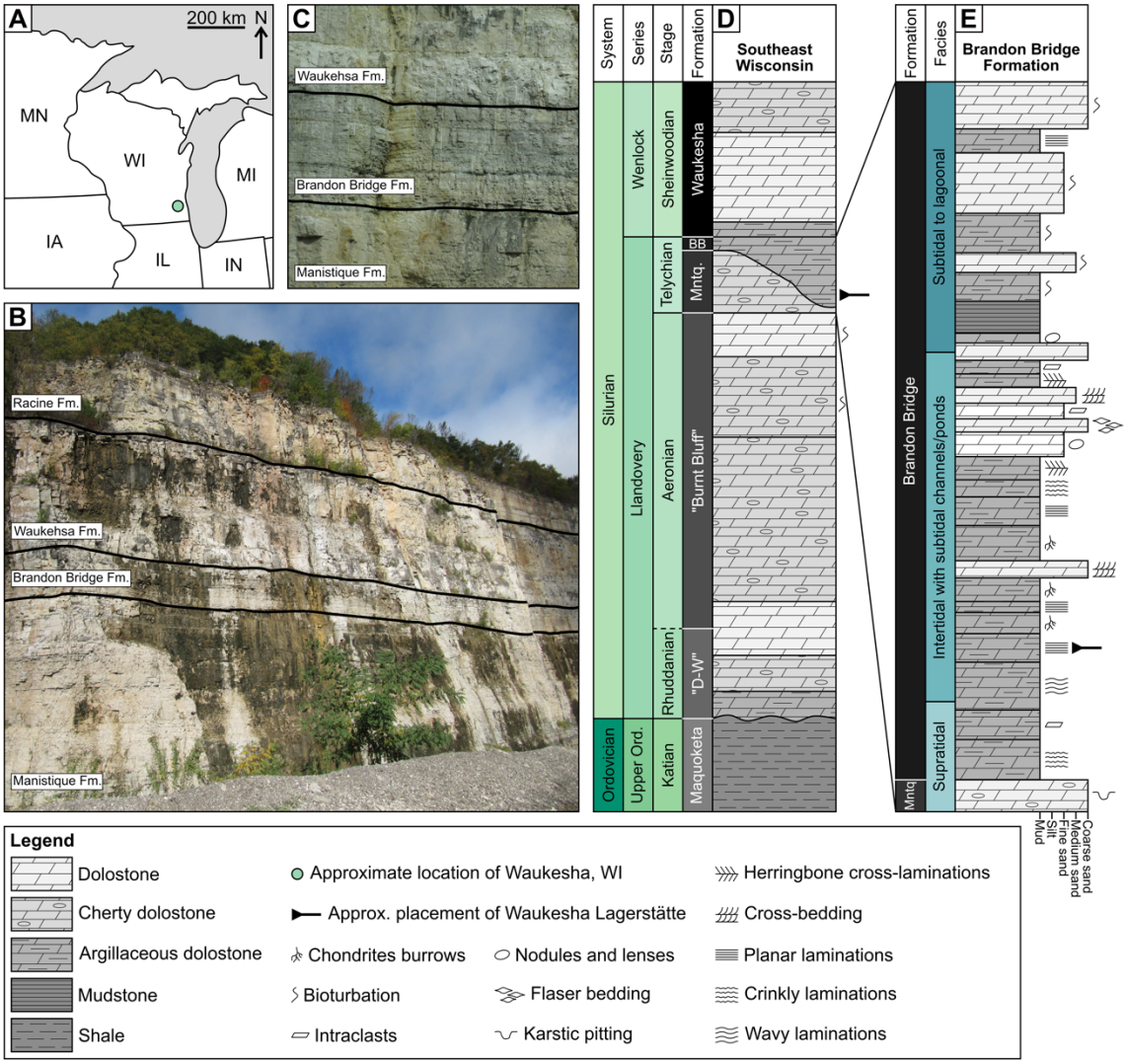

Figure 3-1. Geologic setting of the Waukesha Lagerstätte. A) Map showing the approximate location of Waukesha, WI and both quarries where the Brandon Bridge Formation is exposed (green circle). B and C) Field photographs from the Waukesha Lime & Stone Co. quarry where the Brandon Bridge is exposed well above the quarry floor; hence, no scale is available. D) Uppermost Ordovician and lower Silurian stratigraphic column of southeast Wisconsin (after Wendruff et al., 2020b). E) Idealized stratigraphic column of the Brandon Bridge Formation (after Kluessendorf, 1990) showing the overall deepening upward facies package. In both D) and E) the Brandon Bridge Formation has a maximum thickness of eight meters; the horizon bearing the Waukesha Lagerstätte is located approximately two meters above the underlying paleoslope and is denoted by the inverted black arrow.

The Brandon Bridge Formation was deposited in a peritidal setting, as evidenced by the presence of planar-, cross-, and herringbone cross-laminations, bioturbation, ripple marks, and desiccation features (Fig. 3-1; Kluessendorf, 1990; Kluessendorf & Mikulic, 1996). The unit displays an overall deepening upward trend, transitioning from supratidal to shallow subtidal (Kluessendorf, 1990; Kluessendorf & Mikulic, 1996). The unconformity between the Brandon Bridge Formation and the underlying Manistique Formation is interpreted as a sequence boundary, with the deepening upward Brandon Bridge Formation thus corresponding to a transgressive systems tract (Kluessendorf, 1990; Kluessendorf & Mikulic, 1996). Karstic surfaces within the supratidal portion at the base of the section and desiccation cracks within the overlying intertidal portion indicate that the unit was periodically subaerially exposed, although the absence of evaporites and caliches indicate that this exposure was short-lived (Kluessendorf, 1990). Bioturbation is prevalent in the subtidal and intertidal portions of the section but absent from the basal supratidal section (Kluessendorf, 1990). Lithologically, the Brandon Bridge Formation is dominated by pale green to reddish brown argillaceous dolomite, with lesser calcarenite beds. Individual beds are typically thin and planar, although some crinkly and wavy laminations are observed (Fig. 3-1; Kluessendorf, 1990; Kluessendorf & Mikulic, 1996).

The paleoslope underlying the Brandon Bridge Formation is approximately 8 meters in relief and is capped by a cherty dolomitic horizon (Kluessendorf, 1990; Mikulic et al., 1985a; 1985b; Kluessendorf & Mikulic, 1996). While the surface of this slope is relatively planar overall, a period of subaerial exposure and karstification prior to deposition of the Brandon Bridge resulted in the development of localized troughs and scallops. This irregular topography produced anoxic sediment traps along the base of the paleoscarp; it is only within these traps that the soft-bodied fauna of the Waukesha Lagerstätte are preserved in localized

beds of greenish-gray laminated mudstone (Kluessendorf, 1990). The exceptionally preserved fossils described in this and other studies were largely collected from a 12 cm-thick bed approximately 2 meters above the base of the Brandon Bridge Formation at the Waukesha Lime & Stone Co. quarry (Fig. 3-1; e.g., Mikulic et al., 1985a; 1985b; Smith et al., 1987; Kluessendorf & Mikulic, 1996; Moore et al., 2005; Haug et al., 2014; Jones et al., 2015; Wendruff et al., 2020).

3.3 Materials & Methods

Tens of specimens of the new genus of interest to this study were collected in the 1980s and 1990s when the lagerstätte was initially exposed during quarrying activity (Mikulic et al., 1985a; 1985b). These specimens are now housed at the University of Wisconsin-Madison Geology Museum (UWGM), 23 of which were borrowed for this study.

Photomicrographs were taken using a Nikon SMZ1500 stereomicroscope and affixed Nikon D600 and D3300 DSLR cameras. Fossil material in these photographs was traced in Affinity Designer and used as the foundation for living reconstructions of the organisms. In addition, high-resolution photomosaics were collected for the two designated types using a GIGAmacro Magnify2 robotic camera system with a Canon EOS Rebel T6i DSLR camera.

A Zeiss Sigma 500 VP scanning electron microscope (SEM) at the University of Missouri X-Ray Microanalysis Core was used to image the specimens for further description and analysis. A cascade current low vacuum secondary electron (SE) detector was used to collect topographic information from the specimens. A 5-segment high-definition backscattered electron (BSE) detector and dual co-planar Bruker Xflash energy dispersive X-Ray spectroscopy (EDS) units were used to collect elemental and compositional data from the

specimens. All SEM imaging was conducted with a beam accelerating voltage of 20 keV and current of 40 nA, an aperture size of 60 μm, and at a chamber vacuum of 20 Pa (chamber atmosphere = 99.999% nitrogen). Working distance varied as a result of sample thickness and topography, but was generally maintained at 16 mm ± 1 mm. All EDS analyses were conducted at identical operating conditions to SEM imaging, but with an aperture size of 120 μm to improve x-ray count rate (~150 kilocounts per second with both EDS detectors used in tandem). The ATLAS microscopy workflow (Fibics Incorporated) was used to stitch individual SEM images into a single composite image of each analyzed specimen, as well as overlay BSE and SE images to better correlate topographic and compositional information.

The phylogenetic analysis was conducted with PAUP* 4.0a (Swofford, 2003), using the character matrix from Aria & Caron's (2017) study of basal mandibulates from the Burgess Shale. The resultant character matrix comprises 91 taxa (including the new genus) described by 212 individual character states. Ambiguity in some character states and character interpretation necessitated multiple iterations of analyses. Strict consensus trees were computed with heuristic searches using the technique of Aria and Caron (2017) as well as maintaining their taxonomic backbone. Specifically, trees were constructed using tree bisection-reconnection with starting trees generated by random stepwise addition using 1000 replicates, a seed of 1, and a maximum of 10 trees with a score above 1 stored for each replicate. Branch support was evaluated through Bremer analysis, as well as Bootstrap and Jackknife tests. The Bremer analysis was conducted via heuristic searches, using random stepwise addition with 100 replicates and a random seed, saving no more than 10 optimal trees with a score ≥ 1 for each replicate, regardless of whether they were optimal over all replicates. This way, suboptimal trees could be retained for the Bremer analysis, which was initiated 5 steps beyond the most parsimonious tree. Bootstrap and Jackknife analyses were both

conducted as "Fast" stepwise-addition searches with 10,000 replicates. For Jackknife analyses a 30% deletion resampling method was used.

3.4 Systematic Paleontology

3.4.1 Genus *Acheronauta*

Arthropoda von Siebold, 1848

Unranked clade **Mandibulata** Snodgrass, 1938

Genus ***Acheronauta*** gen. nov.

(Figs. 3-2 to 3-9 3-11)

Derivation of name. From Latin, *Acheronta*, Latin form of the Greek word *Acheron*, the River of Woe, one of the five rivers of the Greek underworld, and *nauta*, sailor. *Acheronauta* thus translates to "sailor on the River of Woe," in reference to the harsh tidal environment that allowed for the preservation of the Waukesha biota.

Type species. *Acheronauta stimulaplis* gen. et sp. nov. (Fig. 3-2) from the Brandon Bridge Formation, Waukesha Lime & Stone Co. quarry, Waukesha, WI, USA.

Diagnosis. Vermiform arthropod bearing a cephalic carapace. Ocular somite bearing two tear-drop shaped faceted eyes. Five pairs of head appendages, considered as antennules, antennae, mandibles, maxillules, and maxillae. Antennae, maxillules, and maxillae terminally sub-chelate. Conterminant hypostome-labrum complex present. First three trunk segments reduced, bearing stenopodous maxilliped pairs. Homonomously segmented trunk bearing one pair of small, setose, paddle-shaped appendages per segment. Trunk terminus contracted without an obvious telson.

Dimensions. Ranges from 0.22 cm x 0.93 cm to 0.60 cm x 5.86 cm.

Occurrence. Silurian Brandon Bridge Formation in southeast WI, USA.

Remarks. Although this taxon has not been officially named by any prior publications, and thus requires no formal synonomy list, representative samples have been imaged and briefly discussed: Mikulic et al. (1985a & 1985b) described a single specimen (UWGM_4001/3, their figs. 2C and 15, respectively) as a "worm-like arthropod"; Wendruff (2016) and Wendruff et al. (2020b) referred also to a single specimen (UWGM_2451, their figs. 2.5M and 5M, respectively) as a "vermiform arthropod with large headshield and small grasping appendage"; and Westberg (2019) designated this taxon as "Vermiform arthropod sp. 1" in their description of two specimens (sample numbers unreported, their fig. 4a-b). Our investigation reveals that this taxon belongs to a unique genus of arthropod, which likely comprises two separate species as described below.

Although more work is necessary to document the full range of taphonomic expressions present in the Waukesha Lagerstätte, this study demonstrates that there is a wide variety of taphomorphs within *Acheronauta* gen. nov. (Fig. 3-3). This variety of preservational style has likely resulted in other *Acheronauta* gen. nov. specimens being referred to as markedly different taxa. For example, Westberg (2019) describes one moderately well-preserved specimen, which displays a homonomous trunk, potential cephalic carapace, and blunt trunk terminus, as a "putative arthropod" (Westberg, 2019, fig. 8a). A second, more poorly preserved "putative arthropod" is shown in their fig. 8b which appears to display a long homonomous trunk and potential cephalic carapace with suggestions of head limbs extending beyond its perimeter. Likewise, Wendruff et al. (2020b) illustrates specimens that appear morphologically similar to the *Acheronauta* gen. nov. specimens described herein as entirely different taxa. Their fig. 5f (described as an "arthropod with two pairs of antenniform appendages") shows an organism with a small head bearing one or two pairs of laterally splayed appendages, followed

by a long, multisegmented trunk. The anterior trunk segments are apparently reduced, but subsequent segments show a fairly consistent size along the trunk's length, ending with a blunt terminus. Wendruff et al.'s (2020b) fig. 5e and Westberg's (2019) fig. 5e both show poorly preserved specimens of markedly similar appearance: a curved, partially preserved trunk with dark and light banded pleurites extending beyond the margin. In both publications, these specimens are described as lobopods. There are, however, notable similarities between the specimens shown in these publications and our specimens UWGM_2780, UWGM_3413, and UWGM_3762 (Fig. 3-3). Note also that the vast majority of samples investigated in this, and previous, studies comprise lateral views of the fossil and thus descriptions are limited in terms of what can be said about said about some of the features.

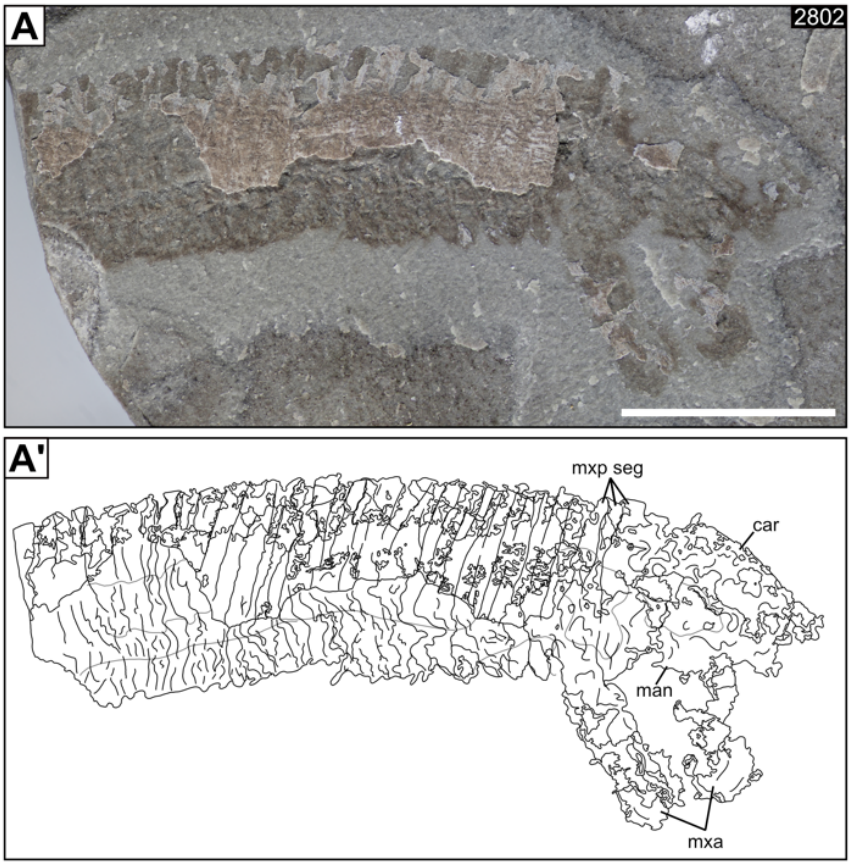

Figure 3-2. *Acheronauta stimulapis* gen. et sp. nov. holotype. A & A') GIGAmacro image of UWGM_2802 and corresponding trace. UWGM_2802 has been designated as the holotype despite being a partial specimen as it is the only specimen to bear both clearly identifiable mandibles and the eponymous boxing glove-esque sub chelae on the antennae, maxillules, and maxillae. Abbreviation list: car = cephalic carapace; mxa = maxilla; mxp = maxilliped; seg = segment. Scale bar = 5 mm.

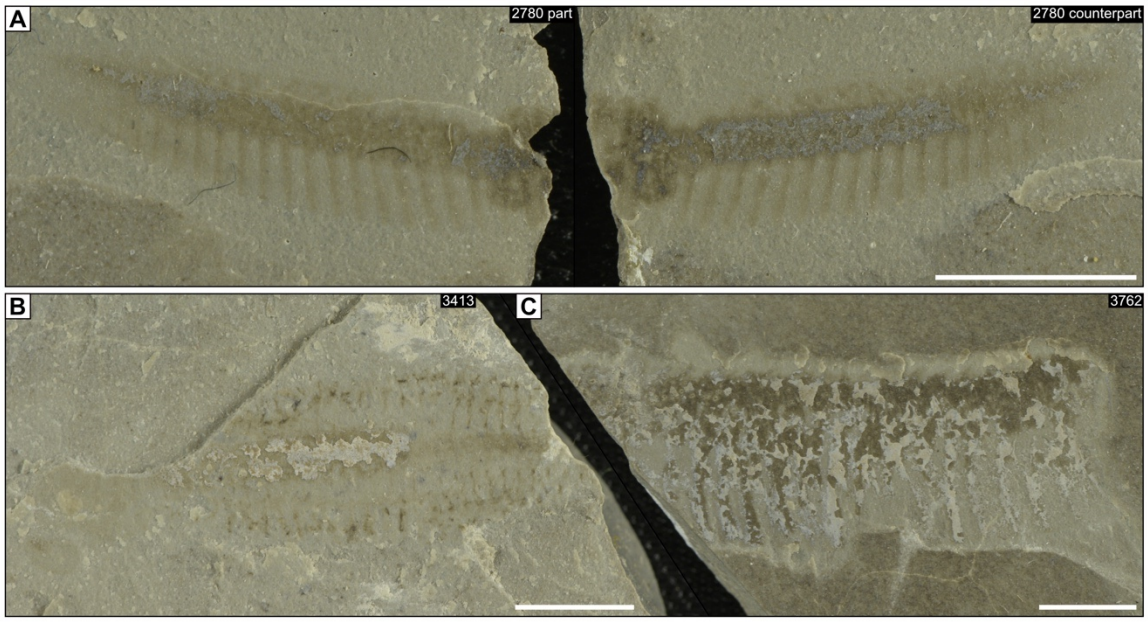

Figure 3-3. Taphomorphs of *Acheronauta* gen nov.. Differential preservation resulted in several taphomorphs of *Acheronauta*; three of the more poorly preserved forms are shown here. In all three specimens, pleural bands are visible, extending beyond the margin of the trunk. A) UWGM_2780 part and counterpart. This partial specimen is missing the anterior portion of the head region; note that the color banding in the pleurites is reversed relative to other specimens. B) UWGM_3413, partial specimen, part of the head is present but very faint. Concentrated phosphate (white mineralization) along the midline potentially follows a gut tract or inner viscera. C) UWGM_3762, partial specimen missing the head region. Phosphate mineralization (white) is concentrated along pleurae and the main trunk. All scale bars = 5 mm.

3.4.2 *Acheronauta stimulapis*

Acheronauta stimulapis sp. nov.

(Figs. 3-2 to 3-8, & 3-11)

Diagnosis. Same as for genus with two additional specifications: blunt anterodorsal corner on the cephalic carapace, sometimes with a faceted eye protruding beyond this margin; rounded trunk terminus lacking pronounced pre-terminal contraction.

Dimensions. Ranges from 0.22 cm x 0.93 cm to 0.76 cm x 4.64 cm.

Derivation of name. From Latin, *stimulus*, sting, *apis*, bee. The terminal podomeres on the raptorial appendages of some specimens are shaped like a boxing glove. The specific name of this organism translates to "sting like a bee" in honor of famed American boxer Muhammad Ali.

Holotype. UWGM_2802, partial specimen (Fig. 3-2, 3-6, & 3-11), from Waukesha Lime & Stone Co. quarry, Waukesha, WI, USA.

Paratypes. UWGM_2759, whole specimen (Fig. 3-4 & 3-6); UWGM_2770, whole specimen (Fig. 3-4 & 3-5); UWGM_4639, whole specimen (Fig. 3-4 & 3-7). All specimens from Waukesha Lime & Stone Co. quarry, Waukesha, WI, USA.

Additional material. UWGM_2728, partial specimen (Fig. 3-8); UWGM_2780 (Fig. 3-3), part and counterpart of partial specimen; UWGM_2813, whole specimen (Fig. 3-7); UWGM_2828, partial specimen (Fig. 3-5 & 3-7); UWGM_2833, part and counterpart of partial specimen (Fig. 3-6); UWGM_2951, partial specimen; UWGM_3413, partial specimen (Fig. 3-3); UWGM_3511, partial specimen (Fig. 3-8); UWGM_3762, partial specimen (Fig. 3-3); UWGM_3800, partial specimen; UWGM_3805, whole specimen; UWGM_3991, whole specimen (Fig. 3-6); UWGM_4438, partial specimen; UWGM_4634, partial specimen;

UWGM_4635, partial specimen; UWGM_4648, partial specimen (Fig. 3-8). All specimens from Waukesha Lime & Stone Co. quarry, Waukesha, WI, USA.

Hypodigm. Total number of specimens identified = 21, as listed above. Additional specimens may be present in the UWGM collections, though not formally assigned.

Occurrence. The Silurian Brandon Bridge Formation in southeast WI, USA.

Description. Specimens of *Acheronauta stimulapis* gen. et sp. nov. are composed of two tagmata: 1) a head bearing a cephalic carapace and a suite of head appendages; 2) a long, multisegmented trunk (up to 44 segments observed, though most specimens have 20–30) bearing small, setose swimming appendages, one pair per somite, along its length. The carapace is limited in its coverage of the organism, enclosing only the head and up to the first three segments of the trunk. This carapace was likely bivalved, but a lack of well-preserved dorsally oriented specimens precludes confirmation a clearly defined hinge line.

An ocular somite is present on the anterior edge of the head, bearing two tear-drop shaped lateral eyes, with well-preserved facets observed in some specimens (Fig. 3-5). In most specimens with preserved eyes, the eye protrudes beyond the anterior margin of the cephalic carapace (Fig. 3-5A & B). A series of five head appendages is found behind the ocular somite, the first of which is a pair of apparently arthrodized antennules bearing no extensions, setae, or chelae (Fig. 3-6), although these appendages are generally not well-preserved. The second, fourth, and fifth pairs of head appendages (antennae, maxillules, and maxillae, respectively) are self-similar; they are apparently uniramous, although their bases are not distinguishable, are stout and without setae, and the terminal two podomeres form a sub-chelate structure, appearing like a tiny boxing glove (Figs. 3-2, 3-4 & 3-6). There is ambiguity in the precise number of podomeres on these three appendages, with counts ranging from 3 to 5 plus the terminal sub-chelate podomeres. Posteriorly, however, the appendages grow more robust,

with each subsequent appendage adding an extra podomere. The third pair of head appendages are mandibles, which are recessed relative to the neighboring appendages and do not protrude from the head, only differentiable under raking light on several key specimens (Figs. 3-2 & 3-6A & B). The mandibles do not appear to bear palps, and instead display parallel rows of simple teeth on a likely grinding surface. A conterminant hypostome-labrum complex is located anterior to the mandibles, although this feature is only displayed on two specimens (UWGM_3991 and UWGM_2833; Fig. 3-6C, E & F).

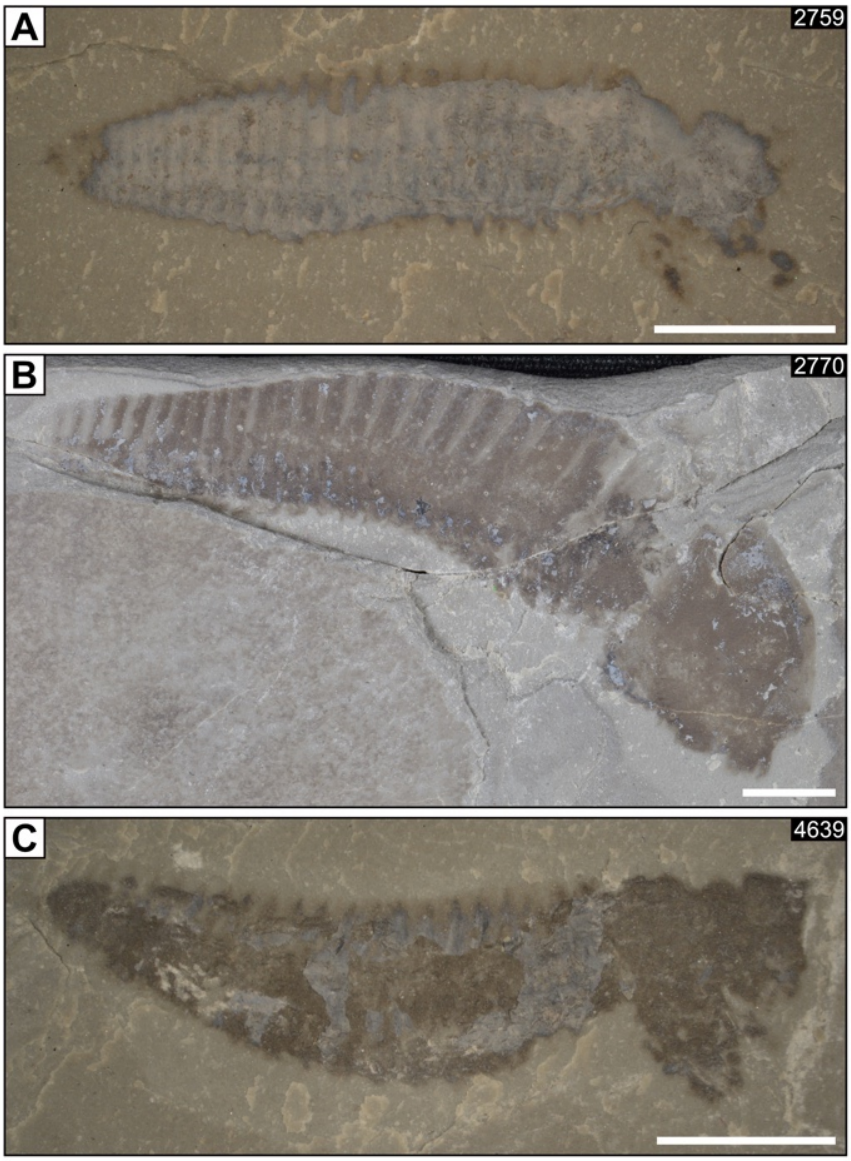

Figure 3-4. *Acheronauta stimulapis* gen. et sp. nov. paratypes. A) UWGM_2759. Cephalic carapace is missing, B) UWGM_2770. C) UWGM_4639. All scale bars = 5 mm.

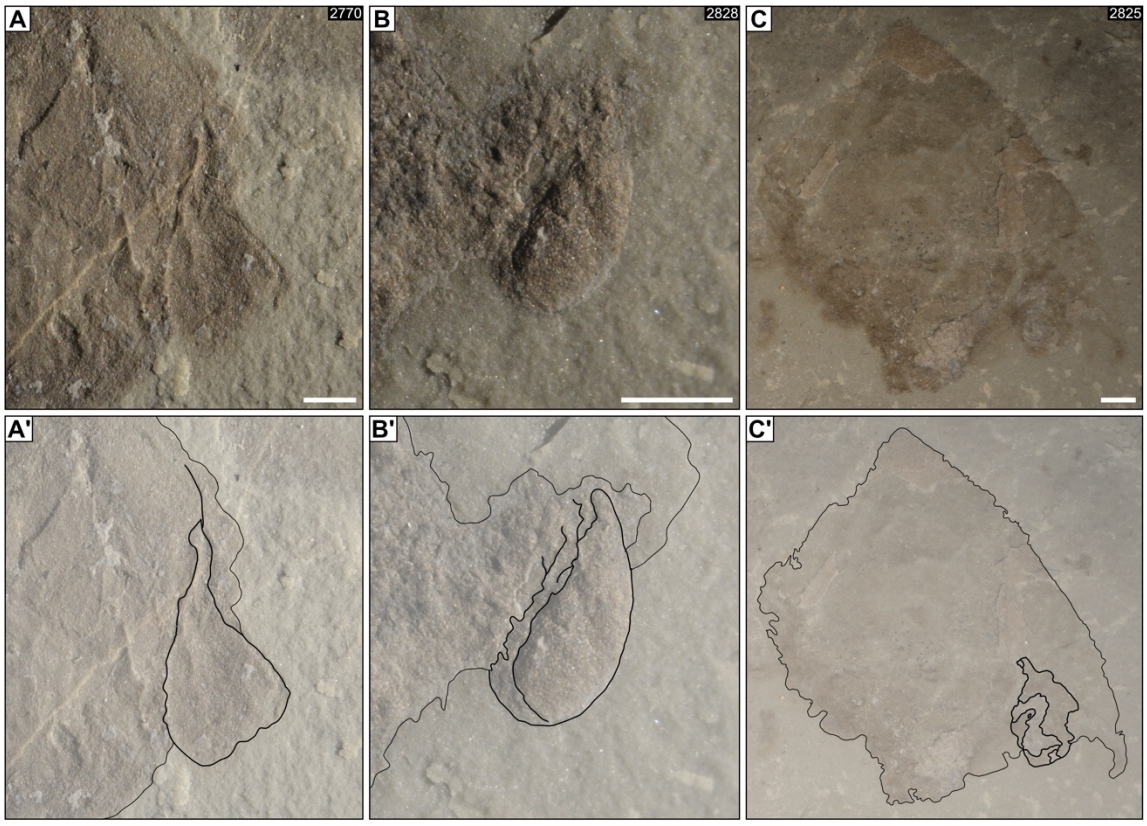

Figure 3-5. Placement of compound eyes. In most specimens with preserved eyes, the eye extends either to or beyond the anterior margin of the cephalic carapace. In one specimen, however, the eye is recessed into the head, with a carina on the carapace extending well beyond it. A & A') UWGM_2770 photomicrograph and corresponding trace. Full specimen shown in Fig. 3-4. B & B') UWGM_2828 photomicrograph and corresponding trace. Full head region shown in Fig. 7. While this eye appears to be slightly distorted, facets are clearly visible in panel B. C & C') UWGM_2825 photomicrograph and corresponding trace. Full specimen shown in Fig. 9, note the recessed placement of the eye relative to A and B. All scale bars = 1 mm.

Figure 3-6. Head appendages and musculature. A) UWGM_2802; holotype; full specimen shown in Fig. 3-2. Maxillae with terminal sub-chelae are well preserved in this specimen. The left maxilla may have the subsequent maxilliped preserved along the left margin, giving the appendage it's more robust appearance relative to the right maxilla. B & B') UWGM_2802; closeup of head region and corresponding trace. This specimen bears the best-preserved mandibles, with grooves clearly visible in the surface. Potential muscle attachments for the maxillae are outlined with dashed lines. C & C') UWGM_3991; the smallest complete specimen investigated herein. Several head appendages are partially preserved, including a potential attachment point of the antennules, the antennae (which appear to drape around the hypostome), and leg bases of both maxillules and maxillae. D & D') UWGM_2759; full specimen shown in Fig. 3-4. The head region is preserved at an oblique angle. It is unclear whether the anteriormost appendages are antennules or antennae; the orientation suggests antennules, but the placement relative to other appendages suggests antennae. Maxillae with partially preserved terminal sub chelae are prominent. At least one maxilliped appendage is preserved along the posterior margin of the left maxilla. E) UWGM_2833; this specimen provides a unique dorsoventral view of *Acheronauta* gen. nov.. The imbricated trunk segments are clearly visible, with minor kerogen concentrated along segment boundaries. F & F') UWGM_2833; close up of the head region, showing antennulate antennules and maxillae extending away from the carapace. A hypostome is visible, but partially obscured by epoxy. Abbreviation list: anu = antennule; ant = antenna; man = mandible; mxl = maxillule; mxa = maxilla; mxp = maxilliped; car = cephalic carapace; hyp = hypostome; mus = muscles. All scale bars = 2 mm.

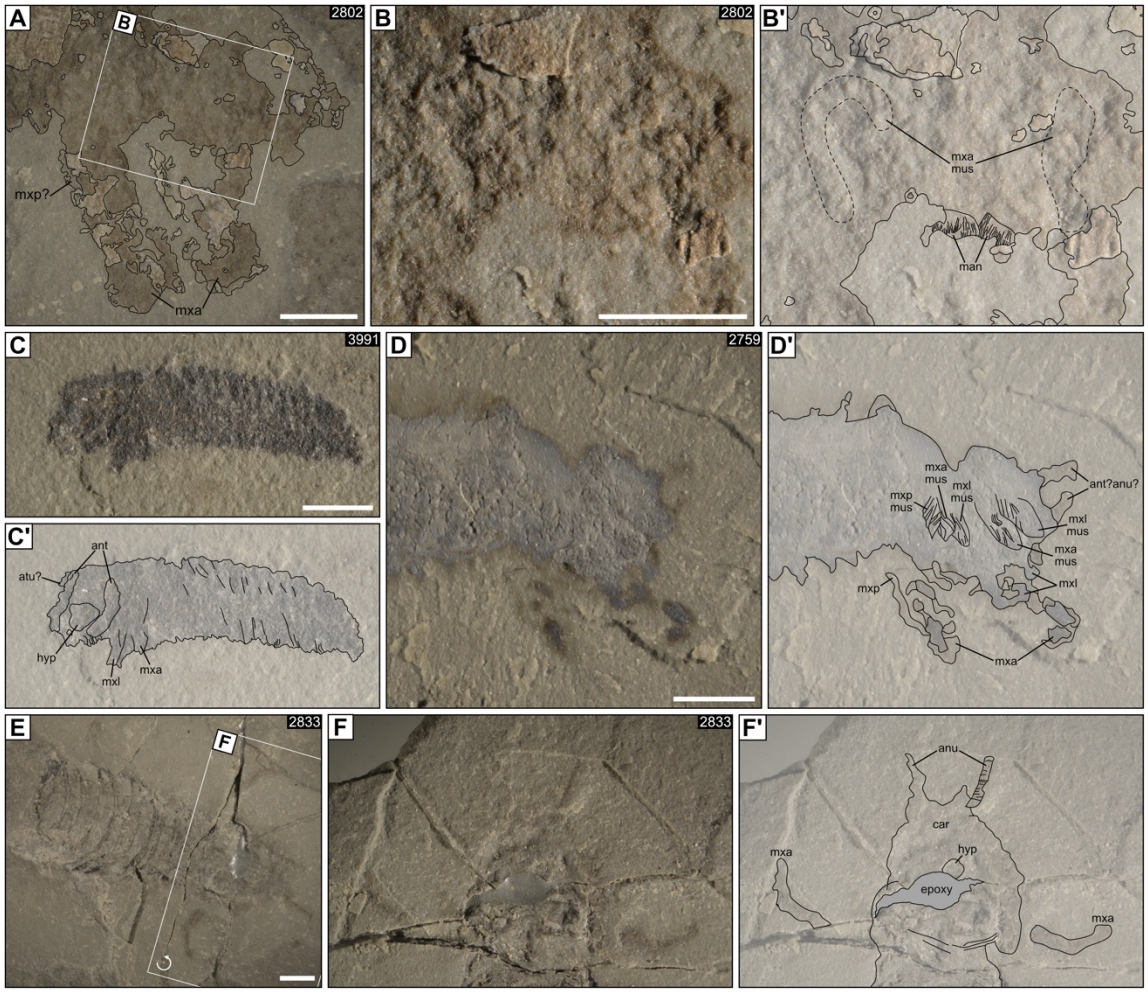
A
2802
B
mxp?
mxa
B
2802
B'
mxa
mus
man
C
3991
C'
ant
atu?
hyp
mxl
mxa
D
2759
D'
mxa
mus
mxl
mus
mxp
mus
ant?anu?
mxl
mus
mxa
mus
mxl
mxp
mxa
E
2833
F
F
2833
F'
anu
car
mxa
hyp
epoxy
mxa

The first three trunk segments are reduced relative to the others, and while they are morphologically part of the trunk, functionally they belong to the head as each bears a single pair of well-developed maxillipeds comprising approximately 5 to 7 podomeres, although there is some ambiguity in podomere number based on the fossils analyzed herein (Fig. 3-7). These three somites are often positioned at an angle relative to the following trunk segments (Fig. 3-7C & D). Similar to the head appendages, the maxillipeds lack outgrowths; however, they do not display chelae, and instead terminate in a single claw.

The remaining trunk segments are homonomous, with semi-annular tergites flanked by relatively short (transversely) pleurae. The pleurae often appear banded, with a laterally sloping border separating a light-colored anterior from a discolored posterior that often bears a thin phosphate coat. In one specimen, this pattern appears reversed (Fig. 3-3A), though this could be a taphonomic effect. Sternites are not readily distinguishable. Each trunk segment bears a single pair of small, setose, paddle-shaped appendages plausibly used for swimming (Fig. 3-8). The main ramus appears multisegmented, with up to nine short, disc-like podomeres (denoted by label i; Fig. 3-8B' & D'). Some specimens preserve what is possibly a frilly epipod near the leg base (denoted by label ii; Fig. 3-8B' & D').

Figure 3-7. Maxillipeds and their placement. A & A') UWGM_2828; photomicrograph and corresponding trace. Three maxillipeds partially preserved, along with a single maxilla. The eye is well preserved, as shown in Fig. 3-5. B & B') UWGM_4639; photomicrograph and corresponding trace. Full specimen shown in Fig. 3-4. While the majority of the head appendages and their corresponding segments are jumbled, some appendage structures are visible. One to two maxillipeds are preserved along the posterior margin of the head appendage mass, with the sub-chelae of a maxilla, maxillule, and both antennae present along the anterior margin. The mandibles are not identifiable, but the corresponding musculature is visible near the top of the head. C) UWGM_2813; photomicrograph of full specimen. This specimen bears 44 trunk segments, the most of any of the specimens described herein. The head is preserved obliquely, with twisting localized along the three maxilliped segments oriented at an angle to the homonomous trunk segments. D & D') UWGM_2813; closeup of the offset maxilliped segments and corresponding trace. The oblique preservation of the head leads to overprinting of the offset maxilliped segments with maxilla musculature; a single maxilla is only partially preserved. It is unclear whether the anteriormost musculature corresponded to antennae or maxillules; mandibular musculature is located higher within the head. Abbreviation list: ant = antenna; man = mandible; mxl = maxillule; mxa = maxilla; mxp = maxilliped; car = cephalic carapace; mus = muscles; seg = segment. All scale bars = 2 mm.

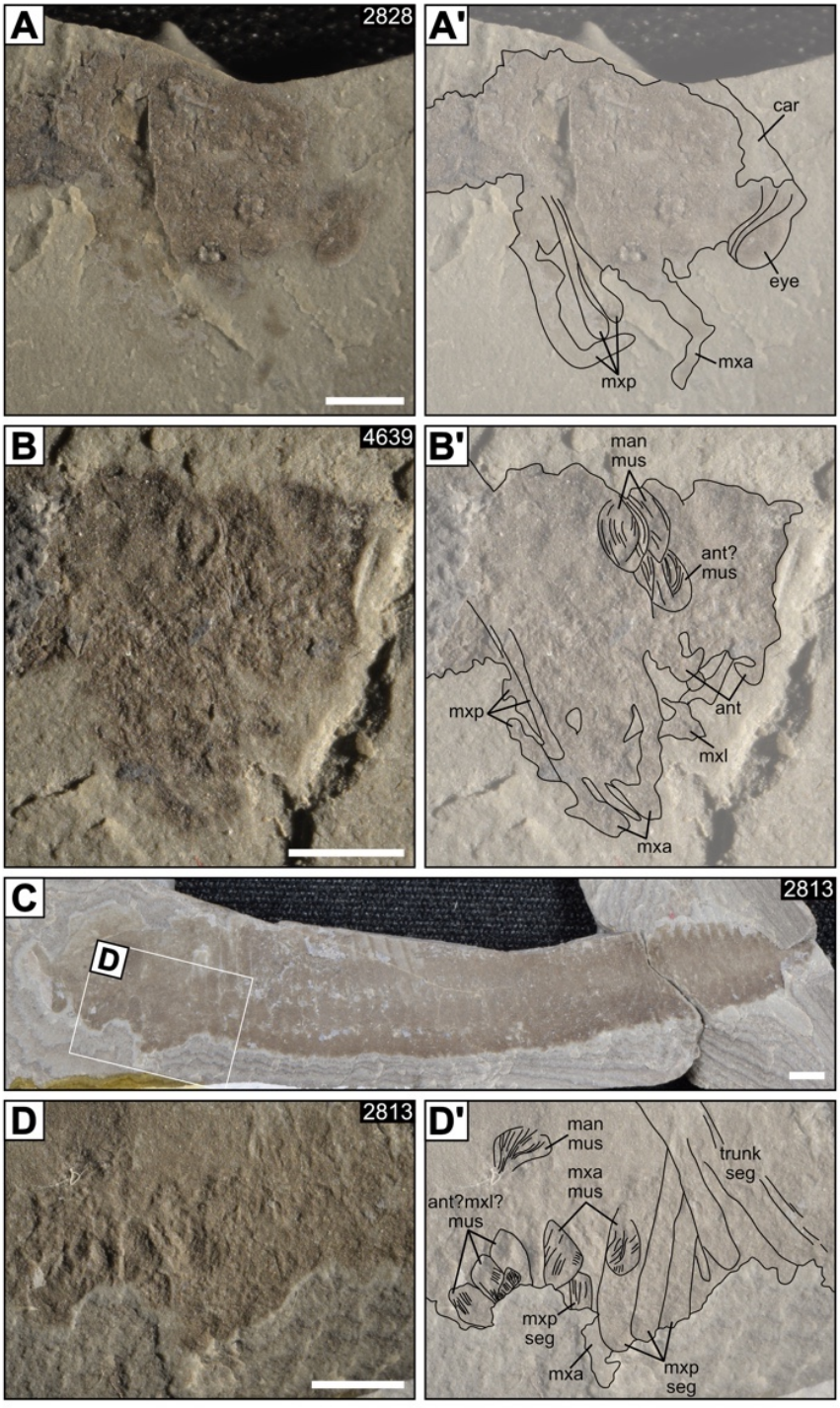
A
2828
A'
car
eye
mxa
mxp
B
4639
B'
man
mus
ant?
mus
mxp
ant
mxl
mxa
C
2813
D
D
2813
D'
man
mus
mxa
mus
ant?mxl?
mus
trunk
seg
mxp
seg
mxa
mxp
seg

Figure 3-8. Trunk limb structure. A) UWGM_2728; photomicrograph of full specimen. UWGM_2728 is one of the only specimens providing a ventral view of the organism. The head limbs are jumbled underneath the carapace, but the trunk limbs are preserved. B & B') UWGM_2728; photomicrograph and corresponding trace of trunk limb closeup. Setose swimming appendages are visible and comprise two structures; the rightmost appendage has been twisted and lies in out of sequence. C) UWGM_3511; photomicrograph of full specimen. This specimen has been twisted along the maxilliped segments, with the trunk preserved 180° from the typical position. D & D') UWGM_3511' photomicrograph and corresponding trace of trunk limb closeup, with several appendage groups outlined. In both B' and D', separate limb structures have been labelled with Roman numerals: i) main ramus, tenably an exopod; ii) small frilly bit, plausibly an epipod; iii) potential structure near the limb base, visible on very few limbs, possibly an endopod. E) UWGM_4648; photomicrograph of full specimen. Black arrow indicates a three-dimensionally preserved turdlet. F & F') UWGM_4648; photomicrograph and corresponding trace of trunk limb podomeres. Podomeres are short and disc-like, with a maximum number of nine visible in a single limb. Area of greatest relief in podomeres is outlined in F'.

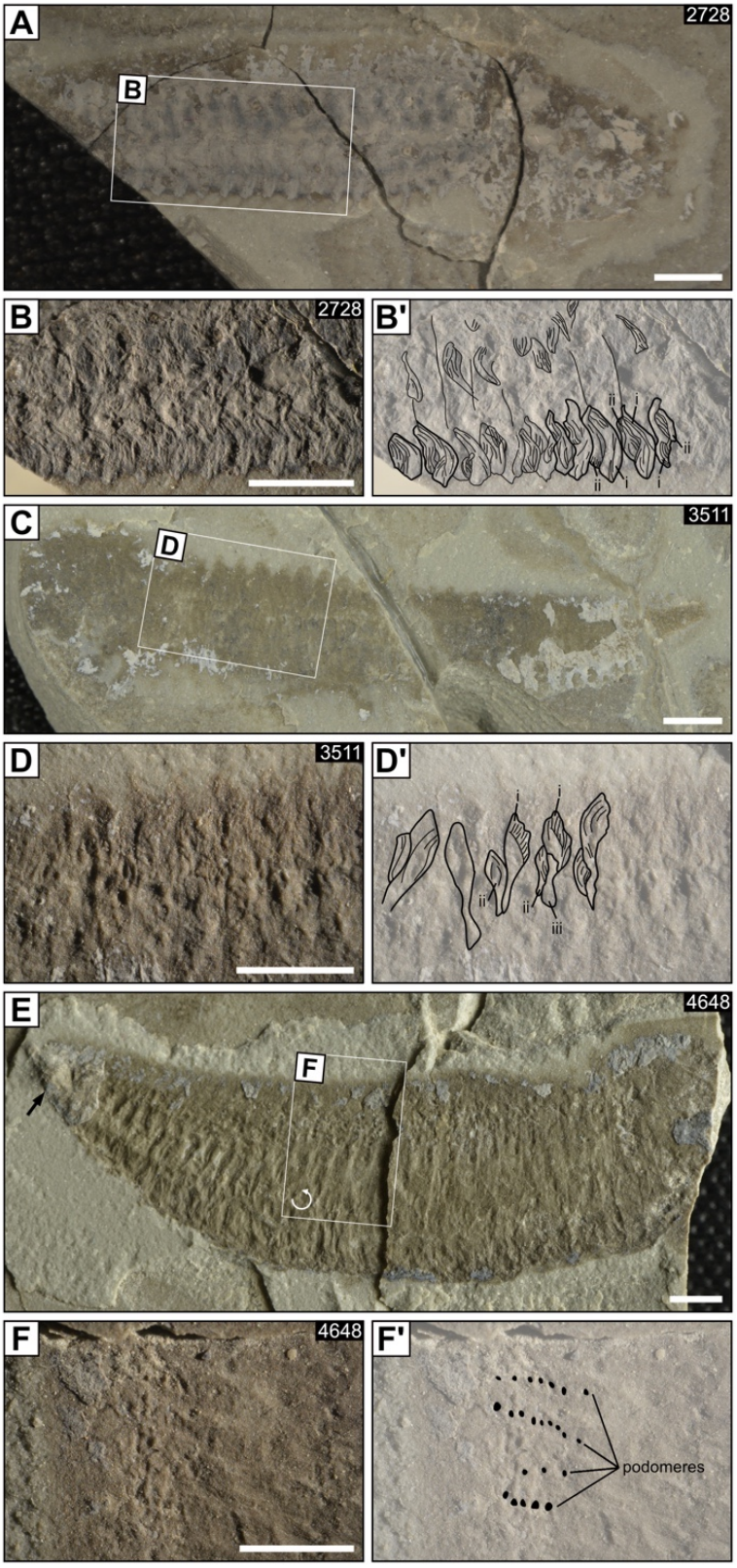
A
2728
B
B
2728
B'
ii
i
ii
ii
i
i
C
3511
D
D
3511
D'
i
i
ii
ii
iii
E
4648
F
F
4648
F'
podomeres

The trunk segments generally maintain a consistent diameter along much of the trunk length. Near the terminus of the trunk, segment diameter contracts sharply, resulting in a blunt termination of the trunk; while the terminus is sclerotized, no telson or other terminal process is observed in any specimen. Occasionally, a three-dimensionally preserved turdlet is found along the midline of the animal, near its terminus. Truly labile material (e.g., nervous system, stomach) is not preserved except in a few rare examples of poorly preserved potential gut tracts (Fig. 3-3). There is some evidence of muscle fibers within the head of some specimens (Figs. 3-6 & 3-7), although it is difficult to differentiate between muscle fibers and setae elsewhere in the organism (e.g., trunk appendages).

Remarks. There is uncertainty as to whether the tiny boxing glove on the second, fourth, and fifth head appendages could represent either endopods or exopods, although it is more likely for an endopod to exhibit the sturdy, sub-chelate morphology that is displayed by these specimens. Similarly, while the small swimming appendages along the trunk are preserved in many specimens, often in fine enough detail to observe setae, there is no clear evidence to confirm whether the main ramus of the limb is an exopod or endopod. While it is tenable that the main leg ramus (denoted by label i; Fig. 3-8B' & D') is an exopod based on the overall paddle-shape morphology and abundance of setae (and is thus the interpretation made herein), the possibility that the main ramus (denoted by label i; Fig. 3-8B' & D') is instead an endopod, and the presumed epipod (denoted by label ii; Fig. 3-8B & D) thus a reduced exopod, cannot be ignored (Fig. 3-8). Alternatively, as suggested by a single well-preserved limb outlined in Fig. 3-8D', the primary appendage could comprise an endopod-exopod pair (labels i & iii) with a frilly epipod (label ii) near the base.

As mentioned previously, the majority of specimens represent lateral views of the organism. However, some specimens appear twisted, with the trunk oriented at an angle to

the laterally preserved head, thus providing an oblique dorsal view of the trunk (UWGM_2813; UWGM_3511; Figs. 3-7C & D, 3-8C & D). In these cases, the twisting is localized within the first three segments of the trunk which bear the maxilliped pairs.

3.4.3 *Acheronauta leonidas*

Acheronauta leonidas sp. nov.

(Figs. 3-5, 3-9, & 3-11)

Diagnosis. Same as for genus with two additional specifications: Presence of carina on anterodorsal margin of cephalic carapace; Pronounced contraction in tergite width anterior to trunk terminus.

Dimensions. The single complete specimen measures 0.60 cm x 5.86 cm.

Derivation of name. From Greek, Leonidas was a warrior king of the Greek city-state of Sparta ca. 480 BC. Hoplites, Greek citizen soldiers, commonly wore helmets adorned with vertical horse-hair plumes; the front edge of the cephalic carapace on *A. leonidas* gen. et sp. nov. bears a resemblance to this plume and is thus named for king Leonidas.

Holotype. UWGM_2825, part and counterpart of whole specimen (Figs. 3-5, 3-9, & 3-11), from Waukesha Lime & Stone Co. quarry, Waukesha, WI, USA.

Additional material. UWGM_3684, partial specimen, from Waukesha Lime & Stone Co. quarry, Waukesha, WI, USA.

Hypodigm. Total number of collected specimens identified = 2. Additional specimens may be present in the UWGM collections, though not formally assigned.

Occurrence. The Silurian Brandon Bridge Formation in southeast WI, USA.

Remarks. It is important to note that this species designation is based on only two specimens: UWGM_2825 (complete) and UWGM_3684 (incomplete). UWGM_2825 is the only specimen to bear both an anterior keel on the cephalic carapace and a pronounced contraction of the trunk anterior to the terminus. UWGM_3684 is poorly preserved, and only shows the trunk, which does exhibit a pronounced contraction in posterior tergite width. The overall marked similarity of *A. Leonidas* gen. et sp. nov. to *A. stimulapis* gen. et sp. nov. is notable, and it could be argued that the designation of two separate species is unwarranted because the key differences between the proposed species possibly represent taphomorphs or alternatively may be the result of sexual dimorphism. However, given that only one of the 23 *Acheronauta* gen nov. specimens analyzed in detail herein, as a subset of the tens of specimens that have been collected, has been identified to bear both a contracted posterior trunk and anterior carina on the cephalic carapace, neither of these arguments seem tenable. If these traits were the result of sexual dimorphism, we would expect a higher proportion of the fossils to display one or both of these characteristics. As for the possibility of the presence or absence of a carina being a product of taphonomic distortion, we feel that the absence of a carina on such well-preserved *A. stimulapis* gen. et sp. nov. specimens like UWGM_2770 and UWGM_4634, argues against the possibility of a missing carina being the result of poorer preservation (compare cephalic carapaces in Figs. 3-4, 3-5, 3-8A, & 3-9; compare trunk termini in Figs. 3-4, 3-6 to 3-9). Additionally, while the presence of a carina is the most obvious feature present in *A. Leonidas* gen. et sp. nov., the carapace also appears to be somewhat deeper (dorsoventrally) than that of *A. stimulapis* gen. et sp. nov., with an anteroventral "cheek guard" extension on *A. Leonidas* gen. et sp. nov.. These morphological differences are somewhat more subtle than the anterodorsal carina, so we are hesitant to include these traits in the diagnosis. Furthermore, while the compound eye on *A. stimulapis* gen. et sp. nov. specimens protrudes

beyond the anterior margin of the cephalic carapace, UWGM_2825 shows the eye located in a slightly more posterior location beneath the carapace, with the keel protruding beyond it (Fig. 3-5). Thus, while further analysis of the remaining collection of *Acheronauta* gen. nov. specimens at the UWGM is warranted to support or refute our morphological interpretations, we have opted to designate a second species within the *Acheronauta* genus.

Figure 3-9. *Acheronauta Leonidas* gen. et sp. nov. holotype. A & A') GIGAmacro image of UWGM_2825 part and corresponding trace. B) GIGAmacro image of UWGM_2828 counterpart. UWGM_2825 is the only identified specimen to bear both key characteristics distinguishing *A. Leonidas* gen. et sp. nov. from *A. stimulapis* gen. et sp. nov.: an anterodorsal carina on the cephalic carapace, and pronounced contraction of the trunk segments anterior to the terminus. Abbreviation: mxp = maxilliped. Scale bar = 5 mm.

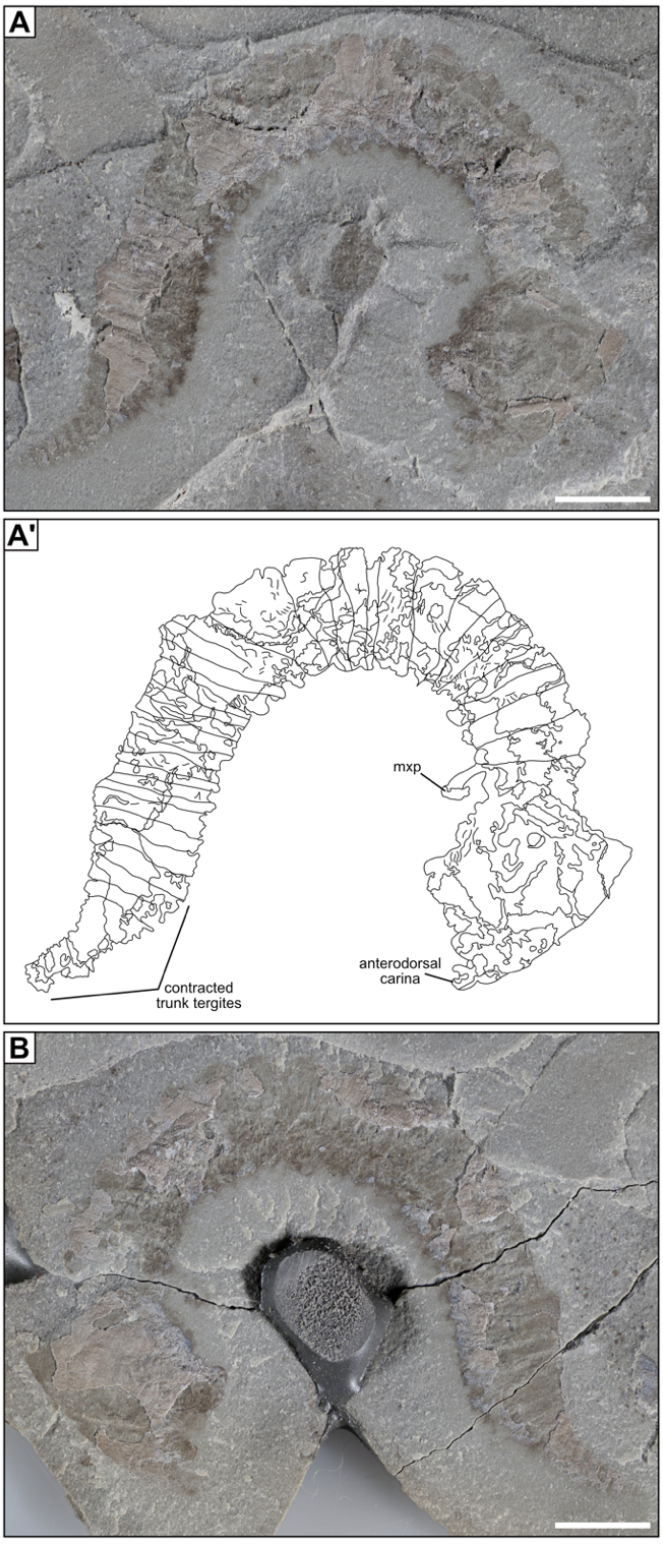
A
A'
mxp
anterodorsal
carina
contracted
trunk tergites
B

3.5 Discussion

3.5.1 Phylogeny & Autecology

Owing to ambiguity in some of the characters when coding *Acheronauta* gen. nov. to the cladistic matrix of Aria & Caron (2017), we have chosen to provide four phylogenetic trees (Fig. 3-10). First, the predominant ambiguous character is the series of small swimming appendages attached to the trunk segments. Poor preservation, coupled with a lack of clear ventral views on the majority of specimens, provided little evidence as to whether the main ramus of each appendage represents an endopod or exopod (labeled i; Fig. 3-8). Second, the lack of well-preserved specimens in a dorsoventral perspective means that there is no clear view of the dorsal margin of the cephalic carapace; thus, it is unclear whether this carapace is bivalved. Third, the predominance of lateral views coupled with the overlying cephalic carapace results in a paucity of well-preserved mouth parts. As such, while there are preserved mandibles in the holotype of *A. stimulapis* gen. et sp. nov. (Fig. 3-6A & B; UWGM_2802), there is no clear evidence for or against the presence of an atrium oris, although the mandibles are recessed into the head relative to the other cephalic appendages. Finally, there is ambiguity in the total number of podomeres in the cephalic appendages, with counts ranging from three to seven.

Figure 3-10. Phylogenetic trees and branch analyses. Four strict consensus phylogenetic trees were constructed for *Acheronauta* gen. nov. with characters coded in the following manner: A) Our favored tree. Main ramus of trunk limb = Exopod. Other ambiguous characters = assumptive "certain" states. B) Main ramus of trunk limb = Exopod. Other ambiguous characters = "?". C) Main ramus of trunk limb = Endopod. Other ambiguous characters = assumptive "certain" states. D) Main ramus of trunk limb = Endopod. Other ambiguous characters = "?". Branch analysis results are labelled at each node. In A) Bremer analysis values are denoted in regular font, boostrap analysis values are denoted in bold, and jackknife analysis values are denoted in italics. For B–D, bootstrap analysis values are denoted in bold at each node. In all cases, "–" indicates that a particular node is missing in the corresponding branch analysis. Values in parentheses indicate that, while the specific node was present in both the branch analysis and strict consensus trees, the topology of the contained taxa is different.

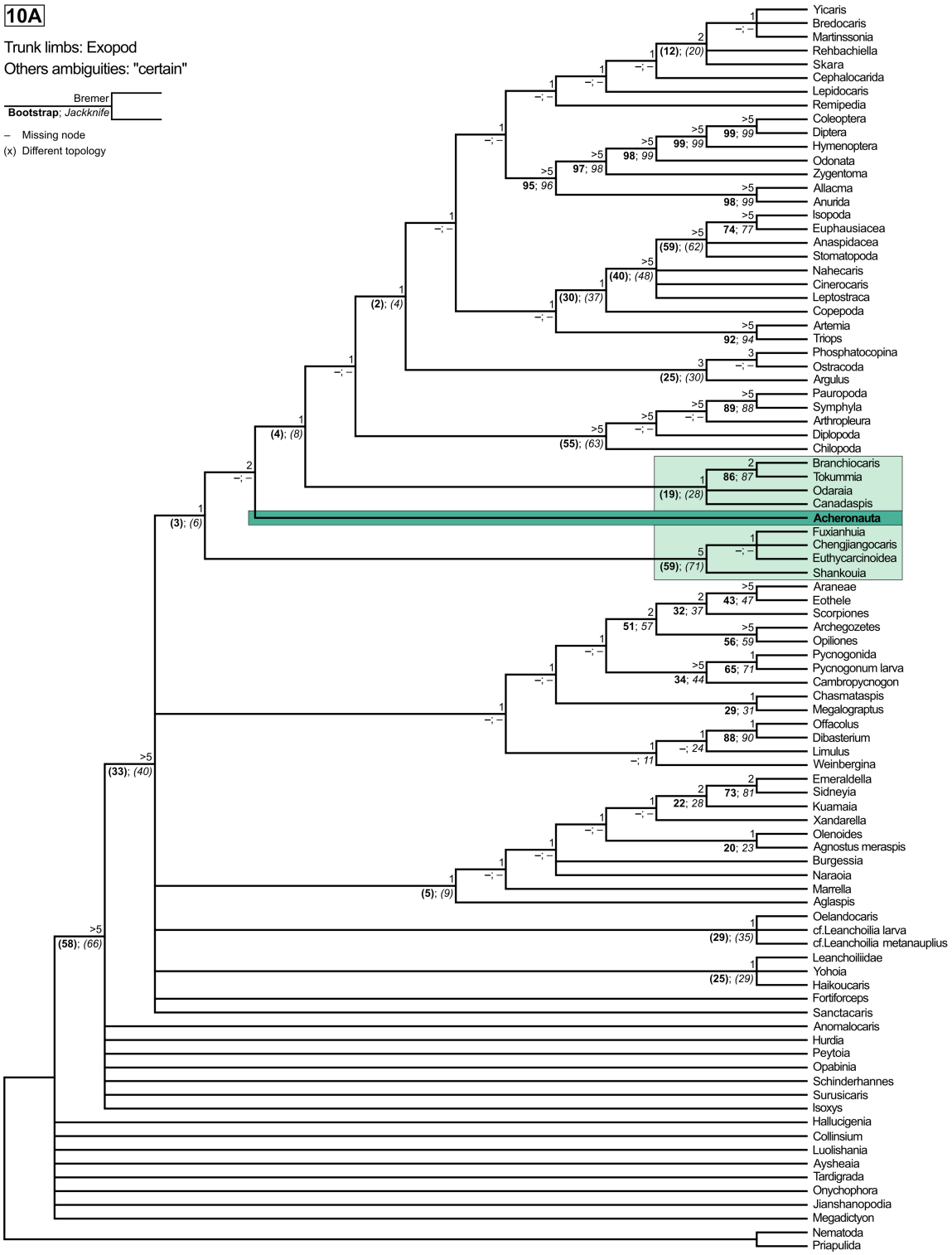
10A
Trunk limbs: Exopod
Others ambiguities: "certain"
Bremer
Bootstrap; Jackknife
– Missing node
(x) Different topology
Yicaris
Bredocaris
Martinssonia
Rehbachiella
Skara
Cephalocarida
Lepidocaris
Remipedia
Coleoptera
Diptera
Hymenoptera
Odonata
Zygentoma
Allacma
Anurida
Isopoda
Euphausiacea
Anaspidacea
Stomatopoda
Nahecaris
Cinerocaris
Leptostraca
Copepoda
Artemia
Triops
Phosphatocopina
Ostracoda
Argulus
Pauropoda
Symphyla
Arthropleura
Diplopoda
Chilopoda
Branchiocaris
Tokummia
Odaraia
Canadaspis
Acheronauta
Fuxianhuia
Chengjiangocaris
Euthycarcinoidea
Shankouia
Araneae
Eothele
Scorpiones
Archegozetes
Opiliones
Pycnogonida
Pycnogonum larva
Cambropycnogon
Chasmataspis
Megalograptus
Offacolus
Dibasterium
Limulus
Weinbergina
Emeraldella
Sidneyia
Kuamaia
Xandarella
Olenoides
Agnostus meraspis
Burgessia
Naraoia
Marrella
Aglaspis
Oelandocaris
cf.Leanchoilia larva
cf.Leanchoilia metanauplius
Leanchoiliidae
Yohoia
Haikoucaris
Fortiforceps
Sanctacaris
Anomalocaris
Hurdia
Peytoia
Opabinia
Schinderhannes
Surusicaris
Isoxys
Hallucigenia
Collinsium
Luolishania
Aysheaia
Tardigrada
Onychophora
Jianshanopodia
Megadictyon
Nematoda
Priapulida

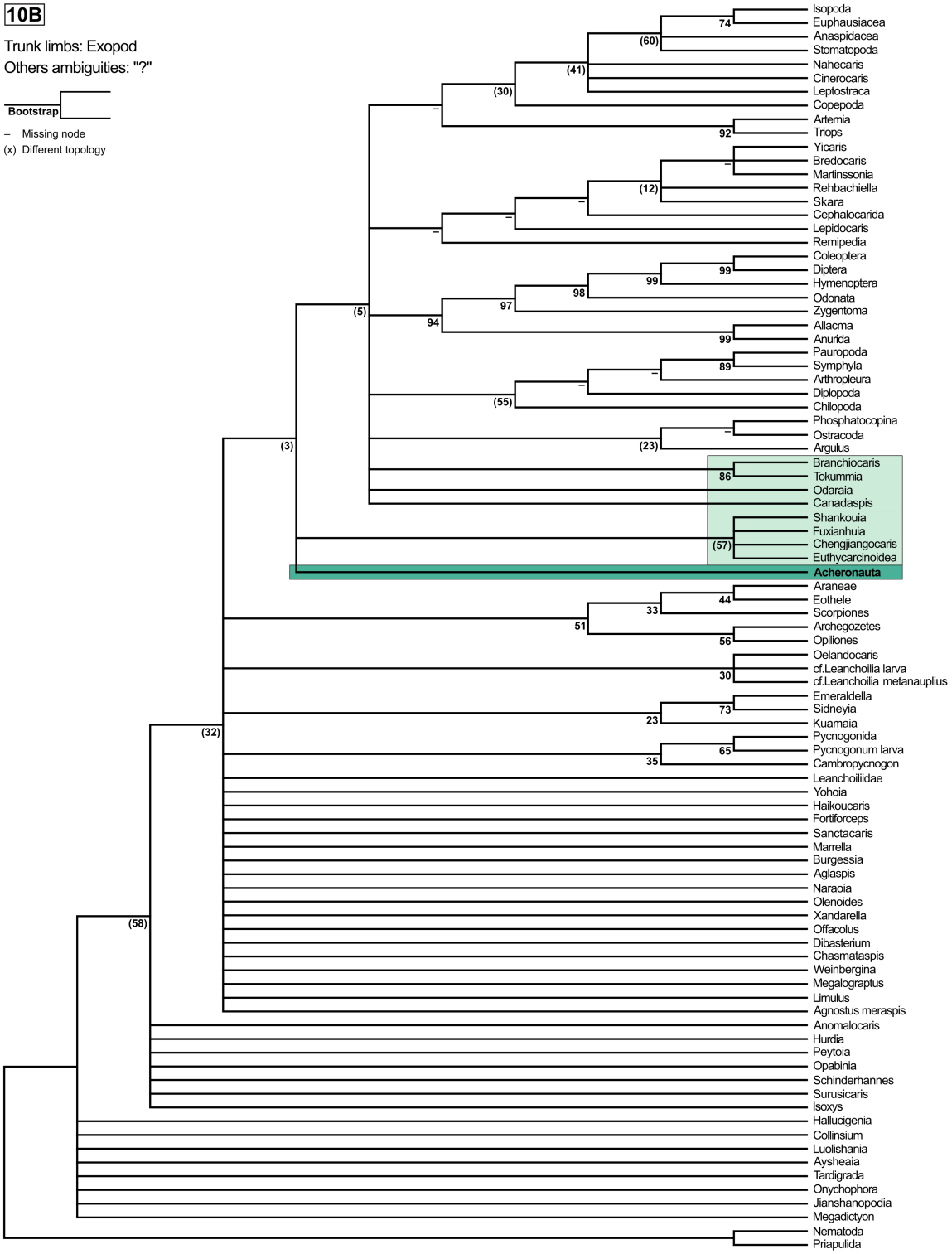
10B
Trunk limbs: Exopod
Others ambiguities: "?"
Bootstrap
– Missing node
(x) Different topology
Isopoda
Euphausiacea
Anaspidacea
Stomatopoda
Nahecaris
Cinerocaris
Leptostraca
Copepoda
Artemia
Triops
Yicaris
Bredocaris
Martinssonia
Rehbachiella
Skara
Cephalocarida
Lepidocaris
Remipedia
Coleoptera
Diptera
Hymenoptera
Odonata
Zygentoma
Allacma
Anurida
Pauropoda
Symphyla
Arthropleura
Diplopoda
Chilopoda
Phosphatocopina
Ostracoda
Argulus
Branchiocaris
Tokummia
Odaraia
Canadaspis
Shankouia
Fuxianhuia
Chengjiangocaris
Euthycarcinoidea
Acheronauta
Araneae
Eothele
Scorpiones
Archegozetes
Opiliones
Oelandocaris
cf.Leanchoilia larva
cf.Leanchoilia metanauplius
Emeraldella
Sidneyia
Kuamaia
Pycnogonida
Pycnogonum larva
Cambropycnogon
Leanchoiliidae
Yohoia
Haikoucaris
Fortiforceps
Sanctacaris
Marrella
Burgessia
Aglaspis
Naraoia
Olenoides
Xandarella
Offacolus
Dibasterium
Chasmataspis
Weinbergina
Megalograptus
Limulus
Agnostus meraspis
Anomalocaris
Hurdia
Peytoia
Opabinia
Schinderhannes
Surusicaris
Isoxys
Hallucigenia
Collinsium
Luolishania
Aysheaia
Tardigrada
Onychophora
Jianshanopodia
Megadictyon
Nematoda
Priapulida

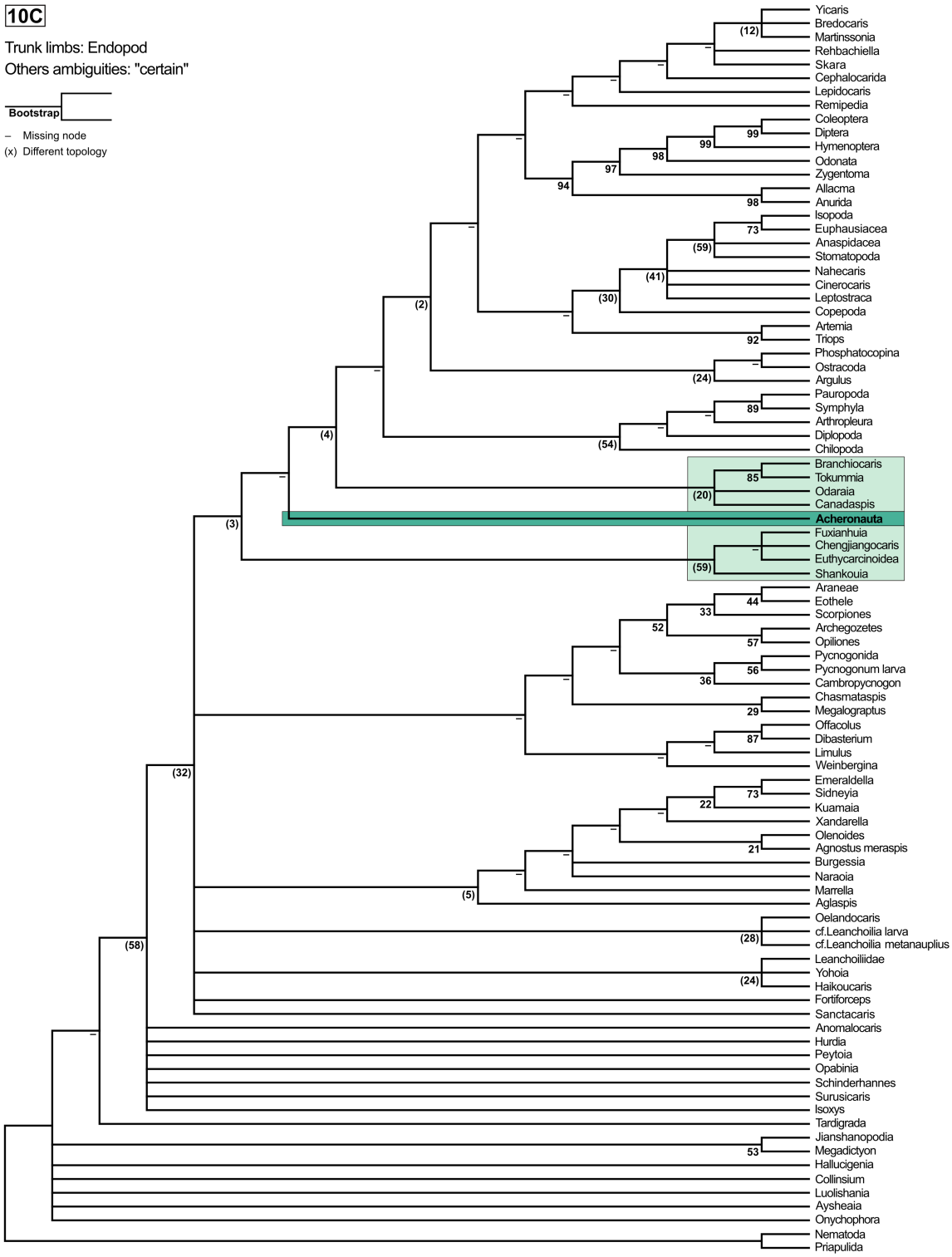
10C
Trunk limbs: Endopod
Others ambiguities: "certain"
Bootstrap
– Missing node
(x) Different topology
Yicaris
Bredocaris
Martinssonia
Rehbachiella
Skara
Cephalocarida
Lepidocaris
Remipedia
Coleoptera
Diptera
Hymenoptera
Odonata
Zygentoma
Allacma
Anurida
Isopoda
Euphausiacea
Anaspidacea
Stomatopoda
Nahecaris
Cinerocaris
Leptostraca
Copepoda
Artemia
Triops
Phosphatocopina
Ostracoda
Argulus
Pauropoda
Symphyla
Arthropleura
Diplopoda
Chilopoda
Branchiocaris
Tokummia
Odaraia
Canadaspis
Acheronauta
Fuxianhuia
Chengjiangocaris
Euthycarcinoidea
Shankouia
Araneae
Eothele
Scorpiones
Archegozetes
Opiliones
Pycnogonida
Pycnogonum larva
Cambropycnogon
Chasmataspis
Megalograptus
Offacolus
Dibasterium
Limulus
Weinbergina
Emeraldella
Sidneyia
Kuamaia
Xandarella
Olenoides
Agnostus meraspis
Burgessia
Naraoia
Marrella
Aglaspis
Oelandocaris
cf.Leanchoilia larva
cf.Leanchoilia metanauplius
Leanchoiliidae
Yohoia
Haikoucaris
Fortiforceps
Sanctacaris
Anomalocaris
Hurdia
Peytoia
Opabinia
Schinderhannes
Surusicaris
Isoxys
Tardigrada
Jianshanopodia
Megadictyon
Hallucigenia
Collinsium
Luolishania
Aysheaia
Onychophora
Nematoda
Priapulida

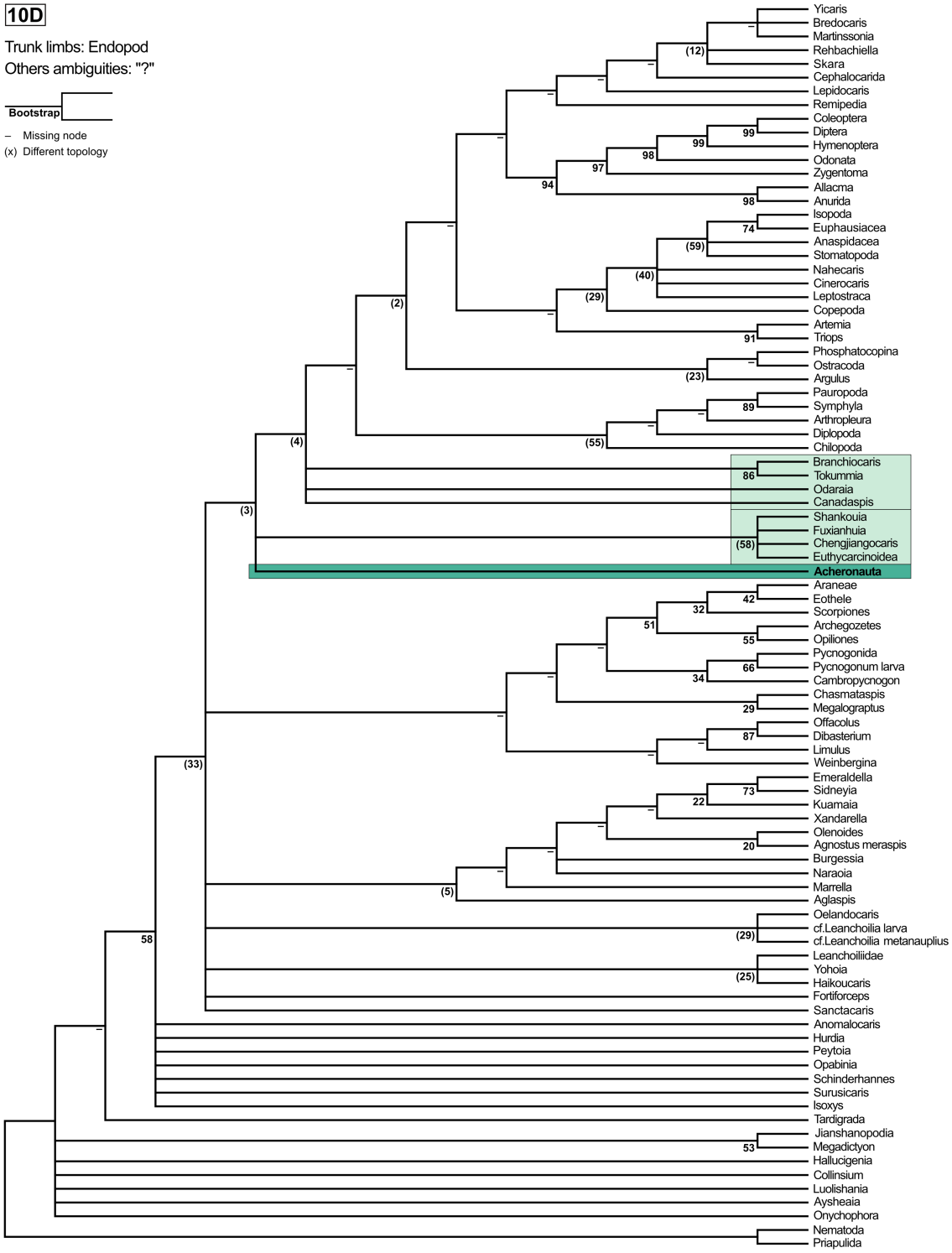
10D
Trunk limbs: Endopod
Others ambiguities: "?"
Bootstrap
– Missing node
(x) Different topology
Yicaris
Bredocaris
Martinssonia
Rehbachiella
Skara
Cephalocarida
Lepidocaris
Remipedia
Coleoptera
Diptera
Hymenoptera
Odonata
Zygentoma
Allacma
Anurida
Isopoda
Euphausiacea
Anaspidacea
Stomatopoda
Nahecaris
Cinerocaris
Leptostraca
Copepoda
Artemia
Triops
Phosphatocopina
Ostracoda
Argulus
Pauropoda
Symphyla
Arthropleura
Diplopoda
Chilopoda
Branchiocaris
Tokummia
Odaraia
Canadaspis
Shankouia
Fuxianhuia
Chengjiangocaris
Euthycarcinoidea
Acheronauta
Araneae
Eothele
Scorpiones
Archegozetes
Opiliones
Pycnogonida
Pycnogonum larva
Cambropycnogon
Chasmataspis
Megalograptus
Offacolus
Dibasterium
Limulus
Weinbergina
Emeraldella
Sidneyia
Kuamaia
Xandarella
Olenoides
Agnostus meraspis
Burgessia
Naraoia
Marrella
Aglaspis
Oelandocaris
cf.Leanchoilia larva
cf.Leanchoilia metanauplius
Leanchoiliidae
Yohoia
Haikoucaris
Fortiforceps
Sanctacaris
Anomalocaris
Hurdia
Peytoia
Opabinia
Schinderhannes
Surusicaris
Isoxys
Tardigrada
Jianshanopodia
Megadictyon
Hallucigenia
Collinsium
Luolishania
Aysheaia
Onychophora
Nematoda
Priapulida

In light of these uncertainties, we have produced four viable phylogenetic analyses with corresponding strict consensus trees. Two of these trees (Figs. 3-10A & B) code the main ramus of the small trunk appendages as exopods, while the other two code the primary rami as endopods (Figs. 3-10C & D). For each of these endopod and exopod analyses, one has the remaining ambiguous characters coded as "?" in the character matrix (Figs. 3-10B & D), while the other is coded as their most plausible "certain" state (i.e., the carapace is bivalved; an atrium oris is present; head limbs comprise seven or fewer podomeres; Figs. 3-10A & C). We favor Fig. 3-10A as the most tenable phylogeny of *Acheronauta* gen. nov., which has the swimming limbs coded as exopods (based on the prevalence of setae and the overall paddle-shape), and the other characters coded as their assumptive "certain" states as opposed to a "?" in the matrix.

Our initial analysis of these specimens, prior to any character coding (as documented in a published abstract; Pulsipher et al., 2019), suggested an affinity with either the crustacean class Thylacocephala or Remipedia, an interpretation based primarily on the overall morphology of these specimens. Thylacocephalans, which have been previously documented in the Brandon Bridge Formation (*Thylacares brandonensis* Haug et al., 2014), are known from the Lower Silurian to the Upper Cretaceous, though their range may extend into the Cambrian (Vannier et al., 2006; Haug et al., 2014). Remipedes, on the other hand, have a poor fossil record extending only into the Carboniferous (Neiber et al., 2011). Both thylacocephalans and remipedes, interpreted by some to have a sister-group relationship (Haug et al., 2014), are characterized by long, segmented trunks, three pairs of anterior raptorial appendages, and a suite of small posterior swimming appendages (Neiber et al.., 2011; Haug et al., 2014; Schram et al., 1999). Importantly, thylacocephalans are almost entirely enclosed in a bivalved carapace (Schram et al., 1999). Remipedes have no carapace, and, unlike other extant crustaceans, have

only one trunk tagma (Neiber et al., 2011). Thus, while direct assignment to either Remipedia or Thylacocephala was problematic, we originally supposed that these specimens may be thylacocephalans without a whole-body carapace, carapace-bearing remipedes, or a unique class of arthropods plausibly related to one or both groups. The phylogenetic analysis presented herein instead indicates that *Acheronauta* gen. nov. is not closely related to Remipedia which is much more derived, as shown in Fig. 3-10. Thylacocephala is not coded in the Aria & Caron (2017) matrix, however, and thus cannot be directly compared to *Acheronauta* gen nov. in this context.

Phylogenetic analysis based on the specimens described herein places *Acheronauta* gen. nov. as a basal mandibulate, closely related to the fuxianhuiids and/or hymenocarinids (Aria & Caron, 2017; n.b. we here use Fuxianhuiida in the paraphyletic sense, as both our cladograms and those of Aria & Caron 2017 resolve the Euthycarcinoidea within the fuxianhuiids. However, recent evidence by Edgecombe et al. [2020] suggests a much closer affinity of the euthycarcinoids to the myriapods. Thus, while the fuxianhuiids and euthycarcinoids may yet prove to be related, it is the comparison to the better-understood fuxianhuiids which is important to our discussion here). In both assumptive "certain" trees, regardless of the status of the main rami of the trunk limbs, *Acheronauta* gen. nov. falls between the hymenocarinids and fuixianhuiids (Figs. 3-10A & C). In both "?" coded trees, again regardless of the endopod/exopod status of the trunk limbs, *Acheronauta* gen. nov. plots in an unresolved polytomy with the fuxianhuiids and crown-group Arthropoda (Fig. 3-10B & D). This phylogenetic placement is markedly similar to the reinterpretation of *Parioscorpio venator* Wendruff et al., 2020b by Anderson et al. (*in press*), which places this taxon as a sister-group to the fuxianhuiids and hymenocarinids in some of their alternate state analyses. Branch support analysis of the phylogenetic trees, particularly bootstrap, is notably weak in all cases

(Fig. 3-10). In our preferred tree (Fig. 3-10A), Bremer support collapses the node containing *Acheronauta* gen. nov. in two steps, which is more robust than many of the interorder relationships among the Crustacea which collapse in one step.

Regarding inferences of their autecology, *Acheronauta* gen nov. was likely a scavenger, as well as an opportunistic predator as evidenced by the specialization of the cephalic appendages and its relatively large size compared to smaller taxa in the Waukesha Lagerstätte (i.e., paleoscolecids, polychaetes, synziphosurines, other juvenile arthropods, etc.). This interpretation is bolstered by the apparent phylogenetic affinity of *Acheronatua* gen. nov. with fuxianhuiids and hymenocarinids. The fuxianhuiids have been interpreted as scavengers, using their specialized head appendages, posterior to the antennae, to plow the sediment in search of food (Yang et al., 2013). The hymenocarinid clade comprises both scavengers and predators. *Tokummia katalepsis* Aria & Caron, 2017, with its large size and prominent chelate maxillipeds, was likely able to grasp and cut up its prey (Aria & Caron, 2017). *Canadaspis*, however, is interpreted to have subsisted on coarse food particles raked from the sediment and passed along a "conveyor belt" of appendages toward the mouth parts (Briggs, 1978; Hou & Bergström, 1997).

While *Acheronauta* gen. nov. is not closely related phylogenetically to Remipedia, and potentially not to Thylacocephala either, a brief description of their life modes is warranted given their apparent morphological convergence. Modern remipedes have been documented almost exclusively in the deepest waters of anchialine caves, in low nutrient, low oxygen settings where they are opportunists, functioning as both predator and scavenger (Neiber et al., 2011). Conversely, the life mode of thylacocephalans is uncertain; hypotheses include benthic scavenger, necto-benthic ambush predator, nektonic predator, or some combination of the three (Broda et al., 2015). Importantly, however, the raptorial appendage specialization

of *Acheronauta* gen. nov. and its placement of these morphologies in the antennae, maxillules, and maxillae (as opposed to adjacent limbs) are unique features not observed in other arthropods. The remipede *Godzillius robustus* Schram et al., 1986 is somewhat of an exception; *G. robustus* bears uniramous maxillules, maxillae, and maxillipeds which have a similar curvaceous, boxing glove-esque appearance terminating in a single claw. Unlike *Acheronauta* gen. nov., however, these specialized appendages are adjacent, setose, and, in the case of the maxillae and maxillipeds, the more terminal podomere nests tightly against the other (Schram et al., 1986).

3.5.2 Taphonomy

The taphonomy of the Waukesha Lagerstätte was initially investigated by Mikulic et al. (1985a; 1985b) and more recently by Wendruff et al. (2020b), as summarized below; the results presented herein augment these studies. Perhaps one of the most unique features of the Waukesha Lagerstätte is its bias towards the preservation of soft-bodied, rather than shelly, organisms (Mikulic et al., 1985a; 1985b; Moore et al., 2005; Wendruff et al., 2020b). Whereas Silurian carbonates of the midwestern US are rather well-known for their shelly taxa, such as brachiopods, echinoderms, and corals, the Waukesha instead provides an uncommon glimpse into arthropod diversity at this interval in life's history—preserving soft-bodied or sclerotized organisms via secondary phosphatization (Mikulic et al., 1985b; Jones et al., 2015; Wendruff et al., 2020b; Anderson et al., *in press*). Moreover, it seems that when biomineralized taxa are present in the Waukesha Lagerstätte, they are demineralized (Mikulic et al., 1985b). For example, trilobites appear totally decalcified (Kluessendorf, 1990), while leperditicopids have

their calcite shells replaced by phosphate (Jones, 2016). Conulariids, which biomineralize with apatite, show partial demineralization (Miller et al., 2020).

The particular depositional setting of the Waukesha very likely played a critical role in promoting or facilitating this mode of preservation. This lagerstätte represents a conservation trap-style deposit, whereby organisms (or their molts) were swept into localized and presumably anoxic/dysoxic sediment traps (Kluessendorf, 1990; Kluessendorf & Mikulic, 1996; Wendruff, 2016; Wendruff et al., 2020b). Differential preservation of organisms versus molts could be a partial cause of the taphomorphs discussed previously in section 4 and illustrated in Fig. 3-3. Paleoecological and preservational characteristics of the Waukesha assemblage suggests that these organisms were transported to the sediment trap environments, potentially during tidally or otherwise influenced burial events (e.g., Mikulic et al., 1985b; LoDuca et al., 2003; Moore et al., 2005) before being "entombed" by microbial accumulations (*sensu* Wendruff et al., 2020b after Varejão et al., 2019). The subsequent geochemical changes imposed by early decay in a reduced permeability setting are suggested to have facilitated the dissolution of shelly materials as well as the mineralization of soft tissues by francolite and pyrite in the earliest taphonomic stages (Briggs et al., 1996; Briggs, 2003). Given the small physical size of the sediment trap that comprised the Waukesha, the precise values of physical and chemical burial variables were likely subject to fluctuation, and this variability, in conjunction with differential biostratinomic histories of the bodies and molts of *Acheronauta* gen. nov. that made their way to the sediment trap, likely explains the range of taphomorphs seen in the genus.

From SEM-EDS imaging and analyses (Fig. 3-11), including both SE and BSE large-area micrograph mosaics of the holotype specimens of *A. stimulapis* gen. et sp. nov. (Fig. 3-11A & B) and *A. leonidas* gen. et sp. nov. (Fig. 3-11C–F), it is observed that the fossils are

incompletely replicated or encrusted by a compositionally variable fluorapatite. This material is distinguishable in the mixed-signal mosaics (Fig. 3-11A & C) as the lighter greyscale patches against the darker grey carbonate-cemented siliciclastic host-rock. The fluorapatite contains somewhat appreciable sulfur in some cases (Fig. 3-11E), which would generally define it mineralogically as francolite. Minor amounts of pyrite are observable in some specimens (see disseminated yellow speckles in Fig. 3-11E), but pyritization is not pervasive across the suite of fossils examined herein, nor even within single specimens (compare Fig. 3-11E with Fig. 3-11D & F), and is thus not likely to be taphonomically relevant, at least in this taxon. Jones et al. (2015) documented similar elemental compositions in two-dimensional compressions of phyllocarids from the Waukesha, with the outer cuticle of the fossils enriched in both phosphorus and calcium (which they interpret as apatite), with minute amounts of pyrite crystals in and around some of the specimens. The authors also documented that the host rock comprises common clay minerals and quartz silt, and is thus enriched in Al, K, Si, Mg, Na, and Fe (Jones et al., 2015).

The original taphonomic investigation of the Waukesha by Mikulic et al. (1985b) proposed that the fossils were preserved through the infilling of diagenetic fluorapatite. However, Jones et al. (2015) instead argued that phosphatization of their phyllocarid specimens occurred via replacement of the outer cuticle either during or following sediment compaction. Our investigation of *Acheronauta* gen. nov. specimens suggests a similar taphonomic pathway: the primary mode of preservation is through secondary phosphatic encrustation and tissue replacement of lightly sclerotized and soft tissues, respectively (Mikulic et al., 1985b; Jones et al., 2015; Wendruff et al., 2020b; Anderson et al., *in press*).

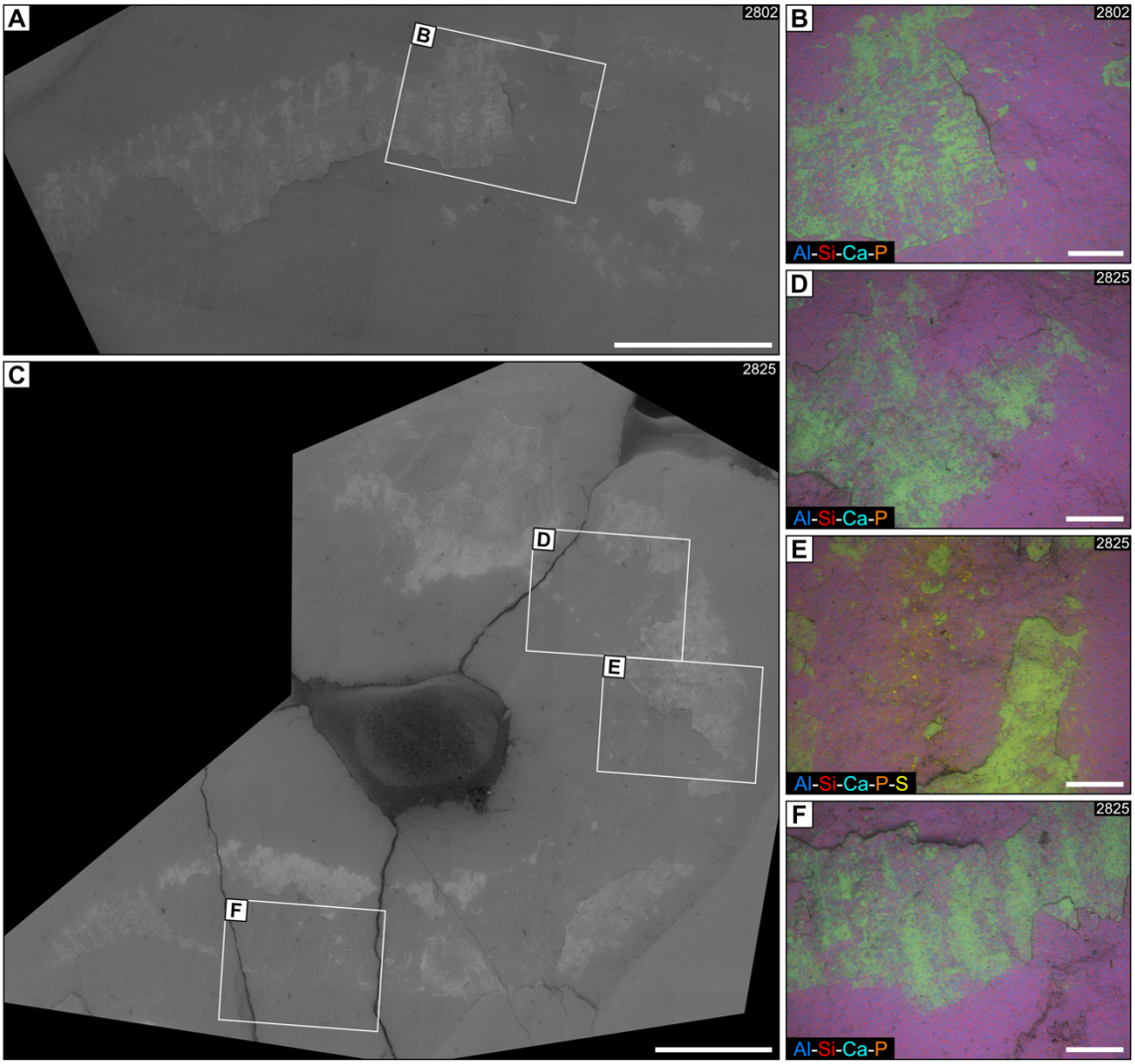

Figure 3-11. SEM-EDS analyses. A) UWGM_2802 SE and BSE large-area micrograph mosaic of the *A. stimulapis* holotype. B) UWGM_2802; EDS compositional map. C) UWGM_2825; SE and BSE large-area micrograph mosaic of the *A. leonidas* holotype. D–F) UWGM_2825; EDS compositional maps. In both A and C, fossil material is visible as the lighter gray patches. In B & D–F, the pink coloration represents mixed aluminum and silica signals; the green patches represent mixed calcium and phosphate signals; the yellow hue represents a sulfur signal. Scale bars in A & C = 5 mm; scale bars in B & D–F = 1 mm.

3.6 Conclusions

The taxonomic evaluation of a vermiform arthropod from the Silurian Waukesha Lagerstätte presented herein reveals a novel genus comprising two species: *Acheronauta stimulapis* gen. et sp. nov. and *Acheronauta leonidas* sp. nov. These arthropods are characterized by a cephalic carapace, a suite of head appendages including specialized antennae, maxillules, and maxillae which terminate in boxing glove-esque sub-chelae, three pairs of maxillipeds used for walking, and a long, homonomously segmented trunk, with small, setose swimming appendages on each tergite. The rarer taxon, *A. leonidas* gen. et sp. nov., is distinguished from the abundant *A. stimulapis* gen. et sp. nov. by the presence of an anterodorsal keel on the cephalic carapace and by a pronounced contraction of the trunk tergites anterior to the terminus. SEM-EDS imaging and analyses indicate that these specimens are preserved as carbonate-fluorapatite compressions in a fine-grained, aluminosilicate host rock. Phylogenetic analysis suggests that this genus represents a basal mandibulate, closely related to the fuxianhuiids and/or the hymenocarinids, similar to *P. venator,* which is also known from the Waukesha (Wendruff et al., 2020b; Anderson et al., *in press*).

The Waukesha Lagerstätte prominently records a diverse assemblage of soft-bodied organisms, mostly comprising unique arthropod genera, like *Acheronauta* gen. nov. , rather than the shelly biota typical of other Silurian faunal assemblages (Mikulic et al., 1985a; 1985b; Moore et al., 2005; Wendruff et al., 2020b). This biota thus provides a unique glimpse onto an interval of arthropod evolution that is otherwise sparsely known. In an ecological sense, the Waukesha is not unlike a Silurian Burgess Shale (Gould, 1989; Briggs et al., 1994), albeit preserved in carbonate rocks. The arthropods preserved in these rocks—and other small Ordovician and

Silurian lagerstätten on the Laurentian paleocontinent—serve as a potential bridge between soft-bodied arthropods found in Cambrian and later Paleozoic deposits. Although much work has been done on Burgess Shale-type arthropods, and to decipher how they might be the predecessors or stem-group cousins of modern taxa, it has proven difficult to make much sense of the taxonomic or ecological role of some arthropods, such as those of the late Cambrian Orsten meiofauna or the Hunsrück Slate of the early Devonian. While the significance of chronologically or faunally isolated biota may be viewed as curious but intractable, lagerstätten like the Waukesha may provide evidence of evolutionary connections or continuities heretofore unavailable. The intertidal and shallow subtidal environments of the Silurian in effect may have served as the laboratory where the Cambrian, Paleozoic, and Modern arthropod faunas first mixed, some set to evolve to a bright and diverse future, others doomed to obscurity or extinction. More investigation is necessary, of course, to see just how valuable the Waukesha and other Paleozoic deposits prove to be, but the results shown so far, including the morphology and taphonomic diversity of *Acheronauta* gen. nov., suggest that this will be a fruitful endeavor.

3.7 References

Anderson, E. P., Schiffbauer, J. D., Jacquet, D. M., Lamsdell, J. C., Kluessendorf, J., & Mikulic, D.G. In press. Stranger than a scorpion: a reassessment of *Parioscorpio venator*, a problematic arthropod from the Llandoverian Waukesha Lagerstätte. *Palaeontology*.

Aria, C. & Caron, J.-B. 2017. Burgess Shale fossils illustrate the origin of the mandibulate body plan. *Nature*, 545, 89–92, doi: 10.1038/nature22080.

Briggs, D. E. G. 1978. The morphology, mode of life, and affinities of Canadaspis perfecta (Crustacea: Phyllocarida), Middle Cambrian, Burgess Shale, British Columbia. *Philosophical Transactions of the Royal Society B: Biological Sciences*, 281, 439–487.

Briggs, D. E. G., Erwin, D. H., & Collier, F. J. 1994. The Fossils of the Burgess Shale. Washington: Smithsonian Institution Press.

Briggs, D. E. G., & Wilby, P. R. 1996. The role of calcium carbonate-calcium phosphate switch in the mineralization of soft-bodied fossils. *Journal of the Geological Society, London*, 153, 665–668.

Briggs, D. E. G. 2003. The role of decay and mineralization in the preservation of soft-bodied fossils. *Annual Review of Earth and Planetary Sciences*, 31, 275–301. doi:10.1146/annurev.earth.31.100901.144746

Broda, K., Hegna, T. A. & Zatoń, M. 2015. Fossils explained. Thylacocephalans. *Geology Today*, 31, 116–120, doi: 10.1111/gto.12097.

Edgecombe, G. D., Strullu-Derrien, C., Góral, T., Hetherington, A. J., Thompson, C. & Koch, M. 2020. Aquatic stem group myriapods close a gap between molecular divergence dates and the terrestrial fossil record. *Proceedings of the National Academy of Sciences of the United States of America*, 117, 8966–8972, doi: 10.1073/pnas.1920733117.

Gould, S. J. 1989. *Wonderful Life: The Burgess Shale and the Nature of History*. W. W. Norton & Co, New York, 347 pp.

Haug, C., Briggs, D. E. G., Mikulic, D. G., Kluessendorf, J. & Haug, J. T. 2014. The implications of a Silurian and other thylacocephalan crustaceans for the functional morphology and systematic affinities of the group. *BMC Evolutionary Biology*, 14, 1–15, doi: 10.1186/s12862-014-0159-2.

Hou, X. & Bergström, J. 1997. Arthropods of the Lower Cambrian Chengjiang fauna, southwest China. *Fossils & Strata*, 45, 1–116.

Jones, W. T., Feldmann, R. M. & Schweitzer, C. E. 2015. Ceratiocaris from the Silurian Waukesha Biota, Wisconsin. *Journal of Paleontology*, 89, 1007–1021, doi: 10.1017/jpa.2016.22.

Kleffner, M. A., Norby, R. D., Kluessendorf, J., and Mikulic, D. G. 2018. Revised conodont biostratigraphy of Lower Silurian strata of southeastern Wisconsin. Geological Society of America *Abstracts with Programs*, 50.

Kluessendorf, J. 1990. *Depositional and Taphonomic Aspects of a Silurain (Brandon Bridge, Llandovery-Wenlock) Fossil Konservat Lagerstätte from Waukesha, Wisconsin (U.S.A.), Predictability of North American Silurian Fossil Konservat Lagerstätten, and Some Insights into Ichnofacies*. University of Illinois at Urbana-Champaign, 115 pp.

Kluessendorf, J. & Mikulic, D. G. 1996.An Early Silurian sequence boundary in Illinois and Wisconsin. Geological Society of America *Special Paper*, 306, 177–185.

Lamsdell, J. C., LoDuca, S. T., Gunderson, G. O., Meyer, R. C. & Briggs, D. E. G. 2017. A new Lagerstätte from the late ordovician Big Hill Formation, Upper Peninsula, Michigan. *Journal of the Geological Society*, 174, 18–22, doi: 10.1144/jgs2016-059.

Liu, H. P., McKay, R. M., Young, J. N., Witzke, B. J., McVey, K. J. & Liu, X. 2006. A new Lagerstätte from the Middle Ordovician St. Peter Formation in northeast Iowa, USA. *Geology*, 34, 969–972, doi: 10.1130/G22911A.1.

LoDuca, S. T., Kluessendorf, J. & Mikulic, D. G. 2003. A new noncalcified Dasycladalean alga from the Silurian of Wisconsin. *Journal of Paleontology*, 77, 1152–1158.

Mikulic, D. G. 1977. A preliminary revision of the Silurian stratigraphy of south-eastern Wisconsin. Pp. A6–A34 in K. G. Nelson (ed) The geology of southeastern Wisconsin, 41st Annual Tri-State Geological Field Conference Guidebook. Milwaukee, University of Wisconsin-Milwaukee.

Mikulic, D. G., Briggs, D. E. G. & Kluessendorf, J. 1985a. A Silurian Soft-Bodied Biota. *Science*, 228, 715–717.

Mikulic, D. G., Briggs, D. E. G. & Kluessendorf, J. 1985b. A New Exceptionally Preserved Biota from the Lower Silurian of Wisconsin , U.S.A. *Philosophical Transactions of the Royal Society B: Biological Sciences*, 311, 75–85.

Mikulic, D. G. & Kluessendorf, J. 1999. Stasis and extinction of Silurian (Llandovery-Wenlock) trilobite associations related to oceanic cyclicity. *Journal of Paleontology*, 73, 320–325.

Miller, A. A., Jacquet, S. M., Anderson, E. P., Huntley, J. W., & Schiffbauer, J. D. 2020. Ecology ad taphonomy of Silurian conulariids from the Waukesha Lagerstätte, Wisconsin. Geological Society of America *Abstracts with Programs*. 52.

Moore, R. A., Briggs, D. E. G., Braddy, S. J., Anderson, L. I., Mikulic, D. G. & Kluessendorf, J. 2005. A new Synziphosurine (Chelicerata: Xiphosura) from the late Llandovery (Silurian) Waukesha Lagerstätte, Wisconsin, USA. *Journal of Paleontology*, 79, 242–250, doi: 10.1666/0022-3360(2005)079<0242:ANSCXF>2.0.CO;2.

Neiber, M. T., Hartke, T. R., Stemme, T., Bergmann, A., Rust, J., Iliffe, T. M. & Koenemann, S. 2011. Global Biodiversity and Phylogenetic Evaluation of Remipedia (Crustacea) Stepanova, A. (ed.). *PLoS ONE*, 6, e19627, doi: 10.1371/journal.pone.0019627.

Pulsipher, M. A., Anderson, E. P., & Schiffbauer, J. D. 2019. Refining arthropod evolutionary history: Investigation of an undescribed crusacean-like fossil from the Waukesha Lagerstätte, Wisonsin. 11th North American Paleontological Convention *Program with Abstracts; PaleoBios* 36.

Schram, F. R., Yager, J., & Emerson, M. J. 1986. Remipedia. Part I. Systematics. *San Diego Society of Natural History Memoir*, 15, 4–60.

Schram, F. R., Hof, C. H. J. & Steeman, F. A. 1999. Thylacocephala (Arthropods: Crustacea?) from the Cretaceous of Lebanon and implications for Thylacocephalan systematics. *Palaeontology*, 42, 769–797.

Smith, M. P., Briggs, D. E. G., Aldridge, R. J., 1987. A conodont animal from the lower Silurian of Wisconsin, USA, and the apparatus architecture of panderodontid conodonts. Pp. 91–104 in: R. J. Aldridge (ed) *Paleobiology of Conodonts*. British Micropalaeontological Society Series Ellis Horwood, Chichester,

Snodgrass, R. E. 1938. Evolution of the Annelida, Onychophora, and Arthropoda. *Smithsonian Miscellaneous Collections*. 97, 1–159.

Swofford, D.L. 2003. PAUP*. Phylogenetic Analysis Using Parsimony (*and Other Methods). Version 4. Sinauer Associates, Sunderland, Massachusetts.

Vaerjão, F. J., Warren, L. V., Simões, M. G., Fürsich, F. T., Matos, S. A., Assine, M. L. 2019. Exceptional preservation of soft tissues by microbial entombment: Insignts into the taphonomy of the Crato konservat-lagerstätte. *Palaios*, 34, 331–348.

Vannier, J., Chen, J.-Y., Huang, D.-Y., Charbonnier, S. & Wang, X.-Q. 2006. The Early Cambrian origin of thylacocephalan arthropods. *Acta Palaeontol.*, 51, 201–214.

von Bitter, P. H., Purnell, M. A., Tetreault, D. K. & Stott, C. A. 2007. Eramosa Lagerstätte—Exceptionally preserved soft-bodied biotas with shallow-marine shelly and bioturbating organisms (Silurian, Ontario, Canada). *Geology*, 35, 879–882, doi: 10.1130/G23894A.1.

von Siebold, C. T. 1848. Lehrbuch der vergleichenden Anatomie der Wirbellosen Thiere. 1–679. In von C. T. Siebold, and H. Stannius (eds) *Lehrbuch der vergleichenden Anatomie*. Verlag von Veit and Company, Berlin, 679 pp.

Wendruff, A. J. 2016. *Paleobiology and Taphonomy of Exceptionally Preserved Organisms from the Brandon Bridge Formation (Silurian), Wisconsin, USA*. The Ohio State University, 240 pp.

Wendruff, A. J., Babcock, L. E., Wirkner, C. S., Kluessendorf, J. & Mikulic, D. G. 2020a. A Silurian ancestral scorpion with fossilised internal anatomy illustrating a pathway to arachnid terrestrialisation. *Scientific Reports*, 10, 1–6, doi: 10.1038/s41598-019-56010-z.

Wendruff, A. J., Babcock, L. E., Kluessendorf, J. & Mikulic, D. G. 2020b. Paleobiology and taphonomy of exceptionally preserved organisms from the Waukesha Biota (Silurian), Wisconsin, USA. *Palaeogeography, Palaeoclimatology, Palaeoecology*, 546, 109631, doi: 10.1016/j.palaeo.2020.109631.

Westberg, M. 2019. *Enigmatic Worm-like Fossils from the Silurian Waukesha Lagerstätte, Wisconsin, USA*. Lund University, 26 pp.

Wilson, H. M., Briggs, D. E. G., Mikulic, D. G., & Kluessendorf, J. 2004. Affinities of the Lower Silurian Waukesha 'Myriapod.' Geological Society of America *Abstracts with Programs*, 36.

Yang, J., Ortega-Hernández, J., Butterfield, N. J. & Zhang, X. 2013. Specialized appendages in fuxianhuiids and the head organization of early euarthropods. *Nature*, 494, 468–471, doi: 10.1038/nature11874.